



NATIONAL TECHNICAL UNIVERSITY OF ATHENS
FACULTY OF APPLIED MATHEMATICS AND PHYSICS

MOLECULAR DYNAMICS AND PHASE TRANSITIONS IN PROTEIN-WATER SYSTEMS

PhD THESIS

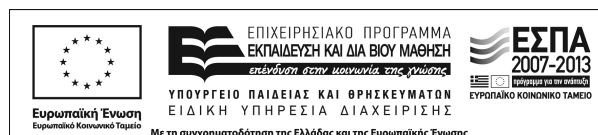
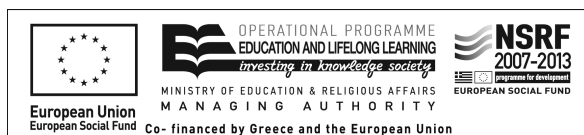
ANNA PANAGOPOULOU

Applications Physicist

SUPERVISOR:

P. PISSIS

Professor NTUA



ATHENS, November 2013



NATIONAL TECHNICAL UNIVERSITY OF ATHENS
FACULTY OF APPLIED MATHEMATICS AND PHYSICS



The PhD Thesis has been financially supported by the program HERAKLEITUS II

MOLECULAR DYNAMICS AND PHASE TRANSITIONS IN PROTEIN-WATER SYSTEMS

PhD THESIS

ANNA PANAGOPOULOU

Applications Physicist

THREE MEMBERED ADVISORY COMMITTEE:

1. P. PISSIS, Professor NTUA
(supervisor)
2. G. NOUNESIS, Director of research
NCFSR Democritos
3. N. SHINYASHIKI, Professor Tokai
University, Japan

SEVEN MEMBERED COMMITTEE:

1. D. GIOVA, Professor NTUA
2. S. HAMODRAKAS, Professor
NKUA
3. T. MAVROMOUSTAKOS,
Professor NKUA
4. A. KYRITSIS, Assistant Professor
NTUA
5. G. NOUNESIS, Director of
research NCFSR Democritos
6. N. SHINYASHIKI, Professor Tokai
University (Japan)
7. P. PISSIS, Professor NTUA

ATHENS, November 2013

Preface

The present PhD thesis has been elaborated in the Physics Department of the Faculty of Applied Mathematics and Physics of the National technical University of Athens (NTUA) during the period May 2009-November 2013. The three-membered advisory committee consisted of Professor P. Pissis (supervisor), Professor N. Shinyashiki, and G. Nounesis (Director of Research).

The object of the thesis was the study of molecular dynamics and phase transitions in protein-water systems. For this purpose thermal and dielectric experimental techniques were employed in NTUA as well as in other collaborating laboratories abroad.

I acknowledge the program HERAKLEITUS II for financial support of this thesis.

I would like to gratefully thank Professor P. Pissis for offering me the opportunity to elaborate this thesis. I am grateful to Professor P. Pissis for his guidance during the elaboration period of the thesis and the transmission of knowledge and way of scientific thinking. Furthermore, the support of Professor P. Pissis should be acknowledged starting from the period of my undergraduate studies and on until now. I appreciate and admire Professor P. Pissis not only for his scientific excellence but also for his incorruptible and loving character. I would also like to thank Assistant Professor A. Kyritsis for the collaboration during the elaboration period of the thesis and his useful and highlighting consulting. I would like to thank Professor N. Shinyashiki in Tokai university (Japan) for his useful advice and support which was at any time available to me despite the geographical distance. I would also like to thank Professors J. L. Gómez Ribelles, M. Monleón Pradas and Dr. R. Sabater i Serra in the Polytechnical University of Valencia (Spain), as well as the rest of the people from Spain, for the experimental collaboration. I gratefully thank Dr. S. Kripotou, who has been my friend and collaborator for many years in the Dielectrics Research Group in NTUA, for her useful scientific advice and support. In addition I would like to thank my friends Dr. K. Raftopoulos, Dr. D. Fragiadakis, Dr. A. Spanoudaki for similar reasons. I would also like to thank all of the members of the Dielectrics Research Group in NTUA. Above all I would like to thank my beloved mother for her support and dedicate this thesis to the memory of my father.

INDEX	i
Introduction	1
1. Principles of the protein structure	5
1.1 The 20 aminoacids and the polypeptide chain.....	5
1.2 Protein structure and function.....	8
2. Water dynamics	15
2.1 Water dynamics overview and the inhomogeneous structure.....	15
2.2 Dynamics of supercooled water.....	19
2.3 Water in non polar confinement.....	24
3. Phase transitions in hydrated proteins	25
4. Experimental techniques	31
4.1 Water Equilibrium Sorption Isotherms (ESI).....	31
4.1.1 Experimental Instruments.....	33
4.2 Differential Scanning Calorimetry (DSC).....	34
4.2.1 Experimental Instruments.....	37
4.3 Dielectric Relaxation Spectroscopy (DRS).....	38
4.3.1 Experimental Instruments.....	42
4.4 Thermally Stimulated Depolarization Currents (TSDC).....	42
4.4.1 Experimental Instruments.....	42
5. Globular Protein BSA	43
5.1 Introduction.....	43
5.2 Materials and Sample Preparation.....	43
5.3 BSA-ESI.....	44
5.4 BSA-DSC.....	45
5.5 BSA-Dielectric Measurements.....	49
5.5.1 BSA-TSDC.....	49
5.5.2 BSA-DRS.....	52
5.6 Discussion -Conclusions.....	59
5.6.1 Critical water contents and crystallization effects.....	59
5.6.2 Glass Transition - α relaxation of the protein water mixture.....	61
5.6.3 The interplay between a secondary relaxation of polar groups triggered by water molecules and the ν relaxation of water.....	66
5.6.4 Excess uncrystallized water and ice.....	71
5.6.5 Conclusions.....	76
6. Fibrous Protein Elastin	79
6.1 Introduction.....	79
6.2 Materials and Sample Preparation.....	80
6.3 Elastin-ESI.....	81
6.4 Elastin-DSC.....	81
6.5 Elastin-Dielectric Measurements.....	88
6.5.1 Elastin-TSDC.....	88
6.5.2 Elastin-DRS.....	91
6.6 Discussion-Conclusions.....	100
6.6.1 The interplay between a secondary relaxation of polar groups triggered by water molecules and the ν relaxation of water.....	100
6.6.2 Dynamical characteristics of the p and w modes.....	103

6.6.3 The w' relaxation mode.....	105
6.6.4 Identifiing the origin of the hydration water related relaxation modes.....	107
6.6.5 Conclusions.....	109
7. Comparative studies of Glass Transition and Water Dynamics in globular proteins, fibrous proteins and other biopolymers	111
7.1 Introduction-Scope.....	111
7.2 Materials and Sample preparation.....	112
7.2.1 Globular protein Lysozyme	112
7.2.2 Fibrous protein Collagen.....	112
7.2.3 Hyaluronic Acid hydrogel (HA).....	112
7.2.4 Casein Peptone.....	113
7.3 Glass Transition and Water Dynamics.....	113
7.3.1 The v relaxation and its relation to the secondary relaxation of polar groups.....	115
7.3.2 The w relaxation and its relation to the liquid-liquid phase transition (LLPT).....	121
7.3.3 Glass transition in hydrated biopolymers.....	122
7.3.4 Ice like structures - Confinement.....	134
7.3.5 Percolation.....	139
8. Conclusions	141
References	147
Summary	165
Περίληψη	167
Εκτενής Περίληψη	169

1. Principles of the protein structure

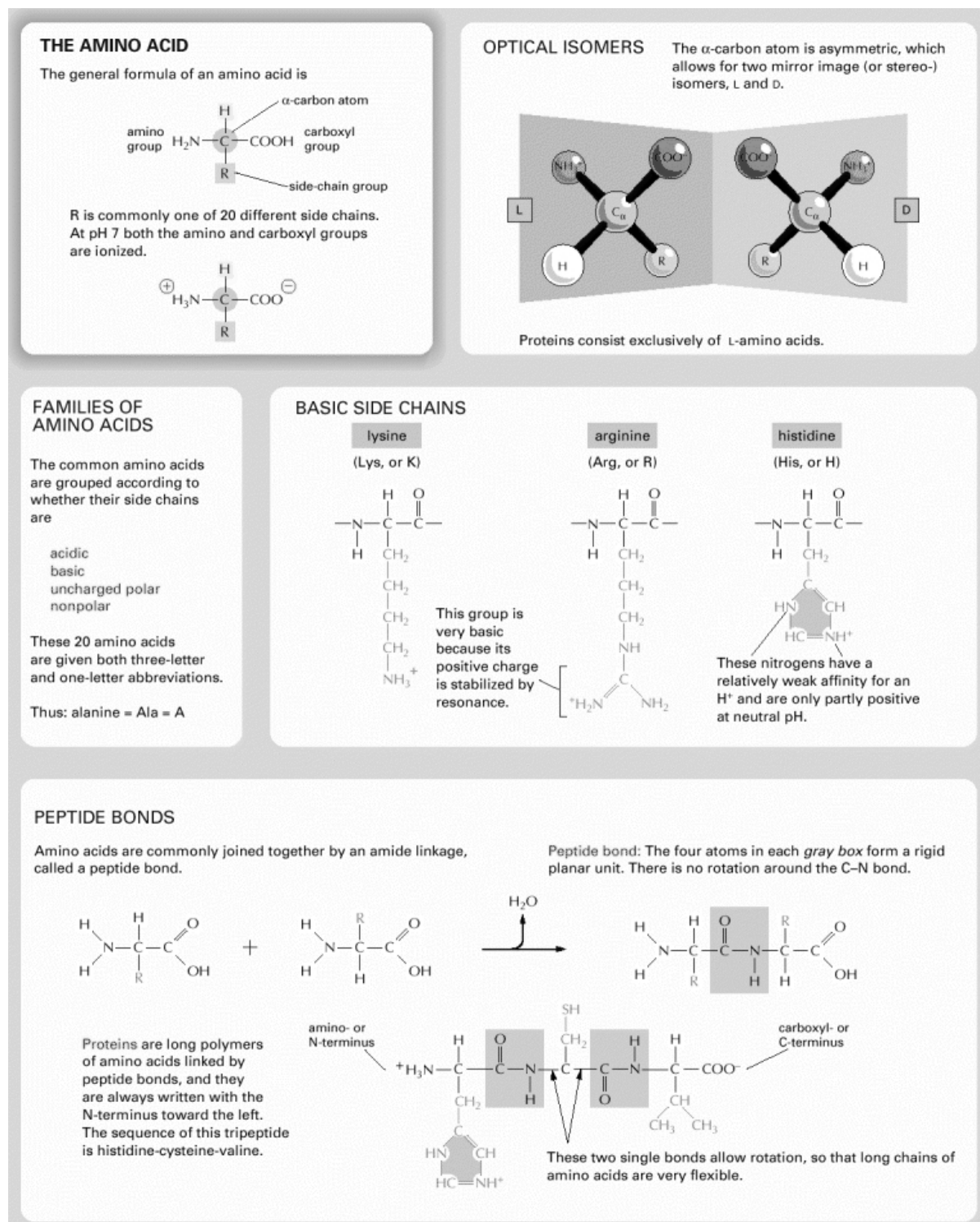
1.1 The 20 aminoacids and the polypeptide chain

The primary structural components of proteins are the aminoacids. The general chemical formula of an aminoacid may be seen in Scheme 1.1. The central α -carbon atom is bonded to an aminogroup (-NH), a carboxyl group (-COOH) and a side chain (-R), or aminoacid residue. There are 20 different side chains and, consequently, 20 different aminoacids. The aminoacids are classified into categories according to the type of their side chains. These may be charged (acid or acidic), polar uncharged or non polar (Scheme 1.1). The chemical types of all 20 aminoacids may be seen in Schemes 1.1 and 1.2. Based on the tendency of a side chain to be in contact with a polar solvent like water, the aminoacid may be classified as hydrophobic (non-polar) or hydrophilic (polar or charged).

Amino acids are put together into a polypeptide chain on the ribosome in a process called protein synthesis. During this process the peptide bond, the covalent bond between two amino acid residues, is formed. The peptide bond is formed between the carboxyl and amino groups of neighbouring amino acids. Examples of peptide bonds may be seen in Scheme 1.1. Sometimes these amino acids are chemically modified in the protein after protein synthesis. In total the number of different proteins, which it is possible to produce from 20 amino acids is enormous. For example for 10 amino acid sequence it is possible to have 20^{10} different sequences, which is approximately equal to 10^{13} or 10 trillions of different structures. The structures build from 2 to 100 amino acids with molecular weight up to 10 kDa are usually called peptides. Longer polypeptide structures are classified as proteins. Some other classifications refer to the conformational stability of the amino acid chain. In this classification peptides have many different conformations and can randomly change them, whereas proteins are structurally rigid with only one preferable conformation. These classifications are not strict and are used only as a guideline.

Proteins are made of aminoacids linked into linear chains, called polypeptide chains, consisting of one or more of the latter. The sequence of the polypeptide chain is defined by a gene with genetic code. Each type of protein differs in its sequence and number of amino acids. Therefore, it is the sequence of the chemically different side chains that makes each protein distinct. A polypeptide chain consists of a polypeptide backbone with attached side chains. The two ends of a polypeptide chain are chemically different: the end carrying the

Chapter 1. Principles of the protein structure



PEPTIDE BONDS

Amino acids are commonly joined together by an amide linkage, called a peptide bond.



Peptide bond: The four atoms in each gray box form a rigid planar unit. There is no rotation around the C-N bond.

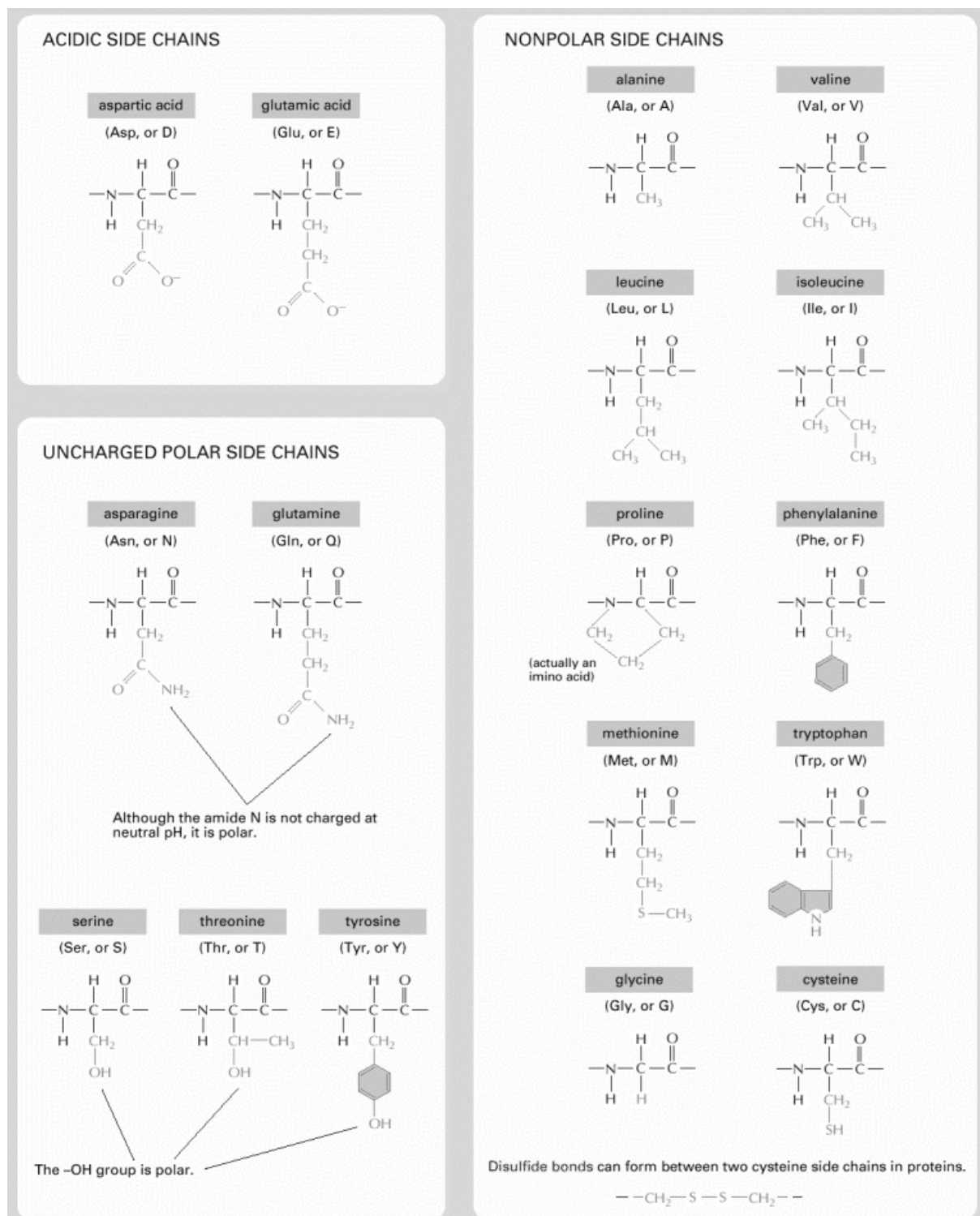
Proteins are long polymers of amino acids linked by peptide bonds, and they are always written with the N-terminus toward the left. The sequence of this tripeptide is histidine-cysteine-valine.



These two single bonds allow rotation, so that long chains of amino acids are very flexible.

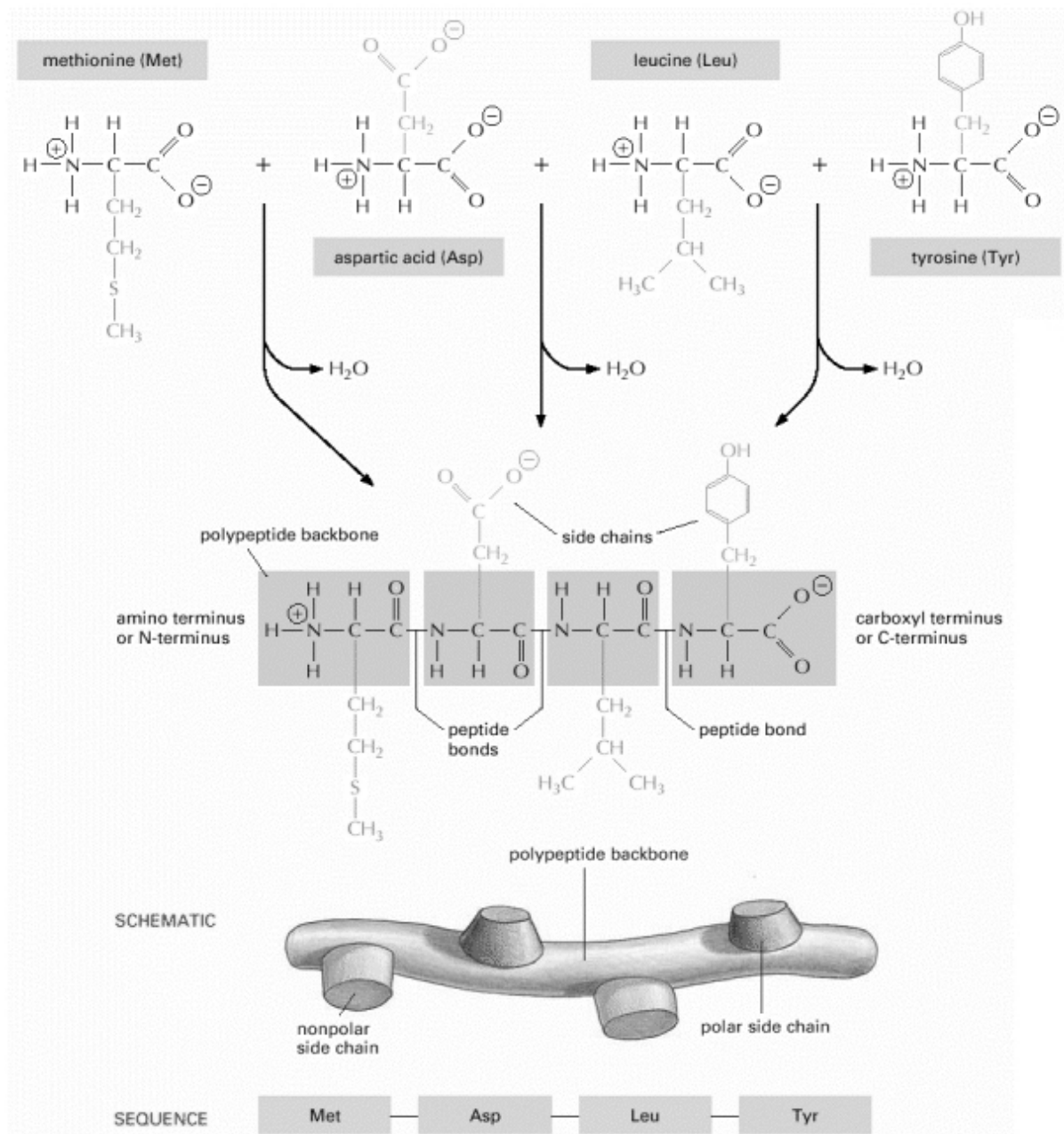
Scheme 1.1 The amino acid chemical type. Basic aminoacids. Examples of peptide bonds. [Alberts 2002]

free amino group (NH_3^+ , also written NH_2) is the amino terminus, or N-terminus, and that carrying the free carboxyl group (COO^- , also written COOH) is the carboxyl terminus or C-terminus. The amino acid sequence of a protein is always presented in the N-to-C direction,



Scheme 1.2 The chemical types of acidic, uncharged polar and non polar aminoacids. [Alberts 2002]

reading from left to right. An example of a sequence of distinct aminoacids forming a peptide chain may be seen in Scheme 1.3.



Scheme 1.3 Schematic representation of a polypeptide chain [Alberts 2002]

1.2 Protein structure and function

Proteins are large biological molecules with molecular weight up to few million Daltons. For convenience, the protein weight is measured in thousands Daltons or kiloDaltons (kDa). The main polypeptide chain, consisting of a sequence of aminoacids is the main structural component of the complex protein structure. Examples of more complex protein structures are described in Scheme 1.4. These are the α helix and the β sheet, two well known conformational structures of the backbone [Petsko 2004, Pauling 1951].

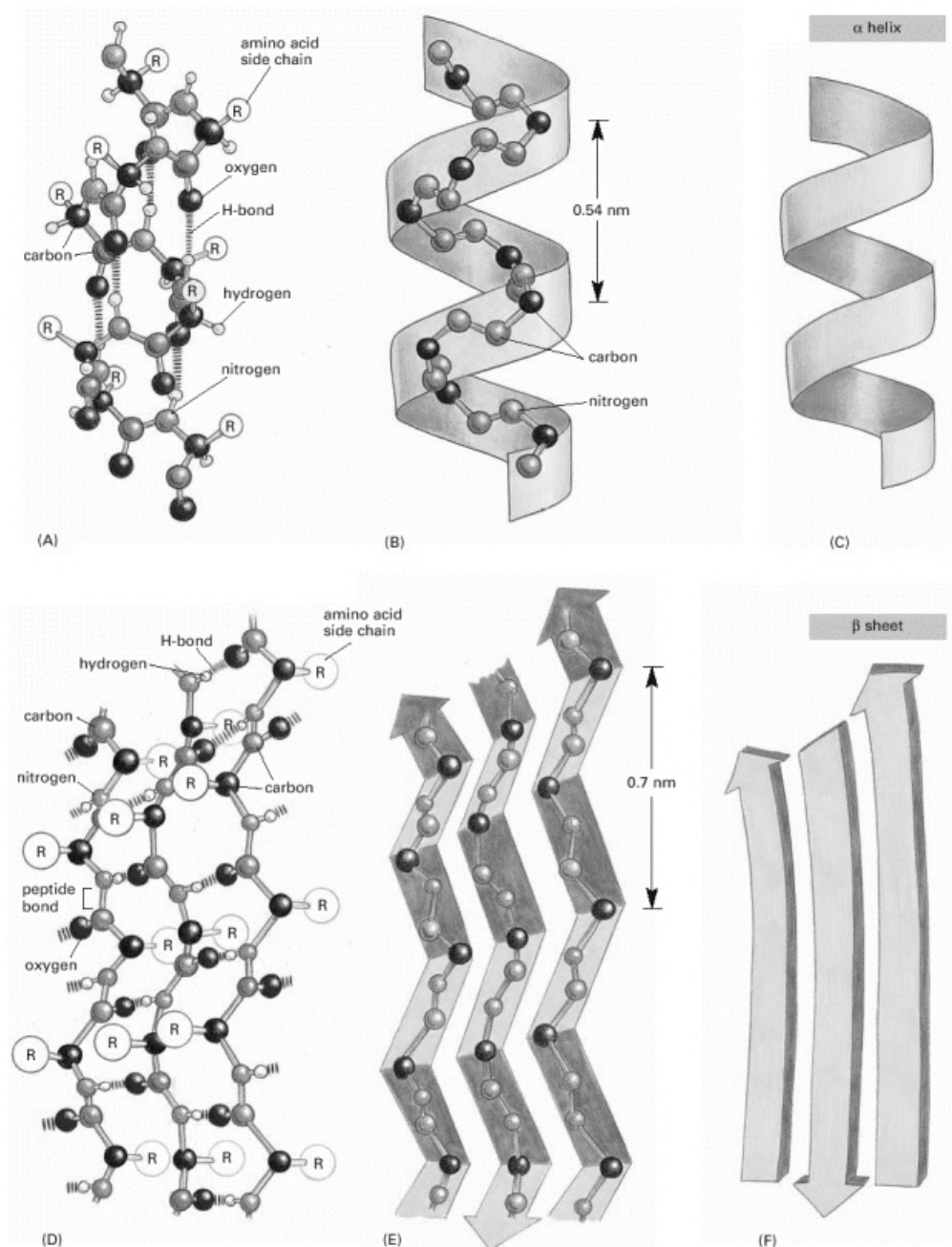
In general, the structural organisation of a protein can be divided into four different levels:

- **Primary structure or protein sequence.** The protein sequence, or amino acid sequence in polypeptide chain defines the protein primary structure. DNA (or RNA in viruses) codes the primary protein structure and this is comprehensive information for the protein structure and functions.
- **Secondary structure.** Segments of polypeptides often fold locally into stable structures, like alpha-helix or beta-sheet. These conformations are classified as a protein secondary structure. A main feature of the protein secondary structure is the local stabilisation by hydrogen bonds.
- **Tertiary structure, protein 3D structure or protein folding.** Tertiary structure or protein folding completely defines the structural organization of the protein molecule in 3d.
- **Quaternary structure.** The interactions between several protein molecules forms a protein complex, with its structure defined as a quaternary structure.

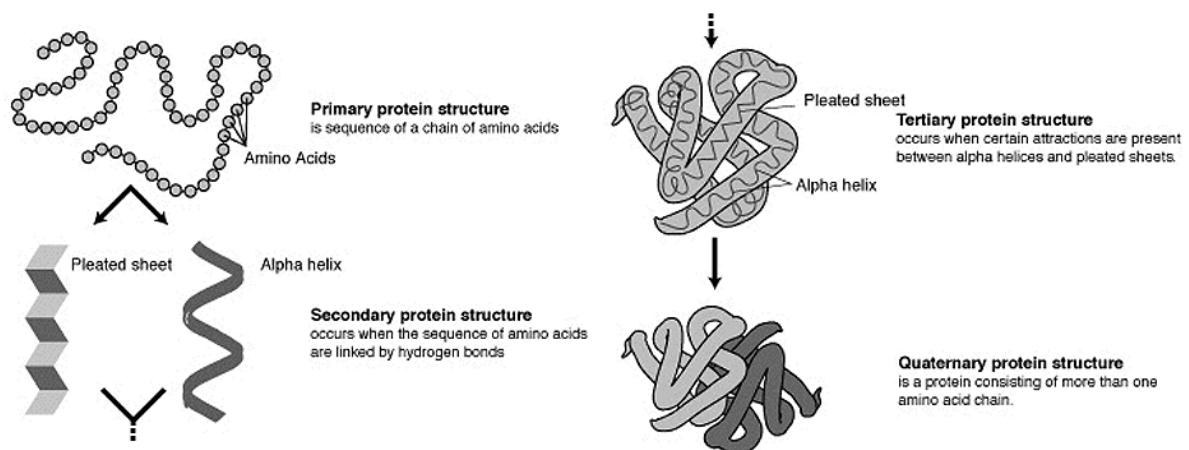
The classification of the protein according to the structure is shown in Scheme 1.5.

Folded proteins are stabilized mainly by weak noncovalent interactions

The amide bonds in the backbone are the only covalent bonds that hold the residues together in most proteins. In proteins that are secreted, or in the extracellular portions of cell-surface proteins, which are not exposed to the reducing environment in the interior of the cell, there may be additional covalent linkages present in the form of disulfide bridges between the side chain of cysteine residues. Except for cross-links like these, however, the remainder of the stabilization energy of a folded protein comes not from covalent bonds but from noncovalent weakly polar interactions. The properties of all the interactions that hold folded proteins together are listed in Table 1.1. Weakly polar interactions depend on the electrostatic attraction between opposite charges. The charges may be permanent and full, or fluctuating and partial. In general, the term electrostatic interaction is reserved for those interactions due to full charges, and this convention is observed in Table 1.1. But in principle, all polar interactions are electrostatic and the effect is the same: positively polarized species will associate with negatively polarized ones. Such interactions rarely contribute even one-tenth of the enthalpy contributed by a single covalent bond (see Table 1.1), but in any folded protein structure there may be hundreds to thousands of them, adding up to a very large contribution. The two most important are the van der Waals interaction and the hydrogen bond. Van der Waals interactions occur whenever the fluctuating electron clouds on an atom or group of bonded atoms induce an opposite fluctuating dipole on a non-bonded neighbor, resulting in a very weak electrostatic interaction. The effect is greatest with those groups that are the most polarizable; in proteins these are usually the methyl groups and methylene groups of hydrophobic side chains such as leucine and valine. Van der Waals interactions diminish rapidly as the interacting species get farther apart, so only atoms that are already close together (about 5 Å apart or less) have a chance to participate in such interactions. A given van der Waals interaction is extremely weak (see Table 1.1), but in proteins they sum up to a substantial energetic contribution. Hydrogen bonds are formed when a hydrogen atom has a significant partial positive charge



Scheme 1.4 The regular conformation of the polypeptide backbone observed in the α helix and the β sheet. (A, B, and C) The α helix. The N–H of every peptide bond is hydrogen-bonded to the C=O of a neighboring peptide bond located four peptide bonds away in the same chain. (D, E, and F) The β sheet. In this example, adjacent peptide chains run in opposite (antiparallel) directions. The individual polypeptide chains (strands) in a β sheet are held together by hydrogen-bonding between peptide bonds in different strands, and the amino acid side chains in each strand alternately project above and below the plane of the sheet. (A) and (D) show all the atoms in the polypeptide backbone, but the amino acid side chains are truncated and denoted by R. In contrast, (B) and (E) show the backbone atoms only, while (C) and (F) display the shorthand symbols that are used to represent the α helix and the β sheet in ribbon drawings of proteins. [Alberts 2002]



Scheme 1.5 The classification of proteins according to their structure [Alberts 2002]

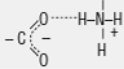
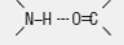
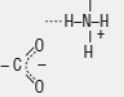
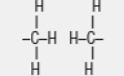
by virtue of being covalently bound to a more electronegative atom, such as oxygen, and is attracted to a neighboring atom that has a significant partial negative charge (see Table 1.1). This electrostatic interaction draws the two non-hydrogen atoms closer together than the sum of their atomic radii would normally allow. So, if two polar non-hydrogen atoms in a protein, one of which has a hydrogen attached, are found to be less than 3.5 Å apart, a hydrogen bond is assumed to exist between them. It is thought that the hydrogen-bonding effect is energetically most favorable if the three-atom system is roughly linear. The atom to which the hydrogen is covalently attached is called the donor atom; the non-bonded one is termed the acceptor atom. If the donor, the acceptor or both are fully charged, the hydrogen bond is stronger than when both are uncharged. When both the donor and acceptor are fully charged, the bonding energy is significantly higher and the hydrogen-bonded ion pair is called a salt bridge (see Table 1.1). The strengths of all polar weak interactions depend to some extent on their environment. In the case of hydrogen bonding, the strength of the interaction depends critically on whether the groups involved are exposed to water [Petsko 2004].

The hydrogen-bonding properties of water have important effects on protein stability

Water, which is present at 55 M concentration in all aqueous solutions, is potentially both a donor and an acceptor of hydrogen bonds. Water molecules hydrogen bond to one another, which is what makes water liquid at ordinary temperatures (a property of profound biological significance) and has important energetic consequences for the folding and stability of proteins.

The ability of water molecules to hydrogen-bond to the polar groups of proteins has important effects on the energy, or strength, of the hydrogen bonds formed between such groups. This is most clearly seen by comparing hydrogen bonds made by polar groups on the surface and in the interior of proteins. The strengths of polar weak interactions depend to some extent on their environment. A polar group on the surface of a protein can make

Table 1.1 Chemical interactions that stabilize polypeptides [Petsko 2004]

Chemical Interactions that Stabilize Polypeptides				
Interaction	Example	Distance dependence	Typical distance	Free energy (bond dissociation enthalpies for the covalent bonds)
Covalent bond	$-C_{\alpha}-C-$	-	1.5 Å	356 kJ/mole (610 kJ/mole for a C=C bond)
Disulfide bond	$-Cys-S-S-Cys-$	-	2.2 Å	167 kJ/mole
Salt bridge		Donor (here N), and acceptor (here O) atoms <3.5 Å	2.8 Å	12.5–17 kJ/mole; may be as high as 30 kJ/mole for fully or partially buried salt bridges (see text), less if the salt bridge is external
Hydrogen bond		Donor (here N), and acceptor (here O) atoms <3.5 Å	3.0 Å	2–6 kJ/mole in water; 12.5–21 kJ/mole if either donor or acceptor is charged
Long-range electrostatic interaction		Depends on dielectric constant of medium. Screened by water. 1/r dependence	Variable	Depends on distance and environment. Can be very strong in nonpolar region but very weak in water
Van der Waals interaction		Short range. Falls off rapidly beyond 4 Å separation. 1/r ⁶ dependence	3.5 Å	4 kJ/mole (4–17 in protein interior) depending on the size of the group (for comparison, the average thermal energy of molecules at room temperature is 2.5 kJ/mole)

interactions with water molecules that are nearly equivalent in energy to those it can make with other surface groups of a protein. Thus, the difference in energy between an isolated polar group and that of the same species when involved in a hydrogen bond with another polar group from that protein, is small. If, however, the interaction occurs in the interior of the protein, away from bulk solvent, the net interaction energy reflects the difference between the group when hydrogen-bonded and when not. It is energetically very unfavorable not to make a hydrogen bond, because that would leave one or more uncompensated partial or full charges. Thus, in protein structure nearly all potential hydrogen-bond donors and acceptors are participating in such interactions, either between polar groups of the protein itself or with water molecules. In a polypeptide chain of indeterminate sequence the most common hydrogen-bond groups are the peptide C=O and N-H. In the interior of a protein these groups cannot make hydrogen bonds with water, so they tend to hydrogen bond with one another, leading to the secondary structure which stabilizes the folded state [Petsko 2004].

Bound water molecules on the surface of a folded protein are an important part of the structure

When the polar backbone groups of a polypeptide chain become involved in secondary and tertiary structure interactions, the water molecules that were interacting with them in the unfolded protein are freed to rejoin the structure of liquid water. But there are many polar groups, both backbone and side-chain, on the surface of a folded protein that must remain in contact with water. Atomic-resolution structures of proteins show a layer of bound water molecules on the surfaces of all folded soluble proteins. These waters are making hydrogen bonds with polar backbone and side-chain groups and also with one another. There are several such water molecules per residue. Some are in fixed positions and are observed every time the structure is determined. However, others are in non-unique positions and reflect an ensemble of water-protein interactions that hydrate the entire surface. A few additional water molecules are trapped inside the protein in internal cavities.

Because bound water molecules make important interactions with groups that would otherwise make none, the waters in fixed positions should be considered as part of the tertiary structure, and any detailed structure description that does not include them is incomplete [Petsko 2004].

Another classification of the protein systems is made according to their shape. Two major categories are:

- **Globular Proteins.** They have complex tertiary and sometimes quaternary structure. Their spherical structure is induced by the tertiary structure. Hydrophobic amino acids are bound towards the molecules interior, whereas hydrophilic amino acids are bound outwards, which explains the solubility of globular proteins. Lysozyme, myoglobin and albumin are examples of globular proteins. Their functional role is mainly metabolic.

and

- **Fibrous Proteins.** They have little or no tertiary structure. They consist out of long, parallel polypeptide chains. They usually have cross linkages at intervals forming long fibers or sheets. They are usually water insoluble. They have mainly structural role. Elastin, keratin and collagen are fibrous proteins.

It must be mentioned at this point, that the protein structure is by far more complex than the one derived out of the preliminary description in this chapter, as numerous secondary structures have been recorded and characterized depending on the protein system, such as the collagen triple helix, the 3_{10} -helix, the α -helix, the β strand [Petsko 2004, Conn 2008] etc. Moreover, the understanding of the protein folding, i.e. the mechanism through which the secondary structure is formed, is not yet fully established and is a main pending task of molecular biology [Petsko 2004].

Protein function

It is a fundamental axiom of biology that the three-dimensional structure of a protein determines its function. Understanding function through structure is a primary goal of structural biology. But this is not always simple, partly because a biologically useful definition of the function of a protein requires a description at several different levels. To the biochemist, function means the biochemical role of an individual protein: if it is an enzyme, function refers to the reaction catalyzed; if it is a signaling protein or a transport protein, function refers to the interactions of the protein with other molecules in the signaling or transport pathway. To the geneticist or cell biologist, function includes these roles but will also encompass the cellular roles of the protein, as judged by the phenotype of its deletion, for example, or the pathway in which it operates. A physiologist or developmental biologist may have an even broader view of function.

There are four biochemical functions of proteins: binding, catalysis, switching, and as structural elements. The functions of all proteins, whether signaling or transport or catalysis,

depend on the ability to bind other molecules, or ligands. The ligand that is bound may be a small molecule or a macromolecule, and binding is usually very specific. Ligand binding involves the formation of noncovalent interactions between ligand and protein surface; these are the same types of bonds that are involved in stabilizing folded proteins and in interactions between protein subunits. Specificity arises from the complementarity of shape and charge distribution between the ligand and its binding site on the protein surface and from the distribution of donors and acceptors of hydrogen bonds. Changes in the conformation of a protein may accompany binding or be necessary for binding to occur. Alternatively, even a small change in the structure of a ligand or protein can abolish binding [Petsko 2004].

A protein in solution is completely surrounded by water. Some of these water molecules will interact more or less tightly with the protein surface. In fact, it is generally accepted that at least a single layer of bound water molecules should be considered an integral part of a protein structure, as previously mentioned. However, in order for a ligand which is itself surrounded by water molecules to bind to a solvated protein, both water layers must be disrupted and, at least partially, displaced. Thus, the protein and the ligand would exchange a layer of waters for favorable interactions with each other, and the enthalpic cost of releasing the surface waters can be balanced by the favorable enthalpy of the new interactions as well as by the hydrogen bonds the water can make with other solvent molecules. The relationship between these energetic contributions is not simple. Although it might seem that the free energy of a water hydrogen bond to a protein group would be comparable to that of a hydrogen bond with another water molecule, the difference in enthalpy could be either positive or negative, depending on the microenvironment on the protein surface. For example, in an environment of reduced polarity, a hydrogen bond between a water molecule and a serine side chain could be stronger than in aqueous solution because the electrostatic attraction is greater in a medium of low polarity. Further, it is likely that some protein-bound waters gain entropy when they are displaced. Thus, the free energy of ligand binding will depend on the tightness of the water interactions with the protein surface. Although there are many potential binding sites on the irregular, largely polar protein surface, the sites where ligands actually bind will be those where favorable interactions can occur and where bound solvent can also be displaced.

The role of water, therefore, is vital not only to the organization of macromolecular structure, but also to participation in enzyme catalysis. It is known that a minimum amount of water is necessary for enzymatic activity of a protein and dielectric results indicated a correlation between the onset of enzymatic activity and of a percolation type displacement process of protons on single macromolecules [Rupley 1991, Careri 1998].

2. Water Dynamics

2.1 Water dynamics overview and the inhomogeneous structure

It is known that, despite the simple structure of the water molecule, bulk liquid water exhibits a rather abnormal behavior, showing a maximum density at 4°C, and an increase in many of its thermodynamic properties, such as heat capacity and isothermal compressibility, as temperature decreases below 0°C [Franks 1972]. The anomalies of thermodynamic and dynamic properties of water become more pronounced in the metastable supercooled liquid state [Debenedetti 2003]. Although dynamics of supercooled water has been studied in the region between the melting point (0°C) and the homogeneous nucleation temperature (-42°C) [Angell 2008, Bertolini 1982, Debenedetti 2003, Masciovecchio 2004, Rønne 1997], the dynamics of water is experimentally inaccessible for the liquid state in a wide temperature range (-123 to -43°C at atmospheric pressure), often called the no man's land. This is due to the fact that, even after quenching to very low temperatures, bulk supercooled water crystallizes upon heating at approximately -123°C.

Figure 2.1a gives a schematic illustration of different temperature domains, at atmospheric pressure, of H₂O. One domain is stable, while the others are metastable. T_M is the melting temperature line and T_H represents the homogeneous nucleation temperature line. The region between the homogeneous nucleation curve T_H and the crystallization curve T_X is a kind of "No Man's Land," as experiments on the liquid phase cannot be performed. T_B is the boiling temperature and T_g the glass transition temperature. Water can also exist in a glassy form at the lowest temperatures [Mishima 1998].

Water has at least two different amorphous solid forms, a phenomenon called polyamorphism [Mishima 1998]. Two forms of glassy water, which correspond to two different local tetrahedral arrangements, have been extensively studied: low-density and high-density amorphous ice (LDA and HDA, respectively). The glassy states differ in structure as revealed by neutron scattering, X-ray diffraction and Raman spectroscopy and in thermodynamical properties such as density. Different routes to the formation of glassy water are possible. LDA is formed by quenching from the liquid state to form hyperquenched glassy water or by low-pressure vapor deposition on a cold plate to form amorphous solid water [Mayer 1991, Mishima 1998]. HDA is traditionally formed by pressure-induced amorphization of ordinary hexagonal ice Ih at -196°C (77 K) [Mishima 1984]. Upon releasing pressure HDA (density of 1.17 g/cm³ at zero pressure) transforms into LDA (0.94 g/cm³ at zero pressure) at $T=-156$ °C (117 K) [Mishima 1985]. In addition to LDA

and HDA another distinct form of glassy water has been also proposed, i.e. the very high density amorphous ice (VHDA) [Loerting 2001, Finney 2002].

The commonly accepted value for the glass transition temperature of water at ambient pressure is $T_g = -137^\circ\text{C}$ (136K) [Johari 1987] assigned to the LDA glass transition. Increasing the temperature leads to the formation of very viscous liquid water (ultraviscous water) and crystallization to cubic ice at 150K (Fig. 2.1a). The two regions of LDA and HDA at temperatures lower than the crystallization curve T_x may be seen in Fig. 2.1b, which is a generalization of Fig. 2.1a, including pressure as a parameter. Recent experimental studies have given more information regarding the glass transition temperatures of both LDA and HDA and an associated pressure dependence [Seidl 2011, Giovambattista 2012]. In particular, the T_g of HDA is located at about -158°C (115 K) at ambient pressure and increases with increasing pressure [Seidl 2011] while the T_g of LDA decreases with increasing pressure, starting from the known value of -137°C (136K), as estimated by molecular dynamics simulations [Giovambattista 2012].

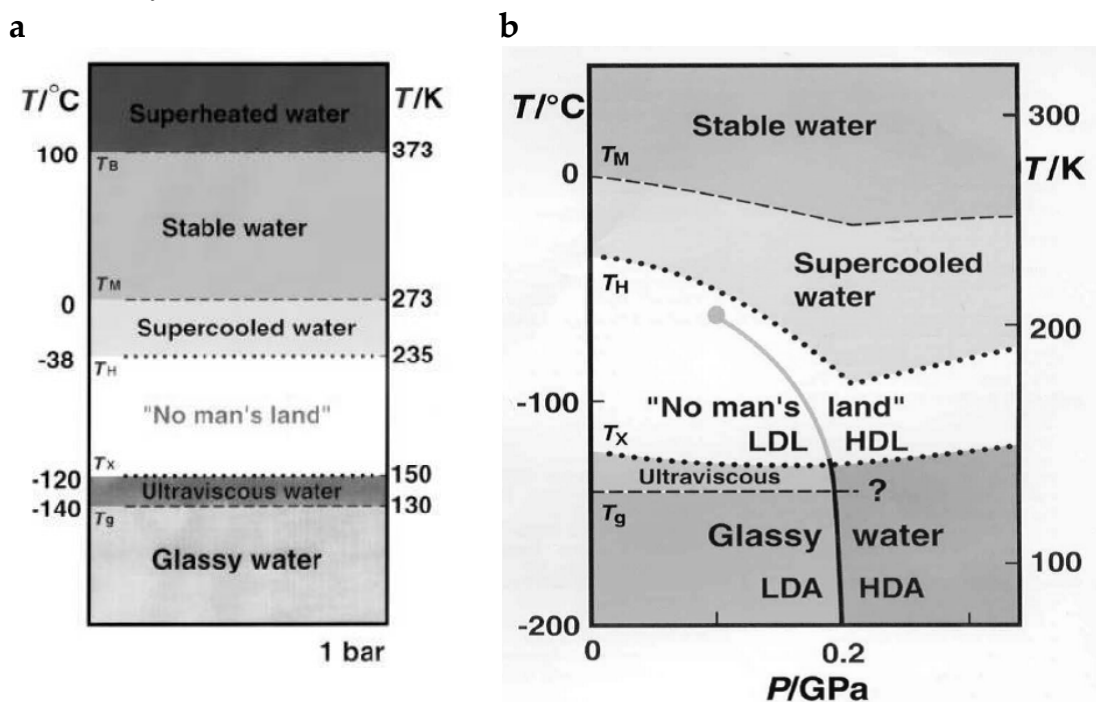


Fig. 2.1 a) Schematic illustration of different temperature domains, at atmospheric pressure, of H_2O b) generalization of (a) to incorporate the pressure as a parameter [Stanley 2000].

Computer simulations may be used to probe the local structure of water. At low temperatures, many water molecules appear to possess one of two principal local structures, one resembling LDA and the other HDA [Harrington 1997, Poole 2002]. Experimental data can also be interpreted in terms of two distinct local structures [Stanley 2000]. Among several approaches to the water problem, a widely accepted but not unambiguously established is the liquid-liquid phase transition (LLPT) hypothesis [Mishima 1998, Mallamace 2011 and references therein]. The LLPT arose from MD studies on the structure and equation of state of supercooled bulk water. According to this model, the transition

between LDA and HDA is a low-temperature manifestation of a first-order transition between two phases of liquid water: low-density liquid (LDL) and high-density liquid (HDL). LDA and HDA are, also in this hypothesis, simply their corresponding vitreous forms. The transition terminates at liquid-liquid (LL) critical point. Below this hypothesized second critical point (grey dot in Fig. 2.1b) the liquid phase separates thus into two distinct liquid phases: a low-density liquid (LDL) phase at low pressures and a high-density liquid (HDL) at high pressures (Fig. 2.1b). Bulk water near the known critical point at 374°C (647K) is a fluctuating mixture of molecules whose local structures resemble the liquid and gas phases. Similarly, bulk water near the hypothesized LL critical point is a fluctuating mixture of molecules whose local structures resemble the two phases, LDL and HDL. The “critical fluctuations” that are enhanced well above the critical temperature influence the properties of liquid bulk water, thereby leading to the observed anomalous behavior (dramatic increase) in quantities such as the isothermal compressibility, isobaric specific heat, and thermal expansion coefficient. The validity of the LLPT is gaining space in the last years. For example, in a recent molecular simulation using two distinct water models taking into account the LLPT or not, it was found that the experimental data on the glass transition temperatures of LDA and HDA are reproduced only in the case where a LLPT is considered [Giovambattista 2012]. Furthermore, an approach to compare optical scattering data on deeply supercooled water (LDA) at low temperatures, water confined in MC41 nanotubes in the no man’s land, and liquid water at high temperatures showed a continuous variation of distinct water populations proportionality, the latter classified as water molecules in the LDL phase and HDL phase (partially hydrogen bonded and non-hydrogen bonded) [Mallamace 2007]. The continuous variation is in agreement to the LLPT. In addition, a genuine LLPT was recently observed experimentally in an aqueous dilute solution of glycerol, showing implications that the transition is driven mainly by the water component [Murata 2012].

Water exists in approximately 13 different crystalline forms, some of which are stable in certain temperature-pressure ranges, while others remain metastable. Figure 2.2 shows a phase diagram of water in the P - T plane. As it may be seen in Fig. 2.2 the phase diagram of water is quite complicated, exhibiting numerous triple points. Only hexagonal ice-one (Ih), ice-three (III), ice-five (V), ice-six (VI) and ice-seven (VII) can be in equilibrium with liquid water, whereas all the other ices, including ice-two (II), are not stable in its presence under any conditions of temperature and pressure. Ice-two, ice-eight (VIII), ice-nine (IX), ice-ten and ice-eleven (both) all possess (ice-nine incompletely) ordered hydrogen-bonding whereas in the other ices the hydrogen-bonding is disordered even down to -273°C (0 K), where reachable. Ice-four (IV) and ice-twelve (XII) are both metastable within the ice-five phase space. Cubic ice (Ic) is metastable with respect to hexagonal ice (Ih). The density of the ordinary hexagonal ice is 0.917 g/cm³. Ice-five (V) has the most complicated structure of all the ice phases. Ice V is formed from liquid water at 500 MPa by lowering its temperature to -20°C. Its unit cell forms monoclinic crystals with each unit cell containing 28 molecules [Kamb 1967]. All molecules form one connected lattice with a density of 1.24 g cm⁻³ at 350 MPa. The hydrogen bonding is disordered and constantly changing as in hexagonal ice. The relaxation time of ice V is identical to the one of ice II [Johari 2001].

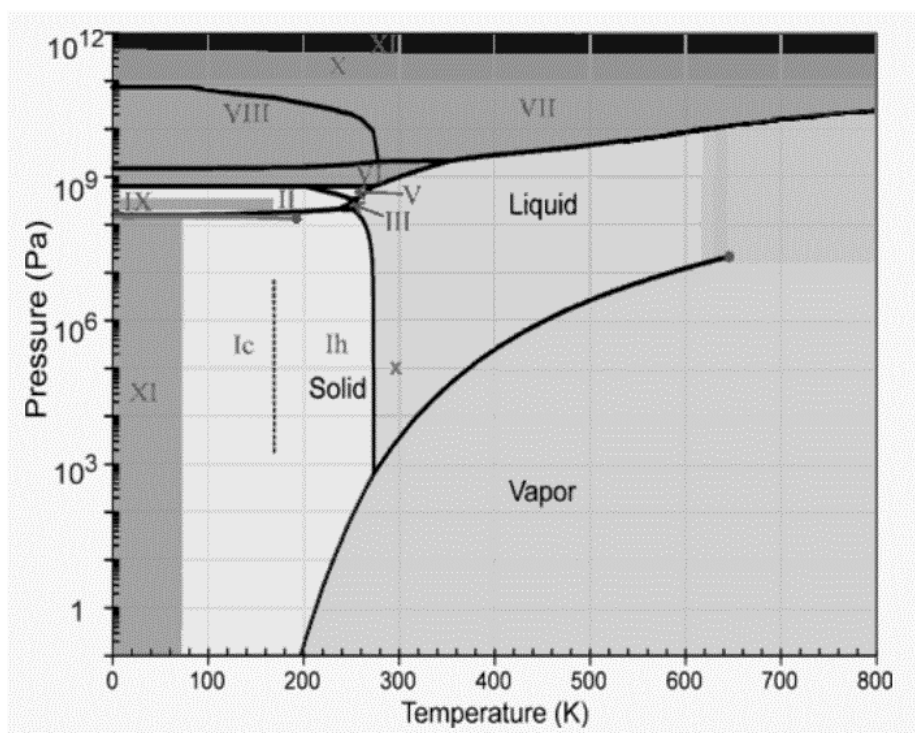


Fig. 2.2 The phase diagram of water in the P-T plane [Vázquez 2010].

The difficulty in approaching the dynamics of supercooled water in the no man's land, i.e. water which is not in a crystalline form, drives several open questions which need to be answered.

A main question is the existence and the localization of its glass transition. As already mentioned, the conventionally accepted value for the T_g of amorphous water is located at about $T_g = -137^\circ\text{C}$ (136K) and is assigned to the glass transition temperature of LDA (Fig. 2.1). Nevertheless, this value has been questioned by numerous experimental approaches, mostly DSC measurements and comparison of dielectric data of hyperquenched water with dielectric data of glass forming water-like aqueous solutions, e.g. $\text{H}_2\text{O}-\text{H}_2\text{O}_2$, [Velikov 2001, Yu 2004] but also by molecular simulation studies [Starr 2003, Giovambattista 2004]. The above mentioned studies localize the glass transition temperature of bulk water in the range of -113 to -93°C (160-180 K) although this reassignment is doubted by recent experimental studies which follow an approach to deduce the T_g of water based on the dynamic properties of binary water mixtures as studied by dielectric spectroscopy and other experimental techniques [Capaccioli 2011, Ngai 2011].

Another major issue is the fact that the relationship between supercooled and glassy water is not clear. A question arises regarding the possibility to derive the dynamic behavior of bulk water in the no man's land by comparing with the properties of confined water. This possibility is questioned, as the confining interfaces are believed to induce alterations to the structural and dynamical characteristics of water. Water molecules in direct contact with the confining medium (interfacial water) have a similar room temperature structure as supercooled bulk water 30°C below room temperature [Teixeira 1997]. Water confined by hydrophilic surfaces exhibits a molecular layering with a mean periodicity of 2.5 \AA

[Israelachvili 1983]. Computer simulations of 2D confined interfacial water in hydrophilic nanopores suggested the formation of two well-defined layers that are already in a glassy state at ambient temperature, displaying very low mobility with respect to bulk water [Gallo 2000]. Beyond these two layers, water shows bulk-like character. Finally, the effect of confinement has been reported to decrease with decreasing dimensionality of confinement [Barut 1998], although it is not diminished.

2.2 Dynamics of supercooled water

In order to confront the difficulty in monitoring water dynamics in the no man's land region, several approaches have been made in literature, aiming to prevent crystallization of water, either by mixing with hydrophilic glass-forming solutes [Cerveny 2005, 2006, 2008, Hayashi 2006, Shinyashiki 2007a] and biopolymers [Shinyashiki 2009, Sugimoto 2008] or by confinement on the nanometer length scale, e.g. within nanopores of silica gels [Oguni 2007] or within a layered vermiculite clay [Bergman 2000]. Homogeneous water solutions of several systems, such as alcohols, ethylene and propylene glycols, sugars or carbohydrates (mono-, di- and polysaccharides) and some hydrophilic macromolecular systems including biopolymers (from polypeptides to several proteins) [Cerveny 2006, 2008, Ngai 2008, Capaccioli 2010], in concentrations of water up to 50% in weight, can be easily supercooled down to form glass, while no crystallization occurs when water molecular clusters are reduced down to sizes smaller than the critical size necessary for homogeneous nucleation, in case of confinement [Oguni 2007]. Another effect of confinement is the disorder induced by the interfaces that prevents the water molecules to form a crystalline lattice.

Water in hydrated systems differing in its properties from bulk water is often called bound water, while the term free is used for water exhibiting bulk dynamics at the same system in question [Miyazaki 2000]. There is not a clearly settled definition for bound water throughout literature, whereas water that does not crystallize neither during cooling nor during heating might consist of more than one contribution. Studies by adiabatic calorimetry in case of protein-water mixtures [Miyazaki 2000, Kawai 2006] and water confined within silica gel nanopores [Oguni 2007], have provided important results, useful to clarify this point. Oguni et al. [Oguni 2007] found that interfacial water on the silica pore walls remains in the uncrystallized state independently of the pore size, while internal water molecules, which are surrounded only by water molecules in the liquid state, remain uncrystallized only when they are confined within pores smaller in diameter than a critical value. These observations show that the interface and the dimensions affect independently water dynamics. Furthermore, Kawai et al. [Kawai 2006] suggested an analogy between uncrystallized water confined within silica nanopores and hydration water at the protein surface, in protein water mixtures. It is known that no crystallization occurs in the water present in the primary hydration layer at the protein surfaces [Sartor 1995]. Therefore, studies of protein-water systems could be aiming to clarify the dynamics of supercooled water.

Dielectric techniques are very effective for studies on the dynamics of binary water systems, since, owing to the strong electric dipole moment of the water molecule, molecular motions of water can be detected as dielectric relaxation processes. Moreover, the extremely

broad frequency range of dielectric measurements of typically more than ten decades allows following on the same sample processes with very different time scales from the liquid to the glassy state. Dielectric studies focused on the dynamics of supercooled water in different host environments in the hydration range 30-50 wt %, all provide one major result concerning the main relaxation of water. Its relaxation time, τ , has an Arrhenius temperature dependence, at least below the glass transition temperature, T_g , of the hydrated system, has an almost universal activation energy, E_{act} , of about 0.45-0.55 eV [Cerveny 2008, Sjöström 2010] shows a symmetric or nearly symmetric shape of its response function on a logarithmic frequency scale and its magnitude increases systematically with increasing water content [Sjöström 2010]. These characteristics apply not only in case of aqueous mixtures, but also in case of water confined in various confining systems [Cerveny 2004]. Another interesting feature of the observed main relaxation is a change in the temperature dependence of its characteristic relaxation time from an Arrhenius to a non Arrhenius one (strong to fragile crossover, SFC), upon increasing temperature, typically at about $-90 \pm 20^\circ\text{C}$ (180 ± 20 K) [Cerveny 2008, Ngai 2008, Swenson 2006]. The SFC has been systematically recorded by Quasi Elastic Neutron Scattering (QUENS) experiments in water confined in 1D, 2D or 3D environments, as well as in water under biological confinement (lysozyme, DNA and RNA) [Chen 2009]. The crossover as measured by QUENS lies in the temperature region of about $-70 \pm 20^\circ\text{C}$ (200 ± 20 K), depending on the dimensionality of confinement, the hydration level and pressure [Mallamace 2011]. It has been suggested to be an integral characteristic of the structure of water, based on experiments and simulation studies [Chen 2009, Mallamace 2012]. However, several experimental studies on hydrated proteins by dielectric relaxation spectroscopy (DRS) and nuclear magnetic resonance (NMR) show no sign of such a crossover [Khodadadi 2008, Gainaru 2009] which has been also suggested to be an artifact of the data analysis method [Doster 2010], the latter being ruled out later on [Magazù 2011]. The crossover observed by QUENS has been alternatively explained by the assumption that it is caused by the main relaxation of water entering the experimental window at the resolution of the spectrometer [Khodadadi 2010, Capaccioli 2011, Ngai 2011].

The interpretation of the main relaxation of water and its association to the viscosity related α relaxation of bulk water, has been highly debated in literature. The dynamic crossover of the main relaxation of water has been interpreted to originate from a transformation of a secondary β relaxation of water in the deeply supercooled regime into a cooperative viscosity related α relaxation above the crossover temperature [Cerveny 2006, 2008, Swenson 2010] or in the fact that at temperatures above the crossover temperature, a merged $\alpha\beta$ relaxation is observed, while the α relaxation disappears at lower temperatures due to confinement effects [Swenson 2006]. On the other hand, the nature of the corresponding relaxation has been discussed in terms of the Johari-Goldstein β relaxation of glass formers in general [Ngai 2008, 2011, Capaccioli 2007, 2010, Shinyashiki 2007b] where the term “ ν relaxation” of water was used. In [Shinyashiki 2007, Ngai 2011] the ν relaxation of water is strongly believed to have exclusively characteristics like a secondary relaxation process, as its dielectric strength $\Delta\epsilon$ universally increases with temperature, unlike in case of a viscosity related α relaxation. In this case the crossover is recorded at temperatures close to the glass transition temperature of the hydrated systems. Additionally, it was shown by numerous experimental results on different systems, that the time scale of the ν relaxation

process depends on the hydration level and a bottom limit for this was suggested [Ngai 2011].

Supercooled water in hydrated proteins as studied by dielectric spectroscopy

In case of hydrated proteins, the main dielectric relaxation of water is usually attributed to contributions of water molecules in the protein hydration shell. Although most dielectric spectroscopy studies are dealing with samples of hydration levels high enough for complete hydration and low enough to prevent crystallization of water (about 0.3 g/g, i.e. g of water per g of hydrated protein), recently efforts are made to study protein dynamics in a broad hydration range, either in partially crystallized solutions [Shinyashiki 2009] or starting at low levels of hydration with hydrated dry samples (powders) [Gainaru 2009, Khodadadi 2010, Jansson 2010]. Studies at low levels of hydration have been able to follow the secondary relaxation of water and to establish an additional contribution from the protein surface itself to the dielectric response [Gainaru 2009]. The complex structure of proteins makes it essential to incorporate the experimental parameter of hydration level, in order to follow step by step the organization of water in the hydration sphere of biomolecules.

Several characteristic literature results, obtained by dielectric spectroscopy measurements (see chapter 4, section 4.3) on hydrated proteins but also on a glycerol-water mixture and bulk water are reported in Fig. 2.3. The experimental results are presented via the temperature dependence of the relaxation times, τ , of the main relaxation of supercooled water, in an Arrhenius diagram (see chapter 4, section 4.3).

The dielectric data of bulk water at temperatures higher than the the no man's land (Fig. 2.3) as recorded in the THz and GHz [Mallamace 2012] frequency regions, are shown in Fig. 2.3, by a unique symbol for both techniques. Starting with the dielectric data recorded in water confined in vermiculite clay [Bergman 2000], an apparent discontinuity exists when compared to the data for bulk water. The first scenario which suggests that the secondary relaxation of water transforms into a combined α and β relaxation, supports an abrupt change in the dynamics of water, in the region of the SFC (which is highlighted in the plot by vertical dotted lines), so that the two data series are smoothly connected (i.e. vermiculite clay and bulk water). It must be mentioned at this point that several results in literature on hydrated proteins but also on confined water, mostly obtained by neutron scattering techniques and nuclear magnetic resonance (not shown here, see [Mallamace 2012] for review), which exhibit the crossover in the exact temperature region of the suggested SFC. The data on a dilute aqueous solution of glycerol (big X, [Murata 2012]) resemble the data of the β secondary relaxation of the mixture at low temperatures. The trace of this relaxation exhibit a crossover at lower temperatures than the region of the SFC. This is located at about $1000/T = 6$, near about the point where the β relaxation crosses the T_g of the system (not shown here). Let us now move on to the data on hydrated proteins. For the hydrated globular protein lysozyme, several dielectric data (not the actual data but only the trace) from [Khodadadi 2008] are shown by lines & triangles. For the dry lysozyme sample (open triangles) which contains only residual water, the main relaxation exhibits much higher relaxation times than the lysozyme sample with a water fraction of 0.28 g/g (solid triangles), the trace of which is similar to the thick grey line from [Ngai 2011] which has been

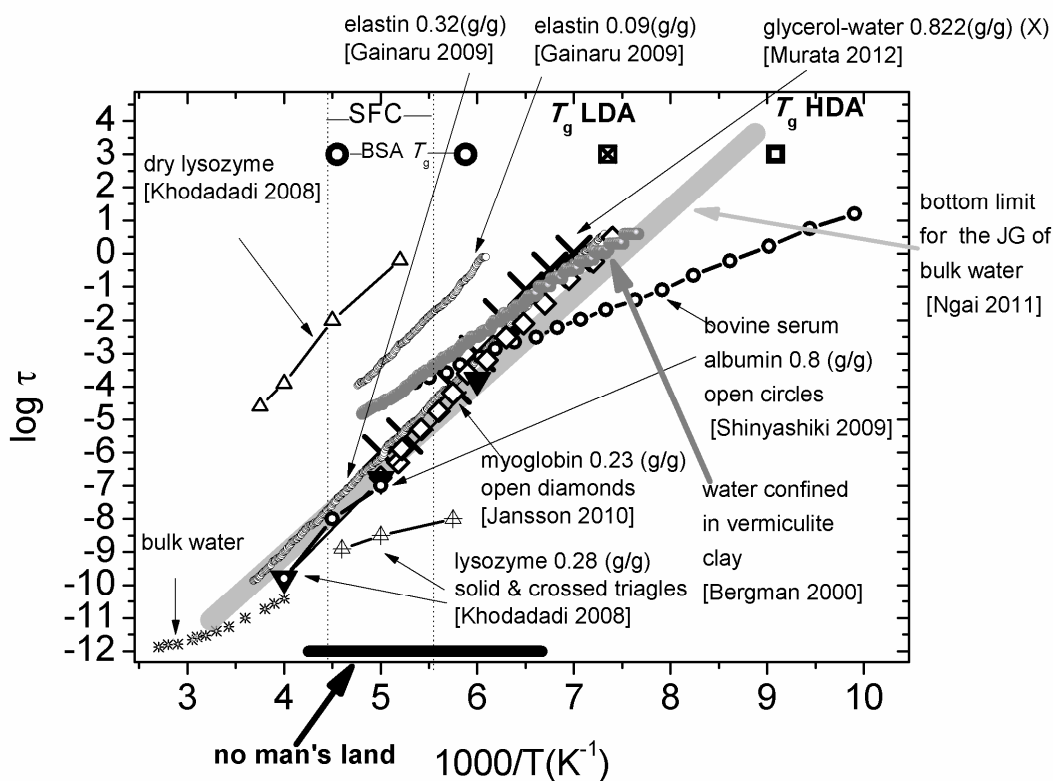


Fig. 2.3 Plots of the logarithm of relaxation times ($\log \tau$) versus reciprocal temperature for several hydrated systems from literature, including bulk water and water confined in vermiculite clay. The water fraction of the hydrated proteins and aqueous solutions are denoted on the diagram reported on the wet basis g/g, i.e. g of water per g of total hydrated mass. The temperature region of the reported strong to fragile crossover (SFC) from literature [Chen 2009] is highlighted in the plot by vertical dotted lines. The enthalpy relaxations of the LDA and HDA at ambient pressure, as well as for the glass transition of a bovine serum albumin (BSA) solution of water fraction 0.8 g/g [Kawai 2000] (range between open circles), having a relaxation time of $\tau=10^3$, are also added in the plot. In addition, the thick grey solid line represents the bottom limit for the relaxation times of bulk water according to [Ngai 2011].

suggested to be the bottom limit for the relaxation times of the ν relaxation of bulk water. The strong hydration dependence of the main relaxation in the case of lysozyme, in combination to the results from neutron scattering on the same relaxation, shows that the response includes protein contributions. A third dielectric relaxation is recorded for hydrated lysozyme (line & crossed triangles), which shows lower activation energy (lower slope in the Arrhenius plot), which is suggested to originate exclusively from hydration water [Khodadadi 2008]. Some dielectric results on the hydrated fibrous protein elastin are also shown in Fig. 2.3. The activation energy is similar to the one of the ν relaxation and a strong dependence on the hydration level is again obvious (compare elastin of 0.09 g/g to 0.32 g/g in Fig.2.3). The contribution of the protein to the main relaxation observed in hydrated elastin has been suggested in [Gainaru 2009]. Finally, the trace of the main relaxation due to uncrystallized water, which has been recorded for a dilute aqueous

solution of the globular protein bovine serum albumin (BSA) of water fraction 0.8 g/g in [Shinyashiki 2009], is represented as line & open circles in Fig. 2.3. The trace of the relaxation in the low temperature side is quite different than the one for the rest hydrated systems and it exhibits lower activation energy. On the other hand, in the high temperature side the trace is similar to the trace of the rest of the hydrated proteins. The discontinuity of the 2 traces (which have been obtained by different equipments covering different frequency ranges) is explained by a change in dynamics at the point where the glass transition of the hydrated system is approached. The corresponding T_g range is highlighted in the plot according to adiabatic calorimetry results in an aqueous BSA solution of the same concentration by [Kawai 2000]. This explanation is suggested for the secondary relaxation of water, or, in other words, the Johari Goldstein relaxation (ν relaxation) [Shinyashiki 2007, Capacioli 2011, Ngai 2011]. According to this scenario, the absence of a crossover in the case of hydrated elastin is attributed to the fact that the glass transition of the hydrated system is located at higher temperatures [Ngai 2011]. Nevertheless, this assumption is not unambiguous. It may also be seen that the SFC region is comparable to the T_g region of BSA solution in Fig. 2.3. Furthermore, the absence of a crossover is evident also in the data for hydrated lysozyme in Fig. 2.3, while other dielectric results on hydrated lysozyme (not shown here) exhibit such a crossover. By the above mentioned observations, it becomes clear that a detailed study on the dielectric processes in hydrated proteins in a wide range of frequencies and water compositions, could be useful to study the dynamic behavior of hydration water in more detail and possibly to clarify its connection to confined water.

Closing this section, a main observation should be stressed which derives from the numerous experimental results on supercooled water. There is a main problem regarding the state of water at very low temperatures in the supercooled state or under confinement. This problem can be described when comparing two different approaches from literature. The first one is the approach by F. Mallamace et.al [Mallamace 2007] to compare optical scattering data on deeply supercooled water (LDA) at low temperatures, water confined in MC41 nanotubes (2D confinement) in the no man's land, and liquid water at high temperatures. A continuous variation of distinct water populations proportionality was found, the latter classified as water molecules in the LDL phase and HDL phase (partially hydrogen bonded and non-hydrogen bonded). The intensity of LDL decreases with increasing temperature. This approach suggests that the confined water molecules in the no man's land resemble the evolution starting from LDA at low temperatures. On the other hand, in the recent scientific work by Murata and Tanaka [Murata 2012], a liquid-liquid genuine transition was recorded in a glycerol-water mixture. In the latter case, the liquid at low temperatures resembles more the structure of HDL, suggesting that glycerol molecules prevent crystallization and simultaneously induce pressure effects in water dynamics. The corresponding secondary relaxation is the one which is reported in Fig. 2.3, and exhibits similar temperature dependence of its relaxation time with other hydrated systems in Fig. 2.3. By this, it becomes clear that the use of different environments to form supercooled water should be explicitly studied having in mind the dynamical alterations induced, although complicated. The recent results on the pressure dependence of the T_g values of the LDA and HDA phases [Debenedetti 2012] makes the situation even more tricky. The difficulty is even more pronounced in the case of complex biological environments, such as

proteins, where the coexisting hydrophilic and hydrophobic domains induce the effects of hydrophilic/hydrophobic hydration.

2.3 Water in non polar confinement

Over the last 20 years the attention of many researchers has been driven to the dynamics of water in non polar, hydrophobic confinement. The aspect of water filling hydrophobic spaces, such as cavities, cylinders or plates, is a special issue, in the sense that normally it is expected that water molecules 'would prefer to go somewhere else'. The existence of confined water molecules inside hydrophobic protein cavities has been proposed initially by Saenger in 1987 [Saenger 1987]. This kind of water was described as 'internal' water and was suggested to be an integral part of the protein structure. The significance of this kind of water to biological function is of great interest.

A review regarding experimental results obtained by X-ray crystallography in comparison to results by molecular simulations, concerning studies of water confined in nanotubes [Hummer 2001], fullerenes and protein cavities [Collins 2005, 2007], is given by Rasaiah et.al [Rasaiah 2008]. It is found that water molecules confined to nonpolar pores and cavities of nanoscopic dimensions exhibit highly unusual properties. Water filling is strongly cooperative, with the possible coexistence of filled and empty states and sensitivity to small perturbations of the pore polarity and solvent conditions. Confined water molecules form tightly hydrogen-bonded wires or clusters. The weak attractions to the confining wall, combined with strong interactions between water molecules, permit exceptionally rapid water flow, exceeding expectations from macroscopic hydrodynamics by several orders of magnitude. The proton mobility along 1D water wires also substantially exceeds that in the bulk. Proteins appear to exploit these unusual properties of confined water in their biological function (e.g., to ensure rapid water flow in aquaporins or to gate proton flow in proton pumps and enzymes). The unusual properties of water in nonpolar confinement are also relevant to the design of novel nanofluidic and molecular separation devices or fuel cells [Rasaiah 2008]. Furthermore, the combination of inelastic neutron scattering experiments and molecular simulations provide information on the specific effects of hydrophobicity in the dynamics of water surrounding biomolecules. In particular, the results show changes in the plasticity of the hydrogen-bond network of hydration water molecules depending on the biomolecular site hydrophilicity. At -73°C (200 K), the measured low frequency density of states of hydration water molecules of hydrophilic peptides is remarkably similar to that of HDA, whereas, for hydrophobic biomolecules, it is comparable to that of LDA behavior. It is therefore suggested that the apparent local density of water is lower in a hydrophobic environment [Russo 2011].

3. Phase transitions in hydrated proteins

Proteins are flexible molecules

The pictures of protein structures that emerge from X-ray crystallography and NMR seem rigid and static. In reality, proteins are highly flexible. Because the forces that maintain the secondary and tertiary folds are weak, there is enough energy available at body temperature to break any particular interaction. When existing weak interactions are broken, the groups that are released can make new interactions of comparable energy. These rearrangements can occur on a time scale that is faster than the time required to determine the structure by tools such as X-ray crystallography. Thus, the three-dimensional structures of proteins determined by physical techniques are average structures. Protein motions can be classified in terms of their relationship to the average structure (Fig. 3.1 a). The fastest motions are atomic fluctuations such as interatomic vibrations and the rotations of methyl groups. Next come collective motions of bonded and non-bonded neighboring groups of atoms, such as the wig-wag motions of long side chains or the flip-flopping of short peptide loops. The slowest motions are large-scale, ligand-induced conformational changes of whole domains [Petsko 2004].

Whole folded domains never undergo large, thermally driven distortions at ordinary temperatures. Transitions from one type of folding motif to another are rarely seen except in pathological cases. An all alpha-helical protein will not normally refold to an all beta-sheet protein, except, for example, in the cases of amyloid and prion diseases. Smaller-scale refolding does occur in some proteins, however. Ligand binding may induce disordered polypeptide segments to become ordered. Ligands can also induce the disordering of a previously ordered strand, although this is less common. Association and dissociation of subunits can also be triggered by ligand binding, and the ligand can be as small as a proton if it changes the charge of a crucial residue [Petsko 2004].

At body temperature, the atoms in most protein molecules fluctuate around their average positions by up to an Ångstrom or occasionally even more, depending on their position in the protein (Fig. 3.1 b). In the tightly packed interior, atomic motions are restricted to less than an Ångstrom. The closer to the surface of the molecule, the greater the increase in mobility until, for surface groups that are not surrounded by other atoms, the mean fluctuation may be several Ångstroms. Proteins have been called “semi-liquid” because the movements of their atoms are larger than those found in solids such as NaCl, but smaller than those observed in a liquid like water. In a protein, the covalent structure of the polymer sets limits on the motions of atoms and groups of atoms. Chemical groups such as methyl groups or aromatic side chains display collective motions. Methyl groups rotate on a picosecond time-scale; aromatic rings, even those in the interior of the protein, flip at

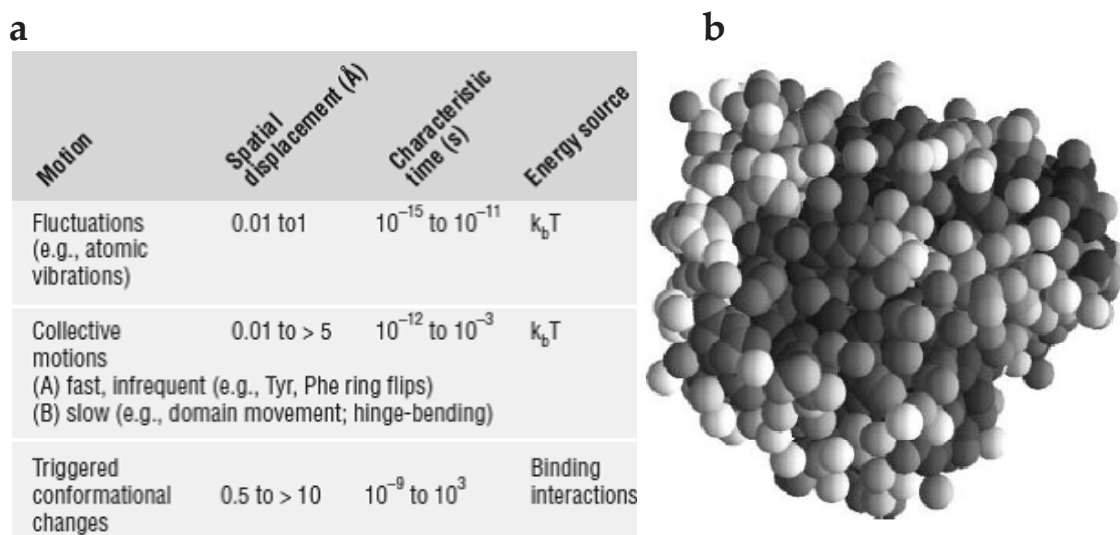


Fig. 3.1. **a**) Types of motion found in proteins (all values are approximate) **b**) Protein shaded according to flexibility. Space-filling model of sperm whale myoglobin in which each atom is shaded according to its average motion as determined by X-ray crystallography. The darker the atom, the more rigid it is. Note that the surface is not uniform in its flexibility. [Petsko 2004].

average rates of several thousand per second. The actual ring flip takes only about a picosecond, but it happens only about once every 109 picoseconds. Flipping an aromatic ring inside a protein, where the packing density is high, requires that surrounding atoms move out of the way. The probability that they will all move in the right direction at the same time is very low: hence the relatively long interval between flips. In the interior of proteins, close atomic packing couples the motions of non-bonded neighboring atoms. If a methyl group in the center of a protein is next to another methyl group, the motions of both will be correlated by virtue of their tendency to collide. Thus both the extent of motion of every group and its preferred directions depend on non-bonded as well as bonded contacts. Only for surface side chains and protruding loops are non-bonded interactions of little importance, and residues in such unrestrained positions are always the most flexible parts of a protein structure. At biological temperatures, some proteins alternate between well-defined, distinct conformations. In order for two conformational states to be distinct, there must be a free-energy barrier separating them. The motions involved to get from one state to the other are usually much more complex than the oscillation of atoms and groups about their average positions. It is often the case that only one of the alternative conformations of a protein is biologically active [Petsko 2004].

Of most importance for protein function are those motions that occur in response to the binding of another molecule. Ligand-induced conformational changes can be as modest as the rearrangement of a single side chain, or as complex as the movement of an entire domain. In all cases, the driving force is provided by ligand–protein interactions. Often, the motion enables some part of the structure to make contact with a ligand [Petsko 2004].

Current picture of water related phase transitions in hydrated proteins

The hydration properties of proteins and water and protein dynamics in protein-water mixtures have been studied in the past several decades by a variety of experimental techniques. The results indicated the significant influence of protein-water interactions on the structure, the dynamics and the biological function of proteins [Fenimore 2004, Grant 1978, Gregory 1995, Kuntz 1974, Ringe 2003, Rupley 1991]. A minimum amount of water is necessary for enzymatic activity of a protein and dielectric results indicated a correlation between the onset of enzymatic activity and of a percolation type displacement process of protons on single macromolecules [Rupley 1991].

Thermal and dynamic studies of fully hydrated proteins revealed the presence of a thermal glass transition in the temperature range from about -110 to -70°C (160-200 K), depending on the protein and the experimental technique employed [Fenimore 2004, Gregory 1995, Ringe 2003, Khodadadi 2010] and a dynamical transition. The latter is associated with an abrupt onset of atomic displacements on the microscopic length and time scale, usually probed by quasielastic neutron scattering in the range from about -75 to -35°C (200-230 K) [Doster 2010]. The mechanism of the dynamical transition, remains a subject of active discussions [Doster 2010, Khodadadi 2010]. The dynamical transition of proteins has been related to "the protein glass transition" and believed to be triggered by the coupling of the protein with the hydration water through hydrogen bonding, since protein hydration water shows a dynamic transition at a similar temperature [Mallamace 2011 and references therein]. On the other hand, several studies suggest that the glass transition should not be confused with the dynamical transition, mainly because they occur in different temperature regions [Khodadadi 2008, 2010].

Another phenomenon governing biological properties of proteins occurs at high temperatures, just below the onset of protein denaturation. A protein is in the native state up to a given temperature and evolves, on increasing T , into a region characterized by a reversible unfolding-folding process. This latter phenomenon depends on the chemical nature of the protein and the solvent. In the case of the water-lysozyme system such a phenomenon occurs in the temperature range from about 40 to 90°C (310–360K). Above 80°C, lysozyme denatures irreversibly. For such a system, calorimetric measurements [Salvetti 2002] show a broad peak in the specific heat around that temperature.

Both transitions occurring in hydrated proteins, i.e, the glass transition and denaturation, are strongly believed to be associated to the characteristic structural and dynamical properties of the hydrogen bond (HB) network in hydration water. Several theoretical approaches provide scenarios aiming to explain the coupled dynamics of protein and water in the hydration shell. The origin of the glass transition of globular hydrated proteins is not fully understood and it is believed to be highly connected to water dynamics. The obvious question raised by observation of a glass transition in protein dynamics is the following: *Is the transition due to a transition in the bulk solvent, the bound solvent, the protein alone, or some combination?* [Ringe2003]

Theoretical studies suggest that the glass transition is driven by the translational reorientation of the HB network on the protein surface [Tournier 2003], while some others also connect the water-protein glass transition to the denaturation of the globular proteins, suggesting that both correspond to energetic sub-states, while an energy criterion for the

onset of mobility of strong protein-water bonds is induced [Porter 2012]. The aim is to explain these phenomena on a molecular level with the idea to highlight the role of water around and inside the macromolecules.

Finally, a schematic presentation summarizing the dynamical features of hydrated proteins in an Arrhenius diagram (see chapter 4, section 4.3), as proposed in [Khodadadi 2008], may be seen in Fig. 3.2.

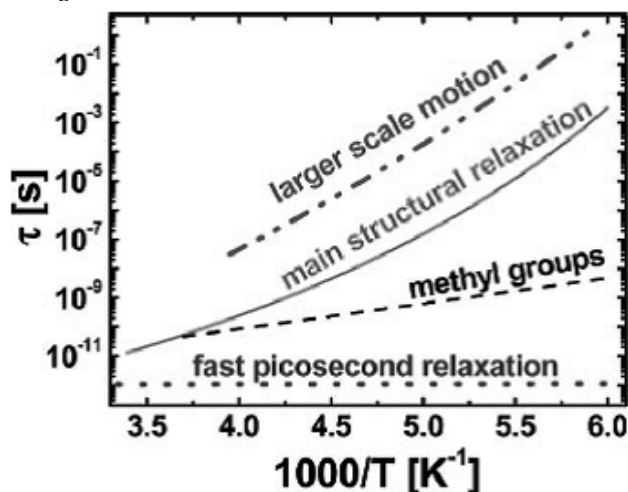


Fig. 3.2. Schematic presentation of the proposed main components in dynamics of hydrated protein and their temperature dependence [Khodadadi 2008]

In Fig. 3.2 the fast components of protein dynamics, i.e. the fast picosecond relaxation and the rotation of methyl groups, are suggested to be independent of hydration. The main structural relaxation is suggested to present cooperative motions of aminoacids between different conformational states strongly coupled to motions of hydration water. It has a slightly super-Arrhenius (see Arrhenius equation, eq. 4.14) temperature dependence and it is the main cause of the dynamical transition. It shows a strong dependence on hydration level [Khodadadi 2008]. At this point we should highlight the correspondence of this relaxation to the main relaxation of water which was described in chapter 2 (section 2.2). Finally, the slower relaxation is suggested to represent larger scale motions, e.g. kinds of hinge-bending or domain motions. It exhibits strong hydration dependence and its temperature dependence seems to follow the one of the main structural relaxation [Khodadadi 2008].

The protein glass transition has been also been described according to the theory of glass formers in general. This scenario involves the secondary β relaxation of water in the mixture (corresponding to the main relaxation in Fig. 3.2) and the main segmental α relaxation of the hydrated mixture (corresponding to the larger scale relaxation in Fig.2.3), which is responsible for the thermal glass transition observed. An analogy to hydrated proteins has been suggested in [Ngai 2008].

Finally, it is stressed that the microscopic mechanism that governs the protein glass transition is still not quite clear. In particular, when the transition is studied through calorimetric or rheological measurements, it is found that it is tricky to detect, it is exceptionally broad and, thus, covers a large temperature dependence [Jansson 2010]. The origin of this broadening has been suggested to be due to a large distribution of relaxation

Chapter 3. Phase transitions in hydrated proteins

times within the protein-water system [Sartor 1994] or even due to a size distribution of water clusters on the protein surface [Doster 1986].

Chapter 3. Phase transitions in hydrated proteins

4. Experimental Techniques

4.1 Water Equilibrium Sorption Isotherms (ESI)

Studies on isothermal hydration provide valuable information on the interactions of water molecules with the hydrated material at the molecular level. The sorption isotherm describes the thermodynamic relationship between water activity and the moisture content of a material in equilibrium and at constant temperature and pressure. The typical shape of an isotherm reflects the way in which water binds to the system.

The water sorption in polymers and biomaterials is a special case of the vapor sorption in amorphous solids in general. The sorption isotherms have been classified according to their shape and the associated vapor-solid interactions into 5 different types by Brunauer et al. [Brunauer 1940]. The Brunauer classification in the case of water sorption is seen in Fig. 4.1.

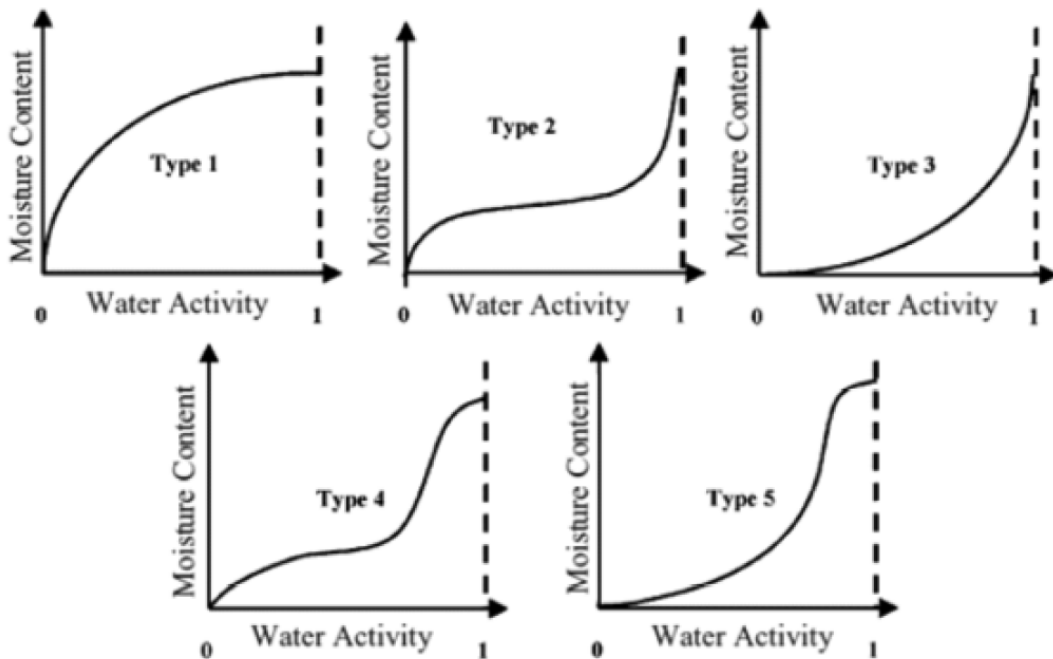


Fig. 4.1 Classification of water sorption isotherms [Mathlouthi 2003]

The isotherm of Type 1 presents a characteristic increase of moisture content approaching a maximum value and describes the sorption process in microporous materials according to the Langmuir theory. According to this theory all the available sorption sites are identical and the sorption takes places exclusively in a monolayer. The isotherms of Types 2 and 3 take into account the existence of multiple sorption layers and strong or weak interactions between the adsorbed molecules and the components of the host material. The isotherms of Types 4 and 5 describe monolayer and multilayer sorption, respectively, accompanied by capillary condensation processes.

A widely accepted mathematical model to describe sigmoidal shaped, multilayer water sorption isotherms is the Brunauer-Emmet-Teller (BET) equation [Brunauer 1938]

$$\frac{h}{h_m} = \frac{ca_w}{(1-a_w)[1+(c-1)a_w]} \quad (4.1)$$

where, h is the water content (g of water per g of dry mass), α_w is the water activity (relative humidity, rh), h_m is the water content corresponding to water molecules in the first sorption layer and c is a parameter associated to the total free energy in the hydrated system. The BET equation is associated to the isotherms of Types 2 and 3 in Fig. 4.1. In addition to describing water sorption isotherms in the case of multilayer hydration, it is often used for the determination of specific surface areas. Typically, the BET equation is valid at low α_w values and, particularly, in the range of $\alpha_w < 0.4$ [Zhang 2000].

In order to extend the validity of the BET equation in a more broad range of water activities, the Guggenheim-Anderson-de Boer (GAB) equation [Timmermann 1989] was proposed:

$$\frac{h}{h_m} = \frac{cfa_w}{(1-fa_w)[1+(c-1)fa_w]} \quad (4.2)$$

In this equation h_m is the water content corresponding to water molecules directly attached to sorption sites (primary hydration sites, first sorption layer), whereas c and f are parameters related to the energy difference between water molecules in the first sorption layer and in the second and higher sorption layers, and between water molecules in the second and higher sorption layers and bulk water, respectively. The validity of the GAB equation may be extended up to α_w values as high as 0.9 and more modifications of the latter have been proposed [Blahovec 2007]. The water sorption isotherms of polymers, biopolymers and food materials are usually well described by the GAB model.

An isotherm can be typically divided into three regions, as it may be seen in Fig. 4.2. The water in region A represents strongly bound water, and the enthalpy of vaporization is considerably higher than the one of pure water. The bound water includes structural water (H-bonded water) and monolayer water, which is sorbed by the hydrophilic and polar groups. Bound water is unfreezable and it is not available for chemical reactions. In region B, water molecules bind less firmly than in the first zone. The vaporization enthalpy is slightly higher than the one of pure water. This class of constituent water can be looked upon as the continuous transition from bound to free water. The properties of water in region C are similar to those of the free water that is held in voids, large capillaries, crevices. An apparent

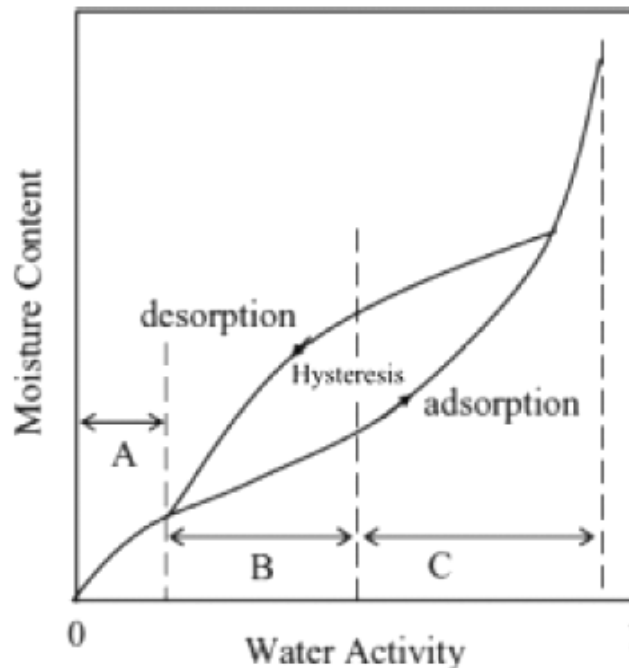


Fig. 4.2 Sorption isotherm showing a hysteresis [Andrade 2011]

deviation from the initial linear behavior in region B is observed by entering region C. This departure from the initial linear trend is typical for hydrophilic materials such as hydrogels and is explained in terms of clustering of water molecules [Pandis 2011]. Moreover, hysteresis is related to the nature and state of the components of the material, reflecting their potential for structural and conformational rearrangements, which alters the accessibility of energetically favorable polar sites [Andrade 2011]. The hysteresis may be also related to swelling/deswelling of materials exhibiting high degrees of elasticity [Lee 2013].

Analysis of sorption data

The analysis of the water sorption data in this thesis has been made according to the GAB equation (eq. (4.2)).

4.1.1 Experimental Instruments

ESI measurements in this thesis were performed in the Physics Department of the National Technical University of Athens (NTUA).

For water ESI measurements solid samples were used, prepared by compressing an amount of powder ~100 mg to a cylindrical pellet of thickness 0.6-0.8 mm and diameter about 14 mm. ESI measurements were performed at room temperature by exposing the samples to various controlled water vapor atmospheres in sealed jars above saturated aqueous salt solutions [Greenspan 1977]. By this way, the water activity α_w (relative humidity, rh) was systematically varied between about 0.02 and 0.98. The attainment of equilibrium and final weights were determined via continuous monitoring of sample weight using a Bosch SAE 200 balance with 10^{-4} g sensitivity. The sorption and desorption

procedures took place successively. The above mentioned procedure was followed in the case of the studied systems lysozyme, BSA, elastin and casein peptone. In the case of collagen and HA, ESI measurements were performed at $T=25^{\circ}\text{C}$, in controlled nitrogen atmosphere, using a TA Instruments VTI-SA-plus Analyser. The dry mass of the samples was obtained by drying at $T=40^{\circ}\text{C}$ and 60°C , for HA and collagen, respectively. The HA sample was a solid hydrogel piece of an approximate dry mass of 5mg (instead of a compressed pellet). The water activity a_w (relative humidity) was systematically varied between 0.05 and 0.95 in a step of 0.05. The resulting error in the determination of water content was less than ± 0.001 .

4. 2 Differential Scanning Calorimetry (DSC)

Differential Scanning Calorimetry (DSC) is a thermal analysis (TA) technique, conventionally employed for studying thermal transitions of materials [Hatakeyama 1994]. The quantity measured by this technique is the energy needed so that the temperature of the sample studied, T_s , is maintained comparable to the one of an inert reference material, T_r , while the two samples are either heated or cooled at a constant rate, or their temperature is controlled isothermally.

There are two main types of DSC experimental instruments/modes: i) power compensated and ii) heat flux. In the power compensated mode, T_s and T_r are controlled independently, by two distinct furnaces. The power supply of each furnace is controlled separately, so that $T_s=T_r$, and determines the heat flow of the system. In the heat flux mode, the measured sample and the reference are sufficiently thermally contacted through a metallic disc and are surrounded by a common furnace. The enthalpy and heat capacity changes which take place in the studied sample result in an alteration of T_s with respect to T_r . This temperature difference, ΔT , is measured and the heat flow is calculated according to the known values of thermal resistance. In fact, a heat flux DSC is the commercially used DTA (Differential Thermal Analyser) [Hatakeyama 1994]. Typical DSC thermograms may be seen in Fig. 4.3, where the glass transition, crystallization and melting, if present, are recorded as a heat capacity step, an exothermic and an endothermic peak, respectively. It may be seen in Fig. 4.3 that the recorded transitions depend strongly on the thermal history of the sample.

Analysis of melting and crystallization peaks

From the crystallization and melting peaks the characteristic temperatures T_c and T_m may be estimated. At the same time, the crystallization and melting enthalpies, ΔH_c and ΔH_m , respectively, may be calculated by the peak area. The crystallinity (X_c) of a polymer, is calculated via:

$$\chi_c = \frac{\Delta H}{\Delta H_{100\%}} \quad (4.3)$$

where ΔH and $\Delta H_{100\%}$ are the measured enthalpy of melting of the sample and the enthalpy of melting of a 100% pure crystalline sample of the same polymer.

Bound water content

Owing to the effect of water on the performance of commercial polymers and the crucial role played by water-polymer interactions in biological processes, hydrated polymer systems are widely investigated. In the presence of excess water a polymer may become swollen, exhibiting large changes in mechanical and chemical properties. Water can plasticize the polymer matrix or form stable bridges through hydrogen bonding, resulting in an anti-plasticizing effect. The behavior of water may vary in the presence of a polymer, depending on the degree of chemical or physical association between the water and polymer phases. Water whose melting/crystallization temperature and enthalpy of melting/crystallization are not significantly different from those of normal (bulk) water is called freezing water. Those water species exhibiting large differences in transition enthalpies and temperatures, or those for which no phase transition can be observed calorimetrically, are referred to as bound water. It is frequently impossible to observe crystallization exotherms or melting endotherms for water fractions very closely associated with the polymer matrix. These water species are called non-freezable. Less closely associated water species do exhibit melting/crystallization peaks, but often considerable super-cooling is observed and the area of the peaks on both the heating and cooling cycles are significantly smaller than those of freezing water (see above). These water fractions are referred to as freezing-bound water. The sum of the freezing-bound and non-freezing water fractions is the bound water fraction. These different water species are illustrated in Fig. 4.4 which presents the DSC crystallization curves for water sorbed on poly(4-hydroxystyrene). The water content is given by the mass of water in the polymer divided by the dry mass of the sample, expressed in units of g/g. At the lowest water content no exothermic peak is observed. All of the water in the polymer at this water concentration is non-freezing water. At a higher water content a freezing exotherm is observed at 225 K which is located at significantly lower temperature than the one for bulk water. This peak is due to freezing-bound water in the system. At even higher water content 2 crystallization peaks are present, one in the low temperature side and one at a higher temperature, exhibiting a maximum which is comparable to the one of the crystallization peak of bulk water. In this case the two peaks correspond to water populations of different connectivity. At the highest water content a large exotherm is observed comparable to that of bulk water. This exotherm is ascribed to the crystallization of the freezing water in the hydrated polymer. In addition, in some cases crystallization of water during heating may occur (cold crystallization).

There is not a clearly settled definition for bound water throughout literature, whereas water that does not crystallize neither during cooling nor during heating might consist of more than one contribution [Miyazaki 2000]. Usually, a safe way to define bound water is to assume that this refers to the water molecules which remain uncrystallized during both cooling and heating for DSC measurements at certain cooling and heating rates. The term uncrystallized water (UCW) is by this way straightforward. The fraction of uncrystallized water in the hydrated material may be calculated by the fraction of total amount of crystallized water which is given by the enthalpy of melting and the melting enthalpy of bulk water (333 J/g)[Dean 1999].

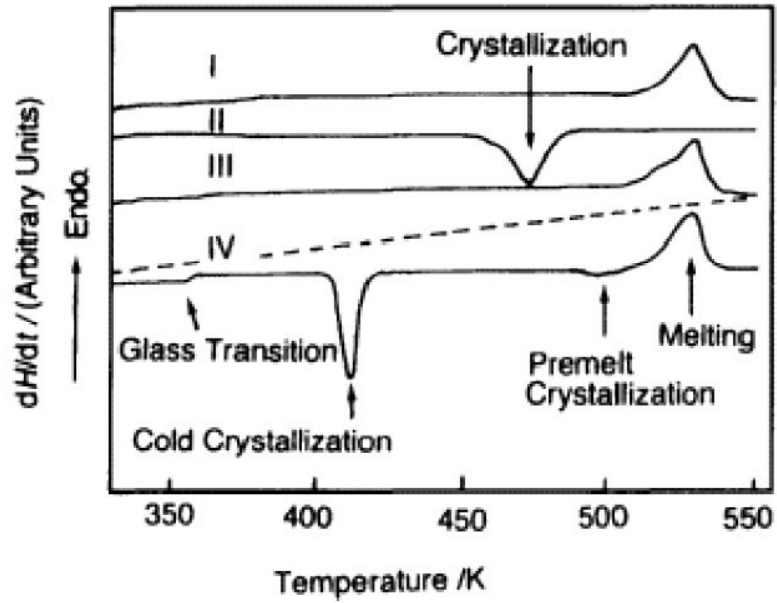


Fig. 4.3 DSC curves of poly(ethylene terephthalate): (I) heated after storage at RT, (II) cooled at 10K/min, (III) heated at 10K/min and (IV) heated at 10K/min following quenching [Hatakeyama 1994]

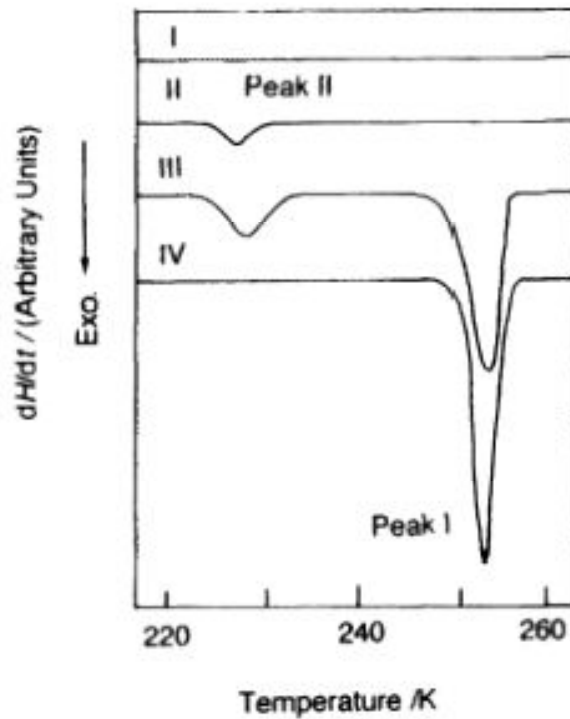


Fig 4.4 DSC crystallization curves of water sorbed on poly(4-hydroxystyrene): (I) WT = 0.079 g/g (II) WT = 0.107 g/g (III) WT = 0.263 g/g; (IV) pure water [Hatakeyama 1994]

Glass Transition Temperature Calculation

Due to the fact that the glass transition is recorded as a heat capacity step, the estimation of the glass transition temperature, T_g , is not straightforward. For that reason, several conventions are made regarding the methodology of calculation. A widely used convention is the so called 'Half C_p Extrapolated' method of calculation (or the midpoint of ΔC_p step). An example of the latter may be seen in Fig. 4.5. The glass transition temperature, T_g , is defined as the temperature at which the change in heat capacity, ΔC_p , equals the half of the total. The total ΔC_p is defined as the extrapolation of the crossing points of the tangents of the experimental curve at temperatures lower and higher than the T_g , where linear regions dominate, with the tangent at the inflection point, to the y axis. In addition, the extrapolation of the crossing points to the x axis, denote the onset (T_{onset}) and end (T_{end}) temperatures of the transition. The T_g is defined by the extrapolation of the experimental point, where the change in heat capacity is $\Delta C_p/2$.

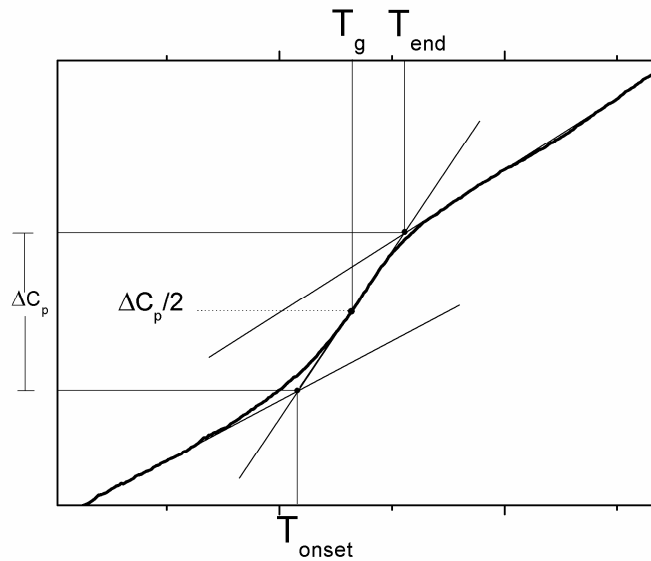


Fig. 4.5 Calculation of the glass transition temperature, T_g , in a DSC thermogram, according to the Half C_p Extrapolated method

4.2.1 Experimental Instruments

DSC measurements in this thesis were performed at three different DSC instruments. A Mettler Toledo 823e calorimeter in the Center of Biomaterials of the Polytechnical University of Valencia (UPV) was employed to perform measurements on the hydrated proteins BSA and lysozyme, in the temperature range $-150 \leq T \leq 40^\circ\text{C}$. A Pyris DSC 6 calorimeter in the Physics Department of the National Technical University of Athens (NTUA), was employed to perform measurements on hydrated collagen, HA and casein

peptone, in the temperature range of $-120 \leq T \leq 40^\circ\text{C}$, or in some cases up to 230°C . A TA Q200 series DSC instrument in the Physics Department of NTUA was employed to perform measurements on hydrated elastin in the temperature range $-120 \leq T \leq 120^\circ\text{C}$, or in some cases up to 200°C . All of the above mentioned experiments were performed in nitrogen atmosphere, on samples between 5 and 15 mg, sealed in aluminum pans. In the case of hydrated elastin the solid samples were encapsulated in Tzero hermetic aluminium pans, and so the water loss during the measurement was eliminated. Finally, standard cooling and heating rates of $10^\circ\text{C}/\text{min}$ were used in all cases.

4.3 Dielectric Relaxation Spectroscopy (DRS)

Dielectric relaxation spectroscopy (DRS) is used in order to measure the complex dielectric function (known also as dielectric permittivity and dielectric constant), $\varepsilon^* = \varepsilon'(\omega) - i\varepsilon''(\omega)$, in a broad frequency range (10^{-5} - 10^{12} Hz). The dielectric properties of a material give information on the molecular mobility, as they are defined by the fluctuations of the dipole moments attached on the molecules.

The complex dielectric function connects the external electrical field, $E(t)$, of an angular frequency, ω , which is applied to a material, to the response of the material, i.e. polarization, $P(t)$. If a stationary periodic disturbance $E(t)(\omega) = E_0 \exp(-i \omega t)$ is applied to the system, it is given [Kremer 2002] that:

$$P(t)(\omega) = \varepsilon_0 (\varepsilon^*(\omega) - 1) E(t)(\omega) \quad (4.4)$$

where $\varepsilon^*(\omega)$ is the dielectric function ($\varepsilon^*(\omega) = \varepsilon'(\omega) - i\varepsilon''(\omega)$). The real part of the dielectric function, $\varepsilon'(\omega)$, is proportional to the energy stored reversibly in the system and the imaginary part, $\varepsilon''(\omega)$, is proportional to the energy which is dissipated per period. The complex dielectric function $\varepsilon^*(\omega)$ in its dependence on angular frequency $\omega = 2\pi f$ (f frequency of the external electrical field) and temperature originates from different processes (Fig. 4.6): (i) displacement of the electron density relative to the nucleus it surrounds (electronic polarization), (ii) displacement of atoms or ions (atomic polarization), (iii) microscopic fluctuations of molecular dipoles (rotational diffusion) and (iv) the propagation of mobile charge carriers (translational diffusion of electrons, holes or ions). In addition, the accumulation of charges at interfaces gives rise to an additional polarization. The latter can take place at inner dielectric boundary layers (Maxwell-Wagner-Sillars-polarization) on a mesoscopic scale and/or at the external electrodes contacting the sample (electrode polarization) on a macroscopic scale [Kremer 2002]. In the frequency domain of Dielectric Spectroscopy it may be assumed that atomic and electronic polarization follow instantly the applied electric field and so they are not observed.

In order to study the molecular mobility and relaxation it is essential to define a relaxation function $\Phi(t)$, or auto correlation function [Kremer 2002]:

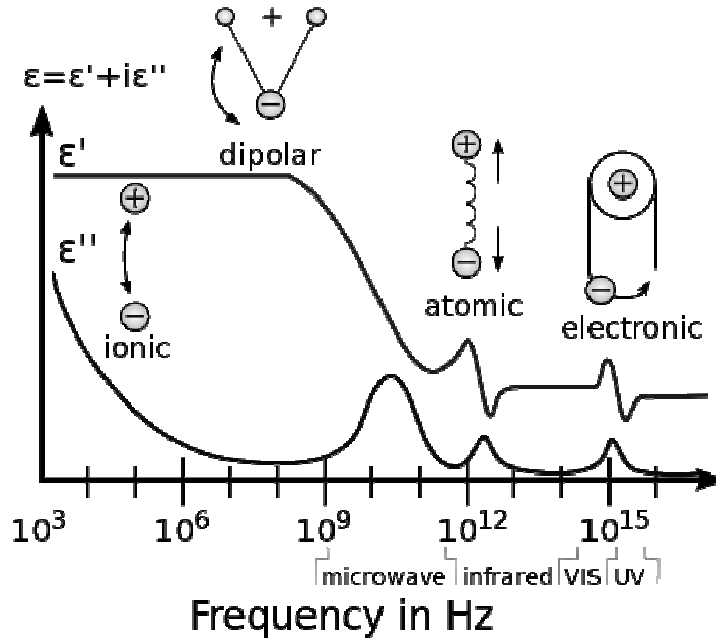


Fig. 4. 6 Types of polarization in the frequency domain

$$\Phi(t) = \frac{\langle \Delta P(t) \Delta P(0) \rangle}{\langle \Delta P^2 \rangle} \quad (4.5)$$

where t denotes the time variable. The relaxation function describes the evolution of the auto correlation of the polarization value $P(t)$ to equilibrium after the application of a disturbing electrical field, at the given time $t=0$. The complex dielectric function is related to $\Phi(t)$ (where electronic and atomic polarization are excluded) according to the equation [Fragiadakis 2006]:

$$\frac{\epsilon^*(\omega) - \epsilon_\infty}{\epsilon_s - \epsilon_\infty} = 1 - i\omega \int_0^\infty \Phi(t) e^{i\omega t} dt \quad (4.6)$$

where ϵ_s is the static dielectric constant and ϵ_∞ the real part of the dielectric function at extremely high frequencies, i.e. including only contributions due to atomic and electronic polarization. The real and imaginary part of the dielectric function are related to each other through the Kramers-Kronig relations [Böttcher 1978]:

$$\epsilon'(\omega) - \epsilon_\infty = \frac{2}{\pi} \int_0^\infty \frac{u \epsilon''(u)}{u^2 - \omega^2} du \quad (4.7)$$

$$\epsilon''(\omega) = -\frac{2\omega}{\pi} \int_0^\infty \frac{\epsilon'(u) - \epsilon_\infty}{u^2 - \omega^2} du \quad (4.8)$$

Because the real and imaginary part of the dielectric function include the same information, frequently the analysis of the dielectric spectra is focused on the imaginary part, $\epsilon''(\omega)$, where, usually, the dielectric relaxations may be observed more clearly.

Analysis of Dielectric Spectra by model functions

Assuming a relaxation function as a simple exponential distribution with a relaxation time , τ , $\Phi(t)=\exp(-t/\tau)$, the dielectric function is related to the angular frequency through the relation:

$$\varepsilon^*(\omega) = \varepsilon_\infty + \frac{\varepsilon_s - \varepsilon_\infty}{1+i\omega\tau} = \varepsilon_\infty + \frac{\Delta\varepsilon}{1+i\omega\tau} \quad (4.9)$$

known as the Debye equation. The quantity $\Delta\varepsilon$ is called dielectric strength of the relaxation and corresponds to the contribution of the relaxation to the static dielectric constant. The real and imaginary part of the dielectric function versus frequency, according to the Debye equation, are plotted in Fig. 4.7 as dashed lines. The imaginary part shows a dielectric loss peak, exhibiting a maximum at $f_{\max}=1/(2\pi\tau)$, while the real part is represented by a step of a corresponding height $\Delta\varepsilon$, around the same frequency. The area beneath the dielectric loss peak is related to the dielectric strength, $\Delta\varepsilon$, via:

$$\Delta\varepsilon = \frac{2}{\pi} \int_{-\infty}^{+\infty} \varepsilon''(\omega) d(\ln \omega) \quad (4.10)$$

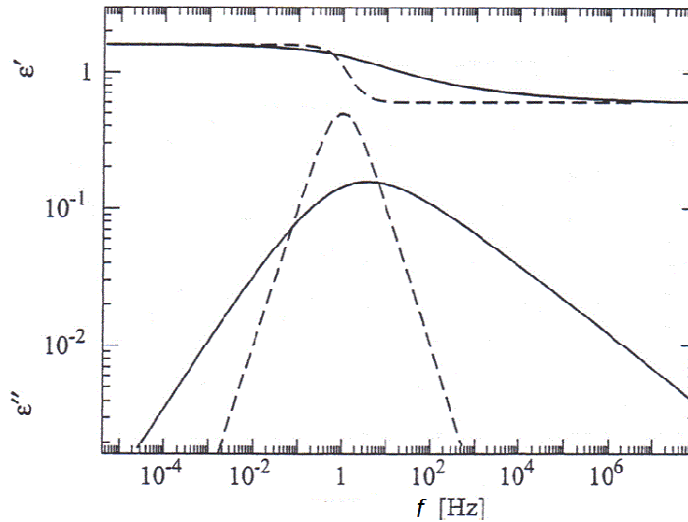


Fig. 4. 7 Real, ε' , and imaginary, ε'' , part of the dielectric function versus frequency, f , for a Debye dielectric relaxation (dashed line) and a relaxation expressed by the Havriliak-Negami equation (solid line)

In most of the experimental cases, the observed dielectric loss peaks are broader than the Debye peak and usually obtain a non-symmetric shape. There are several empirical equations, mostly generalized forms of the Debye equation, which describe the broadening and/or asymmetry of the peak. The most frequently used are the Cole-Cole equation [Cole 1941]:

$$\varepsilon^*(\omega) = \varepsilon_\infty + \frac{\Delta\varepsilon}{1 + (i\omega\tau)^\beta} \quad (4.11)$$

and the Cole-Davidson equation [Davidson 1951]. A combination of the two above mentioned equations is the Havriliak-Negami equation [Havriliak 1966]:

$$\varepsilon^*(\omega) = \varepsilon_\infty + \frac{\Delta\varepsilon}{[1 + (i\omega\tau_{HN})^\beta]^\alpha} \quad (4.12)$$

The parameters α, β , describe the asymmetric and symmetric broadening of the peak, respectively, while it holds $\alpha\beta \leq 1$. The Debye, Cole-Cole, and Cole-Davidson equations are derived out of eq. (4.12) for $\alpha=\beta=1$, $\alpha=1$ and $\beta=1$, respectively.

Finally, apart from contributions due to the fluctuation of dipoles, conductivity contributions due to the translational motion of free current carriers are also present in the dielectric response. In the case of dc conductivity, σ_0 , the latter does not contribute to ε' , and an additional contribution to the losses is expressed as:

$$\varepsilon''(\omega) = \frac{\sigma_0}{\varepsilon_0\omega} \quad (4.13)$$

The dielectric loss spectra for a given dielectric material may include several contributions and the total dielectric response may be expressed through a sum of the contributions. By the analysis, several parameters are derived for each contribution, such as the relaxation time, τ , the dielectric strength, $\Delta\varepsilon$, and the shape parameters of the respective equation employed, as a function of temperature T . Usually the data obtained for the relaxation time, τ , are represented in an Arrhenius diagram, which is obtained by plotting the logarithm of the relaxation time, $\log(\tau)$, versus the inverse temperature (usually $1000/T(K^{-1})$). The equations which are usually used in order to describe the temperature dependence of the relaxation time are the Arrhenius equation:

$$\tau(T) = \tau_0 \exp\left(\frac{E_{act}}{kT}\right) \quad (4.14)$$

where τ_0 is a preexponential factor and E_{act} the activation energy of the relaxation, and the Vogel-Tammann-Fulcher (VTF) equation [Vogel 1921]:

$$\tau(T) = \tau_0 \exp\left(\frac{B}{T - T_0}\right) \quad (4.15)$$

where τ_0, B are temperature independent parameters and T_0 is the Vogel temperature, i.e. the temperature where the τ becomes infinite.

The Arrhenius equation describes secondary relaxations of local character, while the VTF equation describes relaxations of cooperative nature, such as the α relaxation which is associated with segmental dynamics in glass forming systems.

4.3.1 Experimental Instruments

The DRS measurements in this thesis were performed using a Novocontrol Alpha Analyzer in combination with a Novocontrol Quatro Cryosystem, in the Physics Department of the National Technical University of Athens. For DRS measurements the complex dielectric function, $\varepsilon^*(f) = \varepsilon'(f) - i\varepsilon''(f)$, was determined as a function of frequency, f , (10^{-1} - 10^6 Hz) at constant temperature (-150 to 30°C, controlled to better than ± 0.1 K). For measurements, the solid samples were placed between two electrodes forming a cylindrical capacitor 12 mm in diameter. The solutions was placed between electrodes 20 mm in diameter kept apart by silica spacers 50 μm in thickness. Our electrode configurations include no insulating electrodes aiming at recording the net dielectric response of the system under study.

4. 4 Thermally Stimulated Depolarization Currents (TSDC)

TSDC is a dielectric technique in the temperature domain, which corresponds to measuring dielectric loss as a function of temperature at a fixed low frequency in the range 10^{-4} - 10^{-2} Hz (equivalent frequency) [Turnhout 1980]. By this technique the sample is inserted between the plates of a capacitor and polarized by the application of an electric field E_p at temperature T_p for time t_p , which is large compared to the relaxation time of the dielectric relaxation under investigation. With the electric field still applied, the sample is cooled to a temperature T_0 , which is sufficiently low to prevent depolarization by thermal energy, and then is short-circuited and reheated at a constant rate b . The discharge current generated during heating is measured as a function of temperature with a sensitive electrometer. The technique is characterized by high sensitivity and high resolving power [Turnhout 1980]. A normal TSDC measurement is analogous to a DRS measurement at constant frequency. The equivalent frequency is estimated as $f_{\text{eq}} = 10^{-2}$ - 10^{-3} Hz. We refer to references [Turnhout 1980] & [Vanderschueren 1979] for a detailed presentation of the technique.

4.4.1 Experimental Instruments

TSDC measurements in this thesis were carried out using a Keithley 617 electrometer in combination with a Novocontrol sample cell for TSDC measurements, in the Physics Department of NTUA, in the temperature range from -150 to 20 °C. Typical experimental conditions were -20 °C and 0°C for T_p , 1 kV/cm for E_p , 5 min for t_p , 10 °C/min for the cooling rate to $T_0 = -150$ °C, and 3 °C/min for the heating rate b .

Only global TSDC thermograms were obtained in the framework of this thesis.

5. Globular Protein BSA

5.1 Introduction

Bovine Albumin Serum (BSA) is a globular protein and belongs to the family of serum albumins. Serum albumin is the most abundant plasma protein in mammals. Plasma, is the straw-colored/pale-yellow liquid component of blood that normally holds the blood cells in suspension. The main biological role of albumin is to regulate the colloid osmotic pressure of blood. The human serum albumin includes three subunits, resulting in a heart-shaped structure [He 1992]. BSA is the serum albumin found in cows. Two of its main characteristics are the high amount of α helices and the high stability of its structure in a broad range of salt and protein concentration in solution [Zhang 2007]. It is widely studied as a model protein system.

5.2 Materials and sample preparation

Albumin from bovine serum (BSA) in form of lyophilized powder (Sigma 3294) was purchased from Sigma – Aldrich (Mr~66.000) and used as received. Water with 10 μ S/cm conductivity was employed for preparation of solutions for DSC and for dielectric measurements.

DSC, TSDC and DRS measurements, to be described in the following, were performed at various levels of water content h , calculated on the dry and the wet basis, h_d and h_w , respectively, by

$$h_d = \frac{m_{water}}{m_{dry}} \quad (5.1)$$

$$h_w = \frac{m_{water}}{m} \quad (5.2)$$

In these equations m is the mass of the hydrated protein sample, m_{dry} the mass of the dry sample and $m_{water} = m - m_{dry}$ the mass of water inside the sample. The dry mass m_{dry} was determined by drying the protein sample in vacuum for 72 h at room temperature (RT). The term *water content* is used for h_d , while the term *water fraction* is used for h_w .

They are related to each other by:

$$h_d = \frac{h_w}{1 - h_w} \quad (5.3)$$

For water ESI measurements solid samples were used, prepared by compressing an amount of protein powder ~100 mg to a cylindrical pellet of thickness 0.6-0.8 mm and diameter about 14 mm. ESI measurements were performed at RT by exposing the samples to various controlled water vapor atmospheres in sealed jars above saturated aqueous salt solutions [Greenspan 1977]. By this way, the water activity a_w (relative humidity, rh) was systematically varied between about 0.02 and 0.98. The attainment of equilibrium and final weights were determined via continuous monitoring of sample weight using a Bosch SAE 200 balance with 10^{-4} g sensitivity (see also chapter 4, section 4.1, 4.1.1).

For DSC measurements BSA powder was dried in vacuum for 72h to remove traces of humidity. 30% wt aqueous solution of BSA was prepared by dissolving a specified quantity into water. The solution was placed into open aluminum pans (40 μ l) at room ambient for different times to obtain several water contents. After that, the pans with hydrated protein were sealed. DSC measurements were performed in a Mettler Toledo 823e calorimeter on samples between 5 and 15 mg. The hydrated protein samples were cooled down from 25°C to -150°C followed by a heating scan up to 40°C, both at 10°C/min (see also chapter 4, section 4.2, 4.2.1).

Samples for dielectric (TSDC and DRS) measurements were either in the form of solution (for high water fractions, h_w higher than 0.36, corresponding to $h_a=0.56$) or in the form of solid compressed pellets, similar to those used for ESI measurements (for low water fractions, h_w equal to or lower than 0.36). For solutions, BSA was dissolved in water and, for homogenization of the samples, the mixtures were kept at 4°C for at least two days before the measurement. Solid samples were hydrated to the required degree by equilibration for more than 3 days (to constant weight) above saturated salt solutions in sealed jars (similar to ESI measurements), or above open water in sealed jars (100% rh) for a selected period of time and a subsequent equilibration in sealed boxes for at least 2 days. For dielectric measurements, the solid samples were placed between two electrodes forming a cylindrical capacitor 12mm in diameter. The solutions were placed between electrodes 20mm in diameter kept apart by silica spacers 50 μ m in thickness (see also chapter 4, sections 4.3, 4.3.1 and 4.4, 4.4.1).

5.3 BSA-ESI Measurements

The hydration of BSA was recorded by water equilibrium sorption-desorption (ESI) measurements at RT. Figure 5.1a shows the water content h , calculated on the dry basis (g of water per g of dry protein) versus water activity a_w , during sorption and desorption.

As seen in Fig. 5.1a, an initial linear region for water activity up to 0.8 is observed, followed by a departure from linear behavior for $a_w > 0.8$, which is explained in terms of clustering of water molecules (see chapter 4, section 4.1). The desorption data are in good agreement to the sorption data. The GAB equation (eq. (4.2), see chapter 4, section 4.1) was fitted to the experimental data as it can be seen in Fig. 5.1b. The GAB fit is satisfactory (see the solid line in Fig. 5.1b).

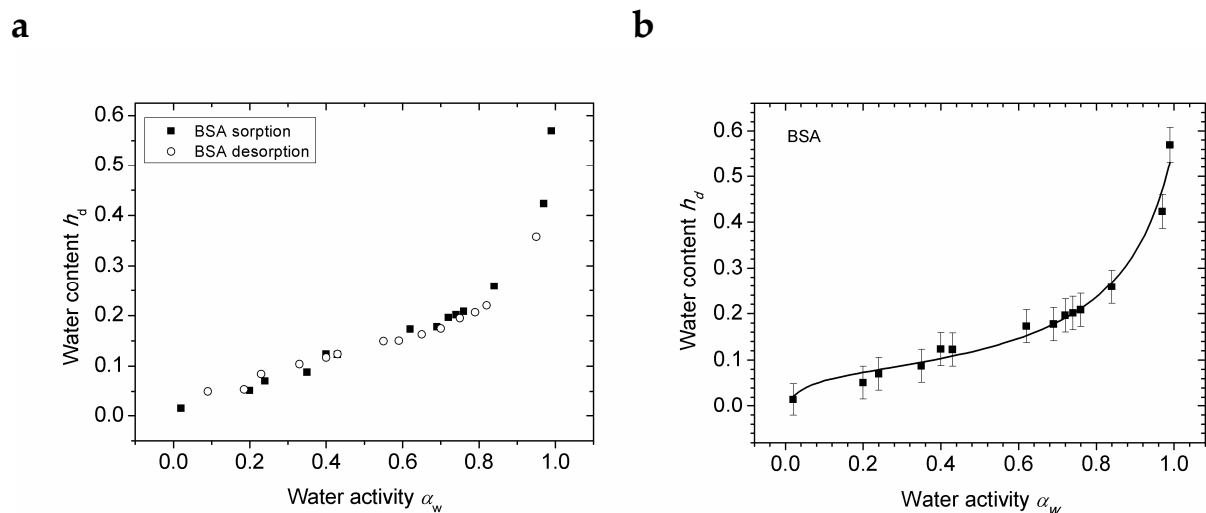


Fig. 5.1 a) Water content h_d against water activity α_w at 25 °C for a BSA sample, during sorption (•) and desorption (◦) **b)** Water content h_d against water activity α_w at 25 °C for a BSA sample. Points are experimental data and the solid line is the fit of GAB equation (eq. (4.2)) to the data.

For the parameter h_m , which corresponds to the content of water molecules attached to primary sorption sites (first sorption layer), a value of 0.073 was obtained for BSA. Another critical water content is estimated by the data, although less unequivocal, namely the water content where significant clustering occurs and the sorption data deviate strongly from the roughly linear behavior in the middle region of water activities. That is at around $h_d=0.25$ (equal to $h_w=0.2$), corresponding to water activities around 0.8. Measurements at smaller α_w steps in this region and analysis in terms of the clustering function [Pandis 2011] are necessary to determine more accurately that critical water content and to study clustering of water. Nevertheless, this value is consistent with the reported value of water content at which water starts to condensate onto weakly interacting unfilled patches of the protein surface, in case of globular proteins [Careri 1998].

5.4 BSA-DSC Results

DSC cooling and heating scans, both at a rate of 10°C /min, were recorded for BSA-water mixtures at various hydration levels. The water fraction values h_w of all the samples measured, along with the corresponding water content values h_d , are listed in Table 5.1 for reference.

Table 5.1 Water fractions h_w and corresponding water contents h_d for BSA samples measured by DSC

h_w	0	0.07	0.10	0.14	0.17	0.18	0.21	0.22	0.23	0.26	0.28	0.30	0.32	0.34	0.35	0.43	0.67
h_d	0	0.75	0.11	0.16	0.20	0.23	0.27	0.28	0.30	0.35	0.38	0.42	0.47	0.52	0.54	0.76	1.99

Cooling and heating thermograms recorded on several BSA-water mixtures, characterized by water fraction h_w , are shown in Figures 5.2a and 5.2 b, respectively. The scale of Fig. 5.2 allows us to observe clearly the crystallization and melting peaks of water. The first water fraction h_w in which crystallization is observed on cooling is 0.30, while melting on heating is first observed for $h_w=0.21$ (traces of melting that cannot be appreciated

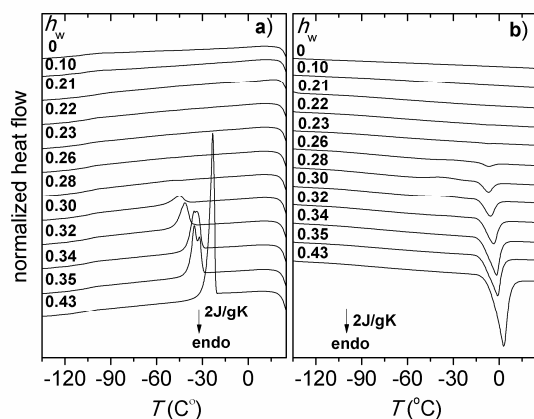


Fig. 5.2 Normalized heat flow during cooling (a) and heating (b), both at $10^\circ\text{C}/\text{min}$, in BSA-water mixtures at different water fractions h_w indicated on the plot

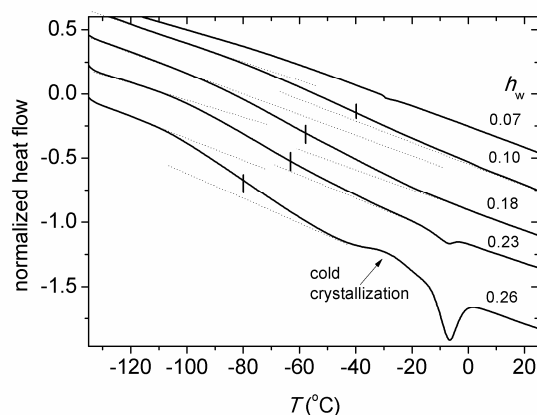


Fig. 5.3 A magnification in the area of the glass transition during heating scan, for characteristic BSA-water mixtures of water fractions h_w indicated on the plot. T_g values calculated as the midpoint of the heat flow step are highlighted by vertical marks.

with the scale of Fig. 5.2 but the melting enthalpy has been listed in Table 5.2 (see below), a clear melting peak is first observed at $h_w=0.26$). The crystallization peaks in Fig. 5.2a seem to consist of more than one contribution, which is more clear for water fractions $h_w=0.34$ and 0.35 . For these two samples it is also obvious that the relative proportion of these contributions differs for varying water fractions.

In the heating thermograms in Fig. 5.2b we also observe a broad glass transition step for most of the samples, as well as a cold crystallization exothermic peak above the glass transition, for water fractions that exhibit no crystallization of water during cooling. A magnification of the thermograms during heating for five characteristic water fractions, $h_w=0.07$, 0.10 , 0.18 , 0.23 and 0.26 , is shown in Fig. 5.3. For $h_w=0.10$ and 0.18 , only the glass transition can be seen, as a heat capacity step. No glass transition is observable for the lower water fractions studied, that is for $h_w=0.07$ and the dry sample (Fig. 5.2b). For $h_w=0.23$ and 0.26 , the glass transition is followed by a cold crystallization peak of water and a subsequent melting peak, the former being more clear in case of $h_w=0.26$.

The crystallization and melting temperatures of water in the mixtures, determined by the cooling and heating peak temperatures, T_c and T_m , respectively, as well as the glass transition temperature, T_g , calculated as the midpoint of the heat capacity step in the heating thermograms (see chapter 4, section 4.2), are plotted in Fig. 5.4 against water fraction h_w , for all samples studied. T_c increases significantly with increasing water fraction, from a value of approximately -55°C for low water fractions until values close to zero for high water fractions. T_m increases in general with increasing water fraction from -10°C to 0°C . In more detail, we can identify in Fig. 5.4 three distinct water fraction regions, with respect to the h_w dependence of T_m . Within the first region, $0.21 < h_w < 0.30$, which is in fact the cold crystallization region and is highlighted in the plot by two vertical dotted lines, the melting temperature seems to remain stable at about -10°C , suggesting that the size of water crystals in this area is more or less unique [Mathot 1994]. For higher water fractions, T_m increases

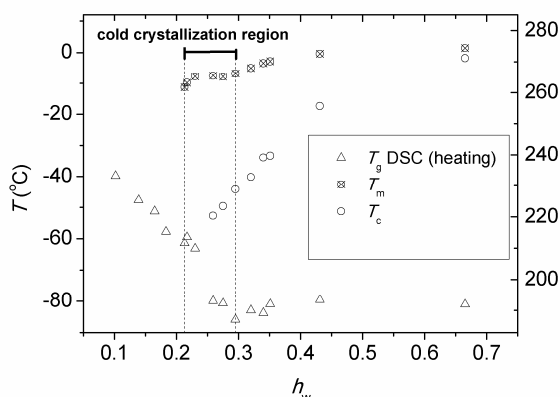


Fig. 5.4 Characteristic temperatures calculated from DSC thermograms for BSA mixtures: glass transition temperature, T_g , melting temperature, T_m , and crystallization temperature, T_c , are represented against water fraction h_w . Vertical dotted lines highlight the cold crystallization water fraction region.

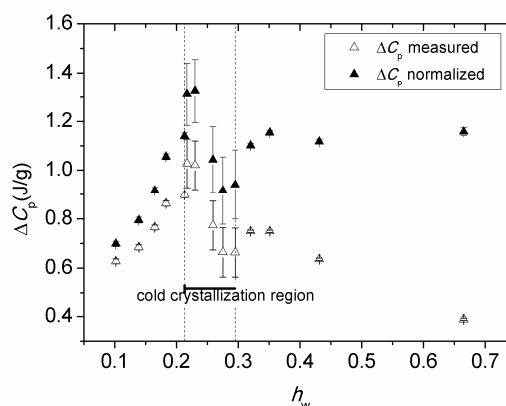


Fig. 5.5 Heat capacity step, ΔC_p , of the glass transition of BSA-mixtures against water fraction h_w . The normalized values of ΔC_p with respect to the fraction of protein mass in the samples are added to the diagram

from a value of -10°C to temperatures close to zero for a water fraction $h_w=0.43$ (second region), where it finally stabilizes (third region).

T_g was detected for water fractions equal to or higher than $h_w=0.10$ (see Fig. 5.3), while no glass transition was detectable for lower water fractions or the dry sample. In Fig. 5.4, it is shown that T_g decreases systematically with increasing water fraction, from a value of approximately -40°C to a value of about -85°C , at the onset water fraction for crystallization during cooling ($h_w \sim 0.3$). Further addition of water causes no further decrease of T_g that stabilizes at about -80°C . The heat capacity step, ΔC_p , of this glass transition is plotted in Fig. 5.5 against water fraction h_w . Assuming that the corresponding glass transition arises from the cooperative motion of protein chains plasticized by water molecules [Miyazaki 2000, Panagopoulou 2011a], we employ a normalization of ΔC_p to the fraction of protein in the samples [Stathopoulos 2011]. These normalized values are added in Fig. 5.5. We observe that the normalized ΔC_p increases systematically with water fraction, until the cold crystallization region is reached. This can be attributed to the increase in the number of configurations available to the polymer chains in the mixtures with water molecules suggesting that protein chains move more intensively interacting with water molecules, or that more chains contribute to the dynamics being accessible to water. Further addition of water causes a significant reduction of the heat capacity step within the cold crystallization region and then stabilization for $h_w>0.3$ occurs. This is consistent with the hypothesis that no more water contributes to the plasticization of the T_g for hydration levels at which water crystallizes either during cooling or heating. This fact will be verified later on, where it will be shown that the fraction of uncrystallized water does not increase further after crystallization effects set in. Additionally, the reduction of the heat capacity step in the cold crystallization region reflects also the reduction of the number of configurations available to the polymer chains probably due to the formation of initial water crystal nuclei during cooling. It must be mentioned at this point that the values calculated for the T_g and

the heat capacity step in the cold crystallization region are rather tentative, due to the fact that cold crystallization peaks interfering in the region of the glass transition make the tangents obtained as baselines less reliable. Nevertheless, the monotonic reduction of the values is systematic enough.

From the cooling and melting enthalpies, calculated from the area under the corresponding peaks, and the melting enthalpy of bulk water (333.55 J/g [Dean 1999]), the content of crystallized water for the corresponding thermal history can be obtained (see also chapter 4, section 4.1). In this work the content of crystallized water of each mixture $h_{d,cw}$ (dry basis) has been obtained from the melting thermograms as the ratio of the melting enthalpy ΔH_m of that mixture (Table 5.2) and the melting enthalpy of bulk water. Table 5.2 lists $h_{d,cw}$ together with the content of uncrystallized water, $h_{d,ucw}$, given by the difference $h_d - h_{d,cw}$.

Table 5.2 Results of DSC measurements, water fraction h_w (wet basis) and water content h_d (dry basis), melting enthalpy of water ΔH_m , water contents of crystallized ($h_{d,cw}$) and uncrystallized water ($h_{d,ucw}$), fractions of crystallized (X_{cw}) and uncrystallized water (X_{ucw}), and number of water molecules per BSA molecule total (n), crystallized (n_{cw}) and uncrystallized (n_{ucw})

h_w	h_d	ΔH_m (J/gr)	$h_{d,cw}$	$h_{d,ucw}$	X_{cw}	X_{ucw}	n	n_{cw}	n_{ucw}
0.18	0.23	0	0	0.225	0	1	825	0	825
0.21	0.27	-0.17	0.001	0.270	0.002	0.998	993	2	991
0.22	0.28	-0.34	0.001	0.276	0.005	0.995	1015	5	1010
0.23	0.30	-0.66	0.002	0.297	0.009	0.991	1096	10	1086
0.26	0.35	-3.27	0.013	0.337	0.038	0.962	1283	49	1234
0.28	0.38	-8.49	0.045	0.334	0.092	0.908	1390	129	1261
0.30	0.42	-14.36	0.061	0.358	0.146	0.854	1536	224	1312
0.32	0.47	-24.23	0.106	0.365	0.226	0.774	1726	390	1336
0.34	0.52	-34.4	0.156	0.360	0.303	0.697	1891	573	1318
0.35	0.54	-37.34	0.173	0.369	0.318	0.682	1987	632	1355
0.43	0.76	-65.33	0.344	0.413	0.454	0.546	2775	1260	1515
0.67	1.99	-150.7	1.348	0.639	0.678	0.322	7283	4938	2345

Often such results are discussed in terms of the fractions of crystallized and uncrystallized water, X_{cw} and X_{ucw} , respectively ($X_{cw}+X_{ucw}=1$), which are also listed in Table 5.2. The water contents $h_{d,cw}$ and $h_{d,ucw}$ are plotted in Fig. 5.6a as functions of the (total) water content h_d . The striking result in Fig. 5.6a is that $h_{d,ucw}$ is not constant, but increases significantly with increasing water content, initially more steeply in the cold crystallization region of water contents, and then more smoothly but systematically for higher water contents, in the water content region where water crystallizes during cooling. This fact suggests a reorganization of the structure of water at each new hydration level. On the other hand, if the amount of non freezable water is examined in terms of weight fraction in the hydrated protein system as a whole, then it can be seen in Fig. 5.6b that it remains stable and equal to about 0.25 within the cold crystallization region and to about 0.21 for higher water fractions (at least within the range of our measurements). It must be mentioned at this point,

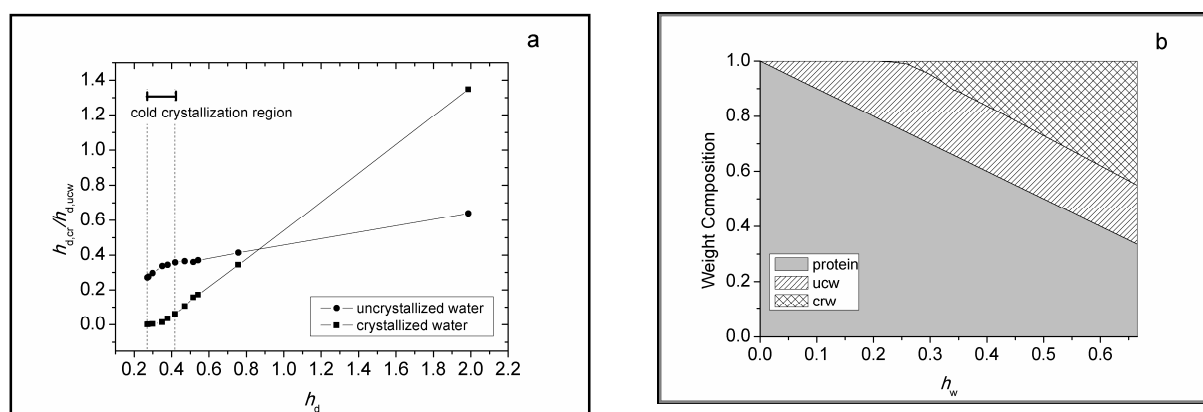


Fig. 5.6 a) Water contents of crystallized and uncrystallized water, $h_{d,cw}$ and $h_{d,ucw}$, respectively, against (total) water content h_d of the BSA-water mixtures and **b)** composition diagram for the BSA-water mixtures, showing the fractions of dry protein, crystallized and uncrystallized water in the mixture, against water fraction h_w .

that the amount of uncrystallized water of Table 5.2 and Fig. 5.6 corresponds to water that remains in the uncrystallized phase throughout the whole measurement and does not crystallize neither during cooling nor heating (both at the rate of $10^\circ\text{C}/\text{min}$).

5.5 BSA-Dielectric Measurements

5.5.1 BSA-TSDC

Figure 5.7 shows TSDC thermograms in the temperature range from -150 to 0°C for several BSA-water mixtures, including solutions (numbers 1-4) and hydrated solid pellets (numbers 5-15). For the sake of clarity, four of the thermograms are replotted in the inset to Fig. 5.7. The TSDC thermograms have been normalized to the same thickness (polarizing field) and the same surface area of the samples. Thus, results for different compositions can be compared to each other not only with respect to the temperature position of the peaks (time scale of the corresponding relaxations), but also with respect to their magnitude (dielectric strength of the corresponding relaxations).

Starting at low water fractions and low temperatures, a broad peak is observed in the solid pellets, already for the practically dry sample (sample 15 at about -110°C , Fig. 5.7), which shifts to lower temperatures with increasing water fraction (located at about -130°C for sample 9) and increases in magnitude. In agreement with previous work on proteins [Anagnostopoulou-Konsta 1987, Pissis 1989] and other biopolymers [Pissis 1991], this peak is attributed to a local, secondary relaxation of small polar groups of the biopolymer, plasticized by water. For low water fractions, that is for $h_w < 0.13$ (samples 10-15), this peak is very broad and an unequivocal assignment of a temperature maximum is not possible. This region of hydration levels corresponds to the water content region of $h_d < 0.15$, where water interacts principally with polar protein surface groups and/or charged groups for lower water contents ($h_d < 0.07$) [Careri 1998]. A fluctuation in the size and arrangement of water clusters in that case [Careri 1998] is consistent with a distribution of relaxation times and a broad peak. At higher water fractions, it is likely that additional contributions, probably due

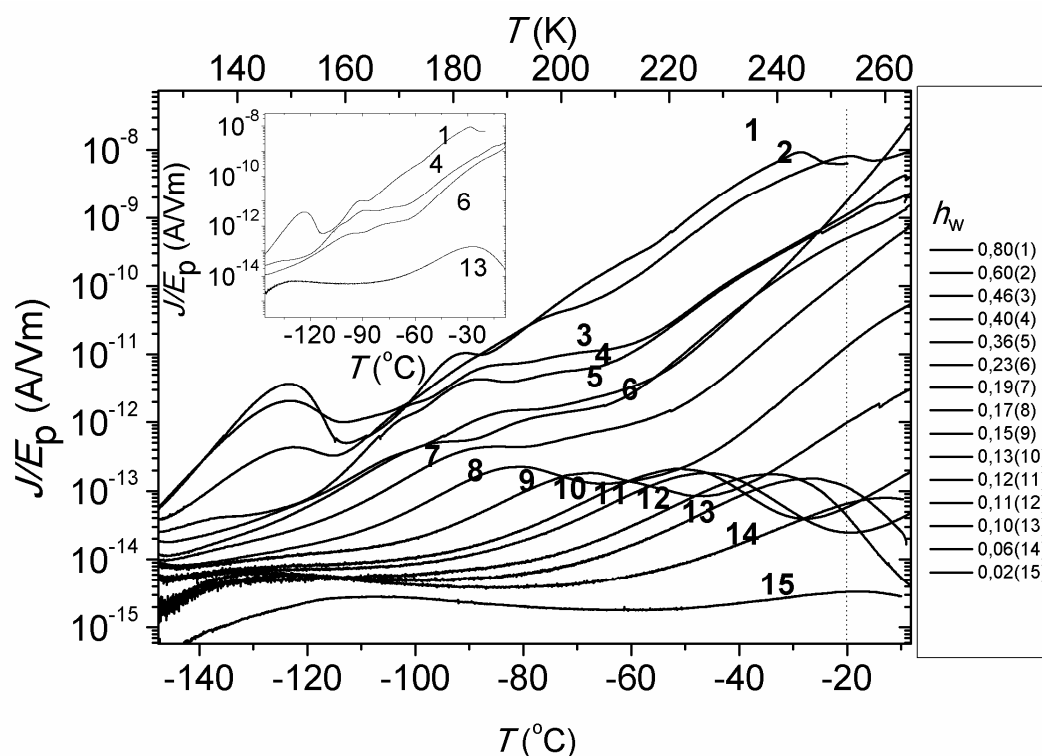


Fig. 5.7 Normalized TSDC thermograms (density of depolarization current divided by polarizing electric field, J/E_p) against temperature T for the BSA-water solutions (samples 1-4) and the hydrated solid pellets (samples 5-15), of water fractions h_w indicated on the plot. The vertical line at -20°C indicates the polarization temperature T_p . The inset shows four of these thermograms for the samples 1, 4, 6 and 13.

to water either in the uncrystallized or in the crystallised phase, are interfering in the low temperature side of the diagram, overlapping the observed peak in question, as seen by the superlinear increase in magnitude for that region.

At low water fractions and high temperatures a peak is observed in Fig. 5.7 (at about -30°C for sample 13 and about -80°C for sample 8), shifting significantly to lower temperatures and increasing in magnitude with increasing water fraction (please note the logarithmic scale). On the basis of this strong plasticization by water and the stabilization of the temperature position of the peak at about -90°C for higher water fractions (see below), i.e. in the range of reported values of T_g in fully hydrated proteins [Gregory 2003, Ringe 2003, Fenimore 2004, Khodadadi 2010], and also because the position of this peak is in the range of the T_g obtained by the DSC results in section 5.4, the peak is attributed to the α relaxation associated to the glass transition of the hydrated protein. This assignment is less clear for the samples 14 and 15 with water fractions h_w lower than about 0.07. For these compositions the peak is located at higher temperatures than the polarization temperature T_p , so that interpretation of the peak is ambiguous [Turnhout 1980]. At this point, we recall that the glass transition was not observable by DSC for water fractions lower than $h_w=0.07$. For samples 6 and 7, the α peak ceases to be unique and is followed by an additional contribution at higher temperatures (peaks at about -95°C and -75°C , respectively, for sample 6 in the inset). Given that these samples are in a hydration range near the cold crystallization region according to the DSC results (section 5.4) and, consequently, accepting

that they were not crystallized during cooling (cooling rates identical for both DSC and TSDC), we assume that a microphase separation occurs in the samples causing the appearance of an additional α relaxation peak. A possible scenario is that, for hydration levels h_w near about 0.2, i.e. the critical water content for significant clustering according to ESI measurements (see section 5.1), some domains of the protein become accessible to water due to swelling of the protein [Kyritsis 1995], and therefore keep on being plasticized in the same manner as for lower water fractions, while in other domains the advanced level of water clustering and the possible creation of initial nuclei of water crystals result in reduced number of water molecules being involved in the macromolecular motions and, thus, in a smaller degree of protein plasticization [Salmeron-Sanchez 2002]. These assumptions are ambiguous, mainly because a splitting of the glass transition is not observable in DSC for the corresponding water fractions. The broadness of the glass transition in DSC along with the high sensitivity and high peak resolving power of TSDC, however, can explain this difference.

At higher water fractions the TSDC response in Fig. 5.7 increases significantly, in particular at higher temperatures, where conductivity and interfacial and space charge polarizations are expected to make significant contributions [Anagnostopoulou-Konsta 1987, Pissis 1989,1991]. The high values of conductivity do not allow unambiguous assignment of the individual TSDC peaks in the temperature region above about -80°C to specific processes. Measurements using insulating thin foils between the sample and the electrodes and special peak resolving TSDC techniques [Turnhout 1980, Pissis 1991], could shed more light on this point. In what follows the focus is on dipolar relaxations observed at lower temperatures. Several relaxations contribute to the TSDC response at higher water fractions and temperatures lower than about -80°C , giving rise to complex, overlapping peaks. In the three solutions with the highest water fractions, samples 1, 2 and 3 in Fig. 5.7 with $h_w=0.80$, 0.60 and 0.46, respectively, a strong peak is observed at about -125°C . Based on previous work with TSDC measurements on various forms of polycrystalline ice (pure ice [Pissis 1981], ice microcrystals dispersed in oil [Pissis 1982] and frozen aqueous saccharide solutions [Daoukaki-Diamanti 1984]), the peak is attributed to relaxation in bulk ice. Finally, the peaks observed at higher temperatures, at about -100°C and -90°C for the solutions (samples 1,3,4, for sample 2 there is not a clear peak discerned) are identified as the α peaks, which seem to become stabilized at these temperatures for the compositions where a part of water crystallizes during cooling. We recall that a splitting of the α peak was observed already at lower water fractions. The peak temperatures of the α peaks and of the peak attributed to relaxation in ice crystals are plotted in Fig. 5.8 as functions of the water fraction h_w . The temperature of the TSDC α peak in glass forming materials is considered as a good measure of the calorimetric glass transition temperature T_g , mainly because of the similar time scales of DSC and TSDC [Turnhout 1980, Pissis 1991], so we employ T_g for T_α in Fig. 5.8. Particularly, for samples where a double α peak was observable during heating (see above), we employ $T_{g,2}$ for the additional peak, so finally we employ $T_{g,1}$ for the main α peak observed by TSDC.

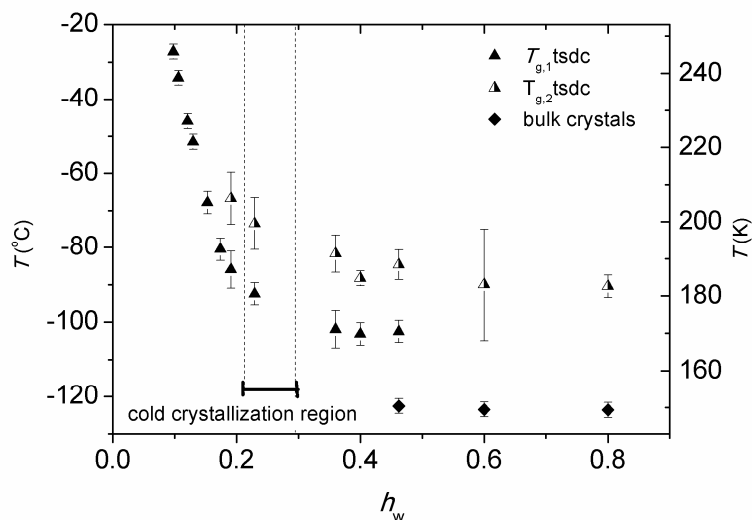


Fig. 5.8 Characteristic temperatures calculated by TSDC data for BSA mixtures, for glass transition temperature, $T_{g,1}$ and $T_{g,2}$ and relaxation peaks due to bulk ice crystals against water fraction h_w . Vertical dotted lines highlight the cold crystallization region.

5.5.2 BSA-DRS

DRS measurements provide the possibility to vary both frequency and temperature over wide ranges (in the present work 10^{-1} - 10^6 Hz and -150 to 20°C , respectively) and so to analyze dynamics in more details than by TSDC. In order to use DRS data to identify processes in the samples in comparison to TSDC and facilitate discussion on their origin, isochronal (constant frequency) presentation of the data is very convenient [Kremer 2002]. In Fig. 5.9b isochronal plots of the dielectric loss against temperature, $\epsilon''(T)$, are presented for the dry sample and BSA-water mixtures of $h_w=0.02, 0.07, 0.13, 0.18, 0.4$ and 0.6 , while the TSDC plots for samples with practically the same hydration levels (at least for most of the samples), samples 15, 13, 10, 8, 4 and 2 from Fig. 5.7, respectively, are shown in Fig. 5.9a. To facilitate comparison with TSDC data, a low frequency, 0.2 Hz, has been selected out of the frequency range of DRS measurements which were carried out isothermally. We recall that the equivalent frequency of TSDC measurements is in the range 10^{-4} - 10^{-2} Hz and we point out that the lower equivalent frequency of TSDC shifts the peaks to lower temperatures (see chapter 4, section 4.4). Starting with the sample of $h_w=0.020$, the broad relaxation which was previously attributed to a relaxation of side polar groups of the protein plasticized by water (TSDC), is observed by DRS at about -75°C . For the next three solid pellets, in terms of increasing water fraction, namely DRS samples with $h_w=0.07, 0.13$ and 0.18 , the dielectric dispersions consist of two contributions in quite good accordance to TSDC data. At low temperatures, we observe the relaxation of small polar groups of the protein, which is plasticized by water (at about -100°C for the sample of $h_w=0.07$). At higher temperatures, the α peak is observed, although masked by conductivity at the high temperature side, plasticized by water. At this point it is obvious that conductivity contributions in TSDC may be suppressed, presumably because the steps of applying the stimulus and of recording the response, i.e. polarization and depolarization step, are separated from each other, as it was

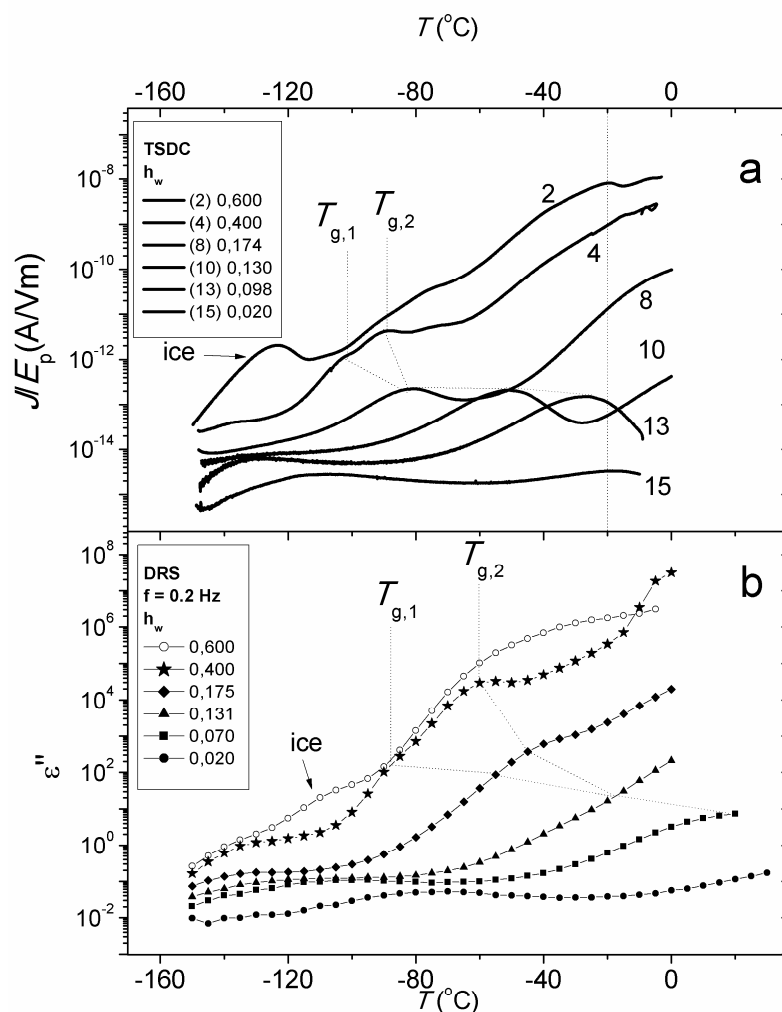


Fig. 5.9 Comparative TSDC thermograms and isochronal plots of dielectric loss, for compressed BSA-pellets and solutions, at the water fractions h_w indicated on the plot. **a)** Normalized TSDC thermograms (density of depolarization current divided by polarizing electric field, J/E_p , against temperature T) for the BSA-water solutions (samples 2,4) and the hydrated solid pellets (samples 8,10,13,15), of water fractions h_w . **b)** isochronal plots of dielectric loss at the frequency of $f=0.2$ Hz for the BSA-water samples of water fractions h_w indicated on the plot.

described in section 4.4. For the solution of $h_w=0.40$ we observe three relaxation processes, instead of two in case of solid pellets. These are, with respect to the TSDC thermogram of the same water fraction, the relaxation of small polar groups which is plasticized by water at about -130°C and two α relaxations associated to the glass transition, which are denoted as $T_{g,1}$ at about -90°C and $T_{g,2}$ at about -60°C . Finally, regarding the sample of the highest water fraction in this diagram, $h_w=0.60$, we observe all three relaxations mentioned for the sample of $h_w=0.40$, though more vaguely for temperatures higher than about -70°C , due to high conductivity contributions, plus an additional peak at about -110°C due to bulk ice crystals. This good agreement between the data by DRS and TSDC suggests that the same mechanisms are at the origin of the peaks measured by the two techniques.

DRS Raw Data

Figure 5.10 shows dielectric loss versus frequency, $\epsilon''(f)$, isothermal data, for the dry BSA pellet, at selected temperatures indicated on the plot. As it can be seen, the dielectric response is very low for this sample, and we present it separately, so that information is not eliminated due to scaling, when represented in comparative diagrams with the rest of the hydrated samples. Two relaxation processes can be detected within the experimental temperature range. At low temperatures, a broad peak enters the experimental window, centred at about 0.5 and 1 kHz at -140 and -90°C, respectively. At higher temperatures, a symmetric peak enters the experimental window at -60°C, centred at about 1, 20 and 200 Hz at -40, -20 and 0°C respectively.

The frequency dependence of the real and imaginary part of the dielectric function, ϵ^* , measured at $T=-15^\circ\text{C}$ is shown in Fig. 5.11, for several samples of different hydration levels. At this temperature a relaxation peak (α relaxation), which is associated with the glass transition of the hydrated protein, is within the experimental window for most of the samples, as is indicated by the main step in the $\epsilon'(f)$ plots (Fig. 5.11a) and the low frequency peak in the $\epsilon''(f)$ plots (Fig. 5.11b). Looking at the dielectric loss curves in Fig. 5.11b we observe that the α relaxation peak is absent for the sample of $h_w=0.02$. The low intensity peak which is within the experimental window, centered at about 800 Hz for the sample of $h_w=0.02$, corresponds to a relaxation of small polar groups of the protein triggered by water, as it will be shown later. For $h_w=0.07$ the maximum of the α peak is not observable and is probably located at lower frequencies (measurements at higher temperatures reveal the existence of the α relaxation peak). The α peak is observable in Fig. 5.11b for $h_w=0.13$ as a shoulder, while its maximum is clearly visible for $h_w=0.18$. Although conductivity contribution is large at this relatively high temperature, rough estimations of the peak position (based also on the corresponding $\epsilon'(f)$ plots) are highlighted in Fig. 5.11b by arrows.

Dielectric permittivity versus frequency, $\epsilon'(f)$, and dielectric loss versus frequency, $\epsilon''(f)$, isothermal data at temperature $T=-90^\circ\text{C}$, are plotted in Fig. 5.12a and 5.12b, respectively, for several samples of different hydration levels (samples of Fig. 11). In Fig. 5.12a we observe that the measured dielectric permittivity increases with increasing water fraction, in the whole frequency range measured, up to $h_w=0.28$, whereas for $h_w=0.40$ it drops to lower values at the high frequency part of the spectrum and then increases again for $h_w=0.60$. In addition, the $\epsilon'(f)$ plots show that for $h_w>0.18$ the dielectric permittivity increases remarkably at low frequencies implying the activation of strong polarization processes at that water fraction range. Dielectric loss spectra shown in Fig. 5.12b reveal the existence of a relaxation process which depends strongly on the hydration level. More specifically, the sample of $h_w=0.02$ exhibits a relaxation peak at the low frequency side of the experimental window, the maximum of which is not clearly detectable, as it is probably located at lower frequencies. For the sample of $h_w=0.07$ a broad relaxation peak is observed centered at about 30 Hz. This peak corresponds to a relaxation of small polar groups of the protein which is triggered by water in the hydration shell and is shifted with respect to the peak for the sample of $h_w=0.02$ (plasticized by water). The plasticization of the underlying molecular process for higher water fractions can be followed in Fig. 5.12b. Arrows in the diagram indicate the maximum frequency of the peak, which is at about 500 Hz for $h_w=0.13$ and 50 kHz for $h_w=0.18$. The position and the magnitude of the peak seem to saturate for samples of

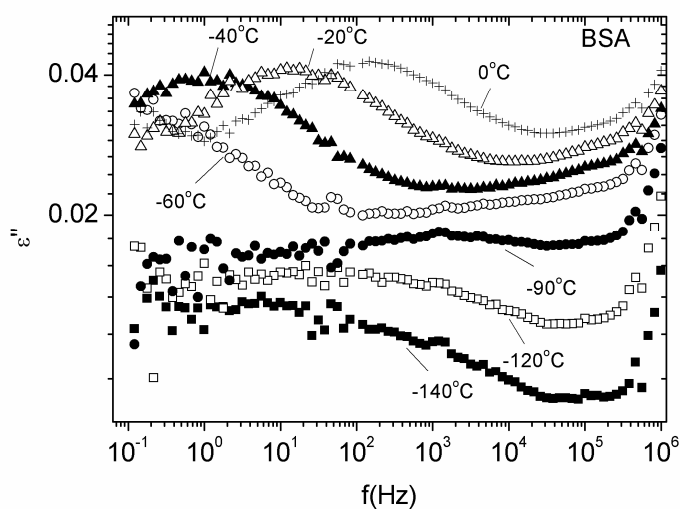


Fig. 5.10 Dielectric loss versus frequency, $\epsilon''(f)$, for a dry BSA sample at selected temperatures T indicated on the plot

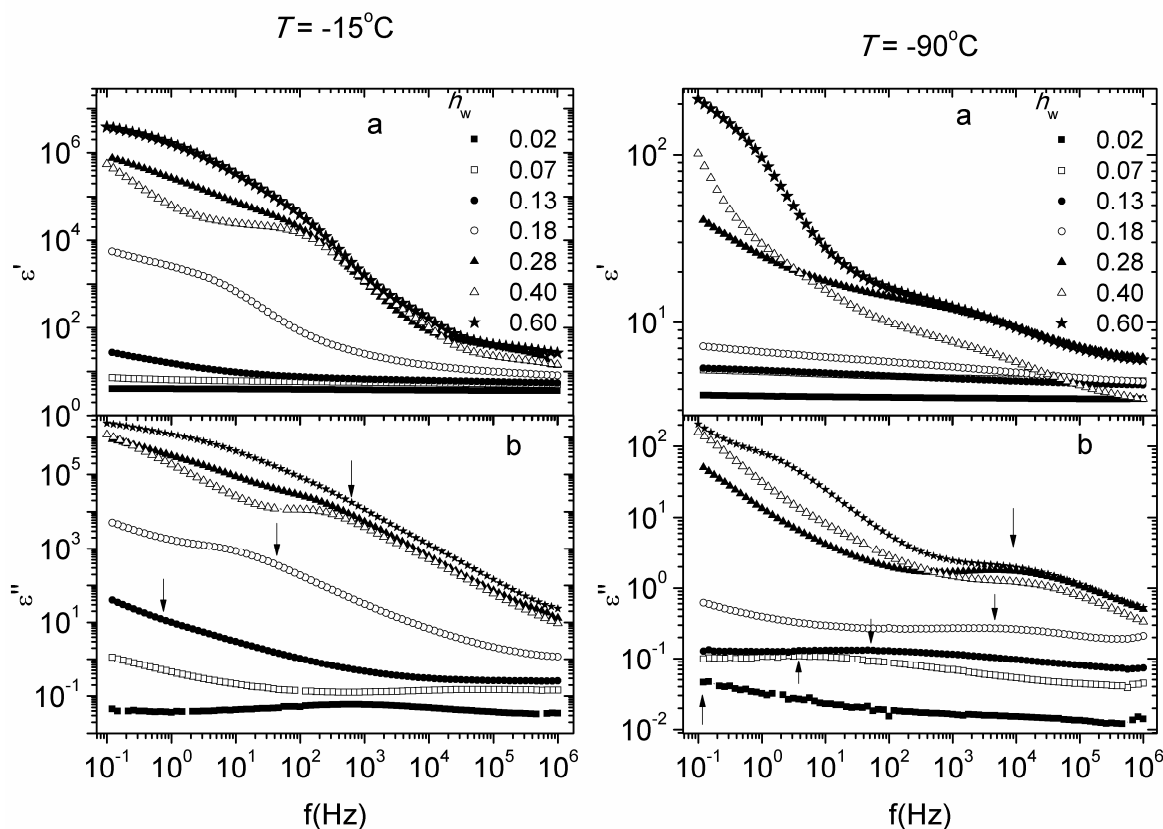


Fig. 5.11 (a) Real part of the dielectric function against frequency, $\epsilon'(f)$, and **(b)** Imaginary part of dielectric function (dielectric loss) against frequency, $\epsilon''(f)$, at -15°C , for BSA-water mixtures at several water fractions indicated on the plot. The arrows indicate rough estimations of the overall α relaxation peak maximum.

Fig. 5.12 (a) Real part of the dielectric function against frequency, $\epsilon'(f)$, and **(b)** Dielectric loss against frequency, $\epsilon''(f)$, at -90°C , for BSA-mixtures at several water fractions indicated on the plot. The arrows indicate the estimated peak maximum.

$h_w=0.28, 0.40$ and 0.60 , centered at about 10 kHz. As it will be shown it what follows, the secondary relaxation of polar groups is the precursor of the secondary relaxation of water in the protein hydration shell, denoted as ν relaxation of water [Ngai 2011] and so the relaxation of polar groups will be called ν relaxation in the high water fraction range, where the loss peaks saturate in position ($h_w=0.18, 0.28, 0.40$ and 0.60). At this point we would like to highlight the increase of the measured low frequency dielectric loss for $h_w>0.18$. Taking into consideration also the remarkable increase of $\epsilon'(f)$ at that water fraction and frequency range we may conclude that the conductivity of the samples is significantly enhanced for that water fraction range implying that the conduction process becomes now a percolative type process [Rupley 1991].

Fitting Results

Dielectric data corresponding to the samples of $h_w<0.18$, have been expressed as the sum of two or three Cole-Cole functions and a conductivity term (see chapter 4, section 4.3), at temperatures where this was necessary. The two samples of lowest hydration levels ($h_w=0$ and 0.02) exhibit two secondary relaxations and no α relaxation associated with the glass transition of the protein. The peaks of these relaxations are clearly visible for the dry sample and have been presented in Fig. 5.10. The high temperature peak originates from the movement of small polar groups of the protein surface, while the low temperature peak will be further analyzed later on. The data corresponding to the samples with $h_w=0.07, 0.13$ and 0.18 exhibit, except from the relaxation of polar groups, a peak corresponding to the α relaxation associated with the glass transition of the hydrated system.

Fitting of the dielectric loss curves for the samples of higher water fractions, that is, $h_w=0.28, 0.40$ and 0.60 has revealed additional peaks entering the experimental window, originating possibly from new forms of water organization (excess water or ice), as the water fraction increases. The complexity of the dielectric response (multiple interfering peaks) along with the large conductivity contribution at high water fractions, make the detection of the peaks rather tentative, in contrast to lower water fractions where the curves are more simple. Help may often be provided by using a derivative method:[Wübbenhorst 2002]

$$\epsilon''_{der}(f) = -\frac{\pi}{2} \frac{\partial \epsilon'(f)}{\partial \ln f} \approx \epsilon''_{rel} \quad (5.4)$$

where ϵ''_{rel} is the ohmic-conduction-free dielectric loss, provided that conductivity makes no significant contribution to ϵ' . For that reason the dielectric loss calculated by the derivative method is added to diagrams containing fitting of dielectric loss at high water fractions.

An example of the fitting of the dielectric loss curves for the samples of $h_w=0.07, 0.18, 0.28$ (inset) and 0.40% , at a characteristic temperature of -90°C , where the relaxation of polar groups and the ν relaxation of water is within the experimental window, is shown in Fig. 5.13. Starting with the data corresponding to $h_w=0.07$, a broad peak corresponding to a relaxation of polar groups of the protein can be seen centered at about 1 Hz. A peak at higher frequencies (dotted line) is necessary to fit the data, but it is not dealt with in this thesis, as its maximum is located mainly out of the frequency range of the experimental window. The same applies for other such peaks in the fitting procedure. At higher water fractions, that is, $h_w=0.18, 0.28$ (inset) and 0.40 , a peak corresponding to the ν [Ngai 2011]

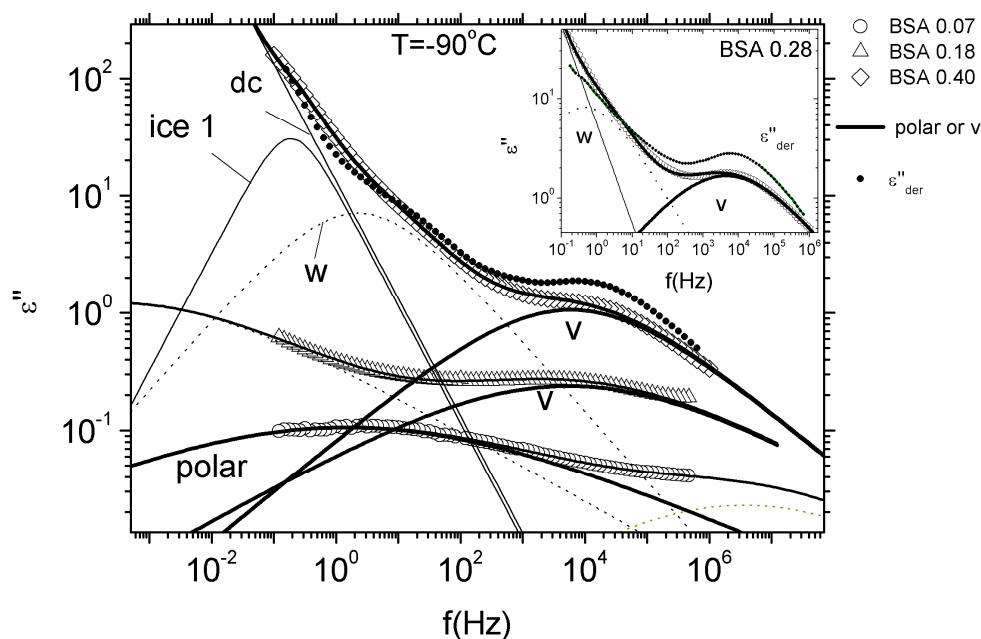


Fig. 5.13 Dielectric loss against frequency, $\varepsilon''(f)$, at $T=-90^\circ\text{C}$, for BSA-water mixtures of water fractions $h_w=0.07, 0.18, 0.28$ (inset) a BSA-water solution of $h_w=0.40$. The solid circles correspond to dielectric loss calculated by the derivative method [Wübbenhorst 2002]. The solid lines which show the peaks corresponding to the relaxation of polar groups for $h_w=0.07$, the v relaxation of water for $h_w=0.18$ and 0.40 , the w and $ice1$ relaxations for $h_w=0.40$ are highlighted in the plot. The solid lines through experimental data correspond to the sum of the contributions.

relaxation of water (see chapter 2, section 2.2) can be seen centered at about 10^4 Hz. An additional peak named w , centered at about 1 Hz for the samples of $h_w=0.28$ and 0.40 , is presented as dotted line, because its maximum could not be clearly discerned at any temperature of our measurements. Its existence is alternatively verified indirectly e.g. by the change of slope of the dielectric loss, which is more pronounced in the derivative data ($h_w=0.40$, solid circles) and of course by the fact that fitting was not possible without taking process w into account. In our fittings we assumed a value of $\beta_w=0.6$ (see eq. (4.11)) for the fractional exponent of process w , which was set as a constant during the fitting procedure. Finally, a peak, better fitted as Debye (i.e. $\beta=1$ in eq.(4.11)), signed as $ice1$ is centered at about 0.1 Hz, in case of the sample of $h_w=0.40$.

Figures 5.14 and 5.15 are examples of the fittings at selected temperatures, -35 and -105°C respectively, for $h_w=0.40$. Fig. 5.14 shows the peaks contributing to dielectric spectra at a high temperature, $T = -35^\circ\text{C}$, for $h_w=0.40$. Starting at low frequencies, a Debye peak named p on the plot is hidden below the dc conductivity contribution. The maximum of this peak is clearly visible at higher temperatures and the peak is necessary to fit the data, but it will not be further studied in this paper, so it is plotted as a dotted line. Similar dielectric responses are often encountered in dielectric measurements on water containing systems and are usually interpreted as interfacial polarization processes due either to localized conduction processes within the samples or to electrode polarization effects [Shinyashiki 2009, Gutina 2002, Suherman 2002, Richert 2011]. In addition, such a relaxation process is usually

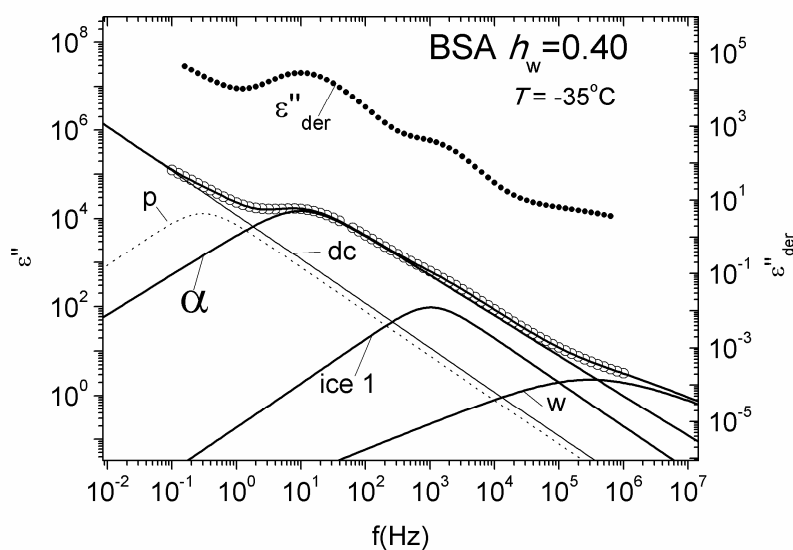


Fig. 5.14 Dielectric loss against frequency (open circles), $\epsilon''(f)$, at -35°C , for a BSA-water solution of water fraction $h_w=0.40$. Green solid circles correspond to dielectric loss data calculated by the derivative method [Wübbenhorst 2002]. Solid and dotted lines correspond to contributions to dielectric loss calculated by fitting of the data by a sum of Cole-Cole functions and a conductivity term. The solid line through experimental data (open circles) corresponds to the sum of the contributions.

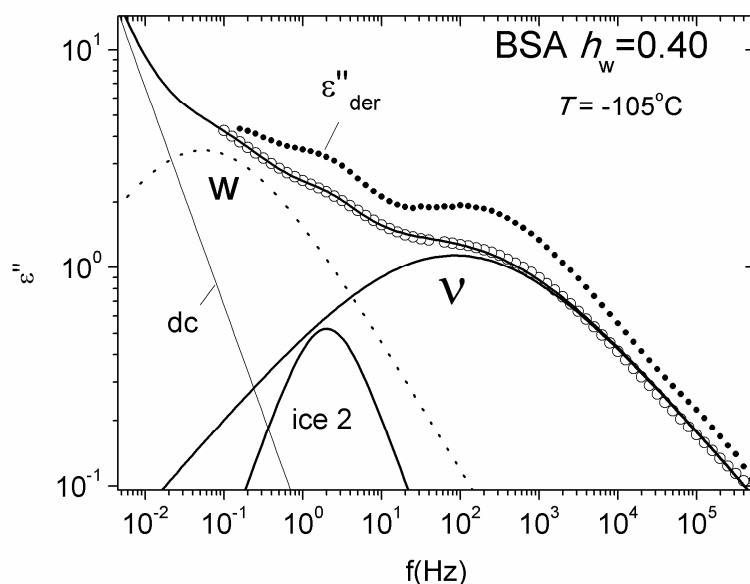


Fig. 5.15 Dielectric loss against frequency (open circles), $\epsilon''(f)$, at -105°C , for a BSA-water solution of water fraction $h_w=0.40$. Solid circles correspond to dielectric loss data calculated by the derivative method.⁵⁰ Solid and dotted lines correspond to contributions to dielectric loss calculated by fitting of the data by a sum of Cole-Cole functions and a conductivity term. The solid line through experimental data (open circles) corresponds to the sum of the contributions.

by a Debye relaxation process [Richert 2011]. Analogous peaks were used for fitting the data for $h_w > 0.07$. At higher frequencies in Fig. 5.14 additional peaks follow, namely, the α peak associated with the glass transition of the hydrated protein, centered at about 10 Hz, a Debye peak probably due to ice, signed as *ice 1*, centered at about 1 kHz, and a peak signed as *w* (which has been discussed above, Fig. 5.13). The position of the peaks seems to correlate well with that calculated by the derivative method (solid circles). Moving on to lower temperatures ($T = -105^\circ\text{C}$, Fig. 5.15) a Debye process signed as *ice 2* is observable (in addition to the ν and the *w* peak), centered at about 2 Hz at -105°C . The peaks denoted as *ice 1* in Fig. 5.14 and *ice 2* in Fig. 5.15 are attributed to relaxation processes in the ice phase, because they were detected only for the sample of $h_w = 0.40$, where ice crystals have been formed during cooling (DSC, section 5.4), while they were absent in the case of $h_w = 0.28$, where DSC studies show no significant ice formation during cooling. Finally, for $h_w = 0.60$ a single relaxation due to ice, denoted as *ice1* was recorded by the fittings (not shown here) throughout the entire temperature range studied, in addition to the p , α , ν and *w* relaxations.

The fitting parameters $\tau_j(T)$ (relaxation time) and $\Delta E_j(T)$ (dielectric strength) calculated for each process j are plotted in Figures 5.17-5.21 against temperature, while the parameters $\beta(T)$ for the processes of polar groups of the protein triggered by water, at low hydration levels, and for the ν relaxation of water associated with the main relaxation of uncrystallized water at high hydration levels, are listed in Table 5.3. The data of Fig. 5.17 for the relaxation of polar groups of the protein triggered by water and the ν relaxation of water have been expressed by an Arrhenius equation (chapter 4, eq. (4.11)). The corresponding values of the activation energy E_{act} , as well as the logarithm of the pre-exponential factor $\log f_0$, are listed in Table 5.4.

5.6 BSA-Discussion-Conclusions

5.6.1. Critical water contents and crystallization effects

By ESI measurements two critical water contents are obtained for BSA-water mixtures at room temperature. The first critical content, h_m , is the water content corresponding to water molecules directly attached to sorption sites (primary hydration sites), in other words to the content of water molecules directly attached to the amino acid residues of the protein. With the values of molecular weights of 66.000 for BSA, 18 for water and for $h_m = 0.073$ (grams of water per grams of dry protein), we conclude that 270 water molecules are directly bound to a BSA molecule. This means that out of the 607 residues of a BSA molecule, only the 270 are accessible to water, the rest being hidden in the globular structure or engaged in other interactions. This value is very close to the water content $h_a = 0.07$, which is the reported water content below which water interacts mainly with charged groups of the protein surface in case of globular proteins [Careri 1998]. The second critical water content is in the range of $h_a = 0.25$ and corresponds to the water content above which clustering is significant.

In Fig. 5.6a the amount of uncrystallized water, $h_{d,ucw}$, increases with increasing water content, not only within the cold crystallization region but also for higher water contents, reaching for the higher water contents measured a value of 0.639 (compare Table 5.2). This

increase of $h_{d,ucw}$ is consistent with the concept of new primary hydration sites becoming accessible to water, as a result of the swelling of the protein with increasing water content, and the formation of new water clusters around these primary sorption sites. Until a hydration level of $h_w=0.35$, corresponding to $h_d=0.54$ (see Table 5.2), the amount of uncrystallized water, $h_{d,ucw}$, is within the range 0.3-0.4, i.e. within the range of the reported values for uncrystallized primary hydration water [Kawai 2006, Sartor 1992, 1994a,b, 1995], and can, therefore, be assigned to water at the primary hydration shell of the protein [Kawai 2006, Cooke 1974, Franks 1977, Harvey 1972, Kimmich 1990, Kotitschke 1990]. The primary hydration shell of the protein corresponds to a monolayer of water molecules at the surface of the protein, which includes water molecules directly attached to primary hydration sites, as well as water molecules that connect the prementioned water molecules to each other, for the completion of the first water monolayer [Careri 1998, Nakasako 2002]. Water molecules in layers at the vicinity of the primary hydration shell are described as secondary hydration shell. These water molecules are loosely bound on the molecules in the primary hydration shell, by hydrogen bonds, but are able to diffuse over a long period of time. Consequently, they remain unfrozen by quenching but are able to crystallize by warming up to -73°C or during annealing above this temperature [Kawai 2006]. The amount of water in the secondary hydration layer is reported to be in the hydration range of 0.4-0.7 (grams of water per grams of dry protein) [Kawai 2006, Sartor 1992, 1994a,b, 1995]. Although it is expected that, for high experimental timescales (which is the case in our study), the water in the secondary hydration shell would completely crystallize, it has been shown, in the case of hydrated proteins [Kawai 2002, Sartor 1992, 1994b, 1995] that some water remains unfrozen because of confinement between small openings of the protein. This kind of water was first described as 'internal' water by Saenger [Saenger 1987] and was suggested to be an integral part of protein structure. Kawai et al. [Kawai 2002] employing adiabatic calorimetry measurements on a BSA-water solution of $h_w=0.8$, suggested that water in the primary hydration shell and 'internal' water of a protein must be intimately connected with the interfacial and internal water molecules confined within silica pore gels, respectively. Interfacial water in this case is meant the amount of water molecules which form hydrogen bonds with silanol groups, while internal water refers to the water molecules that are centered in the pore and interact only with other water molecules [Oguni 2007]. Oguni et al. [Oguni 2007] showed, through experiments by adiabatic calorimetry, that internal water remains unfrozen down to -193°C when confined within pores less than about 1.6 nm in diameter. These observations would explain the additional increase in $h_{d,ucw}$ in Fig. 5.6a for values of hydration level $h_w=0.43$ (corresponding to $h_d=0.76$) and 0.67 (corresponding to $h_d=1.99$), (compare Table 5.2), noting that its value is in the hydration range of 0.4-0.7, which, as mentioned earlier, corresponds to the amount of water in the secondary hydration layer of the protein. Particular geometrical formations of the protein would then play the role of a nanosized pore, e.g. consider that the distance between two segments of an alpha helix, forming a turn, is only 0.54 nm [Pauling 1951]. These observations suggest that there is a considerable amount of 'internal' water in the mixtures studied.

Apart from uncrystallized water, we tried also to identify the water populations in the crystal phase. The critical water fractions by DSC for the appearance of crystallization and melting events, $h_w=0.30$ and 0.21, respectively, are in the range of the second critical

water content estimated by ESI of about $h_d=0.25$, suggesting that crystallization and melting events are first observed in the range of water contents where clustering sets in. The melting temperatures in Fig. 5.4 suggest the existence of two main populations of ice microcrystals in the frozen samples. The first population appears for hydration levels below about $h_w=0.4$, where T_m increases with increasing water content, reflecting the increasing size of water clusters [Mathot 1994], as indicated by ESI measurements. A relaxation corresponding to the first population of water crystals was not clearly observable in TSDC. Nevertheless, the increase in magnitude for sample 4 in Fig. 5.7 and the observed peak at about -135°C could correspond to a contribution due to crystal phase. The corresponding dielectric relaxation (*ice2*) observed by DRS only for $h_w=0.45$ will be discussed in section 5.6.3 regarding the dynamics of water. The second crystalline water population appears for water contents higher than about $h_w=0.45$, where T_m is around 0°C , resembling the behaviour of bulk water. This is consistent with the observation in TSDC measurements (Fig.5.7), where the peak which was attributed to relaxation in bulk ice appears for $h_w=0.46$ at -125°C , whereas it is not present for $h_w=0.40$. The relative temperature position of these relaxations suggests that the smaller ice crystals that are formed at lower water fractions must contain smaller amount of defects than the ones assigned to 'bulk' ice, as previous work on various forms of ice [Pissis 1981,1982, Daoukaki-Diamanti 1984] has shown that the time scale of the relaxation depends on the concentration of defects in the ice crystals and the peak temperature of the relaxation increases with increasing defect concentration.

5.6.2. Glass Transition - α relaxation of the protein water mixture

We turn now our attention to the α relaxation of the protein-water system associated to the glass transition. This relaxation was studied in detail by TSDC and the corresponding peak temperatures, which are good measures of the calorimetric T_g [Turhout 1980, Pissis1991], are plotted in Fig. 5.16 against water content h_w . DSC values for the T_g , calculated as the midpoint of the heat capacity step during heating, are also plotted in Fig. 5.16 (combination of data from Figures 5.8 and 5.4, respectively). $T_{g,1}$ and $T_{g,2}$ by TSDC in Fig. 5.16 shift systematically and significantly to lower temperatures with increasing water content and then stabilize at about -90°C and -100°C respectively, for h_w values higher than about 0.35, i.e. for water contents in the region where a part of water crystallizes during cooling. This is a main result of this thesis. The glass transition observed by DSC is very broad and weak as it was shown in Fig. 5.3, resulting in reduced accuracy of the calculations. Nevertheless, the dependence of the T_g on the water content is systematic enough, and in quite good accordance to the trend observed by TSDC, so we can take it into account. The significant plasticization of the T_g and the stabilization within the temperature range of -100°C to -70°C in the crystallization region, is evident for both TSDC and DSC, and in accordance with various results by literature on fully hydrated proteins [Gregory 1995, Ringe 2003, Fenimore 2004, Khodadadi 2010]. The main difference between the T_g values, as they were observed by the two techniques, is that the plasticization is more smooth in DSC. While T_g values by DSC are comparable to $T_{g,1}$ values by TSDC for the initial water content for which the glass transition is detectable ($h_w\sim 0.1$), the values by DSC for increasing water content seem to correlate better with the values $T_{g,2}$ by TSDC. We recall at this point that a

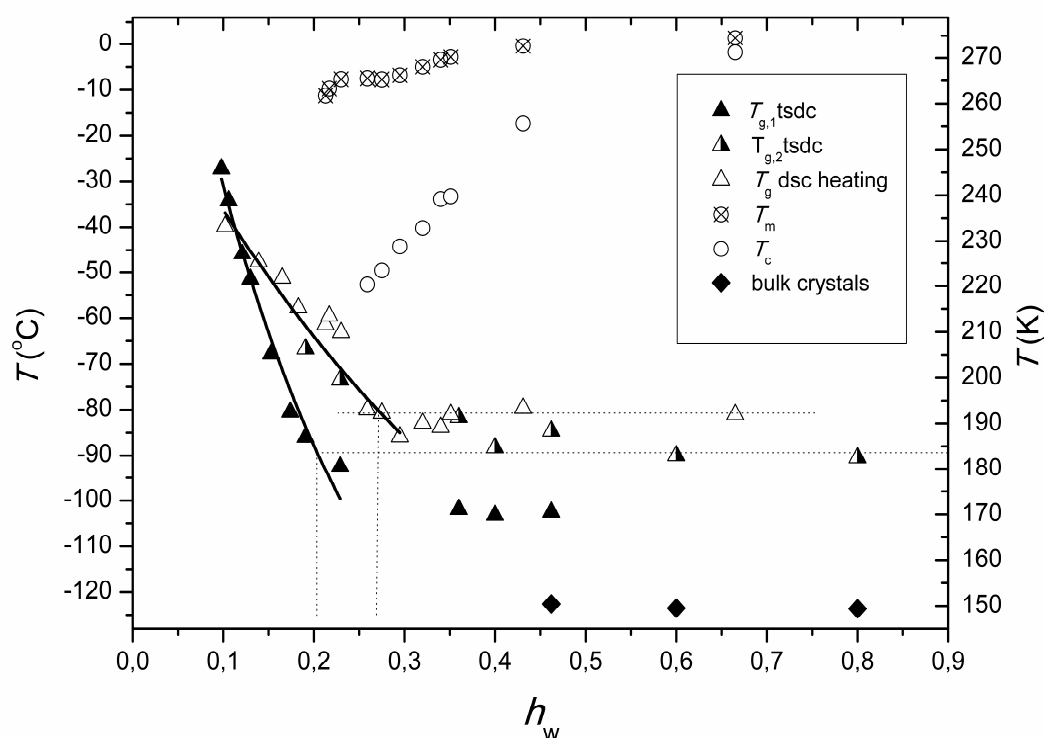


Fig. 5.16 Characteristic TSDC and DSC temperatures, indicated on the plot, against water fraction h_w . The solid lines are fits to the TSDC and DSC data to the Fox equation [Fox 1956]. The dotted lines are added for eye guidance, concerning the estimation of uncrystallized water according to the phase diagram [Rault 1997].

microphase separation was assumed in TSDC (section 5.5.1), resulting in the appearance of an additional α peak ($T_{g,2}$), which was attributed to the motion of protein segments in gels with reduced water content due to the formation of the separate phase of water clusters containing initial nuclei of water crystals. This difference can be explained if we consider the magnitude of the α peaks in TSDC compared to the values for ΔC_p by DSC, that are plotted in Fig. 5.5. We saw that the normalized values of ΔC_p in Fig. 5.5, with respect to the protein fraction in the samples, increase significantly for water contents below the region where part of water crystallizes during cooling. Additionally, the magnitude of the peaks corresponding to $T_{g,2}$ in TSDC (see samples 6 and 7 in Fig. 5.7), is larger compared to that of the respective $T_{g,1}$ peaks. By these facts we conclude that DSC measurements detect the value for the glass transition temperature corresponding to the contribution greater in magnitude, while the other is hidden somewhere within the broad heat capacity step. The comparatively lower equivalent frequency of TSDC, compared to DSC, and the different kind of stimulus for each technique are probably the reasons for the better resolving of the α peaks by TSDC, which is anyway characterized by high peak resolving power [Turnhout 1980]. Nevertheless, the relation between T_g values determined by the two techniques should be further followed in future work, regarding that the thermal history of the samples prior to measurements was different for TSDC (stabilization for at least two days at 4°C) and for DSC (no stabilization).

The solid lines in Fig.5.16 are fits of the Fox equation [Fox 1956]

$$\frac{1}{T_g} = \frac{h_w}{T_{g,w}} + \frac{1-h_w}{T_p} \quad (5.5)$$

to the DSC data and TSDC data ($T_{g,1}$). The data by DSC reflect the glass transition of the whole hydrated system, while data for $T_{g,1}$ reflect the ‘ideal’ plasticization of protein molecules by uncrystallized water, according to the prementioned observations. In this equation $T_{g,w}$ and $T_{g,p}$ of the pure components (water and protein, respectively) were left free and the values determined for them, are about 0°C for the dry protein and -165°C for pure water for DSC. The value obtained for water by DSC is close to the value of -163°C, reported as the glass transition temperature of uncrystallized water in hydrated BSA, in a BSA-water solution 80% in water, by Kawai et.al. [Kawai 2006]. We will come back to this comparison later. Additionally, the value for the fraction of uncrystallized water in the sample, which is estimated in Fig. 5.16 as the projection of the intersection of the stabilized T_g value by DSC with the Fox line, to the composition axis (see Fig. 5.16) [Rault 1997], is found equal to 0.27, which is slightly higher than the fraction of uncrystallized water in the samples as calculated by DSC measurements (Fig. 5.6b). This method of calculation is according to the phase diagram [Rault 1997], and is, therefore, based on the assumption that no strong interactions occur between the components of the mixture. The fact that the DSC data are fitted very well by the Fox mixing formula, which does not take into account any interactions between its components, along with the fact that glass transition in completely or nearly dry proteins seems to be absent, may lead to an important conclusion relevant to the origin of the glass transition in hydrated proteins. It is likely that bound water molecules on the primary hydration sites of the protein, being a structural component, are the condition for segmental dynamics in proteins. In other words, we can imagine the protein as a polymer matrix, and primary hydration water molecules as structural part of the latter. In that case, the plasticization of the glass transition is caused by the additional uncrystallized water of the hydration shell or of water molecules confined in other nanosized areas of the protein. This assumption is supported by the value estimated by the Fox equation in the case of the DSC data (-165°C), which is the glass transition of the uncrystallized water, i.e. uncrystallized water of the primary hydration shell [Kawai 2006]. The same analysis has been done for TSDC data (Fig. 5.16). The values of about 76°C for the dry protein and -209°C for pure water have been determined. Similar values were obtained by the same method in case of lysozyme-water mixtures [Panagopoulou 2011a]. With respect to $T_{g,w}$ the estimated value is lower than the values proposed in the literature.

At this point, we should consider another possible scenario arising from the so far analysis of the data, concerning the glass transition. Given that for water fractions where crystallization occurs during cooling, the peak in TSDC which was assigned to $T_{g,1}$ is positioned at about -100°C (see Fig. 5.7), which is near the reported value of -113°C for the T_g of internal water by Oguni et.al. [Oguni 2007] and that of -113 to -108°C predicted for bulk supercooled water by some research groups [Velikov 2001, Starr2003, Yu 2004, Giovanbattista 2004], along with the observation that uncrystallized, ‘internal’, water seems to be significant in the samples studied for water contents higher than the critical water content for completion of the primary hydration layer, there is the possibility that the double α peak observed in TSDC corresponds to the gel phase of protein/water mixture and the

phase of 'internal' water, rather than to two domains of the mixtures with different degree of plasticization. Oguni et.al. in [Oguni 2007] stated that the heat release and absorption effects at around -113 to -108°C observed by adiabatic calorimetry, should not be confused with crystallization effects of water and fusion of the minute ice particles formed, and suggests that a glass transition of bulk supercooled water takes place potentially at -113°C or above due to the development of an energetically more stable hydrogen-bonding network of water molecules at low temperatures. This scenario would explain the difference in T_g values predicted by DSC and TSDC (see above), as well as the unrealistic values estimated by Fox in case of TSDC, as the values for higher water contents correspond no longer to the glass transition of the mixture, but to the one in the separated microphase of 'internal' water. More evidence supporting this aspect will be given later on in the discussion on water dynamics according to the analysis by DRS (section 5.6.4), as well as in chapter 7 (section 7.3).

Figure 5.17a and b show the temperature dependence of the relaxation time for the α relaxation associated with the glass transition of the hydrated BSA, and the corresponding dielectric strength $\Delta\epsilon_\alpha$, respectively. The inset in Fig. 5.17b shows the fractional exponent $\beta(T)$ of the Cole-Cole function of the α peaks. In Fig. 5.17a, a strong plasticization of the α relaxation is observed with addition of water, for water fractions $h_w=0.07$ to 0.28. Further addition of water causes no further change in the timescale of the α relaxation, as the position of the data for $h_w=0.40$ and 0.60 follow the same trace with that of $h_w=0.28$. This behavior is consistent with the calorimetric results mentioned previously. Additionally, an extrapolation of the data to the equivalent relaxation time for calorimetric measurements ($\tau=100$ s), seems to coincide with the stabilized T_g value from DSC. Furthermore, data from reference [Shinyashiki 2009] which correspond to the dielectric process III associated with the glass transition of a BSA-water solution of $h_w=0.80$ (filled stars in Fig. 5.17a), are similar with our data. This value for the T_g of hydrated BSA after stabilization is in the range of the values reported in literature for the thermal glass transition of various proteins, that is, in the range of -110 to -70°C, depending on the protein, the hydration level and the experimental technique employed [Gregory 2003, Ringe 2003, Fenimore 2004, Khodadadi 2010, Miyazaki 2000, Panagopoulou 2011a]. The prementioned observations provide strong evidence that the data in Fig.5.17 correspond to the α relaxation. The presentation of the plasticization of the protein α process in an Arrhenius diagram is, to the best of our knowledge, a novel result.

Considering the relaxation strength $\Delta\epsilon_\alpha$ of the α process, it can be seen in Fig.17b that it increases superlinearly with hydration level. Furthermore, a clear increase of $\Delta\epsilon_\alpha$ with temperature decrease (which is typical for the α relaxation of glass forming materials [Ngai 2011]), is observed only for the samples of $h_w=0.18$ and 0.40. Considering the sample of $h_w=0.28$, this inconsistency can be explained by the fact that this water fraction value is within the water fraction range where cold crystallization effects occur (0.21 to about 0.30) as seen by DSC. Cold crystallization of ice in this case could be interfering in the temperature range of the α relaxation affecting the values of the dielectric strength. In the case of the samples of low water fractions, that is of $h_w=0.07$ and 0.13, we know that cold crystallization

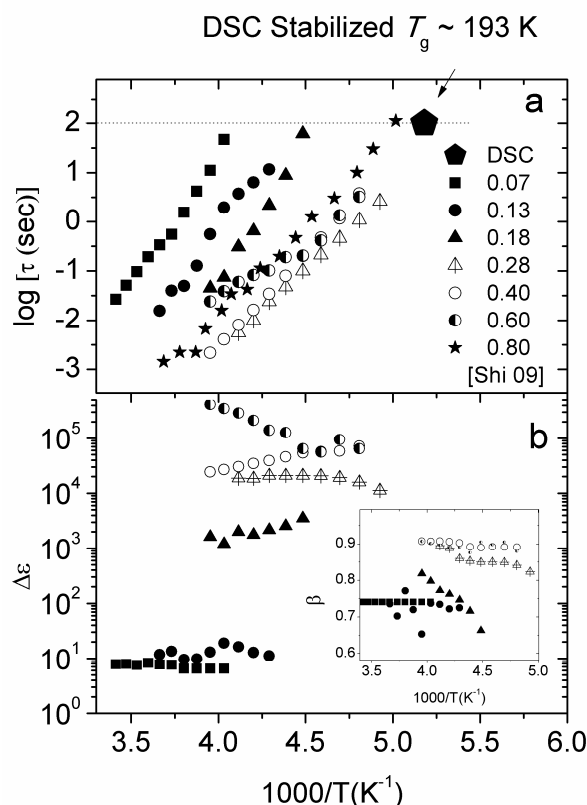


Fig. 5.17 (a) Temperature dependence of the relaxation times for the α relaxation associated with the glass transition of the hydrated BSA for samples of different water fractions indicated on the plot. Solid stars are data from reference [Shinyashiki 2009] on a BSA-water solution of $h_w=0.80$ **(b)** Relaxation strength $\Delta\epsilon_\alpha$ of the α relaxation associated with the glass transition of the hydrated BSA for samples of different water fractions indicated on the plot. The inset shows the fractional exponent $\beta(T)$ of the Cole-Cole function of the α relaxation peaks.

is absent. On the other hand, the low intensity of the α peak at these low water fraction values along with its high relaxation time, when compared with the other samples, result in an increased uncertainty of the fitting results, as conductivity contributions are large in proportion to the magnitude of the peaks. This difficulty in monitoring the α peak is more obvious in case of the $h_w=0.13$, where it can be seen in the inset of Fig.5.17b, that there is significant scattering of the fractional exponent $\beta(T)$. It is obvious that the difficulty in monitoring the peak applies also for the sample of the highest h_w studied here, i.e. 0.60. Considering the sample of $h_w=0.07$ in particular, we may also highlight the fact that this is a value close to the onset water fraction for the appearance of the protein glass transition and that it was fitted without an additional Debye p peak (see section 5.5.2), which was needed for the other samples at higher water fractions. The origin of the glass transition in hydrated proteins is anyway highly debated in literature and it has been proposed that it is highly connected to water and, particularly, that it leads to the cooperative motion of water in the hydration shell and protein chains [Miyazaki 2000, Shinyashiki 2009, Panagopoulou 2011a,b, Jansson 2011, Tournier 2003, Matyushov 2011]. This fact may be the reason for the peculiarity of the protein glass transition, compared to that of common glass formers. There are difficulties to analyze in detail the dynamics of the α relaxation of the hydrated protein,

as conductivity contributions and polarization effects are significant in the temperature region where the α relaxation is observed (we also recall the existence of an additional process p near the α peak). More experiments are needed for a thorough analysis. On the other hand, the assignment of the processes associated to the protein glass transition provides help for the interpretation of the relaxations originating mainly from water dynamics. The origin of the protein glass transition will be discussed further in chapter 7 (section 7.3.3).

5.6.3. The interplay between a secondary relaxation of polar groups triggered by water molecules and the ν relaxation of water

A dielectric relaxation due to local polar groups of the protein plasticized by water, overlapped by a relaxation of uncrystallized water (see section 5.5), was detected in TSDC and DRS. This relaxation was studied previously by means of TSDC measurements on hydrated casein pellets with systematic variation of the water content in small steps [Anagnostopoulou-Konsta 1987], but also on hydrated lysozyme samples [Panagopoulou 2011a]. In both cases, the magnitude of the peak, which is a measure of the number of relaxing units, e.g. dipoles, contributing to the peak [Turnhout 1980], increases more steeply for water contents higher than about the respective h_m value from ESI, suggesting that for h_d higher than h_m , water molecules themselves in the uncrystallized water phase make a contribution to the relaxation in question. This is a fact also for BSA results in this chapter, where, in Fig. 5.7, a steeper increase in magnitude occurs for h_d higher than 0.10 (corresponding to $h_w=0.11$, sample 12 in Fig. 5.7), which is slightly higher than the value 0.073 for h_m from ESI. Another interesting observation is that the increase in magnitude is even steeper for water fractions higher than $h_w=0.17$ (sample 8 in Fig. 5.7), which corresponds to a water content of $h_d=0.20$, which is within the critical water content region (0.15-0.25) that corresponds to the percolation threshold where long-range connectivity of the surface water is established in globular proteins [Rupley 1991]. It is interesting to note that similar results to those reported above for proteins (lysozyme, casein, BSA) were obtained by TSDC with polysaccharides [Pissis 1985], seeds [Ratkovic 1997] and plant tissue [Pissis 1990], and by DRS with cellulose [Sugimoto 2008]. At this point it is essential to note that the frequency-temperature range of the observed relaxation at relatively high hydration levels (h_w higher than about 0.3) is highly studied in literature. In fact, the relaxation observed in this area has proven to exhibit similar temperature dependence of its characteristic time scale for a large number of water-containing systems, such as hydrophilic polymers, biopolymers and small glass-forming systems [Cerveny 2008], has comparable time scales with the β (secondary) relaxation of confined water within various confining systems [Cerveny 2004], and has been discussed in terms of the Johari-Goldstein β -relaxation of glass formers in general in [Ngai 2007,2008, Capaccioli 2007,2010], where the terminology ν -relaxation of water was used.

The dynamical characteristics of the secondary relaxation of polar groups and its connection to the ν relaxation at higher h_w , is better followed by DRS. The temperature dependence of the time scale of the relaxations in question (polar groups and ν relaxation peaks in Fig. 5.12b, 5.13) is shown in Fig. 5.18.

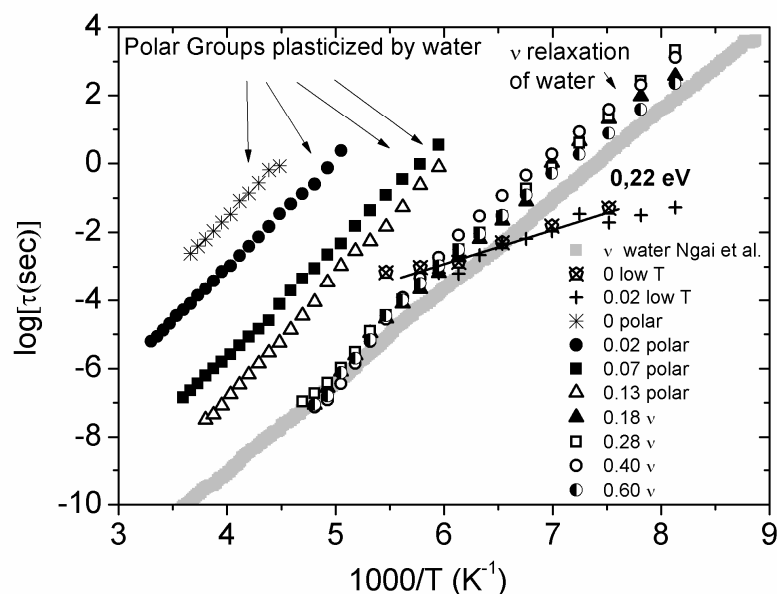


Fig. 5.18 Temperature dependence of the relaxation times for (i) the low temperature relaxation in dry BSA and $h_w=0.02$ (ii) a relaxation of small polar groups of the protein surface triggered by water for BSA-water mixtures of water fractions $h_w=0, 0.02, 0.07$ and 0.13 , and (iii) the ν relaxation of water for hydrated BSA pellets of water fractions $h_w= 0.18$ and 0.28 and BSA-water solutions of $h_w=0.40$ and 0.60 .

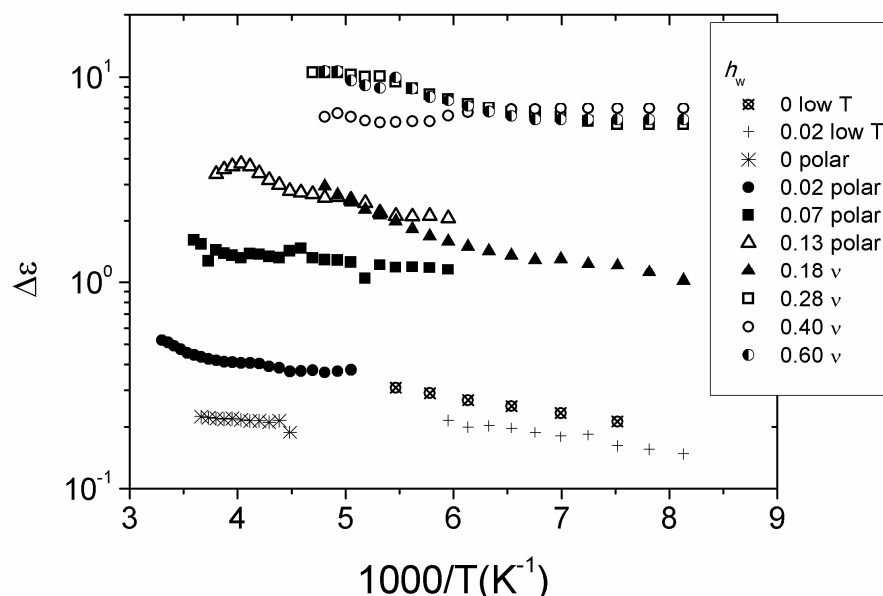


Fig. 5.19 Relaxation strength $\Delta\epsilon$ of (i) the low temperature relaxation in dry BSA and $h_w=0.02$ (ii) a relaxation of small polar groups of the protein surface triggered by water for BSA-water mixtures of water fractions $h_w=0, 0.02, 0.07$ and 0.13 , and (iii) the ν relaxation of water for hydrated BSA pellets of water fractions $h_w= 0.18$ and 0.28 and BSA-water solutions of $h_w=0.40$ and 0.60 .

Table 5.3 Fractional exponent $\beta(T)$ of the Cole-Cole function for the process of polar groups-hydration water for the BSA samples of $0 < h_w < 0.13$ and for the ν relaxation of water for samples of $0.18 < h_w < 0.40$.

h_w	0	0.02	0.07	0.13	0.18	0.28	0.40	0.60
$\beta(T)$	0.38	0.32	0.23	0.15	0.30	0.43	0.43	0.48

Table 5.4 Activation energy, E_{act} , and logarithm of the pre-exponential factor, $\log f_0$, of the Arrhenius equation for the relaxations of small polar groups of BSA which is triggered by hydration water ($0 < h_w < 0.13$) and for the ν relaxation of water ($h_w = 0.18, 0.28$ and 0.40). The activation energy of the ν relaxation has been calculated for temperatures lower than the crossover temperature of about -103°C .

h_w	E_{act} (eV)	$\log f_0$
0	0.67 ± 0.01	14.14 ± 0.20
0.02	0.62 ± 0.01	14.67 ± 0.12
0.07	0.63 ± 0.01	17.60 ± 0.09
0.13	0.70 ± 0.01	20.08 ± 0.15
0.18	0.55 ± 0.02	18.83 ± 0.75
0.28	0.59 ± 0.01	19.92 ± 0.32
0.40	0.50 ± 0.01	16.95 ± 0.19
0.60	0.49 ± 0.01	16.70 ± 0.16

The temperature dependence of relaxation times for an additional low temperature relaxation which was recorded for the dry sample (Fig. 5.10) and the sample of $h_w = 0.02$ (see 'Raw data' in section 5.5.2) can also be seen in the Arrhenius diagram of Fig. 5.18. This low temperature relaxation follows an Arrhenius law and it is characterized by an activation energy, $E_{act} = 0.22$ eV. This value is very close to the energy required to break a single hydrogen bond, and this probes us to assume that this relaxation is probably associated with the reorientation of water molecules dispersed in the protein, in such a way, that they are completely isolated from each other. It is essential to mention that a relaxation of similar E_{act} , although faster, has been recorded in case of lysozyme-water mixtures of high water content studied by NMR [Khodadadi 2008] and there it was assigned again to a form of water. Furthermore, its position in the Arrhenius diagram coincides with that of process I_α from reference [Shinyashiki 2009] in case of a BSA-water solution of water $h_w = 0.8$, and there it was assigned to uncrystallized water. More experimental studies are essential to clarify the origin of the relaxation in question and its evolution with hydration level.

Moving to the high temperature side of Fig. 5.18, we may follow the relaxation of small polar groups, mentioned previously, plasticized by water, until $h_w = 0.13$. The activation energy of this relaxation is in the range of 0.6-0.7 eV (Table 5.4). The interpretation that this relaxation process is assigned to the movement of polar groups rather than water molecules alone, is driven firstly by the observation of this relaxation already for the dry sample and also by its strong plasticization by water, which is very common in case of secondary relaxations in polymeric materials. The plasticization is stronger for low water fractions,

from the dry sample until the sample of $h_w=0.07$. It is obvious that the trace of the data is moving to lower temperatures more smoothly for further increase of h_w from 0.07 to 0.13. The same applies for the increase of the relaxation strength $\Delta\varepsilon$, shown in Fig. 5.19. These results are in agreement to the ones by TSDC observed for BSA (and various systems), described earlier. In both cases, a saturation of the peak position was observed at water fraction values comparable with the critical values for the completion of the first hydration layer estimated by ESI. The saturation of the plasticization along with the superlinear increase of $\Delta\varepsilon$ at even higher water fractions, which has been also recorded in case of hydrated elastin and collagen by DRS [Gainaru 2009], are in consistency with the scenario that at a water fraction of about $h_w=0.07$ the primary sorption sites of the protein surface (first sorption layer, hydrophilic polar groups) is completed, and clustering of the water molecules at the vicinity of the protein surface sets in, resulting in additional contributions of water molecules themselves within the water clusters (ν process). This scenario has been described in detail in a review by Careri [1998], in case of globular proteins. This is also supported by the values of the fractional exponent $\beta(T)$ of the relaxation of polar groups for BSA-water mixtures of $h_w=0, 0.02, 0.07$ and 0.13 (Table 5.3), which decreases from a value of 0.38 for the dry sample to 0.15 for $h_w=0.13$. This shows that the distribution of relaxation times becomes broader as water clustering increases, resulting in a less homogeneous sample. At the same time, at the hydration level where water clustering sets in, the additional water molecules, in the form of extended clusters, interact locally with the protein surface, so that segmental movement appears in the system, observed dielectrically for water fraction $h_w>0.07$. At low hydration levels (water fractions lower than about $h_w=0.20$), the segmental dynamics as studied by dielectric techniques is decoupled from the glass transition detected by calorimetry (where it is detected for water fractions equal to or higher than $h_w=0.10$), as the former probe mainly electrical polarization processes within the water clusters. By this scenario, it is expected that the acceleration and the increase of relaxation strength of the secondary relaxation of polar groups are being gradually saturated, as additional water molecules contribute to a more global movement of the hydrated system, while the extended water clusters are growing in space with the addition of water, leading to the formation of a percolating cluster of the hydration water [Rupley 1991], and the subsequent covering of the entire protein surface. The formation of this percolating water cluster is accompanied by the saturation of the relaxation process of water molecules themselves in the uncrystallized phase (ν process).

Regarding the percolation threshold, our measurements suggest that it is reached at water fractions of $h_w=0.18$. This was verified in more detail by TSDC, at numerous hydration levels in small steps (Fig. 5.7). This value is also consistent with the hydration range between $h_w=0.13$ and 0.20 where the percolation threshold is detected by dielectric measurements for most globular proteins [Careri 1998]. In Fig. 5.18 the temperature dependence of the ν relaxation of water for the samples of water fractions above the percolating threshold is shown. The trace is identical for all four samples of $h_w=0.18, 0.28, 0.40$ and 0.60 . It must be mentioned at this point that the data seem to exhibit a crossover from one Arrhenius behavior at low temperatures to another Arrhenius one at higher temperatures with higher activation energy, at about -103°C . The position of the data correlates well with the thick line in Fig. 5.18, which has been suggested by Ngai et al. in [Ngai 2011] to be the trace of the ν

relaxation of water. Additionally, the activation energy of these relaxations, which has been calculated taking into account only the points at temperatures lower than the crossover, is in the range of the reported values for the main relaxation of water, at about 0.55 eV (Table 5.4). The comparison of numerous measurements in various water containing systems (including hydrated BSA) has shown that water exhibits a common dynamic behavior, expressed by the relaxation named ν [Shinyashiki 2007, Ngai 2011] with a bottom limit of the relaxation times described by the thick line in Fig. 5.18. Finally, regarding a BSA aqueous solution of higher hydration level than the DRS measurements in this thesis, i.e. $h_w=0.80$ [Shinyashiki 2009], a relaxation (I_α) of significantly lower activation energy of about 0.22 eV, dominates in the temperature-frequency region of the ν relaxation. The trace of I_α coincides with the trace of the low frequency relaxations observed at low h_w values ($h_w=0, 0.02$ in Fig. 5.18) and is attributed to uncrystallized water in [Shinyashiki 2009], while it exhibits similar dielectric strength values to the respective ones of the ν relaxation of the measurements in this thesis ($h_w=0.28, 0.40$ and 0.60). The connection of the ν relaxation to relaxation I_α will be discussed further in chapter 7, considering also results on other hydrated systems.

The corresponding relaxation strength of the ν relaxation is shown in Fig. 5.19, together with that of the local relaxation of polar groups at lower h_w . The values of $\Delta\varepsilon$ for $h_w=0.18$ is in the range of the values obtained for the relaxation of polar groups for $h_w=0.13$, at least in the common temperature range where the two relaxations are observed within the experimental window. This fact supports the assumption that the initial water population, which is involved in the dynamics of the ν relaxation, comes from water molecules interacting with protein polar groups at low hydrations. Further increase of hydration level causes an increase of the dielectric strength, showing that the percolating water cluster, the completion of which is gradually achieved, involves higher amount of water molecules. At this point we should highlight the fact that the temperature dependence of $\Delta\varepsilon$ of the ν relaxation of water for samples $h_w=0.18$ and 0.28 , is characteristic of a secondary relaxation [Ngai 2011], as $\Delta\varepsilon$ increases with temperature. Regarding the samples of $h_w=0.40$ to 0.60 , a saturation of the dielectric strength of the ν relaxation is observed. This is consistent with the result from calorimetry (section 5.4 Fig. 5.6b) concerning the fraction of uncrystallized water in BSA-water mixtures calculated by DSC, which showed that it remained stable to about 20% for water fractions higher than about 30%, which is the critical water fraction for crystallization of water during cooling. Finally, in the case of $h_w=0.40$, the temperature dependence of $\Delta\varepsilon$ in Fig. 5.19, is quite different than in the case of $h_w=0.28$ and 0.60 . In particular, $\Delta\varepsilon$ comparable for all three samples at low temperatures, but is lower for $h_w=0.40$ for $1000/T < 6$. This differentiation will be evaluated in section 5.6.4, concerning the dynamics of excess uncrystallized water and ice.

Finally, considering the interplay between the relaxation of polar groups triggered by water and the ν relaxation of water, we may suggest the following: (i) they are both secondary relaxations, as their relaxation strength increases in general with temperature, (ii) the water population involved in the relaxation of polar groups is a part of the larger one which is involved in the ν relaxation (comparable dielectric strengths for $h_w=0.13$ and 0.18 , see above) and (iii) the ν relaxation, although it is related to the relaxation of polar groups, is in fact a separate mode of water in the protein hydration shell, activated as soon as water clustering sets in while its relaxation time saturates when the percolating water cluster is

formed. This last suggestion, is driven by the fact that the ν relaxation is no more plasticized by further addition of water beyond the percolating threshold, as well as by the fact that its magnitude saturates at water fractions where water crystallizes during cooling, where, in parallel, the formation of the primary hydration shell of the protein is completed [Careri 1998, Sartor 1992]. In [Ngai 2011] the ν relaxation is characterized as a secondary Johari-Golstein (JG) relaxation of water, differing from the JG of simple glass formers, because water molecules can rotate and translate after breaking two hydrogen bonds, like in bulk water.

5.6.4. Excess uncrystallized water and ice

The temperature dependence of relaxation times for the additional relaxations observed for the samples of water $h_w=0.28$ and 0.40 , that is, for the relaxations attributed to ice and the relaxation named w in Figures 5.13, 5.14, and 5.15, together with the ones for the ν relaxation for the same samples and for the α relaxation from Figure 5.16a, are plotted in Fig. 5.20, together with experimental data taken from literature.

In order to assign the rest of the relaxations in Fig. 5.20, we take into account DSC results for the same samples. Particularly, the sample of $h_w=0.28$ is in the hydration range where cold crystallization of water is dominant (at temperatures higher than about -40°C), as crystallization during cooling occurs for water fractions higher than about $h_w=0.30$. The sample of $h_w=0.40$, shows crystallization of water during cooling. By these observations, we may conclude that the w relaxation which was detected for both samples of $h_w=0.28$ and 0.40 , probably originates from contributions of excess water near the protein surface, in the sense that it is not crystallized during cooling. In the same aspect, the data for relaxation $ice2$ and $ice1$ in Fig. 5.20 for the $h_w=0.40$, are interpreted as ice contributions, since they do not appear in the spectra of $h_w=0.28$. Dielectric data of Ice Ih by reference [Johari 1981] are added to Fig. 5.20 for comparison. The trace of Ice Ih at low temperatures seems to correlate with the one of the ν relaxation, while the data of $ice2$, although they follow similar slope, they are located at higher temperatures. This fact is not an inconsistency, as it has been shown in case of various forms of ice (polycrystalline pure ice [Pissis 1981], ice microcrystals dispersed in oil [Pissis 1982] and frozen aqueous solutions [Daoukaki-Diamanti 1984]) that the time scale of the relaxation depends on the concentration of defects in the ice crystals and the peak temperature of the relaxation increases with increasing defect concentration. In the high temperature side of Fig. 5.20, the data corresponding to the $ice1$ relaxation can be seen. Surprisingly, the temperature dependence of the relaxation times of this relaxation follows a Vogel-Tammann-Fulcher-Hesse dependence, at temperatures higher than about -90°C ($1000/T=5.5$). A possible scenario explaining the deviation from the Arrhenius behavior, can be that relaxation $ice1$ describes the motion of structural defects in frozen water clusters of small size, which follow the cooperative movement of the global system. On the other hand, the data of $ice1$ relaxation peak agree very well with the temperature dependence of the time scale of the so-called relaxation of percolating protons observed in hydrated lysozyme [Mazza 2011] which has been assigned to a structural rearrangement of the hydrogen bonding network. This comparison is quite interesting, considering that the protons in hydration water diffuse along the H-bonded network of water molecules adsorbed on the

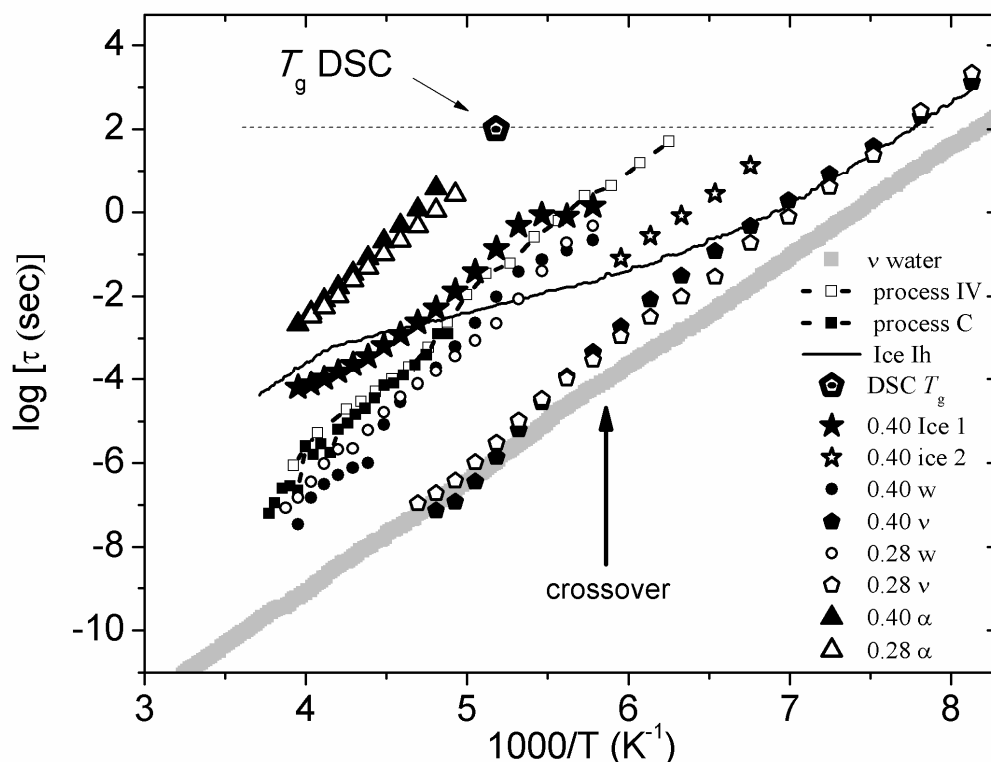


Fig. 5.20 Temperature dependence of the relaxation times for the α relaxation and the relaxations originating mainly from water for a hydrated pellet and a BSA-water solution of $h_w=0.28$ and 0.40 , respectively, i.e. for the ν relaxation of $h_w=0.28$ (open pentagons) and 0.40 (solid pentagons), the w relaxation for $h_w=0.28$ (open small circles) and 0.40 (solid small circles), and relaxations ice 1 (solid stars) and ice 2 (open stars), for a BSA-water solution of $h_w=0.40$. The dotted pentagon shows the T_g of hydrated BSA measured by DSC for $h_w>0.30$ [Panagopoulou 2011b]. The thick solid line shows a bottom limit for the relaxation times of the ν relaxation of water by reference [Ngai 2011]. The solid line shows dielectric response of Ice Ih by reference [Johari 1981]. Lines and squares correspond to the trace of process C (solid) and process IV (open) measured in references [Pagnotta 2010] and [Jansson 2010], respectively.

protein surface in a manner similar to the Grotthuss mechanism for charge transport in ice [Pagnotta 2009]. At temperatures lower than -103°C , where the crossover is observed in case of the ν relaxation, the trace of *ice2* is observed. The relation of the two processes, *ice1* and *ice2*, will be further discussed in what follows in comparison to the results for $h_w=0.60$ and the dielectric strength of the dielectric relaxations (Fig. 5.21) and also in chapter 7.

We turn now our attention to the trace of the w relaxation for $h_w=0.28$ and 0.40 in Fig. 5.20. We recall that the peak of this relaxation could not be clearly discerned in the dielectric loss curves, although it seems that it is essential to fit the data, using a sum of Cole-Cole functions. For that reason, literature data corresponding to relaxations recorded in other hydrated biopolymers are added in Fig. 5.20. A very interesting observation is the fact that the trace of the w relaxation is in quite good accordance to the data for process IV observed in a hydrated myoglobin sample of water fraction $h_w=0.33$, by DRS measurements using insulating thin foils in reference [Jansson 2010], and to the process C observed by the same method in a water-glutathione solution of water fraction $h_w=0.20$ in reference [Pagnotta

2010], and that in both cases the samples showed no crystallization of water during cooling. These processes in both papers were not assigned to any particulate origin. Nevertheless, their existence supports the validity of the points in this work for the w relaxation, at least with respect to the relaxation times. The fact that these processes were recorded for samples at intermediate hydration levels, probably in water fraction region where cold crystallization effects occur, and that they exhibit quite similar temperature dependence of relaxation times, although they are observed in qualitatively different samples, in the sense that hydrated myoglobin in [Jansson 2010] was in the form of a hydrated pellet, like in case of the BSA-water sample of $h_w=0.28$, while the water-glutathione sample in [Pagnotta 2010] was in a form of a solution and the BSA sample of $h_w=0.40$ in the form of a concentrated solution, provide additional support on both, the existence and the validity of the analysis of the w relaxation. The origin of this process is not clear at this point and could be assigned to the layer of molecules adjacent and strongly interacting with the substrate surface. This is the water layer known to have the highest density and slowest translational dynamics compared to the average [Bruni 2011]. Of course, the complexity of the systems studied along with the quality of the results make it difficult to conclude with certainty about the origin of the w relaxation. The possibility that the latter originates to a small amount of “primitive” ice forms or even to protein fluctuations that are enhanced by ice formation (protein cold denaturation) cannot be excluded. The particular relaxation will be further examined in what follows and in chapter 7, in comparison to the results on other hydrated biopolymers.

In order to clarify the picture of the dielectric map, experimental data from Fig. 5.20 are plotted again in Fig. 5.21, together with the results for $h_w=0.60$. In particular, Fig. 5.21A includes, apart from the relaxation times for $h_w=0.60$, two characteristic TSDC thermograms for $h_w=0.40$ and 0.60 (Fig. 5.7) in the upper panel in the plot, together with the characteristic temperatures by TSDC at the equivalent frequency, aiming at direct comparison between the two dielectric techniques. Fig. 5.21B shows a) the temperature dependence of the relaxation times for the w relaxation and the relaxations due to ice and b) the corresponding dielectric strength $\Delta\epsilon$. A first observation in Fig. 5.21A is that process *ice 2* which is detected only for $h_w=0.40$ corresponds to a weak peak detected for the same h_w by TSDC, centered at about -135°C . We recall the assumption made in sections 5.5.1, 5.6.1 that this peak denotes a primitive ice population, a fact which is also supported by DSC (sections 5.4, 5.6.1). Regarding the dielectric strength of *ice 2* it can be seen in Fig. 5.20B that it is quite low when compared to the one of *ice 1* at higher temperatures. Nevertheless, the dielectric strength of *ice 1* decreases abruptly with decreasing temperature, from a value of about $\Delta\epsilon=10^2$, which is the commonly observed dielectric strength of normal ice Ih [Rusiniak 2004], to much lower values approaching the values for *ice 1* (Fig. 5.21Bb)). This fact could explain the discontinuity in the relaxation times observed approximately at the crossover temperature (observed for the v relaxation) which is highlighted in the plot at about -103°C . The picture is different for $h_w=0.60$. In this case only one relaxation due to ice (*ice1*) is detected in the entire temperature range and the temperature dependence of its relaxation time is continuous in Fig. 5.21 A. The extrapolation of the data at the equivalent frequency of TSDC leads to the

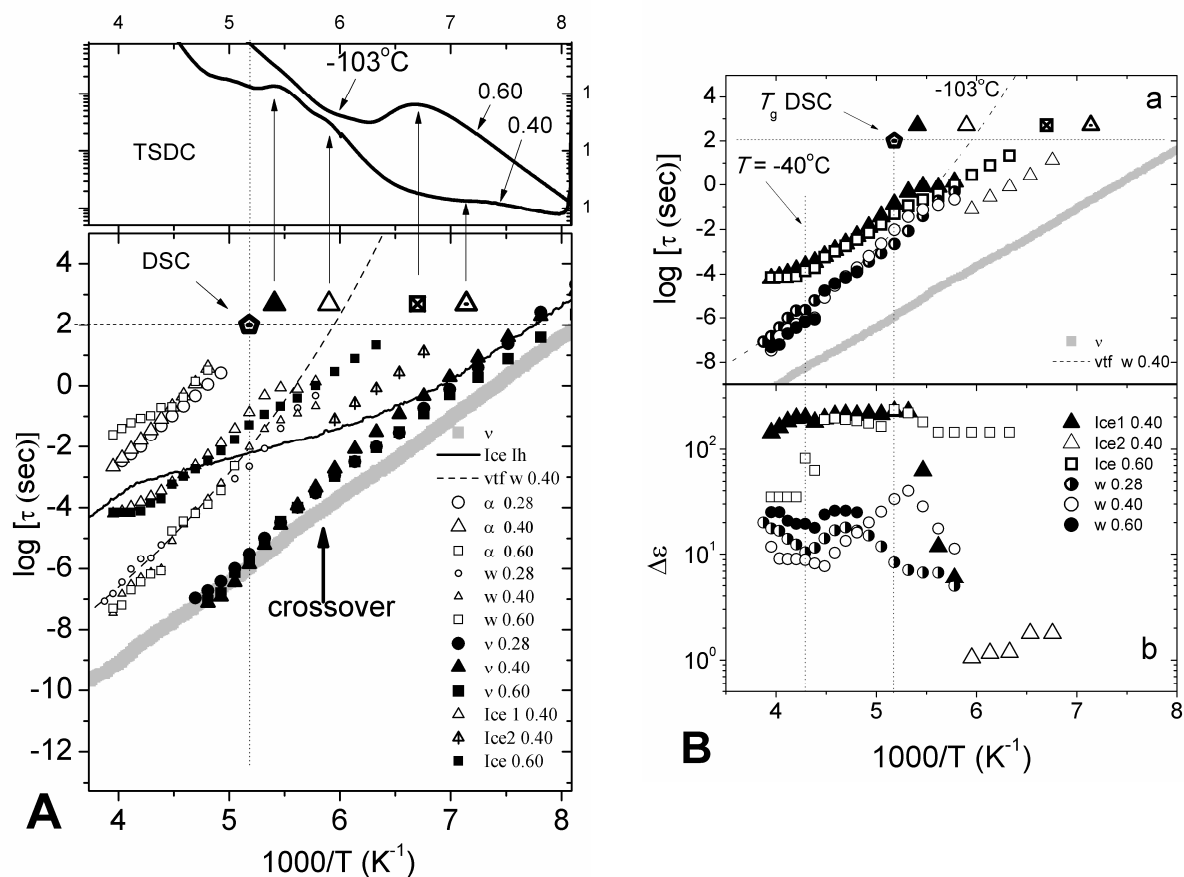
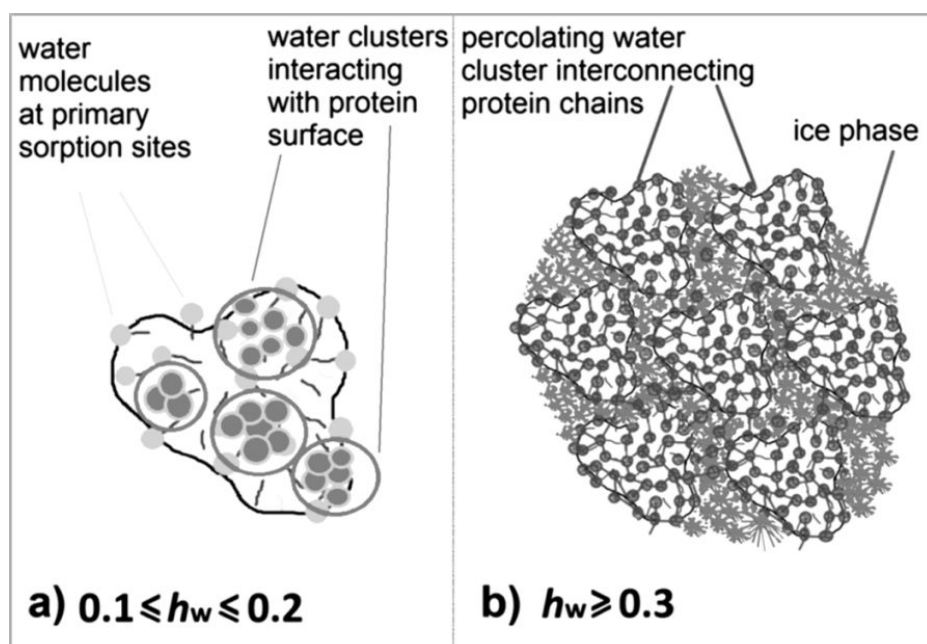


Fig.5.21 A) A reproduction of Fig. 5.20 including the temperature dependence of the relaxation times for the relaxations recorded for a BSA solution of $h_w=0.60$, namely, the α relaxation (open squares), $ice1$ (solid squares), the w relaxation (small open squares) and the ν relaxation (large solid squares). The upper panel shows the TSDC thermograms versus inverse temperature for $h_w=0.40$ and 0.60 . The dashed line through the experimental data is the VTF fit of the data of the w relaxation for $h_w=0.40$ in the temperature range between the T_g of the hydrated system and the homogeneous nucleation temperature ($-80^\circ\text{C}<T<-40^\circ\text{C}$) B) a) Temperature dependence of the relaxation times and b) corresponding dielectric strength, $\Delta\epsilon$, for the w , $ice1,ice2$ relaxations at water fractions $h_w=0.28, 0.40$ and 0.60 . The T_g of the hydrated system and the homogeneous nucleation temperature $T=-40^\circ\text{C}$ are highlighted in the plot by vertical dotted lines. The dashed line through the experimental data is the VTF fit of the data of the w relaxation for $h_w=0.40$ in the temperature range between the T_g of the hydrated system and the homogeneous nucleation temperature ($-80^\circ\text{C}<T<-40^\circ$).

peak centered at about -125°C (upper panel), which has already been attributed to the relaxation in bulk ice (sections 5.4, 5.6.1). The dielectric strength of $ice1$ for $h_w=0.60$ at low temperatures is now comparable to that of bulk ice. Coming back to the w relaxation, it is seen in Fig. 5.21B that its trace is comparable for all, $h_w=0.28, 0.40$ and 0.60 . Its dielectric strength exhibits a non-linear temperature dependence. In particular, the temperature dependence of the w relaxation changes for all of the samples at about $T=-40^\circ\text{C}$, i.e. the homogeneous nucleation temperature, which is highlighted in the plot by a vertical dotted line. In addition, its strength is enhanced for the sample of $h_w=0.40$ in the temperature range

of about $5 < 1000/T < 6$ (Fig. 5.21.Bb). This fact, in combination to the fact that the dielectric strength of the ν relaxation for $h_w=0.40$ was suppressed in the same temperature interval (see Fig. 5.19 and comments in section 5.6.3), implies that the populations of the ν and w relaxations are probably associated, e.g. belonging both to the uncrystallized water fraction in the material. Finally, assuming that the w relaxation corresponds to internal uncrystallized water molecules, a VTF curve is fitted to the experimental data for $h_w=0.40$, in the temperature range between the T_g of the hydrated system and the homogeneous nucleation temperature ($-80^\circ\text{C} < T < -40^\circ\text{C}$). The VTF curve reaches the equivalent relaxation time of DSC ($\tau=100\text{s}$) at $T=-103^\circ\text{C}$, in accordance to the maxima of the peak detected by TSDC for both $h_w=0.40$ and 0.60 at the same temperature. This result would place the T_g of confined internal water at about $T=-103^\circ\text{C}$ and probes us to attribute the phase separation observed by TSDC (see discussion in section 5.6.2) to the formation of a separate phase of internal confined water.

Finally, we present an illustration (Scheme 5.1) regarding the picture deduced from the present study on the glass transition of the BSA-water system. In Scheme 5.1 the representation refers to two water fraction regions which show different behaviour with respect to the glass transition of the system, according to the experimental results of this study. Scheme 5.1a refers to water fractions in the region $0.1 \leq h_w \leq 0.2$. Within this water fraction region, no crystallization of water occurs, while a glass transition step is detected by calorimetry. Dielectric techniques show also a related relaxation process. Here, a single BSA molecule is shown. The red and pink lines correspond to more and less hydrophilic aminoacid residues, respectively. Water molecules attached to primary sorption sites (light blue spheres) are shown as dispersed molecules on the protein surface. Some domains of the protein surface are covered by extended water clusters (bunch of dark blue spheres indicated on the plot), which interact with the protein chains and finally form a percolating water cluster. The combined motion of protein chains and water molecules organized in the water clusters is detected as glass transition by DSC, and its magnitude increases with increasing water fraction, due to gradual swelling of the protein and formation of additional water clusters. Dielectric techniques in this water fraction region probe mainly electrical polarization processes within the water clusters. The segmental relaxation processes detected by DSC and dielectric methods are decoupled from each other in the temperature domain, in the sense that dielectric relaxation occurs at lower temperature than the calorimetric glass transition. Scheme 5.1b refers to water fractions in the region $h_w \geq 0.3$. In this water fraction region, the creation of a separate water phase (ice phase) occurs and the plasticization of the segmental processes is terminated. In Scheme 5.1b a group of BSA molecules is shown. In this water fraction range hydration water molecules have already formed a percolating water cluster (dark blue spheres), interconnecting protein chains. DSC and dielectric techniques detect similar segmental dynamics, that is, combined motion of BSA chains and uncrystallized water molecules, in fully swollen protein. In addition, dielectric techniques detect a slightly faster relaxation process which might originate from a second class of uncrystallized water. The specific features of this new form of organization of uncrystallized water are not yet clarified.



Scheme 5.1

Illustration showing the picture deduced from the present study on the glassy transition of the BSA-water system. a) $0.1 \leq h_w \leq 0.2$, a single BSA molecule is shown. Red and pink lines correspond to more and less hydrophilic polar groups of the protein surface, respectively. Light blue spheres correspond to water molecules attached to primary sorption sites. Dark blue spheres correspond to water clusters on the protein surface. b) $h_w \geq 0.3$, a percolating water cluster (dark blue spheres) interconnects protein chains, while a separate phase of crystalline water (ice) is formed. (color version online [Panagopoulou 2011b])

5.6.5. Conclusions

Glass transition and dynamics of BSA-water mixtures over extreme ranges of composition were studied by thermal and dielectric techniques in comparison to equilibrium water sorption isotherms and were discussed in terms of critical water contents, distinct water populations, crystallization effects of water and the mechanisms by which these factors affect protein structure. Several critical water contents/fractions were estimated: i) $h_m=0.073$ (grams of water per grams of dry protein) for the primary hydration water at ambient conditions (corresponding to 270 out of 607 aminoacid residues in BSA molecule), ii) about $h_d=0.25$ for the onset of significant water clustering and the appearance of cold crystallization of water, iii) $h_w=0.30$ as the onset for crystallization of water during cooling and iv) about $h_w=0.45$ for the formation of bulk ice. The main water populations identified are: A) uncrystallized water of two forms: i) primary hydration water, forming the primary hydration shell, in the range of $h_d = 0.2-0.4$, ii) secondary hydration water forming the secondary hydration shell, or 'internal' water within small openings of the protein structure, in the range of $h_d = 0.4-0.7$, and B) one population of water in the crystal phase (bulk ice crystals). The fraction of uncrystallized water with respect to the total mass of the hydrated protein was found to be stable in the range of 0.21-0.25, for hydration levels where

crystallization effects are present. A rearrangement of the protein structure was concluded to occur at each water content where swelling of the protein seems to play an important role. Several dielectric relaxations are observed by the dielectric TSDC and DRS techniques, in good agreement to each other.

(i) The α relaxation associated with the glass transition of the hydrated system was observed by DRS for water fractions $h_w \geq 0.07$. A strong plasticization by water was observed until a water fraction $h_w = 0.28$. The plasticization stops at higher water fractions, that is, at water fractions higher than the critical water fraction for crystallization of water during cooling (as measured by calorimetry).

(ii) The main relaxation of hydration water was followed over the water composition range of the measurements. It was found that at low water fractions, hydration water triggers a secondary relaxation of small polar groups on the protein surface of an average activation energy value of $E_{act} = 0.6$ eV, which was detected also for the dry sample. A plasticisation of the relaxation of polar groups was detected until a water fraction $h_w = 0.13$. The dielectric strength of the corresponding relaxation was found to increase in general with water content. At higher water fractions, and, specifically, at water fractions $h_w \geq 0.18$, which corresponds to the water fraction for the formation of a percolating conductive cluster, the position of the ν relaxation of water saturates in the Arrhenius diagram and is described by an Arrhenius law with an activation energy of about 0.55 eV. Additionally, the data imply the existence of a crossover at about -103°C . Its dielectric strength increases initially and then saturates at water fractions $h_w > 0.28$. Our results support the claim that the ν relaxation is the secondary Johari-Goldstein relaxation of water, similar to that in bulk water, in the sense that water molecules are able to rotate and translate.

(iii) A relaxation denoted as w is observed for water fractions $h_w = 0.28, 0.40$ and 0.60 . It is suggested that this relaxation originates from excess water, in the sense that it does not crystallize during cooling. It has been found that the time scale of the w relaxation is comparable to the traces of two unknown relaxations observed on other hydrated biopolymers. A possible glass transition temperature $T_g = -103^\circ\text{C}$ is calculated for confined internal water (w)

(iv) Two dielectric relaxations (in different temperature intervals) attributed to ice-like water structures were detected for the sample of $h_w = 0.40$ and a single one for 0.60 .

6. Fibrous Protein Elastin

6.1 Introduction

Elastin is a hydrophobic, insoluble protein which is a main part of several connective tissues such as lung, arteries and skin. It exhibits quite complex structure and hydration dependent functional properties, which are not yet clearly understood, despite the extensive experimental and theoretical studies throughout the previous decades [Debelle 1999]. A variety of structural studies have demonstrated that the elastin molecule consists of tropoelastin subunits physically crosslinked by the enzyme lysyl oxidase [Sandberg 1984]. By this way a three dimensional network is formed, which obtains different conformational states depending on the hydration level and the stress-strain applied. It has been viewed as a random network devoid of any organization [Hoeve 1974], constituted of an aggregate of tropoelastin globules [Partridge 1969], considered as a regular arrangement of successive β turns forming a β spiral [Urry 1984] or composed of isolated and dynamic β turns providing classical entropic elasticity [Tamburro 2003, Tamburro 2006]. The dynamical entropy of the system significantly decreases in the stretched state, and the classical theory of rubber elasticity could be applied to the hydrophobic domains [Li 2002, Mackay 2005]. The biological function of elastin is manifested mainly through the mechanism of elasticity, which depends inextricably on a complex interaction with the solvent, i.e. hydration water. Elastin is elastic only when hydrated [Partridge 1955]. In thermal analysis, elastin undergoes a glass transition phenomenon, dependent on hydration. The glass transition temperature varies from 200°C in the freeze-dried state to approximately 20°C in physiological conditions) and is associated with the amorphous phase [Samouillan 2000, Hoeve 1980, Kakinaya 1975]. Another well known characteristic of elastin is that it undergoes an inverse temperature transition at approximately 20-40°C, a process that results in a reduction of the protein radius of gyration, expulsion of water, and formation of a complex network of hydrogen bonds [Urry 1988]. Recent studies have shown also that this inverse temperature transition depends on the aminoacid sequence in the chains, pointing out that the structuring of water in elastin exists as an inhomogeneous distribution [Ribeiro 2009]. Studies by deuterium Double Quantum filtered NMR [Sun 2010] indicated an increase in order in the surrounding water molecules of the hydration shell in elastin, upon increasing the temperature above temperatures characteristic of the inverse temperature transition. Furthermore, results obtained by T_2 - T_2 exchange NMR measurements, provide information on the exchange rate of distinct hydration water populations (water inside fibers, water on the fiber surface, water between fibers and more free water) [Sun 2011]. Recent dielectric studies on hydrated elastin powders at subzero temperatures and at different levels of

hydration in the hydrated and immersed state, have shown the existence of three dielectric relaxations connected to hydration water [Samouillan 2011]. Two relaxations (β_1 , β_2) are attributed to distinct water populations of the hydration shell, and a third slower relaxation (p_1) is attributed to intrafibrillar water clusters (water between fibers). Finally, dielectric measurements on hydrated elastin samples at various hydration levels showed that the main dielectric relaxation of uncrystallized water in elastin (see chapter 2, section 2.2) exhibits strong hydration dependence and includes contributions from protein segments [Gainaru 2009].

6.2 Materials and Sample Preparation

Elastin from bovine neck ligament in form of powder (**Sigma E1625**), was purchased from Sigma -Aldrich and used as received. Water with $10\mu\text{S}/\text{cm}$ conductivity was used in the sample hydration procedure.

DSC, TSDC and DRS measurements, to be described in the following, were performed at various levels of water content h , calculated on the dry and the wet basis, h_d and h_w , respectively (see also chapter 5, section 5.2, eq.(5.1),(5.2),(5.3)).

For water ESI measurements solid samples were used, prepared by compressing an amount of protein powder ~ 100 mg to a cylindrical pellet of thickness 0.6-0.8 mm and diameter about 14 mm. ESI measurements were performed at room temperature by exposing the samples to various controlled water vapor atmospheres in sealed jars above saturated aqueous salt solutions [Greenspan 1977]. By this way, the water activity a_w (relative humidity, rh) was systematically varied between about 0.02 and 0.98. The attainment of equilibrium and final weights were determined via continuous monitoring of sample weight using a Bosch SAE 200 balance with 10^{-4} g sensitivity (see also chapter 4, section 4.1, 4.1.1).

DSC measurements were performed in nitrogen atmosphere in the temperature range from -120 to 120°C using a TA Q200 series DSC instrument. Solid compressed samples were hydrated to the required degree by a) equilibration above open water in sealed jars (100% rh) for a selected period of time or by b) immersion in deionized water, both followed by a subsequent equilibration in sealed boxes for at least 1 day. The hydrated samples, of an average mass in the range of 10-20mg, were closed in Tzero hermetic aluminium pans. The water loss by this way during the measurement is eliminated. Cooling and heating rates were fixed at $10^\circ\text{C}/\text{min}$ (see also chapter 4, section 4.2, 4.2.1).

Samples for dielectric (TSDC and DRS) measurements were in the form of solid compressed pellets, similar to those used for ESI measurements. Solid samples were hydrated to the required degree by a) equilibration above open water in sealed jars (100% rh) for a selected period of time or by b) immersion in deionized water, both followed by a subsequent equilibration in sealed boxes for at least 1 day. For dielectric measurements, the hydrated samples were placed between two electrodes forming a cylindrical capacitor 12mm in diameter (see also chapter 4, sections 4.3, 4.3.1 and 4.4, 4.4.1).

6.3 Elastin-ESI

Results of water sorption-desorption measurements are shown in Fig. 6.1: water content h_d (g of water per g of dry protein) against water activity α_w at room temperature (25°C) for an elastin sample (sorption, desorption1, solid and open squares respectively). The sorption-desorption procedure for the first sample took place successively. Another set of desorption points is added to the diagram, which correspond to a sample which underwent only the desorption procedure (desorption2), in order to compare in terms of aging (the second sample was prepared approximately 5 months later than the first one and was not subjected to the same hydrating procedure over time at lower relative humidity values, i.e. the sorption process). Starting with the sorption data, as it can be seen in Fig. 6.1, an initial linear region for water activity values from about 0.1 to 0.7 is observed, followed by a departure from linear behaviour for $\alpha_w > 0.7$, which is explained in terms of clustering of water molecules (see chapter 4, section 4.1).

The GAB equation (eq. (4.2)) was fitted to the experimental data. The GAB fit is satisfactory (see the solid line in Fig 6.1). For h_m , which corresponds to the water content of water molecules attached to primary hydration sites, a value of 0.067 ± 0.003 was obtained for elastin. Another critical water content is estimated by the data, although less unequivocal, namely the water content where significant clustering occurs and the sorption data deviate strongly from the roughly linear behaviour in the middle region of water activities (see chapter 4, section 4.1). That is at around $h_d = 0.13$ (equal to $h_w = 0.12$), corresponding to water activities around 0.7. Regarding the desorption data, a pronounced hysteresis loop (see chapter 4, section 4.1) is observed in the water activity range of about 0.2-0.8. Within this region, the water content of the sample is higher at desorption when compared to the respective one at sorption at the same α_w value. Finally, the desorption experimental data coincide between the two different samples (difference in preparation date and hydrating procedure).

6.4 Elastin-DSC

DSC cooling and heating scans, both at a rate of 10°C/min, were recorded for hydrated elastin pellets at various hydration levels. The maximum water uptake when the hydration is achieved through vapor adsorption was determined in section 6.3 to be $h_w = 0.23$. For DSC measurements the hydration of the samples of higher water fraction ($h_w > 0.23$) was achieved by immersion in deionized water (see section 6.2). The water fraction values h_w of all the samples measured, along with the corresponding water content values h_d , are listed in Table 6.1 for reference.

Two successive cooling and heating cycles were performed, starting at 40°C, cooling first to -120°C, then heating to 80°C, then cooling again to -120°C and finally heating again to 120°C or to 80°C, for the hydrated samples through adsorption or immersion, respectively. The two cycles were performed for all the samples studied, except for the dry elastin pellet, where a single cooling and heating cycle was performed (cooling from 40°C to -120°C, heating from -120 °C to 240 °C). Cooling and heating thermograms recorded on several

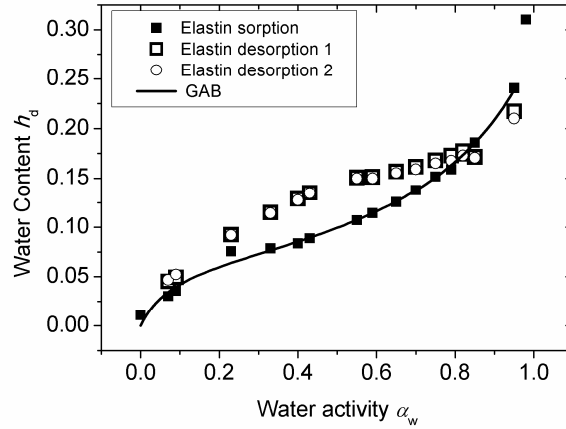


Fig. 6.1 Water content h_d against water activity α_w at 25 °C for an elastin sample, during sorption and successive desorption procedures. Additionally, points during desorption are added for an elastin pellet which underwent only the desorption procedure, for comparison reasons in terms of aging. Points are experimental data and the solid line is the fit of GAB equation (eq. (4.2)) to the sorption data.

Table 6.1 Water fraction h_w , water content h_d , approximation of water molecules per tropoelastin molecule, n , glass transition temperature, T_g and heat capacity step, ΔC_p , for hydrated elastin pellets.

h_w	h_d	n	T_g	ΔC_p
			(°C)	(J/g)
0	0	0	191	0.368
0.100	0.111	444	84	0.320
0.125	0.143	572	60	0.446
0.130	0.149	596	63	0.692
0.187	0.230	920	40	0.835
0.224	0.287	1148	29	0.876
0.320	0.471	1884	-	-
0.390	0.639	2556	-	-
0.450	0.818	3272	-	-
0.530	1.13	4520	-	-

elastin pellets, characterized by water fraction h_w , are shown in Fig. 6.2a and 6.2b, respectively. The heating thermograms for the samples hydrated through vapor adsorption are shown in Fig. 6.3, for clarity reasons.

Elastin-DSC-Hydration through vapor adsorption($0 \leq h_w \leq 0.224$)-Glass Transition

Heating thermograms recorded on several elastin pellets, hydrated through vapor adsorption, characterized by water fraction h_w , are shown in Fig. 6.3. In the corresponding cooling thermograms (Fig. 6.2a) it becomes clear that crystallization effects of water during cooling are absent for the samples hydrated through vapor adsorption studied here, i.e. for $h_w \leq 0.224$. Additionally, the thermograms are identical during the cooling scans of the two successive cycles. The glass transition step of the system, which is observed in the cooling scans for some samples, will be better observed in the heating thermograms.

In Fig.6.3, starting with the dry sample, an intense heat capacity step is observed in the high temperature region. This step is associated with the glass transition of dry elastin, in agreement with literature data [Samouillan 2000]. The evolution of the heating curve is not smooth in the temperature region of the glass transition step for the dry sample, on the contrary it exhibits implications of exothermic broad peaks at temperatures lower and higher than the glass transition temperature T_g . A broad and weak endothermic peak centred at about 110°C is probably due to the evaporation of residual water and has been observed also in previous studies [Samouillan 2000]. The complex dynamics of dry elastin at those high temperatures is out of the scope of this thesis, and the dry sample is studied by DSC only for reference, with respect to the glass transition temperature.

In the case of the hydrated samples in Fig 6.3, two cycles of cooling and heating were performed, as explained in the first paragraph of this section (section 6.4). Starting at low temperatures ($T < 20^\circ\text{C}$), the first observation is that no crystallization of water during heating (cold crystallization) occurs and that the curves coincide for the successive cycles. Moving to higher temperatures, the glass transition step can be seen and the picture is different for the two successive cycles. The first heating scan (solid lines) is performed to 120°C for $h_w = 0.1$, and to 80°C for the higher water fraction values. The hermetic pans used for the measurements prevent water loss from the samples. Nevertheless, the heating during the first scan was limited to 80°C, so that evaporation of water is avoided during the first scan. The exception in the case of $h_w = 0.1$, is because this hydration level is considered to be the most stable (in the sense that it is the water fraction at room temperature and ambient conditions), but also because the T_g for this h_w is higher and the first heating scan is intended to extent at least just over the T_g . In the thermograms of the first scan a T_g step can be seen. For $h_w = 0.1$, the T_g step follows after three successive exo-endo-exothermic peaks, at lower temperatures. For $h_w = 0.125$ and 0.13 two successive exo-endothermic peaks are recorded in the temperature region of the T_g . For $h_w = 0.187$ a single endothermic peak is observed in the T_g region. Finally, for $h_w = 0.224$, a clear glass transition step can be seen. During the second heating scan (dashed lines), those complex exothermic and endothermic peaks near or at the T_g , disappear for all the samples, except of the one of $h_w = 0.1$, as it can be seen in Fig. 6.3. For $h_w = 0.1$ the curve is simplified in the second scan, but still an exothermic peak is observed at temperatures lower than T_g . The origin of those complex peaks will be further discussed in the following paragraphs.

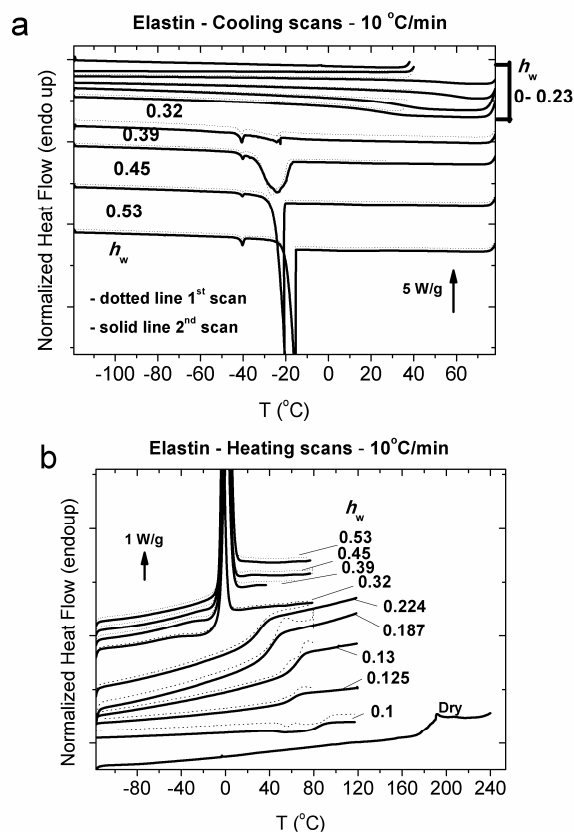


Fig. 6.2 Normalized heat flow during **a)** cooling and **b)** heating for two successive experimental cycles (dotted and solid lines in (a) and (b)), both at 10°C/min, in hydrated elastin pellets at different water fractions h_w indicated on the plot. The samples of $0 \leq h_w \leq 0.224$ have been hydrated through vapor adsorption, while the samples of $0.32 \leq h_w \leq 0.53$ have been hydrated through immersion in deionized water.

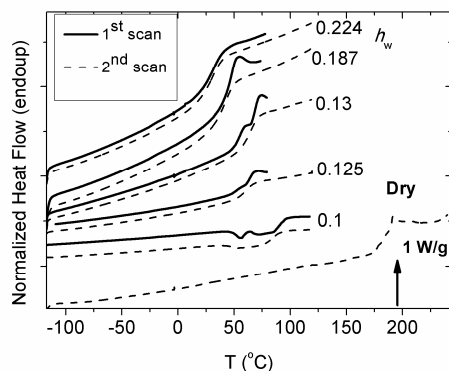


Fig. 6.3 Normalized heat flow during heating, for two successive experimental cycles, both at 10°C/min, in hydrated elastin pellets (hydrated through vapor adsorption) at different water fractions h_w indicated on the plot. A single scan is recorded for the dry sample.

The glass transition of the hydrated system has been analyzed as it was recorded during the second heating scan. The T_g and heat capacity step (ΔC_p) values for the dry sample and the hydrated pellets during the second heating scan are listed in Table 6.1, together with the approximation of water molecules per tropoelastin molecule, n , assuming that the average molecular weight of tropoelastin is 72,000 and that of water 18. The main observation is the plasticizing effect of water on the glass transition of the dry protein. The T_g values reduce from the value 191°C for dry elastin to 29°C for $h_w=0.224$. This plasticization trend is in accordance with results from literature [Van der Sman 2012], where it was found that this trend is very well described by the Flory-Huggins theory for numerous meat proteins including elastin and it was suggested that the thermodynamics in that case may explain the phenomena, without the need for inducing parameters such as bound water. In Table 6.1, the step of the specific heat, ΔC_p , for all the samples is reported. For the dry sample, a value of $\Delta C_p=0.368$ J/g is recorded, lower than but comparable to values given in literature, i.e. 0.45 J/g for dry elastin [Samouillan 2000]. The initial increase of water fraction from the dry sample to the one of $h_w=0.10$, which is actually the water fraction of the protein at room conditions, causes a decrease in ΔC_p , from 0.368 to 0.320 J/g, while further water fraction increase, causes an increase of the ΔC_p as well. The initial decrease is not obviously expected. Probably, in the case of hydrated elastin, it is associated with the complex elastic properties of the elastin molecule. In particular, it is known that the elastic behavior of elastin is highly water dependent and elasticity exists only in the hydrated state [Partridge 1955]. This probes to attribute the initial decrease of ΔC_p to the fact that the dry sample is qualitatively different from the partially hydrated ones. In particular, attenuated total reflectance Fourier transform infrared spectroscopy (ATR-FTIR) measurements on elastin-like polypeptides have shown that the inverse temperature transition is accompanied by a decrease of the β spiral structure and a parallel creation of β sheets, at high temperatures above 43°C [Serrano 2007], while simulation studies have shown that the intensity of the cooperative dynamics in elastin increases with the increase of β spiral intrinsic strands, which is also observed in experimental data [Rossmmeisl 2004]. These findings are in agreement with the reduction in ΔC_p observed in the present study. Nevertheless, the elasticity of elastin and its connection to the glass transition of the hydrated system in detail is out of the scope of this thesis. Another observation that should be stressed at this point, is the fact that the increase in ΔC_p is relatively high (with respect to the h_w increase) when increasing the water fraction from $h_w=0.125$ to 0.13 (0.446 to 0.692 J/g, respectively, in Table 6.1). Recalling that the water fraction value $h_w=0.12$ is found to be the onset of significant water clustering by ESI, it may be assumed that uncrystallized water molecules participating in clusters, are those which mainly contribute to the glass transition of the hydrated system, by effecting the molecules attached to primary hydration sites. This assumption is in agreement with a similar conclusion drawn for the globular protein BSA [section 5.5, Panagopoulou 2011b] and could be of high significance for application in cryoprotection and pharmaceuticals.

In this work, the glass transition has been recorded during two successive scans and an overshoot over the glass transition step was recorded in the first scan, which disappears during the second scan. This overshoot may be associated with physical aging, like in the case of synthetic polymers, where disruption of physical bonds formed during the slow

rearrangement of the glassy material would cause the enthalpic relaxation [Samouillan 2000]. This overshoot has been already observed in DSC measurements on dry elastin [Samouillan 2000]. In this work, the overshoot becomes more and more pronounced as the water fraction of the hydrated pellets increases, and so the glass transition temperature (T_g) of the system moves to lower temperatures near RT. This can be seen in Fig. 6.3 for $h_w=0.10$, 0.125, 0.13 and 0.187. An exception, is found for the sample of the highest h_w studied here, i.e. for $h_w=0.224$, where the overshoot becomes really smooth. The exception observed for the highest h_w value ($h_w=0.224$) may be attributed, either to the fact that the T_g in that case is comparable to RT (so the sample is stored actually not at higher temperature but at the actual T_g or lower), or to the possibility that the inverse temperature transition, which is expected to occur in that particular temperature region, affects the diffusive dynamics of water. At this point, another factor which differentiates the sample of $h_w=0.224$ should be mentioned. In Table 6.1, the number of water molecules per tropoelastin molecule has been calculated. Having in mind that the number of residues of the tropoelastin is about 800 [Urry 2002], it can be seen in Table 6.1 that the number of water molecules per tropoelastin molecule n are 920 for $h_w=0.187$ and 1148 for $h_w=0.224$. By this it is obvious that in the case of the highest hydration level, the number of water molecules exceeds the number of aminoacid residues, by a factor of about 1.4, so the excess water molecules that are not directly bound to aminoacid residues becomes significant. This may be the reason why the diffusion of water in that case is more rapid and, consequently the hysteresis loop is absent (Fig. 6.1). Of course, these assumptions need to be verified with additional experimental studies.

Finally, some additional phenomena, apart from the enthalpic overshoot, were recorded by DSC in the heating thermograms. These additional peaks, were described earlier. They appear only for the samples of $h_w=0.1$, 0.125 and 0.13, and are located at temperatures close to about 50°C. Those peaks disappear in the second scan for the samples of $h_w=0.125$ and 0.13, while for $h_w=0.10$ some peaks disappear but a broad exothermic peak remains at temperatures lower than the glass transition, in the temperature range of about 30-50°C. Possibly, the observed phenomena are connected to the inverse temperature transition (see introduction in this chapter) of the elastin molecule. Those phenomena are not studied in detail in this thesis. Modulated DSC measurements would be very helpful to study such phenomena in future work.

Elastin-DSC-Hydration through immersion in deionized water ($0.32 \leq h_w \leq 0.53$) - Crystallization and melting of water

In Fig. 6.2a and 6.2b the crystallization and melting events of water are clearly observed in the case of the immersed samples. The thermograms corresponding to lower hydration levels (hydration through vapor adsorption) are also shown for comparison. In Fig. 6.2a the first water fraction for which crystallization of water occurs during cooling is $h_w=0.32$. For this h_w value two weak, but clearly distinct crystallization peaks of water are detected, centered at about -20 and -40°C, respectively. The first one, which exhibits a crystallization temperature, $T_c = -20^\circ\text{C}$, increases in magnitude with water fraction increase for $h_w=0.38$, 0.45 and 0.53 and the corresponding T_c slightly increases, more clearly for $h_w=0.53$. The second peak, with $T_c = -40^\circ\text{C}$, is maintained at higher h_w , but its magnitude and

position remain almost stable, independently of water fraction. The results suggest that there are two distinct populations of crystallizable water in the immersed samples. The fact that the second peak does not increase in magnitude with water fraction increase, along with the relatively low T_c observed, suggests that it may correspond to the crystallization of confined water molecules within the protein structure. In Fig. 6.2b the melting of water is observed for all of the immersed samples, exhibiting a single melting peak of a melting temperature $T_m \approx 0^\circ\text{C}$, resembling the melting temperature of bulk water. A broad exothermic peak is observed for $h_w=0.32$ during heating, centered at about $T_c = -20^\circ\text{C}$. This peak corresponds to cold crystallization of water during heating. Analogous crystallization peaks are also observed at higher water fractions, i.e. $h_w=0.39$ and 0.45 , with increased T_c and reduced intensity, while the cold crystallization is eliminated at $h_w=0.53$. At this point it should be mentioned that the heat capacity step which is associated with the glass transition of the hydrated system is probably "hidden" underneath the melting peaks of all of the immersed samples, a fact which is suggested by the observed relative difference in the position of the baseline of the thermograms at temperatures lower and higher than the melting temperature in Fig. 6.2b. For this reason, the analysis of the glass transition could not be done for the immersed samples, and there is no possibility for calculated values to be listed in Table 6.1, like in the case of the samples of lower h_w . Modulated DSC measurements are essential in order to observe the transition. In the present study a main assumption is that the estimated T_g values (i.e. in the range from -10 to 20°C in Fig. 6.2b according to the baseline difference) are in agreement with literature reported T_g values of 20°C in physiological conditions [Hoeve 1980, Kakinaya 1975].

Elastin- DSC -Uncrystallized water

The crystallization and melting enthalpies of water (ΔH_{cr} , ΔH_m , respectively) have been calculated by the crystallization and melting peaks in the thermograms in Fig. 6.2, by the method which is described in section 5.4 for the globular protein BSA (see also chapter 4, section 4.1). For elastin, the fraction of uncrystallized water has been calculated also by the crystallization peaks during cooling, for comparison reasons. The fractions of elastin, uncrystallized water (Ucw) and crystallized water (Crw), for the entire hydration range studied, are shown in the composition diagrams of Fig. 6.4a and 6.4b, against h_w , as calculated from cooling and heating, respectively. By this way it becomes clear that the fraction of Ucw in Fig. 6.4a corresponds to water molecules which remain uncrystallized during cooling, including the fraction of water molecules which crystallize during heating (cold crystallization). On the other hand, Ucw in Fig. 6.4b corresponds to the fraction of water which remains uncrystallized during both, cooling and heating. The main observation is that the fraction of Ucw remains stable in the high hydration range to a value of about $h_w=0.24$ or 0.18 , in Fig.6.4a and 6.4b, respectively. In addition, the fraction of Ucw is significantly enhanced for $h_w=0.32$, in both cases.

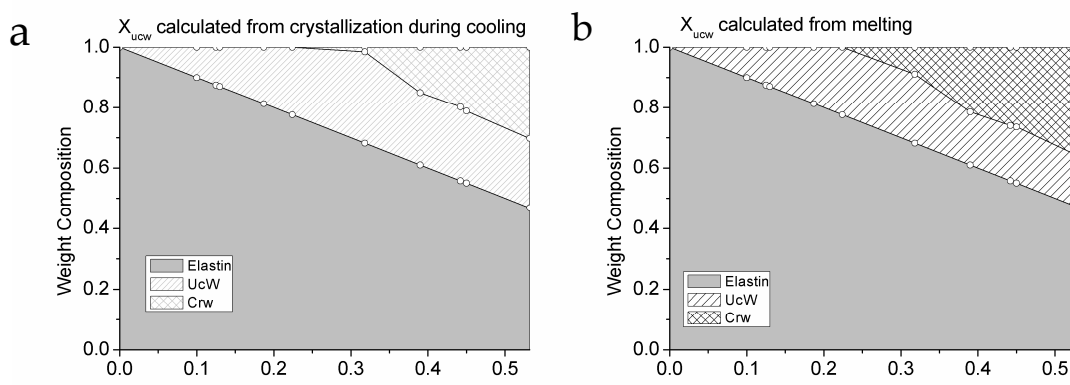


Fig. 6.4 Composition diagrams for the hydrated elastin pellets, showing the fractions of dry protein, crystallized and uncrystallized water in the mixture, against water fraction h_w . The fraction of uncrystallized water, X_{ucw} , has been calculated **a)** from the crystallization peak enthalpy during cooling and **b)** from the melting enthalpy during heating, for comparison.

6.5 Elastin-Dielectric Measurements

A major conclusion which derives from ESI and DSC results, is the fact that no crystallization of water occurs in the hydrated elastin pellets in the water fraction range $0 \leq h_w < 0.23$. The value $h_w = 0.23$ is the maximum water uptake for the hydrated pellets, if they are hydrated in a vapor atmosphere at RT. By this fact it becomes clear that in this hydration range only uncrystallized water is associated with the observed dynamics. For that reason, the results will be described separately for the two cases, i.e. for samples hydrated through vapor adsorption and for immersed samples, two categories which have been already used in the previous section (6.4) regarding the DSC results.

6.5.1 Elastin-TSDC Results

Elastin-TSDC-Hydration through vapor adsorption ($0 < h_w \leq 0.214$)

Two series of TSDC measurements on hydrated elastin pellets, with polarization temperatures $T_p = -20$ and 0°C , were recorded successively for each sample. Fig. 6.5a shows TSDC thermograms with $T_p = -20^\circ\text{C}$, in the temperature range from -150 to 20°C for several hydrated elastin pellets of water fraction h_w indicated on the plot. The TSDC thermograms have been normalized to the same thickness (polarizing field) and the same surface area of the samples. Thus, results for different compositions can be compared to each other not only with respect to the temperature position of the peaks (time scale of the corresponding relaxations), but also with respect to their magnitude (dielectric strength of the corresponding relaxations). Starting at low h_w and low temperatures, a relaxation peak is seen for the almost dry sample (sample (1), $h_w = 0.008$, residual water), centered at about -115°C . This peak is attributed to the local rearrangement of polar groups of the protein surface, triggered by hydration water like in the case of hydrated globular proteins lysozyme [Panagopoulou 2011a] and BSA [Panagopoulou 2011b] (see also chapter 5, section 5.5, 5.5.1). Moving on to higher water fractions, the corresponding peak is moving to lower

temperatures, and generally increases in magnitude. As it will be confirmed by DRS measurements in section 6.5.2, but also by comparison with similar TSDC measurements on hydrated elastin in a broader temperature range (down to -160°C) [Samouillan 2011], the temperature range of the TSDC measurements is not sufficient to observe the complete relaxation at high water fractions, i.e. part of the contributions to this peak is probably manifested at lower temperatures, out of the experimental window. For that reason, the particular relaxation will be analyzed by DRS.

Staying at relatively low temperatures in Fig. 6.5a, the contributions at high water fractions, $h_w \geq 0.10$, become more broad and a slower relaxation is observed, as a shoulder, at higher temperatures, although vaguely (centered at about -90°C for samples (2)-(5) and at about -100°C for samples (6)-(8)). A magnification of two of the thermograms is shown in Fig. 6.5b, where the contribution of the relaxation in question is indicated by dashed lines, drawn for eye guidance. This relaxation has been already observed by TSDC measurements on hydrated elastin [Samouillan 2011] of water contents $h_d=0.1$ and 0.25 (corresponding to $h_w=0.09$ and 0.2 respectively), where it was labelled as β_2 . In this work this relaxation will be named w .

Moving on to the high temperature side of the experimental window in Fig. 6.5a, a well shaped peak is centered at about -10°C for sample (3), ($h_w=0.117$). For the two samples of lower water fractions (samples (1),(2), $h_w=0.008$ and 0.10 respectively), the corresponding peak seems to be absent, and only weak contributions centered at the polarization temperature T_p are observed. The maximum of this peak is moving systematically to lower temperatures with the addition of water (from about -20°C for sample (3) to about -65°C for sample (9)). On the contrary, its magnitude changes non-monotonically with water fraction. It initially increases for water fraction increase from $h_w=0.117$ to 0.169 (sample (3)-(6)), then starts to decrease for water fraction increase from $h_w=0.169$ to 0.188 (samples (6)-(8)) and then increases again for $h_w=0.214$ (sample (9)). This process was also observed previously [Samouillan 2011] for a hydrated elastin sample of $h_d=0.25$. There it was named process p_1 and was attributed to the glassy behavior of hydration water in elastin, or otherwise, the reorganization of the whole hydrogen bonded network. In this work this relaxation has been followed in small steps of hydration in a more wide hydration range, and its characteristics will be further evaluated in this thesis. Here, we will refer to the particular relaxation mode as to p mode.

The maximum temperatures of the relaxation peaks and the normalized depolarization current values at the maximum temperature, for the w and p modes versus water fraction h_w , are shown in Fig. 6.6a and 6.6b respectively (for two series of measurements at different polarization temperatures). In Fig. 6.6.a it is obvious that the position of both peaks is moving to lower temperatures as the hydration level increases. Assuming that these relaxations originate from water, this fact implies that both relaxations are affected by protein components i.e. they correspond to water molecules interacting to some extent with the protein. The temperature decrease is steeper for the p relaxation. The w relaxation is detected for $h_w \geq 0.10$, and the p relaxation for $h_w \geq 0.117$, at least in the experimental temperature range studied in this work. In the case of $h_w=0.214$, the w peak could not be detected by TSDC, but its existence has been verified by TSDC measurements using insulating thin foils at a comparable hydration level in previous studies [Samouilla

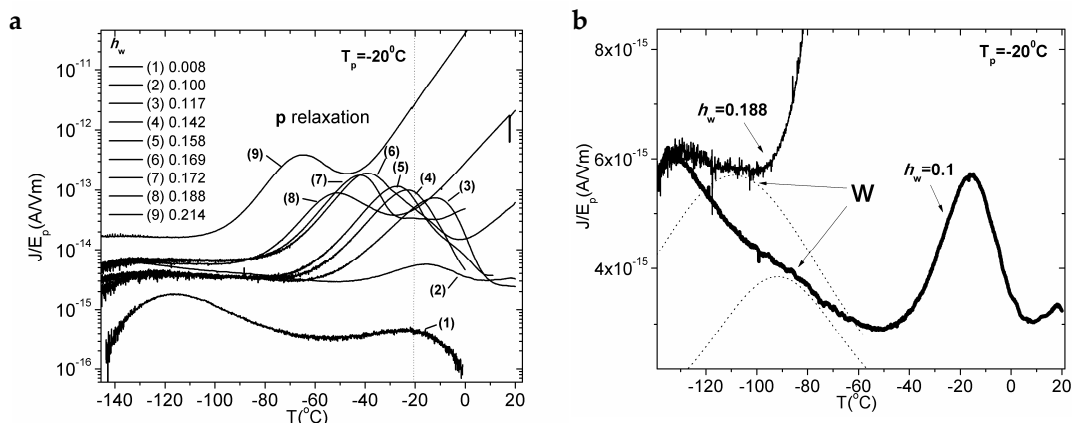


Fig 6.5 a) Normalized TSDC thermograms (density of depolarization current divided by polarizing electric field, J/E_p) against temperature T for hydrated elastin pellets of water fraction h_w indicated on the plot. The vertical line at $T=-20^\circ\text{C}$ indicates the polarization temperature T_p . **b)** The graph is a magnification of two of the thermograms from Fig. 6.5a, showing the w relaxation peak, which appears as a shoulder. The dotted lines are added for eye guidance.

2011]. The novel result in the current study, is the hydration dependence of the particular relaxations. Interesting results arise also from the evolution of the intensity of the relaxations with hydration level. Regarding the intensity of the w relaxation, it can be seen in Fig. 6.6.b, that it remains almost stable in the h_w range of about 0.10-0.14, while it increases at higher h_w , and decreases again for $h_w=0.188$. The increase for $h_w > 0.14$ shows that the w relaxation is enhanced for hydration levels where water clustering is significant according to ESI (for $h_d > 0.13$, see section 6.3). Further water increase causes the reduction of the intensity. This result will be discussed later in comparison with the results by other techniques. Moving to the intensity of the p relaxation, it can be seen in Fig. 6.6.b that it increases continuously in the range of $0.10 < h_w < 0.188$, then decreases for $h_w=0.188$, and increases again for $h_w=0.214$. By these observations, a critical water fraction of about 0.18 may be estimated. This point will be further discussed in comparison with the rest of the results by the other techniques employed in this thesis.

Elastin-TSDC-Hydration through immersion in deionized water ($0.30 \leq h_w \leq 0.50$)

Figure 6.7 shows TSDC thermograms with $T_p=-20^\circ\text{C}$, in the temperature range from -150 to 20°C for several hydrated elastin pellets of water fraction h_w indicated on the plot. The thermograms corresponding to the samples hydrated through vapor adsorption (data from Fig. 6.5a) are also shown in Fig. 6.7, represented by gray solid lines, in order that the evolution of the spectra with hydration level can be followed in a continuous way. Starting at high temperatures in Fig. 6.7, a steep increase may be seen in the spectra around 0°C , for all of the immersed samples (samples (1)-(5)). This increase is due to water melting. This increase is not present in the case of the samples in the hydration range $0 < h_w \leq 0.214$, where there is no crystallization of water. Moving to lower temperatures, a double peak may be observed for the sample of $h_w=0.30$ (sample (1)), exhibiting maxima at about -60 and -80°C . The position and magnitude of those peaks are similar to the ones observed for the p peak

for the sample of $h_w=0.214$ (highlighted by arrow in Fig. 6.7, sample (9) in Fig. 6.5a). The position of these two peaks seems to saturate with further increase of water fraction, i.e. for samples (2)-(5) in Fig. 6.7. The magnitude of the peaks increases in general with h_w increase, with an exception regarding the sample of $h_w=0.50$ (sample (5) in Fig. 6.7, dotted line). The evolution of the p peak leads to the low temperature peak centered at about -80°C in Fig. 6.7, as will be shown later in comparison to the DRS results. The origin of the second peak at higher temperatures is not clear and it might be associated with electrode polarization effects. Finally, moving to the low temperature side of the experimental window, the observed thermograms for the immersed samples are again differentiated when compared to the ones of lower h_w . Two main peaks centered at about -120 and -140°C , are present for samples (1)-(5), generally increasing in magnitude. The origin of those peaks will be evaluated in comparison with the results by DRS.

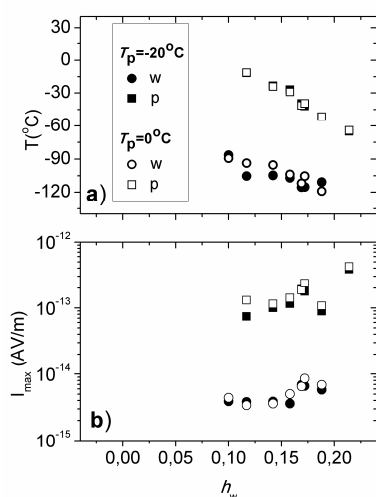


Fig. 6.6 a) Temperature maxima versus water fraction h_w , estimated by TSDC peaks of measurements on hydrated elastin pellets, for two polarization temperature values, for the w and p relaxations b) Normalized depolarization current maximum values, corresponding to the peaks mentioned in a).

6.5.2. Elastin-DRS Results

DRS measurements provide the possibility to vary both frequency and temperature over wide ranges (in the present work 10^{-1} - 10^6 Hz and -150 to 30°C , respectively) and so to analyze dynamics in more details than by TSDC. On the other hand, TSDC proves to be highlighting in the case of high conductivity contributions, for example at high temperatures in the case of hydrated samples, where conductivity contributions are enhanced in DRS spectra and thus overlap the molecular dielectric relaxations. Here, we aim at combining and comparing the two dielectric techniques in order to obtain as much information as possible. For that reason, isochronal (constant frequency) presentation of the DRS data is very convenient [Kremer 2002]. In Fig. 6.8a and 6.8b isochronal plots of the dielectric loss against temperature, $\epsilon''(T)$, are presented for several hydrated elastin pellets of h_w indicated on the plots. To facilitate comparison with TSDC data, a low frequency, 1 Hz, has been selected out of the frequency range of DRS measurements which were carried out isothermally. We recall that the equivalent frequency of TSDC measurements is in the range 10^{-2} - 10^{-4} Hz and point out that the lower equivalent frequency of TSDC shifts the

peaks to lower temperatures (see chapter 4, section 4.4, 4.4.1). Starting at low h_w in Fig. 6.8a, a peak centred at about -70°C is seen for the sample of $h_w=0.01$, which slightly moves to lower temperatures and increases in magnitude for $h_w=0.06$. This peak corresponds to the one observed by TSDC for the sample of $h_w=0.008$ (Fig. 6.5a) and has already been assigned to the local movement of the main polar groups of the protein surface, triggered by hydration water. By comparing with Fig. 6.8a, it becomes clear that the evolution of the particular relaxation with water increase is better followed by DRS, as compared to TSDC (Fig. 6.5a).

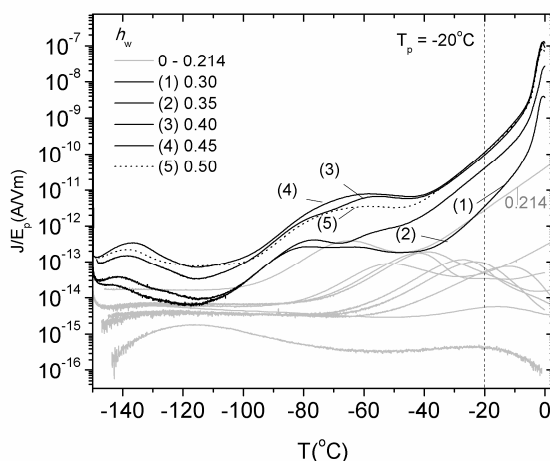


Fig 6.7 Normalized TSDC thermograms (density of depolarization current divided by polarizing electric field, J/E_p) against temperature T for hydrated elastin pellets of water fraction h_w indicated on the plot. The plot focuses on the elastin pellets hydrated through immersion in water and includes the thermograms from Fig. 5 (light gray), for comparison.

The maximum of the peak is located at about $T=-115^\circ\text{C}$ for $h_w=0.10$ and at about -135°C for higher h_w , where it stabilizes at time scales very close to the lower bound of the relaxation times of the secondary process of bulk water (ν process) (see chapter 2, section 2.2) [Panagopoulou 2011a,b]. The corresponding peaks are highlighted by arrows (main polar groups and ν relaxation). At higher temperatures the w relaxation is observed as a shoulder. The position of the shoulder is highlighted by arrows. It can be seen that this shoulder is more pronounced for some of the samples, e.g. for $h_w=0.17$. Finally, on the high temperature side of Fig. 6.8a the p relaxation peak can be seen, centred at about 25 , 5 and -5°C for $h_w=0.16$, 0.17 and 0.18 respectively. The high conductivity contributions at high temperatures make the detection of the p peak impossible for $h_w=0.23$. Regarding the intensity of the p peak, it increases initially for $h_w=0.17$ and then decreases again for $h_w=0.18$. This is in accordance with the TSDC results. It becomes clear at this stage that DRS and TSDC detect the same mechanisms, however more or less clearly in the one or the other technique depending on the specific mechanism (the ν relaxation may be better followed by DRS, while the p relaxation is better observed by TSDC). Finally, in Fig. 6.8b the isochronal plots for the immersed samples appear to be similar to the TSDC measurements in Fig. 6.7.

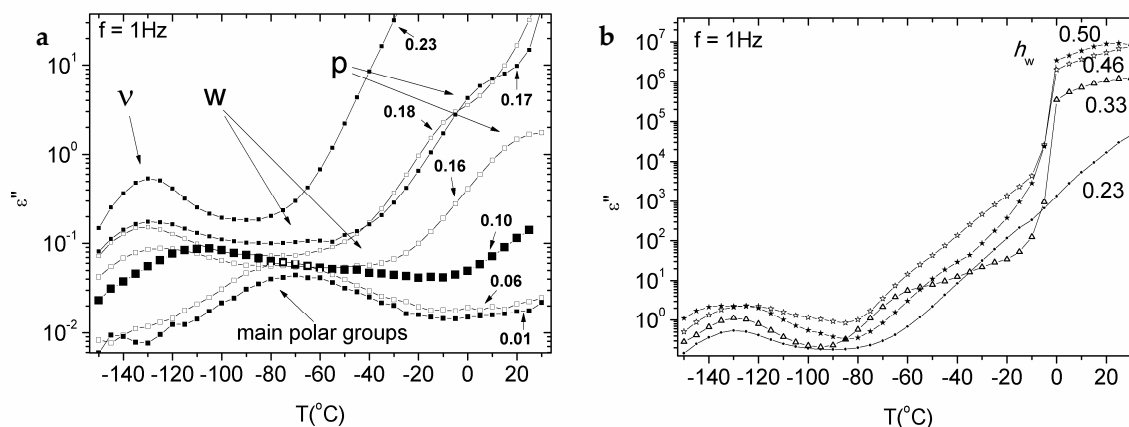


Fig. 6.8 Isochronal plots of the imaginary part of the dielectric function ($\epsilon''(f)$, dielectric loss) at the frequency of $f=1\text{Hz}$, for hydrated elastin pellets of water fraction h_w indicated on the plot. **a)** elastin pellets hydrated through vapor adsorption, **b)** elastin pellets hydrated through immersion in water

Elastin-DRS -Hydration through vapor adsorption ($0 < h_w \leq 0.23$)

Dielectric loss versus frequency, $\epsilon''(f)$, isothermal data at temperature $T=-90^\circ\text{C}$, are plotted in Fig. 6.9 for several samples of different hydration levels. Open symbols are experimental data, and the solid line through them is the sum of the Cole-Cole contributions to the dielectric loss. The thick solid curves correspond to the relaxation of small polar groups of the protein, mentioned previously, plasticized by water, the position of which saturates at the frequency position of the v relaxation of water, at higher h_w . For $h_w=0.01$ and 0.06 the relaxation peak is located at the low frequency side of the experimental window, while its maximum is not clearly detectable in the experimental data, as it is located at lower frequencies. The evolution of the position of the peak for higher water fractions can be followed in Fig. 6.9. The maximum of the peak, is at about 300Hz for $h_w=0.10$ and 6kHz for $h_w=0.16$. The position of the peak seems to saturate for samples of $h_w=0.17$, and 0.23 , centered at about 200kHz . It must be mentioned at this point that other contribution at the high or low frequency side of the experimental window that were needed to fit the data, are not shown for all of the samples, for clarity reasons. Examples of relaxations not shown, are the low intensity contributions at the high frequency side for $h_w=0.01$ and 0.06 and contributions of the w relaxation at the low frequency side for $h_w=0.17$ and 0.23 . An exception is the high frequency contribution for $h_w=0.10$, which is represented by a dash-dotted line. A peak centered at similar frequency is also needed to fit the data for $h_w=0.16$. However, this contribution is not shown, as its low dielectric strength makes it hard for it to be observed in the scale of the plot. Nevertheless, the analysis data of this relaxation, which may be connected with the relaxation in similar frequency region for $h_w=0.10$ (dash and dotted line in Fig. 6.9), will be presented in the discussion section (section 6.5).

An example of the fitting of the dielectric loss curves for water fraction $h_w=0.17$ at a characteristic temperature $T=-20^\circ\text{C}$, is shown in Fig. 6.10. Open circles and open triangles are

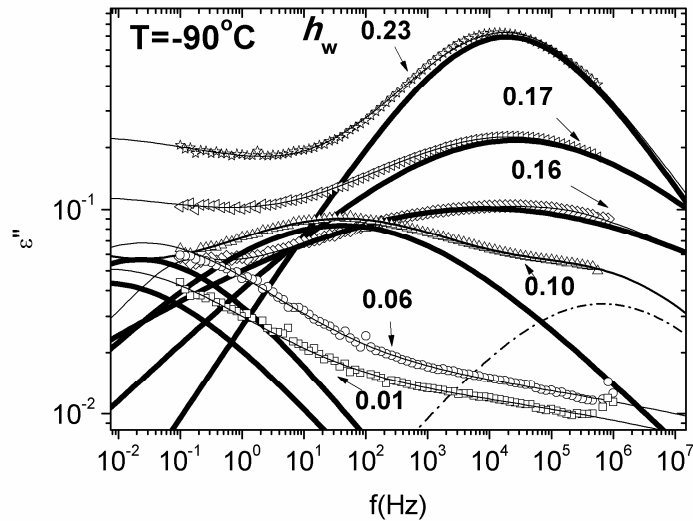


Fig. 6.9 Dielectric loss against frequency, $\epsilon''(f)$, at $T=-90^\circ\text{C}$, for hydrated elastin pellets of water fractions h_w indicated on the plot. Points are experimental data. The thick solid lines are the contribution of the relaxation of polar groups at low water fractions, the position of which is saturated at higher water fractions at the position of the ν relaxation of water. The dash-dotted line at high frequencies is the contribution of an additional relaxation for the sample of $h_w=0.10$. The rest of the contributions which interfere are not shown here, in terms of clarity. The solid lines through the experimental data correspond to the sum of the contributions.

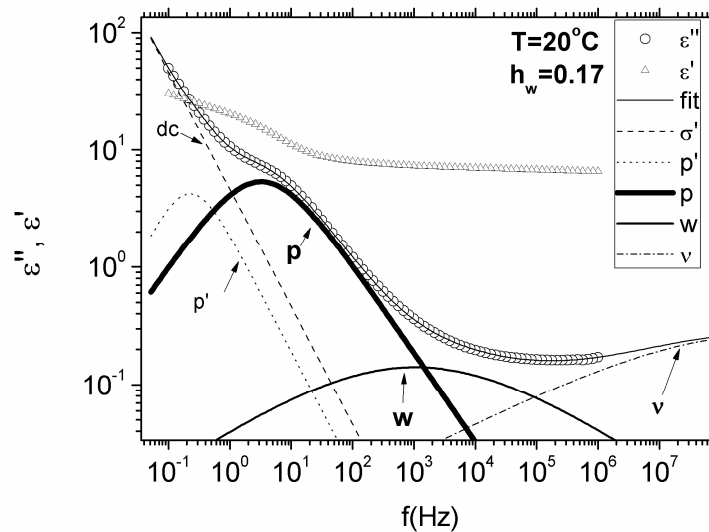


Fig. 6.10 Real and imaginary part of the dielectric function versus frequency f , $\epsilon'(f)$ and $\epsilon''(f)$, respectively, for a hydrated elastin pellet of water fraction $h_w=0.17$, at temperature $T=20^\circ\text{C}$. Several contributions to the dielectric loss are indicated on the diagram. The solid line through the experimental dielectric loss data is the sum of the contributions.

experimental data for the imaginary (dielectric loss, ϵ'') and the real part, ϵ' , of the dielectric function, respectively. The solid line through the dielectric loss data is the sum of the contributions. On the high frequency side of the experimental window the low frequency part of the ν relaxation peak can be seen (dash-dotted line). The ν relaxation peak maximum has already moved out of the experimental frequency range at this temperature, but the evolution of the latter with temperature has been followed from lower temperatures by keeping the shape parameter as a constant, which was the case in the temperature range where the peak could be fully observed. Moving to lower frequencies, the w peak contribution can be seen (solid curve). Here, it becomes clear that the w peak is not directly detectable, due to the fact that its magnitude is relatively low compared to the peaks that are located at higher or lower frequencies. At this point it should be highlighted that this relaxation was better detected by TSDC (Fig. 6.5a) and also by the isochronal representation of the DRS data (Fig. 6.8a) where it was pronounced for the sample of $h_w=0.17$. At even lower frequencies, the p peak can be seen, centered at about 4Hz (thick solid curve). At even lower frequencies, the dc conductivity contribution can be seen as a dashed line. Moreover, a peak better fitted as Debye (chapter 4, section 4.3) (p' , dotted line) is centered at about 0.3Hz. It is worth to say that the maximum of the p' peak coincides with the crossing point of the ϵ' and ϵ'' raw data, implying that this peak may be originated in interfacial polarization effects [Richert 2011]. The p' peak has been also observed in TSDC measurements on hydrated elastin [Samouillan 2011].

The fitting method has been already described in sections 4.3 and 5.5.2. The fitting parameters $\tau_j(T)$ (relaxation time) and $\Delta\epsilon_j(T)$ (dielectric strength) calculated for each process j are plotted in Figures 6.11,6.12 (for the ν relaxation) and Figures 6.13a, 6.13b (for the w and p relaxations) against reciprocal temperature, while the parameters $\beta(T)$ for the ν relaxation of water (small polar groups of elastin which is triggered by hydration water ($0.1 < h_w < 0.16$)) and the ν relaxation of water ($h_w > 0.16$)), the w and p relaxations, are listed in Table 6.2. The data of Fig. 6.11 for the ν relaxation of water have been expressed by an Arrhenius equation (eq.(4.14)). The corresponding values of the activation energy E_{act} as well as the logarithm of the pre-exponential factor $\log f_0$ are listed in Table 6.3.

Table 6.2. Fractional Exponent $\beta_\nu(T)$ of the Cole-Cole function of Polar Groups-Hydration water for low water fractions $0.01 \leq h_w \leq 0.10$ and the ν relaxation of water at higher water fractions $0.16 \leq h_w \leq 0.23$. The term $\beta_\nu(T)$ is used in the Table at both cases. Also, Fractional Exponent $\beta_w(T)$ and $\beta_p(T)$ of the Cole-Cole function of processes w and p respectively.

h_w	0.01	0.06	0.10	0.16	0.17	0.18	0.23
$\beta_\nu(T)$	0.38	0.30	0.20	0.28-0.32	0.24-0.29	0.28-0.32	0.42-0.50
$\beta_w(T)$	-	-	-	0.20-0.40	0.20-0.40	0.20-0.40	0.2-0.9
$\beta_p(T)$	-	-	-	0.71-0.75	0.72-0.74	0.74-0.77	-

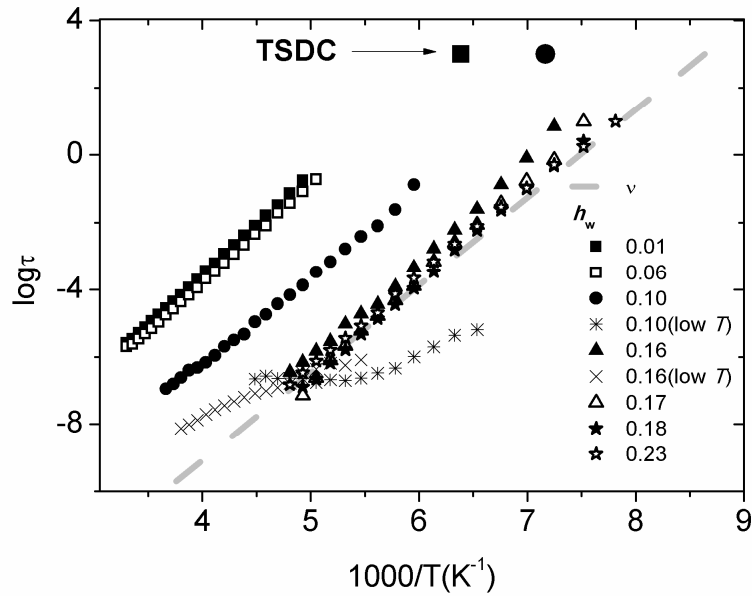


Fig 6.11 Temperature dependence of the relaxation times for the ν relaxation of uncrystallized water for several elastin hydrated pellets of water fractions h_w indicated on the plot. An additional relaxation at lower temperatures than the ν relaxation is shown for $h_w=0.10$ and 0.16 . The TSDC maximum temperature values are added at the equivalent frequency of about 10^{-3} - 10^{-4} Hz, for $h_w=0.01$ and 0.10 .

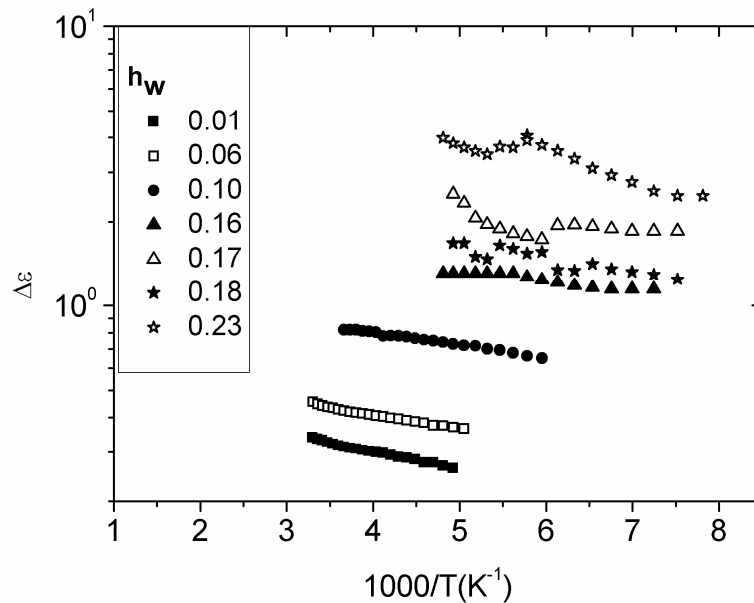


Fig 6.12 Dielectric relaxation strength $\Delta\epsilon$ of the ν relaxation for several elastin hydrated pellets of water fractions h_w indicated on the plot

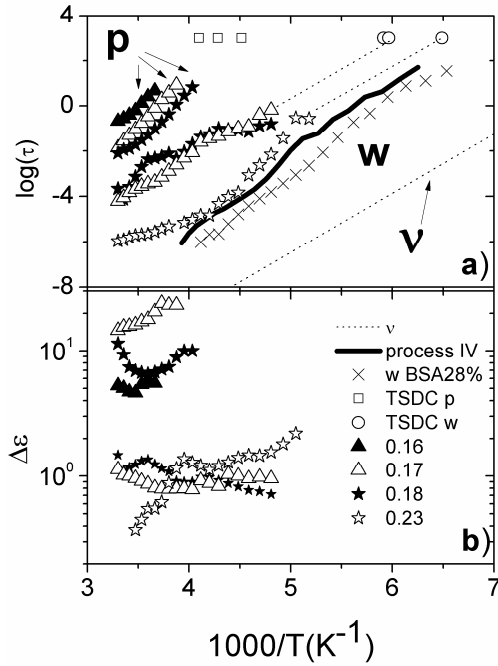


Fig 6.13 [Panagopoulou 2013a]

a) Temperature dependence of the relaxation times for the p and w relaxations for several elastin hydrated pellets of water fractions h_w indicated on the plot. The TSDC maximum temperature values are added at the equivalent frequency of about 10^{-3} - 10^{-4} Hz, for similar h_w values. Literature data for the relaxation time of the w relaxation in hydrated BSA of $h_w=0.28$ [Panagopoulou 2012] and hydrated myoglobin of $h_w=0.33$, process IV in reference [Jansson 2010] are also added to the diagram

b) corresponding dielectric strength $\Delta\epsilon$ for the p and w relaxations for several elastin hydrated pellets of water fractions h_w indicated on the plot.

Table 6.3. Activation energy, E_{act} , and logarithm of the pre-exponential factor, $\log f_0$, of the Arrhenius equation for the relaxations of small polar groups of elastin which is triggered by hydration water ($0.1 < h_w < 0.16$) and for the v relaxation of water ($h_w > 0.16$).

water fraction h_w	E_{act} (eV)	$\log f_0$
0.01	0.59 ± 0.01	14.69 ± 0.03
0.06	0.58 ± 0.01	14.63 ± 0.03
0.10	0.51 ± 0.01	15.72 ± 0.13
0.16	0.59 ± 0.01	20.02 ± 0.27
0.17	0.60 ± 0.01	20.96 ± 0.22
0.18	0.57 ± 0.01	20.13 ± 0.12
0.23	0.52 ± 0.01	18.59 ± 0.14

Elastin-DRS-Samples hydrated through immersion in water ($0.29 \leq h_w \leq 0.50$)

Dielectric loss versus frequency, $\varepsilon''(f)$, isothermal data at temperature $T=-65^\circ\text{C}$, are plotted in Fig. 6.14 for several immersed elastin samples of different hydration levels. The data corresponding to the sample of $h_w=0.23$, which has been hydrated through vapor adsorption, are also included to Fig. 6.14 in order to follow the evolution of the spectra with hydration. The contribution of the ν and w relaxations to the dielectric loss for $h_w=0.23$ are also added to the diagram. At the selected temperature, $T=-65^\circ\text{C}$, four relaxation modes (ν , w , w' , p) can be observed simultaneously within the experimental window, for the immersed samples. The ν relaxation peak, centered at about 10^6 Hz for all samples of Fig. 6.14, shows a non linear dependence of its magnitude with hydration level. In particular, its magnitude increases initially from $h_w=0.23$ to 0.29, then decreases slightly for $h_w=0.33$, 0.38 and finally increases again for $h_w=0.38$. An analogous hydration dependence is observed regarding the p peak, which is observed as a shoulder, centered at about 10Hz, for $h_w= 0.29$, 0.33, 0.38 and 0.46. In the intermediate frequency region, starting from $h_w=0.23$, the evolution of the w relaxation with hydration level is followed. The data for $h_w=0.29$ exhibit a pronounced shoulder centered at about $2 \cdot 10^2$ Hz. For $h_w=0.33$, 0.38 and 0.46 an additional peak centered at about $4 \cdot 10^3$ Hz, increasing in magnitude, is denoted as w' in Fig. 6.14.

In Fig. 6.15 the data from Fig. 6.14 are reproduced, where the data for $h_w=0.29$, 0.33, 0.38 and 0.46 are represented by gray solid lines. The dielectric loss experimental data for $h_w=0.50$ are also added to the diagram. It becomes clear in Fig. 6.15 that the spectra are quite different in the case of $h_w=0.50$. The differences regarding the complex contributions of the observed relaxations to the dielectric loss, will be better described by the analysis of the spectra. An example of the fitting of the dielectric loss curves for water fraction $h_w=0.38$ at a characteristic temperature $T=-65^\circ\text{C}$, is shown in Fig. 6.16. Open circles are experimental data for dielectric loss, ε'' . The solid line through the dielectric loss data is the sum of the contributions. On the high frequency side of the experimental window, the contribution of dc conductivity is shown as a dotted line. The Cole-Cole contributions of the p , w , w' and ν relaxations to the dielectric loss are highlighted in Fig. 6.16 by arrows.

The fitting parameters $\tau_j(T)$ (relaxation time) and $\Delta\varepsilon_j(T)$ (dielectric strength) calculated for each process j , for the immersed samples, are plotted in Fig. 6.17a, 6.17b (for the ν relaxation) and Fig. 6.18, 6.19a, 6.19b, 6.19c (for the w , w' and p relaxations) against reciprocal temperature, including data corresponding to the samples hydrated through vapor adsorption (from Fig. 6.11, 6.12, 6.13), in order to bridge the entire hydration range studied. The parameters $\beta(T)$ for the ν relaxation of water, the w , w' and p relaxations, for the immersed samples, are listed in Table 6.4. The data of Fig. 6.17a for the ν relaxation of water have been expressed by an Arrhenius equation (eq.(4.14)). The corresponding values of the activation energy E_{act} as well as the logarithm of the pre-exponential factor $\log f_0$, for the immersed samples, are listed in Table 6.5.

The results presented so far by ESI, DSC, TSDC and DRS are discussed in the upcoming section (section 6.6), covering the broad hydration range studied, starting from practically dry protein, including samples hydrated through vapor adsorption ($0 < h_w < 0.23$) and finally immersed samples ($0.23 < h_w < 0.53$).

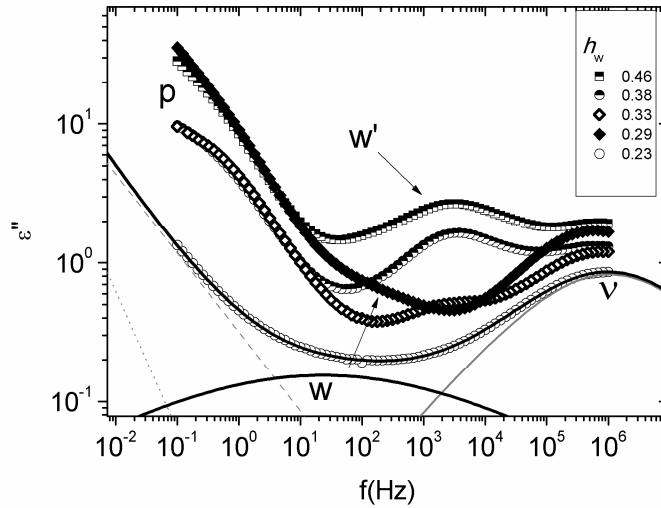


Fig. 6.14 Dielectric loss against frequency, $\epsilon''(f)$, at $T=65^\circ\text{C}$, for hydrated elastin pellets of water fractions h_w indicated on the plot. Points are experimental data. The solid line through the experimental data for $h_w=0.23$ corresponds to the sum of the Cole-Cole contributions to the dielectric loss. The gray and black solid lines are the contributions of the ν relaxation of water and the w relaxation, respectively. The dashed and dotted lines at high frequencies are the contributions of the dc conductivity and an additional relaxation for the sample of $h_w=0.23$.

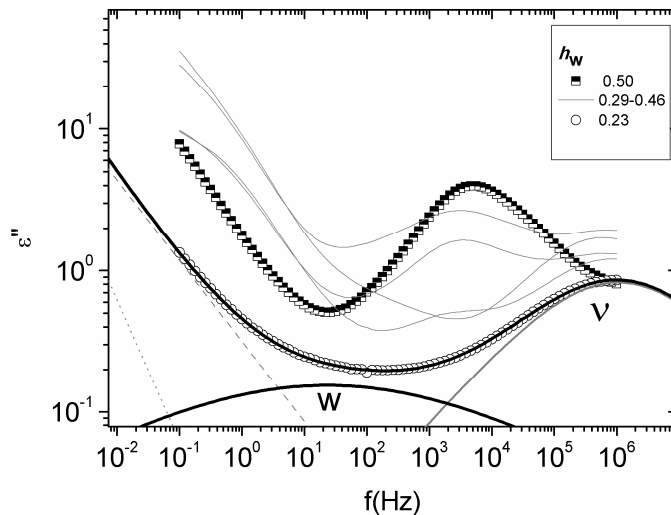


Fig. 6.15 Dielectric loss against frequency, $\epsilon''(f)$, at $T=65^\circ\text{C}$, for hydrated elastin pellets of water fractions h_w indicated on the plot. The plot is a reproduction of Fig. 6.14, including additional data for a sample of $h_w=0.50$. The data corresponding to $0.29 \leq h_w \leq 0.46$ are represented by gray solid lines, for clarity.

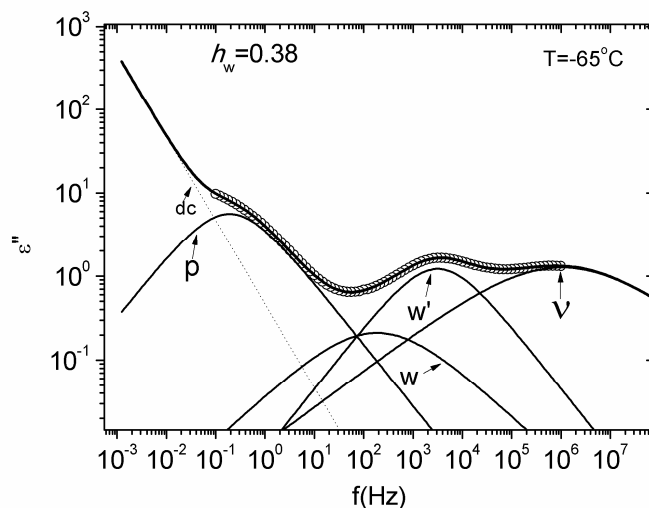


Fig. 6.16 Dielectric loss against frequency f , $\varepsilon''(f)$, for a hydrated elastin pellet of water fraction $h_w=0.38$, at temperature $T=-65^\circ\text{C}$. Several contributions to the dielectric loss are indicated on the diagram. The solid line through the experimental dielectric loss data is the sum of the contributions.

6.6 Discussion-Conclusions

The glass transition of the hydrated elastin samples has been studied by DSC and the results are described in section 6.4 (Elastin-DSC). The overall results show that in the case of dielectric measurements of samples hydrated through vapor adsorption, all samples are studied within a temperature range below the glass transition of the hydrated system and, as it has already been mentioned, all water of hydration is in the uncrystallized phase. Consequently, dielectric studies in the range $0 \leq h_w \leq 0.23$ are dealing with the dynamics of uncrystallized water in the protein hydration shell at temperatures below the glass transition temperature and the inverse temperature transition as well. According to the DSC results on the elastin samples hydrated by immersion in deionized water ($0.32 \leq h_w \leq 0.53$), crystallization of water is evident and, furthermore, at least two distinct populations of water in the crystallized form are expected to be present in the hydrated samples.

6.6.1. The interplay between a secondary relaxation of polar groups triggered by water molecules and the ν relaxation of water

The temperature dependence of the time scale of the secondary relaxation associated with small polar groups of the protein triggered by hydration water (low temperature peaks shown in Fig. 6.8a. and peaks in Fig. 6.9. for $h_w=0.01, 0.06$ and 0.10) and of the ν relaxation of water (low temperature peaks in Fig. 6.8a. and peaks in Fig. 6.9. for $h_w=0.16, 0.17, 0.18$ and 0.23) is shown in Fig. 6.11, while the respective values of the dielectric strength $\Delta\varepsilon$ are shown

in Fig. 6.12. The rate of plasticization is quite slow for an increase in h_w from 0.01 to 0.06. A stronger plasticization is observed for the sample of $h_w=0.10$. The data are in agreement (by extrapolation) with the experimental data from TSDC at the equivalent frequency of the TSDC method [Turnhout 1980]. The TSDC data for $h_w=0.008$ and 0.10 are added to Fig. 6.11. In addition, the trace of the relaxation is in good agreement with the respective one recorded by previous studies on hydrated elastin for similar water fraction values [Gainaru 2009]. The relaxation of polar groups triggered by hydration water is a secondary relaxation, as its dielectric strength increases with temperature, similar to the secondary relaxations observed in many synthetic polymers. The activation energy E_{act} of the relaxation observed in this study, is in the range of 0.5-0.6 eV as it can be seen in Table 6.3. The contribution of the polar groups to the dielectric response of the particular relaxation at low water fractions, has been already proposed for hydrated elastin measured by DRS, at water contents $h_d=0, 0.1$ and 0.2 (corresponding to $h_w=0.09$ and 0.16 respectively), where an apparent superlinear increase of the corresponding dielectric strength was found [Gainaru 2009]. More details regarding the hydration dependent characteristics of the relaxation of polar groups at low hydration levels are given in chapter 7, in a comparative study including hydrated globular, fibrous proteins and other biopolymers.

Moving to higher water fraction values, the trace of the relaxation moves to even lower temperatures and saturates at the position of the bottom limit values of the relaxation times of the ν relaxation of water [Ngai 2011, Panagopoulou 2012] (dashed line in Fig. 6.11, see also chapter 2, section 2.2). Several examples regarding the water fraction dependence of the ν relaxation of water in aqueous polymer mixtures have been previously shown [Cappaccioli 2007]. The trace of the ν relaxation in the water fraction range $0.16 \leq h_w \leq 0.52$, may be seen in Fig. 6.17a, while the corresponding dielectric strength, $\Delta\epsilon$, may be seen in Fig. 6.17b. The saturated trace of the relaxation is maintained for $h_w=0.16, 0.17, 0.18, 0.23, 0.29, 0.33, 0.38$ and 0.46 and is in agreement with the one recorded in previous dielectric studies on hydrated elastin [Gainaru 2009, Samouillan 2011]. As it has been proposed in the case of hydrated BSA (chapter 5, [Panagopoulou 2012]), the saturation of the position of the relaxation in question may be attributed to the rearrangement of uncrystallized water molecules in the hydration shell, following a separate relaxation mode, but being connected to the movement of the polar groups and the water molecules attached to them. The saturation may also be correlated to the formation of a percolating water cluster at the protein surface [Panagopoulou 2011b, Panagopoulou 2012]. The ν relaxation follows an Arrhenius law and its activation energy E_{act} is stated in Tables 6.3 and 6.5. The trace of the relaxation is differentiated for $h_w=0.50$, as it is seen in Fig. 6.17a. A profound difference arises regarding the activation energy, which obtains the value $E_{act}=0.25$ eV for $h_w=0.50$, much lower than the average value of about 0.55 eV at lower water fractions (Fig. 6.17a, Tables 6.3 and 6.5). This kind of evolution of the trace of the ν relaxation at high hydration levels has been also viewed in the case of BSA-water mixtures (section 5.6.3). In Fig. 6.17a it is shown that the trace of the ν relaxation for $h_w=0.50$ is in good agreement with the trace of a relaxation recorded on an aqueous BSA solution of $h_w=0.8$ [Shinyashiki 2009]. The significance of this change will be evaluated in chapter 7, in a comparative study including hydrated globular, fibrous proteins and other biopolymers, regarding the ν relaxation.

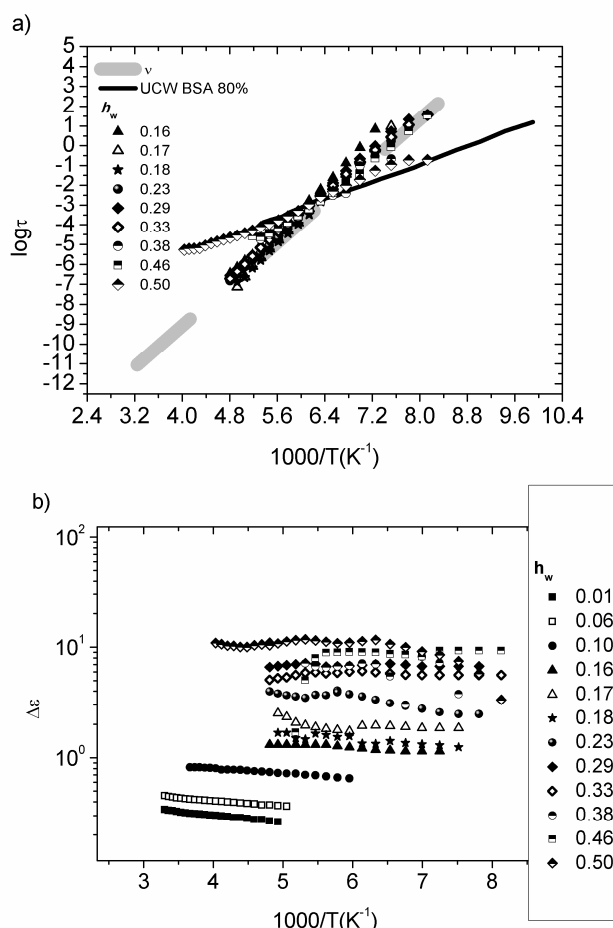


Fig. 6.17 a) Temperature dependence of the relaxation times for the ν relaxation of uncrystallized water for several elastin hydrated pellets of water fractions h_w indicated on the plot. The solid black line corresponds to the trace of the relaxation of uncrystallized water for an aqueous BSA solution of $h_w=0.8$ from reference [Shinyashiki 2009] **b)** Dielectric relaxation strength $\Delta \epsilon$ of the ν relaxation for several elastin hydrated pellets of water fractions h_w indicated on the plot

The dielectric strength of the ν relaxation for hydrated elastin shows a non-linear dependence on the water fraction. In particular, it can be seen in Fig. 6.17b that $\Delta \epsilon$ increases with an increase of the h_w from 0.16 to 0.17, then decreases for 0.18 and finally increases again for $h_w=0.23$. The same observation can be made in the isochronal representation of the dielectric loss in Fig. 6.8a. Increasing further the hydration level causes an increase of $\Delta \epsilon$ for $h_w=0.29$, a slight decrease for 0.33 and 0.38 and then a further increase for $h_w=0.46$, as it can be seen in Fig. 6.17b. The same behavior is also observed in Fig. 6.14 and 6.15, where the dielectric loss data are shown at $T=-65^\circ\text{C}$. The ν relaxation peak for the sample of $h_w=0.50$ in Fig. 6.15 is not clearly observed, as its dynamics is changed, so it is located underneath the pronounced loss peak, together with other contributions. In general, disregarding the slight changes, the magnitude of the ν relaxation seems to saturate at comparable values in the high h_w range, which is an indication that the relaxation is associated to uncrystallized water.

Closing this section, some comments should be made regarding the high frequency relaxation peak in Fig. 6.9 for the sample of $h_w=0.10$ and the one in the same frequency region which was needed to fit the data of $h_w=0.16$. The temperature dependence of the relaxation times of those relaxations is similar, as it can be seen in Fig. 6.11., although their magnitude is different. In particular, the dielectric strength decreases for $h_w=0.16$. The activation energy of this relaxation is relatively low, as it can be seen in Fig. 6.11. A similar relaxation following an Arrhenius law has been reported in the case of hydrated lysozyme studied by NMR [Khodadadi 2008] and there it was assigned to some form of water in the hydration shell of the protein. The study of the particular relaxation is reported here only in terms of completeness.

6.6.2. Dynamical characteristics of the p and w modes

The temperature dependence of the relaxation times for the p and w relaxations and the corresponding dielectric strength $\Delta\epsilon$, as studied by DRS, can be seen in Fig. 6.13a and 6.13b respectively, for selected h_w values, for the samples hydrated through vapor adsorption and in Fig. 6.18 and Fig. 6.19a, 6.19b, respectively, for the immersed samples. In Figures 6.13a, 6.18 the TSDC data at similar h_w values are added to the diagrams. Regarding the p relaxation, all the data, covering the entire h_w range, are included in Figures 6.18 and 6.19a.

Starting with the p relaxation, the plasticization with increasing hydration level can be seen in Fig. 6.18. The trace of the data is in agreement with TSDC points, by extrapolation. The TSDC point at lower temperatures corresponds to $h_w=0.50$, and the value is the temperature maxima of the low temperature peak in TSDC (we recall that two peaks were present in this region in the case of the immersed samples in Fig. 6.7). The plasticization of the trace stops and is followed by a stabilization for the immersed samples in agreement to TSDC (Fig. 6.7). The temperature dependence of the relaxation times for the p relaxation could be an Arrhenius one, or a VTF (eq.(4.15), see chapter 4, section 4.3) of low fragility. A definite decision cannot easily be made. The $\Delta\epsilon$ of the relaxation increases for an increase of h_w from 0.16 to 0.17, and then decreases for 0.18, in agreement with the so far observations by TSDC and DRS (raw data, Fig. 6.5a, 6.8a). The $\Delta\epsilon$ values increase with temperature decrease, for the samples of $h_w=0.16$, 0.17 and 0.29, the increase being more profound for $h_w=0.17$ and 0.29. This fact implies the cooperative nature of the particular relaxation. The same has been also observed for the p_1 relaxation by analysis of experimental data of the thermal sampling technique [Samouillan 2011], for $h_w=0.2$. There, the relaxation has been attributed to a glassy state of water in the clusters formed in the hydration shell. In this work, the detection of the p relaxation at a comparable h_w is not possible because of enhanced conductivity contributions at high temperatures (the p peak could not be recorded for $h_w=0.23$ in DRS), but the cooperativity is confirmed for and extended to $h_w=0.17$ and 0.29. Regarding the sample of $h_w=0.18$, a very peculiar temperature dependence of the $\Delta\epsilon$ is observed, which will be evaluated later on. Moving to higher h_w , the behavior changes and the $\Delta\epsilon$ values decrease with temperature decrease, for $h_w=0.33$ and 0.38, implying a dynamic change concerning the p relaxation. Further increase in h_w causes a further increase of $\Delta\epsilon$ values which finally become temperature independent. The results suggest that the cooperative nature of the p relaxation is lost upon increasing the water fraction. This is probably associated to the formation of ice structures, which is verified by the DSC

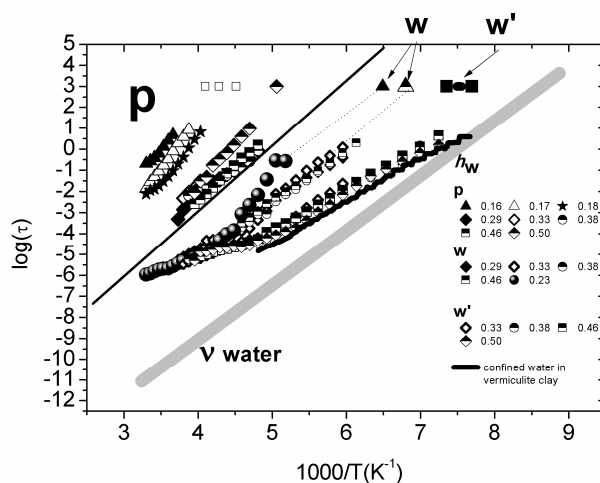


Fig. 6.18 Temperature dependence of the relaxation times for the p , w and w' relaxations for several elastin hydrated pellets of water fractions h_w indicated on the plot. The TSDC maximum temperature values are added at the equivalent frequency of about 10^{-3} - 10^{-4} Hz, for similar h_w values. The relaxation times of water confined in vermiculite clay from reference [Bergman 2000] are also added to the plot

measurements for $h_w \geq 0.32$ (section 6.4, Fig. 6.2). The crystallization of the water molecules which relax following the p relaxation at high hydration levels cannot be excluded, especially when considering that the saturated trace of the p relaxation in Fig. 6.18 is comparable to the trace of deionized ice, reported by Auty and Cole [Auty 1952] and that the $\Delta\epsilon$ values at high hydration levels of about 10^2 are comparable to the values of hexagonal like ice structure observed in BSA solutions [Panagopoulou 2012].

The trace of the w relaxation is followed in Fig. 6.13a, for three h_w values, namely, 0.17, 0.18 and 0.23. The w relaxation could not be detected by DRS for the sample of $h_w=0.10$, probably because its relaxation times are comparable with the ones of the relaxation of polar groups, and due to the comparatively low intensity of the w relaxation when compared to the one of the polar groups. The results for $h_w=0.16$ exhibited high scattering, probably due to low intensity of the w relaxation, and they are not shown here for clarity reasons. A first observation that should be pointed out, is that the trace of the w relaxation is quite in agreement with the TSDC points that are added to the diagram at similar water fraction values. The Arrhenius dependence of the relaxation times and the temperature dependence of the dielectric strength for both $h_w=0.17$ and 0.18 may support the assumption that the relaxation in question is a local secondary relaxation. This was also suggested for the particular relaxation in the work by Samouillan et al. [Samouillan 2011] for a sample of $h_w=0.09$. Moving to the sample of $h_w=0.23$ the trace of the data move to even lower temperatures. The data follow a VTF law rather than an Arrhenius one, and the corresponding $\Delta\epsilon$ increases with temperature decrease. The trace of the relaxation is comparable to the one for the process IV recorded by DRS in hydrated myoglobin at a water fraction $h_w=0.33$ using insulating thin foils as blocking electrodes [Jansson 2010] and for the w process in hydrated BSA at $h_w=0.28$ (chapter 5, [Panagopoulou 2012]), which are added in the diagram for comparison. In both studies, the particular relaxation coexisted with the

main relaxation of deeply supercooled uncrystallized water (ν relaxation), like in the present study, the trace of which is added in Fig. 6.13.a, as a dashed line. This comparison is very important and supports a model which may lead to the evaluation of this controversial relaxation observed in several biopolymers. The evolution of the characteristics of the w relaxation with hydration level is followed in Figures 6.18 and 6.19b. In Fig. 6.18 the trace of the w relaxation is identical for the immersed samples of $h_w=0.29, 0.33, 0.38$ and 0.46 . The extrapolation of the data is in accordance to the TSDC point (half filled triangle, peak maxima in Fig. 6.7 at about -125°C). The trace of the w relaxation for the immersed samples is in agreement with its trace for $h_w=0.23$ in the high temperature range ($1000/T < 4.5$). While the temperature dependence of the relaxation times for $h_w=0.23$ follow clearly a VTF law (eq.(4.15)) for $1000/T < 5$, the trace for the immersed samples follows an Arrhenius law (eq.(4.14)) at $1000/T > 5$ and exhibits a crossover to a VTF behavior at higher temperatures. Regarding the dielectric strength of the w relaxation, it is seen in Fig. 6.19b that the cooperativity observed for $h_w=0.23$ described earlier is lost for $h_w=0.29$, where a decrease of $\Delta\epsilon$ with temperature decrease is observed. In general, the hydration dependence of $\Delta\epsilon$ values is non linear, as it can be seen in Fig. 6.19b. In particular, $\Delta\epsilon$ decreases for $h_w=0.33$ and 0.38 and increases again for $h_w=0.46$, where a cooperative nature seems to be present again, at least within a particular temperature region. The complex evolution of those characteristics with hydration level, although interesting, are rather vague, because of the low intensity of the w relaxation. Nevertheless, the non linear dependence of the intensity of the peak with hydration level may be seen in the raw data, in Fig. 6.14 and 6.15, where the 'shoulder' of the w relaxation is denoted by arrows. A suggestion regarding the origin of the w relaxation will be given in an upcoming subsection regarding the origin of the different relaxation modes observed for the hydrated elastin system.

6.6.3. The w' relaxation mode

The dielectric raw data regarding the w' relaxation have been presented in Fig. 6.7 (low temperature peak in TSDC centered at about -145°C), and in Fig. 6.14, 6.15 and 6.16 (DRS). The magnitude of those peaks increases in general with hydration level. The temperature dependence of the relaxation times of the w' relaxation may be seen in Fig. 6.18 and the extrapolation of the data to the equivalent frequency of TSDC is in agreement with the temperature range of the peak maxima in TSDC, which is added in the plot. The first hydration level for which the w' relaxation is detected is $h_w=0.33$. The trace is identical for the rest of the samples of higher h_w . It is interesting that the trace coincides with the relaxation time of water confined in vermiculite clay [Bergman 2000]. The fractional exponent $\beta(T)$ of the Cole-Cole function for water confined in vermiculite clay, is $\beta=0.55$ at $T=-88^\circ\text{C}$, the same with the fractional exponent of w' for $h_w=0.33$ and 0.38 (Table 6.4). The relaxation times of the w' relaxation for elastin here are recorded to even higher temperatures than the ones for water in vermiculite clay. Here the trace exhibits a crossover from an Arrhenius behavior of higher to one of lower activation energy E_{act} at about $1000/T=5$. The temperature dependence of the relaxation times above the crossover temperature is similar to the one of the w relaxation. The origin of the w' relaxation will be discussed in the upcoming section and in chapter

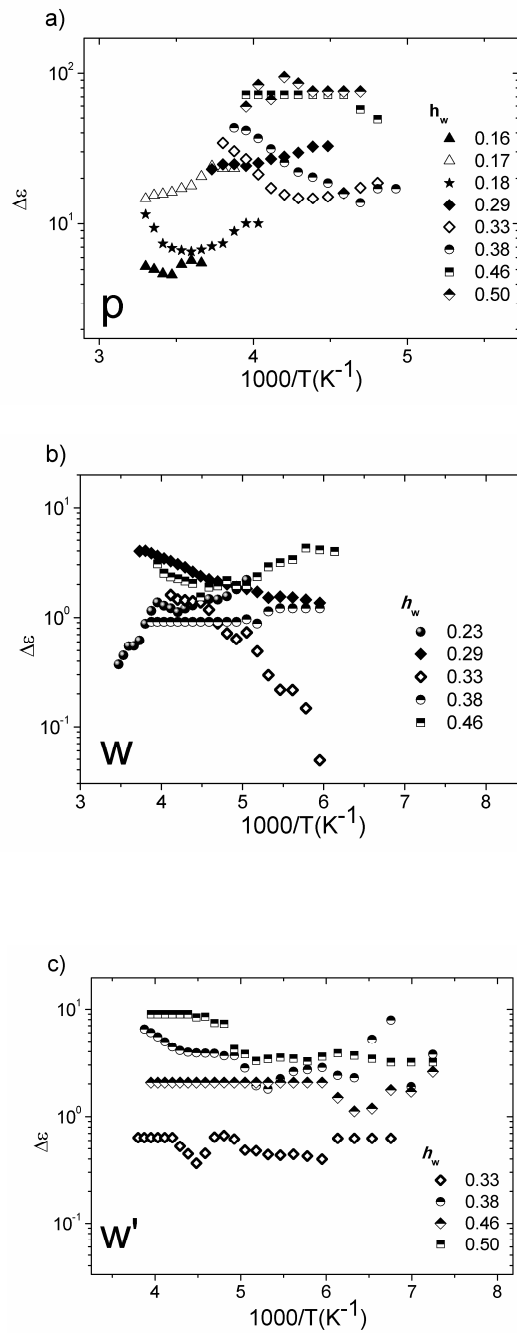


Fig. 6.19 Dielectric strength $\Delta\epsilon$ against reciprocal temperature, $1000/T$, for the a) p b) w and c) w' relaxations for several elastin hydrated pellets of water fractions h_w indicated on the plots

Table 6.4. Fractional Exponent $\beta_\nu(T)$ of the Cole-Cole function of the ν relaxation of water at water fractions $0.29 \leq h_w \leq 0.50$ (immersed samples). Also, Fractional Exponent $\beta_w(T)$, $\beta_{w'}(T)$ and $\beta_p(T)$ of the Cole-Cole function of processes w , w' and p respectively.

h_w	0.29	0.33	0.38	0.46	0.50
$\beta_\nu(T)$	0.50-0.60	0.48-0.56	0.42-0.61	0.43-0.63	0.63-0.73
$\beta_w(T)$	0.47-0.65	0.67-0.74	0.71-0.81	0.47-0.95	-
$\beta_{w'}(T)$	-	0.55	0.55	1	1
$\beta_p(T)$	0.76	0.73	0.74	0.74	0.71-0.84

Table 6.5. Activation energy, E_{act} , and logarithm of the pre-exponential factor, $\log f_0$, of the Arrhenius equation for the ν relaxation of water for the immersed samples ($0.29 \leq h_w \leq 0.50$).

water fraction h_w	E_{act} (eV)	$\log f_0$
0.29	0.53±0.01	18.52±0.09
0.33	0.52±0.01	18.41±0.15
0.38	0.40±0.02	14.73±0.69
0.46	0.44±0.01	15.82±0.33
0.50	0.25±0.01	9.93±0.15

6.6.4. Identifying the origin of the hydration water related relaxation modes

Summarizing the results in this study, we may identify several distinct water populations in the hydration shell of elastin. The first one is dielectrically manifested through the secondary relaxation of hydrophilic polar groups until a water fraction value $h_w=0.10$ (in the experimental h_w range in this work) and by the secondary ν relaxation at higher water fractions. Having in mind that elastin consists mainly of hydrophobic aminoacids and most of the lysines in elastin are involved in crosslinking, it is derived that the only hydrophilic polar groups in elastin are the main chain NH/O polar groups [Darwin 2001]. The ν relaxation corresponds to the formation of a percolating water cluster which is supported by water molecules interacting with polar groups, forming probably a clathrate like formation, which has been observed by cryogenic X-ray crystallography in the case of globular proteins

[Nakasako 2002]. The self association of water molecules themselves is accompanied by the saturation of the position of the ν relaxation. The particular water population corresponds to the one located on the protein surface, detected by NMR at RT [Sun 2011].

The second water population is manifested through the w relaxation. The latter is recorded for water fractions $h_w \geq 0.10$ in this study, i.e. for h_w higher than the one corresponding to the coverage of the primary sorption sites (hydrophilic polar groups, $h_m = 0.067$, section 6.3). A plasticization of this relaxation by water was recorded by TSDC and DRS. This probes to the assumption that the water involved is interacting with protein segments. The fitting results by DRS showed that the w relaxation is a localized secondary relaxation at low water fractions, while it exhibits cooperative behavior for the first time upon increasing water fraction, i.e. for $h_w = 0.23$. Additionally, it was suggested, according to TSDC results, that its magnitude increases more steeply in the water fraction range where water clustering is significant. All the above mentioned remarks, together with the fact that in the case of hydrated elastin, water molecules are approaching voids within the folded monomers, i.e. within the elastin fibers [Debelle 1999], by diffusion, lead to the conclusion that the w relaxation mode is associated with water molecules which are interacting locally with hydrophobic aminoacid residues, within the confined space in the interior of the elastin fibers. The holding of water molecules within the fibers, is supported also by the intense hysteresis loop recorded by ESI (section 6.3). The cooperative nature at $h_w = 0.23$ implies that a condensation of water molecules in the center of the confined spaces occurs, resulting in water molecules surrounded only by water molecules, resembling the characteristics of confined "internal" water [Oguni 2007]. This assumption is also in accordance to the fact that the number of water molecules n per tropoelastin molecule, exceeds the number of residues, in the case of $h_w = 0.23$. Of course, this fact alone is insufficient, because the excess water molecules could be involved in different configurations. Nevertheless, the existence of "internal" water within the protein structure has been already suggested, initially by Saenger [Saenger 1987] and later by other studies [Oguni 2007]. Finally, the similarity of the temperature dependence of the timescale of the w relaxation in elastin, for $h_w = 0.23$, with the one of similar relaxation modes in other proteins (see Fig. 6.13), is very important. This implies the existence of confined "internal" water in other globular proteins. The detection of the w relaxation in elastin at low water fractions is probably facilitated by the majority of hydrophobic aminoacid residues in this protein. The w relaxation corresponds to the one observed by NMR at RT inside the elastin fibers [Sun 2011]. For the immersed samples it has been shown that the dynamics and temperature dependence of the dielectric strength, $\Delta\epsilon$, of the w relaxation, is differentiated, while DSC results in Fig. 6.2a suggest that for $h_w \geq 0.33$, confined ice crystals appear in the system. It may thus be assumed, that the internal water molecules may crystallize at higher h_w values, where the immersion of the matrix causes some expansion of the confining voids and, by this way, the voids become large enough in order for the nanocrystals to be formed.

The third water population is manifested through the p relaxation. The p relaxation was detected for $h_w > 0.117$ by TSDC and DRS. In literature it has been attributed to the cooperative rearrangement in water clusters existing in a glassy state [Samouillan 2011], as studied by dielectric techniques and it may correspond to the population of water between elastin fibers, as recorded by NMR at RT [Sun 2011]. This kind of water population has been

observed in previous studies, e.g. in hydrated keratin [Leveque 1981]. In the current study, the plasticization of this relaxation by water is found, which suggests that the dynamics involved is affected by the global protein dynamics.

Finally, a fourth relaxation denoted as w' , was recorded for the immersed samples. The fact that this relaxation appears in the hydration range, where crystallization during cooling is evident, probes us to assume that it corresponds to the crystalline form of some water population in the protein matrix, although its dynamics is different than the one of normal hexagonal ice (Ih). This relaxation will be further evaluated in chapter 7.

Closing, some comments should be made regarding the peculiar results observed for the samples of a water fraction around about $h_w=0.18$. The results imply that this value is in fact a critical water fraction value for the organization of water in the protein hydration shell. This may be explained by the fact that around this h_w value the number of water molecules per protein molecule exceeds the number of aminoacid residues (800 residues correspond to $h_w=0.17$) and could be associated to swelling of the matrix. This assumption is supported by the fact that, a hysteresis loop was recorded by ESI for a water fraction region lower than this critical one. Up to this point, it was seen that the sample with h_w of about 0.18, shows a reduced intensity for all relaxations studied, i.e. the ν , w and p relaxations, by both DRS and TSDC. The decrease was more intense for the p , then the ν and finally the w relaxation. In addition, a peculiar temperature dependence of the dielectric strength of the p relaxation was found for $h_w=0.18$. Having in mind the origin of the relaxations, it is obvious that the reorganization, i.e. swelling of the matrix, affects more the relaxation modes which are attributed to water molecules less restricted by the surrounding environment.

6.6.5. Conclusions

Dynamics of uncrystallized water and protein dynamics were studied for hydrated elastin pellets by a combination of differential scanning calorimetry (DSC), thermally stimulated depolarization currents (TSDC) and dielectric relaxation spectroscopy (DRS) techniques, in a broad hydration range, including elastin hydrated through vapor adsorption as well as swollen by immersion in water. In addition equilibrium sorption desorption measurements (ESI) were performed at room temperature. The results were discussed in terms of critical water contents, distinct water populations and the mechanisms by which these features affect protein structure.

The glass transition of the hydrated system was studied by DSC and a strong plasticization was observed from $T_g=191^\circ\text{C}$ for dry elastin to $T_g=29^\circ\text{C}$ for $h_w=0.23$. A stabilization of T_g is estimated at higher h_w although the transition is not experimentally accessed. The increment in heat capacity, ΔC_p , of the glass transition was found to depend on water fraction in a non-linear way and this was associated to the change in the protein structure due to hydrophobic collapse. In the temperature range of the glass transition an enthalpic relaxation, as well as phenomena related to the inverse temperature transition, were recorded. Several critical water fractions were estimated: i) $h_w=0.23$ (grams of water per grams of hydrated elastin) for the maximum water uptake by elastin in water vapor equilibrium ii) $h_m=0.067$ (grams of water per grams of dry protein) for the primary hydration water at ambient conditions (corresponding to 261 water molecules per protein molecule),

iii) about $h_d=0.13$ (grams of water per grams of dry elastin) for the onset of significant water clustering and iv) about $h_w=0.18$ for a reorganization of water in the protein hydration shell, and might be related to swelling.

Three dielectric relaxations, related to uncrystallized water, were recorded by TSDC and DRS techniques in good agreement to each other. In the order of increasing temperature/decreasing frequency these are: (i) a local dielectric relaxation of hydrophilic polar groups on the protein surface triggered by water, with contributions of uncrystallized water molecules themselves in the protein secondary hydration shell at high water fractions (ν relaxation), (ii) a local relaxation of water molecules condensed near hydrophobic aminoacid residues inside the protein structure, which shows cooperative characteristics for $h_w=0.23$ (w relaxation), suggesting the manifestation of confined "internal" water, and probably crystallizes for the immersed samples of higher h_w and (iii) a cooperative like relaxation of water clusters between fibers (p relaxation), which was found to be plasticized by increasing water fraction. The results were compared to similar results in the subzero temperature domain and in room temperature at higher water fraction values near the physiological conditions, supporting the existence of these three uncrystallized water populations in the protein hydration shell.

Finally, at high hydration levels, where the hydration was achieved through immersion in water, two distinct population of crystalline forms are believed to be manifested through i) the w dielectric relaxation, corresponding to the crystallization of confined water as previously mentioned, and ii) the w' relaxation, corresponding to another form of ice.

7. Comparative studies of glass transition and water dynamics in globular proteins, fibrous proteins and other biopolymers

7.1 Introduction-Scope

The studies of one hydrated globular protein, bovine serum albumin (BSA) and one fibrous hydrated protein, elastin, in broad ranges of hydration levels, have been presented in chapters 5 and 6, respectively, in detail. The combination of the experimental techniques employed in this thesis, i.e. ESI, DSC, TSDC and DRS, along with inducing the extremely broad hydration range as a parameter, reveals a strong dependence of the experimental results on the hydration level and makes it possible to follow the evolution of the complex contributions of protein and of distinct water populations to the observed dynamics by the dielectric techniques. The information obtained by ESI measurements at room temperature and by DSC measurements, provide the possibility of evaluating the observed dynamics with respect to water organization in the materials (primary sorption sites, crystallization, amount of uncrystallized water). The comparative study of different hydrated systems by the particular methodology, induces more parameters relevant to the structural differences between the systems, i.e. molecular weight, stiffness, aminoacid sequence proportionality etc. This chapter presents comparative results on several hydrated systems and, in particular, two globular proteins, BSA and lysozyme, two fibrous proteins, elastin and collagen, a hydrophilic polysaccharide in the form of a hydrogel (hyaluronic acid, HA) and a simple digest derivative of the globular protein casein (casein peptone). The detailed presentation of the results obtained for the additional hydrated systems (except from BSA and elastin which have been presented thoroughly in chapters 5 and 6) is avoided, as chapter 7 focuses on the comparative discussion according to the major issues arising from the results so far, which are a) the main relaxation of uncrystallized water in the primary hydration shell (ν relaxation and its relation to the polar groups of the hydrated systems), b) the glass transition phenomena observed for the hydrated biomolecules and the extent to which those are affected by water dynamics and c) the dynamics of water beyond the primary hydration shell, the ice-like water structures and the effect of confinement. The results are discussed in comparison to literature results on synthetic polymers, hydrated biopolymers and water under confinement.

7.2. Materials and Sample preparation

Information on the samples and the sample preparation for BSA and elastin are given in sections 5.2 and 6.2, respectively. The information for the rest of the systems discussed in chapter 7 are categorized as follows.

7.2.1 Globular protein Lysozyme

Lysozyme from chicken egg white (62970 Fluka) in form of dried powder, dialyzed and lyophilized was supplied from Sigma-Aldrich (single-chain mol wt 14.3 kD, Mr~14600) and used as received. Water with 10 μ S/cm conductivity was employed for preparation of solutions for DSC and for dielectric measurements. More details can be found in reference [Panagopoulou 2011a]

7.2.2 Fibrous protein Collagen

Collagen from Bovine Achilles Tendon (C9879 Sigma) in the form of white powder was purchased from Sigma-Aldrich and used as received. Water with 10 μ S/cm conductivity was employed for the hydration of the samples. The hydration was achieved either by vapor adsorption ($0 < h_w < 0.33$) or through immersion in deionized water ($h_w > 0.33$) and subsequent equilibration in a hermetically sealed boxes placed in sealed jars at 100% rh atmosphere for 24 hours..

7.2.3 Hyaluronic Acid hydrogel (HA)

The Hyaluronic Acid hydrogels were synthesised in the Center of Biomaterials in the Polytechnical University of Valencia (upv), in Valencia, Spain. The synthesis procedure is described in what follows:

Synthesis: HA A 5 wt% solution of HA (Sigma, HA sodium salt from streptococcus equi sp. 1.63 MDa) was obtained by stirring the salt in a 0.2 M sodium hydroxide (NaOH; extrapure, Scharlau) aqueous solution for 24 h. Next, divinyl sulfone (DVS; 118.15 Da, 97%, Aldrich) was added as crosslinker, at a molar ratio 0.8 and stirred for 1 min before pouring the mixture into 5 cm diameter Petri dishes, 5 ml of the mixture each. The solution was allowed to dry for 24 h at 25°C. After demolding, the films were rinsed in a 40/60 vol % mixture of distilled water/acetone for 15 min to eliminate NaOH and DVS residues, followed by three rinsings in distilled water, dried under vacuum and stored.

The hydration of the samples was achieved through equilibration to constant weight (typically achieved in three or four days) above saturated salt solutions in sealed jars. Weights were determined using a Bosch SAE 200 balance with 10^{-4} g sensitivity. The jars were kept in a dark place, in order to avoid HA degradation due to light exposure. The dry mass m_{dry} was determined by drying the sample in vacuum for 72 h at 40°C. The hydration of the sample of $h_w=0.69$, was achieved through immersion in deionized water and subsequent equilibration in a hermetically sealed box placed in a sealed jar at 100% rh atmosphere for 24 hours. More details can be found in reference [Panagopoulou 2013b].

7.2.3 Casein Peptone

Casein peptone digest of high tryptophan content (403898 PANREAK), in the form of yellow powder, was purchased from Sigma-Aldrich and used as received. The powder exhibits high solubility in water and forms homogeneous aqueous solutions in the hydration range of about $0.40 \leq h_w \leq 0.90$. The sample at ambient conditions exhibits a water fraction value of $h_w = 0.14$. The dry mass m_{dry} was determined by drying the sample in vacuum for 72 h at 70°C. The hydration of the samples was achieved either through weight equilibration above saturated salt solutions or by the preparation of aqueous solutions of various compositions.

7.3 Glass transition and water dynamics

ESI Measurements

The ESI results of the hydrated systems studied in this thesis, are summarized in Fig. 7.1. The results for the HA hydrogel reveal the increased hydrophilicity [Cowman 2005] at water activity values $\alpha_w > 0.6$, where the water uptake is extremely high, despite the crosslinking. The increased adsorption of water at high levels of hydration has been attributed to a reorganization in the material due to swelling. [Servaty 2001, Panagopoulou 2013b]. The h_m value for HA has been calculated as $h_m = 0.114$ which corresponds to $h_w = 0.10$. The ESI results on collagen, show a pronounced hysteresis loop at desorption like in the case of elastin (chapter 6). No hysteresis was recorded for the globular proteins BSA and lysozyme [Panagopoulou 2011a,b]. The hysteresis loop could be associated to the protein structure, in the sense that fibrous proteins being more stiff, may show increased water holding capacity due to swelling/deswelling procedures (see also chapter 4, section 4.1, and [Lee 2013]). The associated water molecules would be the ones which condensate near hydrophobic sites by diffusion (see chapter 6 and [Panagopoulou 2013a]). A comparison of the sorption data between BSA and lysozyme may also be seen in Fig. 7.1. An interesting observation by comparison of the two systems, is that the water uptake is similar for both systems at low water activities and, particularly, for water contents lower than about $h_a = 0.25$, which is the critical water content above which water clustering is significant [Panagopoulou 2011a,b]. At higher water activities BSA absorbs higher amounts of water, in terms of h_a , compared to lysozyme, for the same water activity. This fact supports the idea that despite the difference in molecular weights (14000 for lysozyme, 66000 for BSA), the water uptake is different only if there is a concentrated amount of water molecules out of the primary hydration shell, reflecting the increasing swelling degree with increasing molecular weight, as it was shown for various polymers [Heyd 2006]. On the other hand, in the case of collagen the water uptake is higher when compared to the one of elastin during sorption (Fig. 7.1), in the entire α_w range. Finally, a comparative diagram for sorption data for all of the biopolymers dealt with in chapter 7 is shown in Fig. 7.1. A global observation is the fact that all studied systems exhibit similar water uptake during sorption, at low α_w values. In

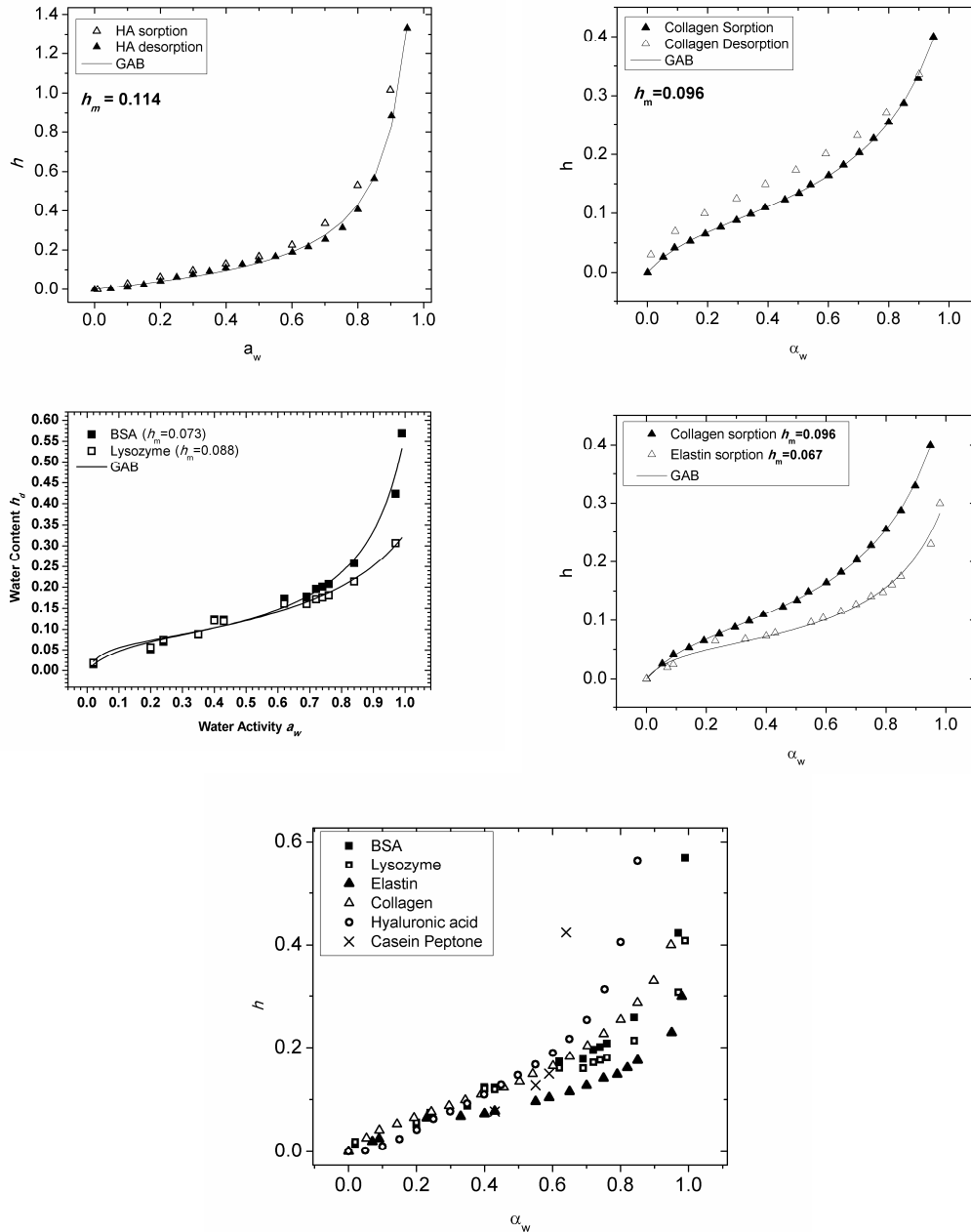


Fig. 7. 1 Water content h_d against water activity α_w at 25 °C for BSA, Lysozyme, Elastin, Collagen, HA and casein peptone, during sorption and/or desorption. Points are experimental data and the solid line is the fit of GAB equation (eq. (4.2)) to the data.

particular, the differences between different samples are visible for $\alpha_w > 0.4$ (corresponding to $h_d \sim 0.10$) and even more pronounced at higher α_w . Regarding the data for casein peptone, the data stop at $\alpha_w = 0.64$, showing a water content $h_d = 0.43$ (corresponding to $h_w = 0.30$). At higher water activity values, the solid samples absorb too much water and they are diluted (casein peptone forms homogeneous aqueous solutions of concentrations in the range of $0.4 \leq h_w \leq 0.9$).

As a conclusion, water adsorption is similar for all the systems below h_m , i.e. the critical water content at which water molecules are attached mainly to primary sorption sites (and before clustering of water molecules sets in). The analysis of sorption data according to the GAB equation (eq.(4.2)) in Fig. 7.1 shows that h_m (h_m is denoted in the plots in Fig. 7) is in the range of $0.067 \leq h_m \leq 0.114$ (corresponding to $0.063 \leq h_w \leq 0.10$), for all systems.

7.3.1 The ν relaxation and its relation to the secondary relaxation of polar groups

The results regarding the main secondary relaxation of uncrystallized water and its relation to a secondary relaxation of polar groups on the protein surface, have been discussed in detail, for the globular protein BSA (chapter 5) and the fibrous protein elastin (chapter 6). In both cases, the rate of plasticization at low water fractions was found to be related to the critical water content, h_m (water molecules attached on primary sorption sites, calculated by ESI), in agreement to several literature results on various systems [Pissis 1985,1990, Anagnostopoulou-Konsta 1987, Ratkovic 1997, Sugimoto 2008, Panagopoulou 2011a,b]. The results obtained by ESI for all of the systems studied were presented in the previous paragraph.

Dielectric loss $\epsilon''(f)$ versus frequency at $T=-90^\circ\text{C}$ for hydrated HA, collagen, casein peptone and lysozyme is seen in Fig. 7.2 a,b,c and d, respectively, at several water fraction values h_w indicated on the plots. At this low temperature the dielectric loss peak corresponding to the relaxation of polar groups and the ν relaxation is within the experimental window for most of the samples. Analogous diagrams for BSA and elastin have been already presented in chapters 5 and 6 at the same or higher temperatures (Fig. 5.12b, Fig. 6.9 and 6.14), while examples of the fittings by a sum of Cole-Cole functions to the dielectric loss spectra including the contribution of polar groups and/or the ν relaxation have been shown in Fig. 5.13, 5.15 for BSA and Fig. 6.9, 6.14, 6.15 and 6.16 for elastin. The methodology of the fitting procedure has been described in detail in sections 4.3 and 5.5.2. The dielectric loss spectra of the systems dealt with in chapter 7 have been fitted accordingly. The temperature dependence of the relaxation times for the relaxation of polar groups and the ν relaxation is shown for HA, collagen, casein peptone and lysozyme, in Fig. 7.3 a, b, c and d, respectively, at selected h_w values indicated on the plots. The trace of the ν relaxation from reference [Ngai 2011] is also added in the diagrams, for eye guidance.

In the raw data of Fig. 7.2 the overall behavior of the relaxation of polar groups and the ν relaxation may be seen for the additional hydrated systems, other than BSA and elastin, where the similarities and differences may be highlighted. Fig. 7.2 a shows the results on hydrated HA hydrogels. The relaxation peak corresponding to the polar groups moves to higher frequencies (plasticization) until a value of $h_w=0.23$. The difference observed in comparison to the rest of the systems is that the magnitude of the peak does not increase constantly with hydration level. Starting from $h_w=0.06$ it increases initially for $h_w=0.08$ and 0.14 and finally decreases steeply for $h_w=0.23$. This behavior is attributed to a structural change in the material, due to swelling, which takes place drastically for HA [Panagopoulou 2013b, Servaty 2001]. This change is reflected in the huge water uptake already seen in ESI measurements (Fig. 7.1). The peak of the ν relaxation in Fig. 7.2 increases significantly in

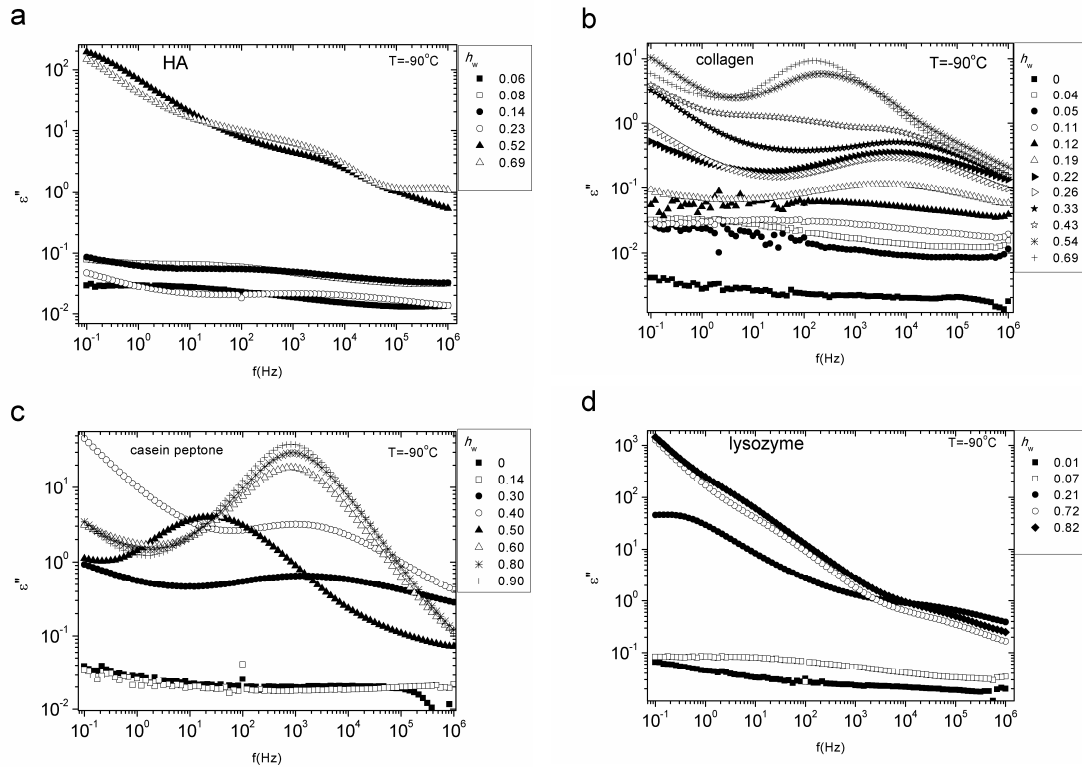


Fig. 7. 2 Dielectric loss $\epsilon''(f)$ versus frequency at $T=-90^\circ\text{C}$ for hydrated a) HA b) collagen c) casein peptone and d) lysozyme, at several water fraction values h_w indicated on the plots

magnitude and its position stabilizes for $h_w=0.52$ and 0.69 , centered at about $5 \cdot 10^3 \text{ Hz}$. The peak is not clearly observed in the raw data, as several contributions interfere at higher and lower frequencies, such as the α relaxation or ice. Nevertheless, as it is shown in the analysis of the results, the dynamics of the ν relaxation differentiates at high water fraction values for HA, exhibiting lower activation energy than the one of polar groups at low h_w values (see Fig. 7.3 a). Moving to the results for hydrated collagen in Fig. 7.2 b, the evolution of the relaxation of polar groups and the ν relaxation with hydration level may be followed. The peak corresponding to the dry sample is located at lower frequencies, out of the experimental window. The main loss peak moves to higher frequencies with increasing water fraction and increases in magnitude. Finally, the peak saturates in position and magnitude, for $h_w \geq 0.33$. The saturation of the position occurs in the temperature frequency range of the ν relaxation, in analogy to the results on BSA and elastin. At $h_w \geq 0.33$, the spectra become more complex, containing contributions of additional relaxation peaks at lower frequencies, corresponding either to an additional relaxation due to uncrystallized water, or to a relaxation due to ice. The contributions due to ice will be evaluated in what follows in section 7.3.4 (Ice-like structures- confinement). The two relaxations due to uncrystallized water exhibit lower activation energy values than the ν relaxation at lower h_w (see Fig. 7.3 b, samples of $h_w \geq 0.43$). Moving to the raw data for casein peptone, the overall behavior is quite different than the observed results on proteins. Starting at low h_w , the relaxation of polar

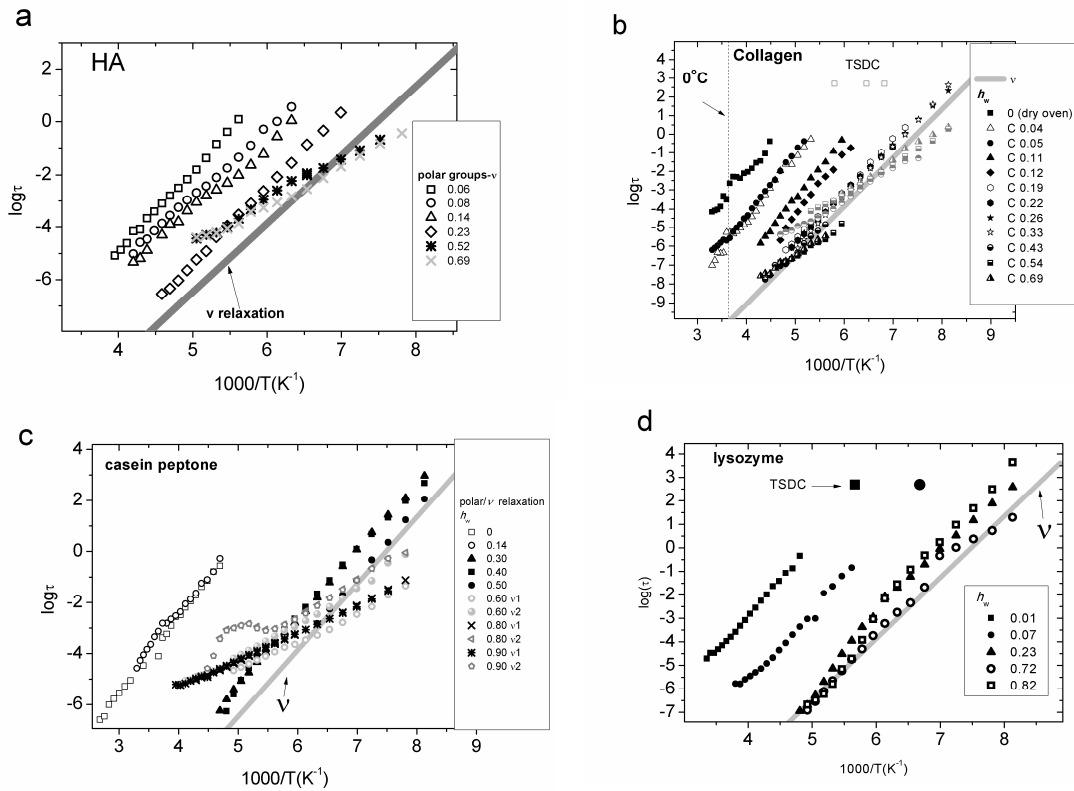


Fig. 7.3 Temperature dependence of the relaxation times for **a)** the relaxation of polar groups/uncrystallized water (ν relaxation) for HA hydrogel **b)** the relaxation of polar groups and the ν relaxation for Collagen (2 relaxations at $h_w = 0.43, 0.54, 0.69$, gray and black symbols) **c)** the α relaxation and the ν relaxation for casein peptone (2 relaxations at $h_w = 0.60, 0.80, 0.90$, gray and black symbols) and **d)** the relaxation of polar groups and the ν relaxation for lysozyme. TSDC data are denoted in the plots.

groups is located out of the experimental window, for both $h_w = 0$ and 0.14 and shows similar temperature dependence of the relaxation times (see Fig. 7.3 c), i.e. no plasticization occurs for the increase of h_w from 0 to 0.14. The relaxation peak observed for the sample of $h_w = 0.30$ is located already in the temperature frequency range of the ν relaxation. The position of the peak stabilizes and the latter increases in magnitude for $h_w = 0.4$. The sample of $h_w = 0.50$ shows a pronounced peak at lower frequencies, which is centered at about 10^1 Hz. By analysis of the data it has been estimated that this peak corresponds to the contribution of ice, rather than of uncrystallized water, and that the contribution of the ν relaxation, which exhibits significantly reduced magnitude, when compared to the one in the case of $h_w = 0.4$, is located in the temperature frequency region of the ν relaxation for $h_w = 0.50$ in Fig. 7.2 c, overlapped by the ice peak in the low frequency side. These results are in agreement with the results by calorimetry, where no crystallization of water during cooling is observed for $h_w \leq 0.40$ and crystallization starts at $h_w = 0.50$ with an apparent decrease in the fraction of uncrystallized water, exhibiting a minimum, as calculated by the crystallization and melting peaks. These DSC results will be described later on in the section concerning the glass transition (see section 7.3.3, Fig. 7.7 and 7.11 a). At this point, we keep in mind that a reorganization of the

water inside the sample occurs for casein peptone around this water fraction range. The reorganization is supported further by the raw data in Fig. 7.2 c at higher water fraction values, where a pronounced peak dominates for $h_w=0.60, 0.80$ and 0.90 in the temperature frequency region of the ν relaxation. As it revealed by analysis of the dielectric loss data, the peak includes contributions from more than one relaxation peaks, and the differentiated dynamics is reflected in the reduction of the activation energy of the observed relaxations (see Fig. 7.3 c, $h_w \geq 0.60$). Finally, in the raw data of lysozyme in Fig. 7.2 d are similar to the respective ones for BSA in Fig. 5.12 b. At this point we recall that in the case of BSA and elastin, a single relaxation of lower activation energy than the one of the ν relaxation was observed for $h_w=0.80$ for BSA [Shinyashiki 2009] and for $h_w=0.50$ for elastin (chapters 5 and 6). The results on lysozyme suggest that the ν relaxation maintains its relaxation time temperature dependence and activation energy values, even at water fraction values as high as $h_w=0.82$ (Fig. 7.3 d).

Finally, the dielectric loss data and the temperature dependence of the relaxation of polar groups for dry samples or almost dry samples containing only residual water, are shown in Fig. 7.4 a and 7.4 b, respectively, for all of the systems studied. The trace of the relaxation is similar for most of the samples. The data which correspond to samples containing residual water ($h_w=0.01-0.02$) exhibit lower relaxation times, as expected (compare BSA of $h_w=0$ (dry) and 0.01). A careful examination of the data for collagen reveals a deviation from the Arrhenius behavior for the relaxation of polar groups at temperatures higher than about 0°C ($1000/T < 3.66$), also seen in Fig. 7.3 b. This is attributed to the melting of some crystalline components of the collagen structure revealed by DSC (see DSC results in section 7.3.3). This fact provides further evidence that the relaxation observed corresponds to the movement of small polar groups, rather than the reorientation of water molecules alone.

In order to better evaluate the hydration dependence of the relaxation of polar groups and of the ν relaxation (at higher h_w), the fractional exponent $\beta(T)$ of the Cole-Cole function corresponding to the dielectric loss peak for each process, as well as the activation energy values, E_{act} , are plotted against water fraction h_w for all systems, in Fig. 7.5 a and b, respectively. For systems where a crossover temperature was observed (see chapter 5) the activation energy has been calculated at temperatures lower than the crossover. In addition, two separate values for $\beta(T)$ and E_{act} are denoted in the graphs, in the case where two relaxations were recorded at high h_w (collagen and casein peptone). Finally, error bars are added in Fig. 7.5 a, which do not refer to experimental errors. In particular, the data points resemble the average value of $\beta(T)$ in the temperature range of the measurements and the error bars indicate the maximum and minimum values. For example, in the case of BSA, where the fractional exponent $\beta(T)$ obtains a stable value in the fitting procedure [Panagopoulou 2012], there are no error bars in Fig. 7.5 a.

In Fig. 7.5 a the values of $\beta(T)$ show a very well defined h_w dependence for the hydrated proteins (excluding HA and casein peptone) in the hydration range where h_w is lower than about 0.13 (for BSA, see Table 5.3 in chapter 5). In particular, $\beta(T)$ decreases with water fraction increase, from a value of about 0.4 for the dry samples, to a value of about 0.15 . The decrease of $\beta(T)$ reflects that the distribution of relaxation times becomes broader

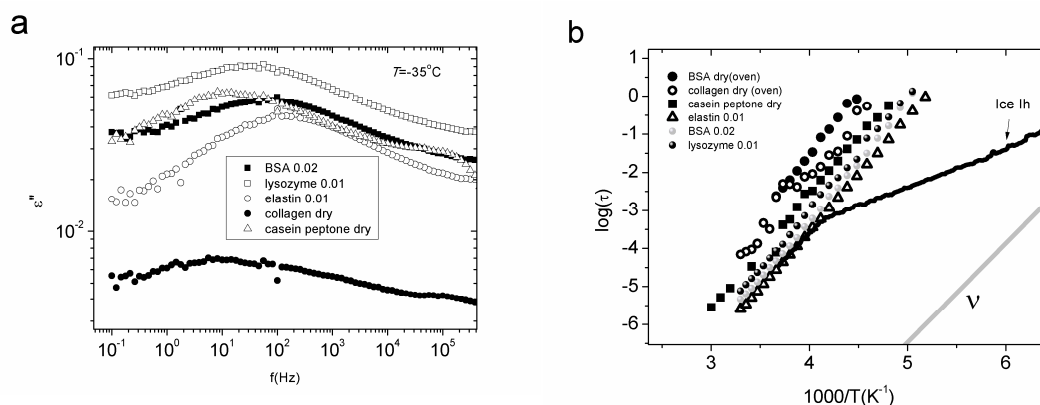


Fig. 7.4 a) Dielectric loss $\epsilon''(f)$ versus frequency for several dry samples (or almost dry, containing residual water) of h_w values indicated on the plot b) the relaxation of polar groups for several dry samples (or containing residual water), at h_w values indicated on the plot

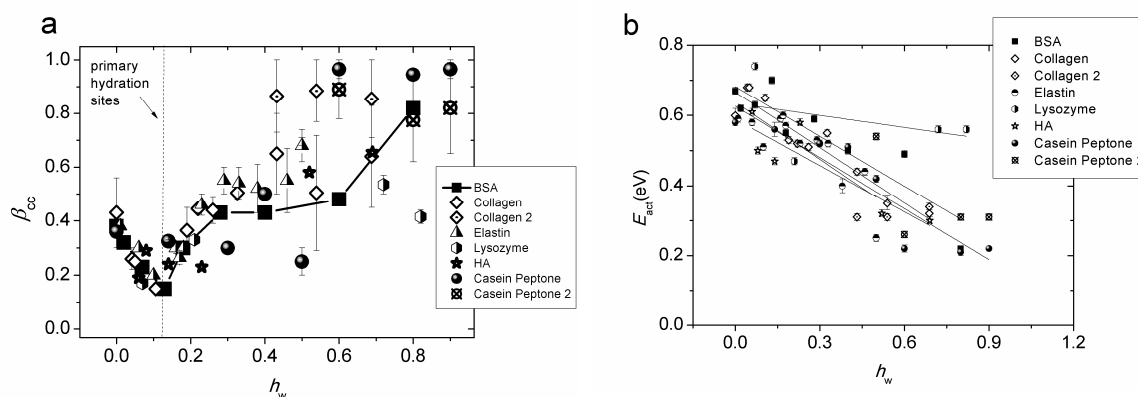


Fig. 7.5 a) Fractional exponent $\beta(T)$ of the Cole-Cole function for the relaxation of polar groups and the ν relaxation versus h_w , for several hydrated systems indicated on the plot. Error bars do not refer to experimental errors. In particular, the data points resemble the average value of $\beta(T)$ in the range of the measurements and the error bars indicate the maximum and minimum values. For example, in the case of BSA, where the fractional exponent $\beta(T)$ obtains a stable value in the fitting procedure [Panagopoulou 2012], there are no error bars. b) Activation energy, E_{act} versus h_w , for the relaxation of polar groups and the ν relaxation versus h_w , for several hydrated systems indicated on the plot. In the case of systems where a crossover is observed, the activation energy is calculated at temperatures lower than the crossover temperature. The solid lines through experimental data are linear fits for each system separately, the one of lower slope corresponding to lysozyme.

as water molecules are being gradually attached on to the primary (hydrophilic, charged or uncharged) polar sites of the protein surface. This means that the polar groups which are hydrated move faster than the rest, resulting in a less homogeneously hydrated surface. At $h_w \geq 0.13$ a change is observed regarding the hydration dependence of the fractional exponent $\beta(T)$. Following the data which correspond to hydrated proteins (excluding HA and casein peptone), the $\beta(T)$ increases with hydration level from a value of about 0.15 to a value of about 0.4 for $h_w \sim 0.3$. This increase reflects the gradual increase of cluster formation. At this point we recall the picture described in chapter 5 for hydrated BSA. The increase of h_w above about 0.10, was accompanied by the appearance of segmental dynamics in the system,

attributed to the combined motion of water clusters with protein chains. For h_w higher than about 0.20, water clustering becomes significant, the formation of a percolating water cluster is gradually achieved and crystallization events of water set in (either during cooling or heating). Coming back to Fig. 7.5 a, the data support this scenario also for lysozyme, elastin and collagen. The $\beta(T)$ values stabilize at a mean value in the range of 0.4-0.5, for water fractions in the range 0.2 to 0.4 approximately. The stabilization reflects the formation of a percolating water cluster around the protein surface. The stabilized value is higher for elastin and collagen compared to BSA and lysozyme. Finally, at higher water fraction values, the differences between the different proteins are enhanced and a general increase of the fractional exponent is seen (with an exception for lysozyme). These differences totally agree with the observation by ESI that at high water activity values the water uptake is different (Fig. 7.1) and with the fact that excess water is organized differently in each system (for example see BSA and elastin in chapters 5 and 6 and collagen in Fig. 7.3b). Regarding the data which correspond to HA and casein peptone in Fig. 7.5 a, it can be seen that the hydration dependence of the fractional exponent $\beta(T)$ is different than in the case of hydrated proteins. The minimum at about $h_w=0.10$ is not evident for casein peptone. The fractional exponent decreases in a linear manner until about $h_w=0.3$ than increases for 0.4 and then decreases again for 0.5. It must be mentioned at this point that at $h_w=0.5$ crystallization of water occurs for the first time upon increasing water fraction, as the sample of $h_w=0.40$ does not exhibit crystallization of water during cooling. As it may be seen in Fig. 7.3 c the dynamics of the ν relaxation changes dramatically at $h_w=0.60$, where two relaxations of much lower activation energy, instead of one, are present. Analogous results may be seen in the case of HA in Fig. 7.5 a and 7.3 a. Like in the case of casein peptone, a structural change also occurs for HA hydrogels at high hydration levels [Panagopoulou 2013b]. The differences support the idea that the dynamics of the polar groups and hydration water are highly dependent on the aminoacid sequence and proportionality, as HA and casein peptone are much simpler than proteins.

The relation of the dynamics to h_m suggests that the polar groups associated with the particular dynamics are mainly the hydrophilic aminoacid residues, i.e. the ones that are located on the outer surface of the protein chains and are more accessible to water molecules, at least in the underhydrated state. The parameter h_m for elastin was determined to $h_m=0.067$. With the values of 72,000 for the molecular weight of tropoelastin and 18 for water, this corresponds to 261 water molecules directly bound to an elastin molecule. Out of the approximately 800 aminoacid residues of the molecule the fraction of about 0.3 (calculated as 261/800) is reasonable for the hydrophilic polar groups of elastin, which are mainly the main chain NH/O groups [Darwin 2001]. Similar calculations for the globular proteins lysozyme [Panagopoulou 2011a] and BSA [Panagopoulou 2011b] gave in both cases a fraction of about 0.45.

Moving on to Fig. 7.5b, the hydration dependence of the activation energy is seen for the relaxation of polar groups and the ν relaxation. The solid lines through experimental data are linear approximations of the evolution for each system. In general, the activation energy decreases with increasing h_w , from a value of about 0.7 for the dry samples, to values as low as 0.2 at high h_w values. An exception holds for lysozyme, where the decrease is less steep and the activation energy value is maintained to about 0.55 eV, i.e. the energy required

to brake two hydrogen bonds. The exception for lysozyme holds also in Fig. 7.5 a, where the fractional exponent does not increase at high hydration levels, like for the rest of the systems (see also the trace of the ν relaxation in Fig. 7.3 d). The hydration dependence of the activation energy suggests that upon increasing water fraction, water molecules which relax via the ν relaxation become more and more dispersed, approaching the activation energy value required to brake one hydrogen bond instead of two. This is accompanied by the involvement of water molecules in different configurations, such as ice-like structures (see examples for BSA and elastin in chapters 5 and 6).

Summarizing, it is shown that the main secondary relaxation of uncrystallized water in the primary hydration shell, is highly associated to the protein surface dynamics in underhydrated conditions and generally shows differentiated dynamics at high hydration levels, due to swelling and or the complex organization of water in the systems, forming ice structures. In the following sections, the discussion will focus on the dynamics of the ν relaxation at water fraction values where the relaxation includes contributions from uncrystallized molecules alone, and corresponds, as it has been already suggested in chapter 5 for BSA [Panagopoulou 2012], to the secondary Johari-Goldstein relaxation of water.

7.3.2 The w relaxation and its relation to the liquid-liquid phase transition (LLPT)

In a recent paper in Nature Materials by Murata and Tanaka [Murata 2012] a liquid-liquid phase transition was observed in a water-glycerol mixture of $h_w=0.835$. The transition from liquid 1 to liquid 2 was recorded experimentally and was found to occur through the mechanisms of nucleation and growth and spinodal decomposition. Liquid 2 was found to be metastable against crystallization. The transition was visualized using phase contrast spectroscopy and the heat capacity was measured by adiabatic calorimetry. It was found that liquids 1 and 2 differ in density, refractive index, structure, hydrogen bonding state, glass transition temperature and stability and that the transition between the two liquids is mainly driven by the local structuring of water rather than of glycerol, suggesting a link to a plausible liquid-liquid transition in pure water.

Fig. 7.6 shows the trace of the α relaxation of liquids 1 and 2, the trace of the β relaxation of liquid 1, from [Murata 2012], together with the trace of the ν relaxation and the w relaxation of BSA of $h_w=0.4$ from chapter 5. In addition, the VTF curve fitted to the w relaxation (see chapter 5, Fig. 5.20) is also added to the diagram. Interestingly enough, there is quite an agreement between the experimental data for BSA and the ones for the water-glycerol mixture. Regarding the ν relaxation it coincides with the trace of the β relaxation of liquid 1 at low temperatures and the recorded crossover (see chapter 5) is in agreement to the one observed in liquid 1. The VTF curve was fitted to the trace of the w relaxation in the temperature region between the T_g of the hydrated system and the homogeneous nucleation temperature ($-80^\circ\text{C} < T < -40^\circ\text{C}$) (see chapter 5, Fig. 5.20). It may be seen in Fig. 7.6 that the trace of the α relaxation of liquid 2 coincides with the VTF curve. The data of the w relaxation at low temperatures deviate from the VTF curve, heading towards the trace of the α relaxation of liquid 1. They also deviate from the VTF curve above the homogeneous nucleation temperature ($T=-40^\circ\text{C}$), which is in agreement with the metastable nature of liquid 2. In

[Murata 2012] it is suggested that liquid 2 contains nanocrystals of cubic ice (Ic). Another option is that the trace of the w relaxation at high temperatures may correspond to the secondary relaxation, which is not recorded clearly in the results. We may assume that the ν relaxation transforms into the β relaxation of liquid 2 in a way that we cannot follow, because the frequencies where this takes place are out of the experimentally observed region.

By this comparison, the assumption made in chapter 5, that the w relaxation corresponds to a separate phase of internal uncrystallized water, or to the relaxation of primary crystal forms, is well supported. In what follows, the VTF curve of Fig. 7.6 will be considered in the discussion of water dynamics and the glass transition in the hydrated systems.

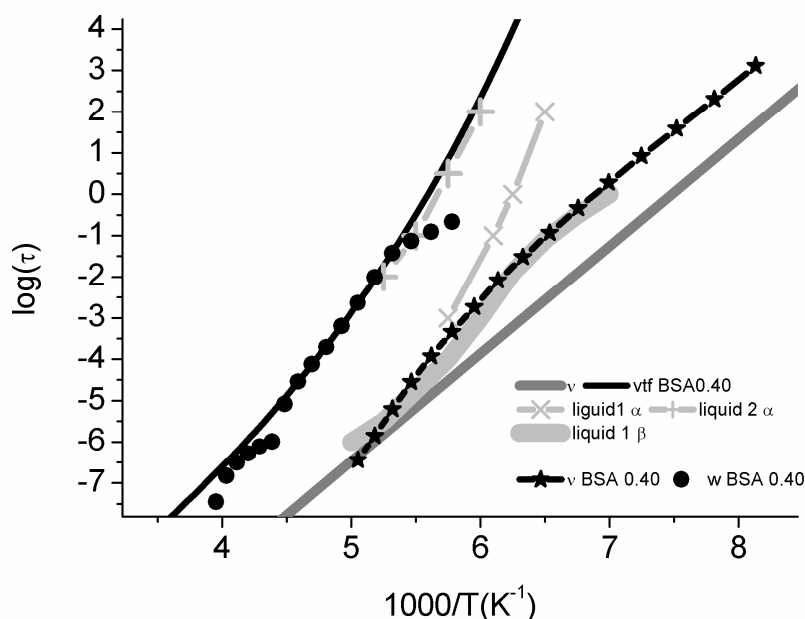


Fig. 7. 6 Temperature dependence of the relaxation times for the ν relaxation and the w relaxation in BSA of $h_w=0.40$ and the α and β relaxations of liquid 1 and the α relaxation in liquid 2, in a water-glycerol mixture by reference [Murata 2012]. The solid line through the experimental data is the VTF fit of the data of the w relaxation for $h_w=0.40$ in the temperature range between the T_g of the hydrated system and the homogeneous nucleation temperature ($-80^\circ\text{C} < T < -40^\circ\text{C}$). The trace of the ν relaxation from reference [Ngai 2011] is also added in the plot.

7.3.3 Glass transition in hydrated biopolymers

Before starting the discussion on the relation of the glass transition to the α relaxation observed by dielectric techniques and the complex dynamics of water in the systems, a quick reference should be made to the results from DSC, so that the picture regarding the glass transition and the states of water in the materials is clear. Cooling and heating thermograms, at cooling and heating rates of $10^\circ\text{C}/\text{min}$, are shown in Figures 7.7, 7.8, 7.9 and 7.10, for

hydrated casein peptone, HA, collagen and lysozyme, respectively. The glass transition temperature was recorded for casein peptone and HA during heating and for lysozyme only during cooling [Panagopoulou 2011a]. The estimated glass transition temperatures as the midpoint of the heat capacity step, are highlighted in the diagrams by vertical solid lines. No glass transition was recorded by DSC for hydrated collagen in the range $-120^{\circ}\text{C} < T < 20^{\circ}\text{C}$ and for dry collagen in the range $-120^{\circ}\text{C} < T < 230^{\circ}\text{C}$ (results not shown here). Starting from the results on casein peptone, it is seen in Fig. 7.7 a, that no crystallization of water takes place during cooling for the dry sample and for the solution of $h_w=0.40$. This h_w value is relatively high when compared to the rest of the hydrated systems, where, as it has been already shown for BSA and elastin and will be shown in what follows for collagen, lysozyme and HA, crystallization during cooling occurs already at about $h_w=0.3$.

The casein peptone solution of $h_w=0.50$ shows crystallization during cooling. The crystallization temperature T_c is located at about $T_c=-40^{\circ}\text{C}$ and seems to include two contributions. As it has been already mentioned in section 7.3.1, a dramatic reorganization of water occurs in the mixture at this h_w value, accompanied by a decrease in the magnitude of the ν relaxation peak in Fig. 7.2. c. At higher h_w values in Fig. 7.7a, the crystallization peak seems to consist of only one contribution and T_c moves to higher temperature values at about -20°C . The heating thermograms for casein peptone are shown in Fig. 7.7 b. A first observation is that no glass transition is recorded for the dry sample, in the experimental temperature range. It must be mentioned that no glass transition was recorded up to $T=80^{\circ}\text{C}$ (measurement not shown here). The sample of $h_w=0.40$ in Fig. 7.7 b exhibits a heat capacity step, corresponding to a glass transition, and the estimated T_g is highlighted by a vertical solid line. The glass transition step is followed at higher temperatures by a cold crystallization exothermic peak and a subsequent melting peak. The heat capacity step for $h_w=0.40$, is enhanced when compared to the ones recorded at higher water fractions, where crystallization of water occurs during cooling. In addition, the T_g values are significantly higher at higher h_w values and obtain a stabilized value at about $T_g=-45^{\circ}\text{C}$, moving slightly to lower temperatures with h_w increase. These observations regarding the glass transition support the already made assumption in the case of lysozyme [Panagopoulou 2011a] and BSA [Panagopoulou 2011b], that the origin of the glass transition is the combined motion of uncrystallized water molecules and the biomolecule segments. More discussion regarding the origin of the glass transition will follow later on in this section. Moving back to the heating thermograms of casein peptone in Fig. 7.7 b, smooth cold crystallization peaks followed by strong melting peaks are observed for the casein peptone solutions of h_w values in the range 0.50-0.80.

The DSC results during cooling for hydrated HA in Fig. 7.8 a, suggest that crystallization of water during cooling occurs for $h_w=0.31$ for the first time upon increasing water fraction (the lower h_w value measured being $h_w=0.17$), exhibiting multiple crystallization peaks. The crystallization peaks become more and more simple with increasing h_w and the T_c values move in general to higher temperatures. In Fig. 7.8 b the heating thermograms are shown at selected h_w values. The glass transition temperatures T_g recorded for $h_w \geq 0.06$ are highlighted by vertical solid lines and no glass transition step is recorded for the sample of $h_w=0.02$. Two cold crystallization peaks are recorded for $h_w=0.31$.

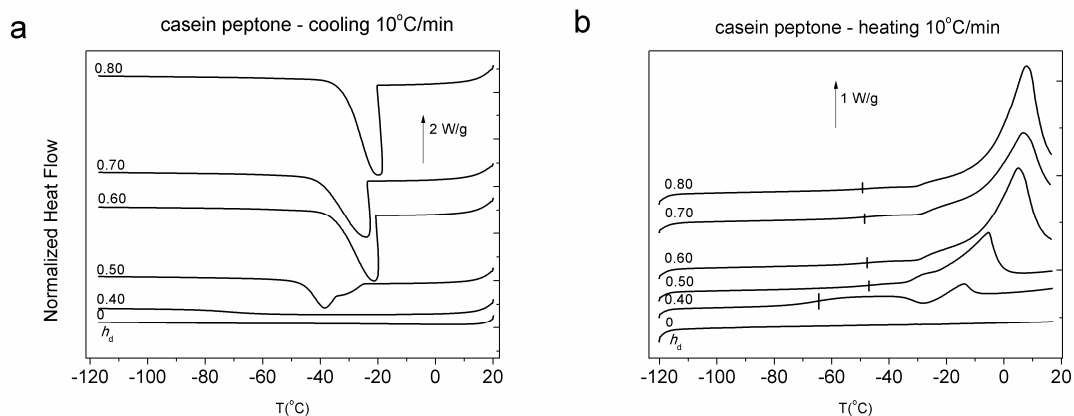


Fig. 7. 7 Normalized heat flow during **a)** cooling and **b)** heating against temperature, both at $10^\circ\text{C}/\text{min}$, for dry casein peptone and its aqueous solutions at different water fraction values h_w indicated on the plots. The estimated glass transition temperature, T_g , during heating, is highlighted on the plot by vertical solid lines

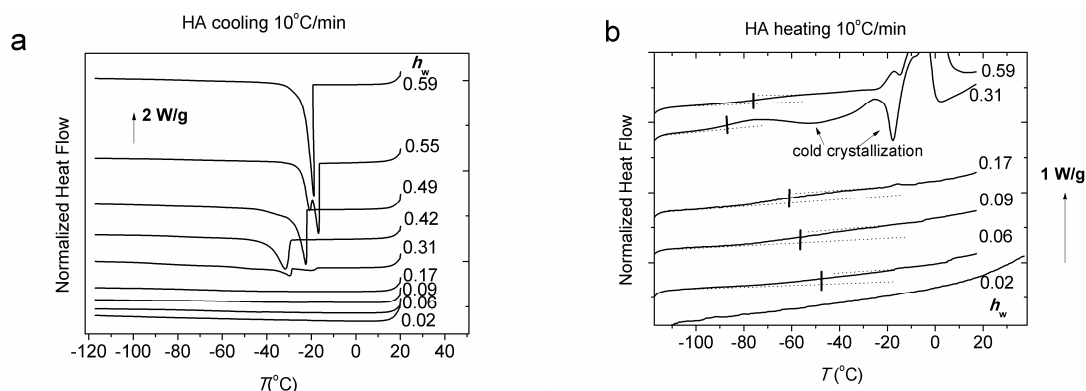


Fig. 7. 8 Normalized heat flow during **a)** cooling and **b)** heating against temperature, both at $10^\circ\text{C}/\text{min}$, for hydrated HA at different water fraction values h_w indicated on the plot. The estimated glass transition temperature, T_g , during heating, is highlighted on the plot by vertical solid lines

The results of hydrated collagen are shown in Fig. 7.9 a and b. The cooling thermograms in Fig. 7.9 a are qualitatively different than the ones observed for BSA (chapter 5), casein peptone and HA. A first observation is that two crystallization peaks during cooling are recorded already for the dry sample. These are a broad crystallization peak centered at about -2°C and a small peak centered at about -45°C . Based on measurements on a dry collagen sample, heated up to 150 , 180 and 230°C , we conclude that the broad peak corresponds to the crystallization of some collagen segments, as the peak is maintained even after water evaporation and heating up to 230°C , which is a reported denaturation temperature for collagen [Brodsky 2005]. Regarding the small peak centered at about -45°C , it is believed to be attributed to the crystallization of strongly bound water, as it is maintained after evaporation of residual water upon heating to 150°C but vanishes after heating above 180°C (results not shown here). The magnitude and position of the peak seem to be independent of hydration level. This peak shows similar characteristics with an analogous peak observed for elastin for the immersed samples of $h_w \geq 0.31$ (see chapter 6, Fig.

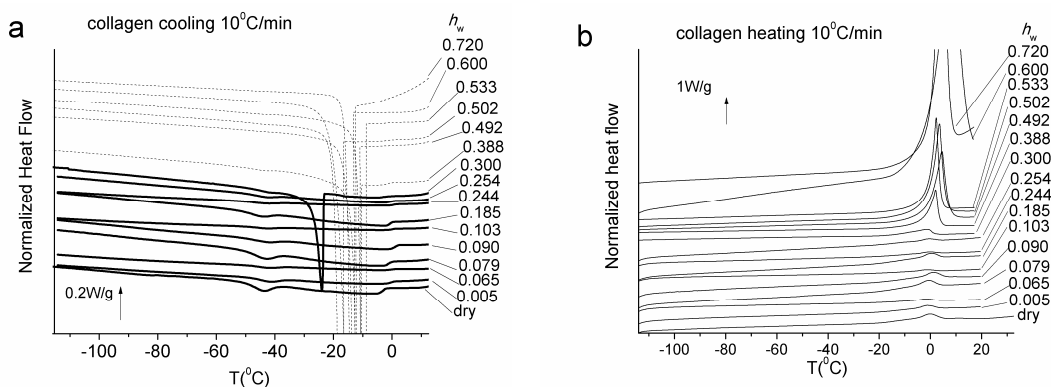


Fig. 7. 9 Normalized heat flow during a) cooling and b) heating against temperature, both at 10°C/min, for dry and hydrated collagen at different water fraction values h_w indicated on the plots. No glass transition is recorded for hydrated collagen in the experimental temperature range

6.2 a). At $h_w=0.30$ in Fig. 7.9 a, a crystallization peak is recorded centered at about -25°C , which is attributed to crystallization of water. At higher h_w , this crystallization peak increases in magnitude and T_c moves to about -15°C , where it stabilizes. At this point it must be mentioned that the two crystallization peaks which are recorded for the dry sample, are also maintained at higher water fractions, although this is not obvious in the scale of Fig. 7.9 a. Moving to the heating thermograms for collagen in Fig. 7.9 b, a first important observation is that no glass transition is recorded for the hydrated collagen samples. Furthermore, no cold crystallization is either observed. A single melting peak, centered at about 0°C , is recorded in the entire h_w range. By comparing the calculated values of the crystallization and melting enthalpies, we conclude that the melting peak at low h_w values below 0.3, includes the melting of both, the peak due to crystallization of protein segments and strongly bound water. It is clear, that DSC results of hydrated collagen are more similar to the ones on elastin, resembling probably the hydrophobic nature and low swelling degree of those fibrous proteins.

Finally, the DSC results on lysozyme may be seen in Fig. 7.10 a and b. The glass transition step is recorded only during cooling with no apparent explanation [Panagopoulou 2011a]. The crystallization during cooling starts already at $h_w=0.218$. The results are similar in general to the ones obtained for BSA and HA, relevant to the evolution of the peaks with hydration level and cold crystallization. A main difference, when comparing with the results for BSA, may be found regarding the melting peaks at high hydration levels. Crystallization and melting peaks of water in DSC measurements have proved to be very helpful to characterize different states of crystalline water in case of different hydrophilic polymers [Ping 2001], or in case of confined water within AOT lamellar mesophases [Prouzet 2010]. By comparative studies with DSC and FTIR measurements it is shown that multiple fusion peaks correspond to distinct water populations with respect to their connectivity [Ping 2001, Prouzet 2010], whereas the maximum temperature of a single fusion peak is independent of the host material surface and gives information on the size distribution of the crystal phase, in case of water confined within the pores of organosilane-modified silica [Oodo 2011]. The melting peaks observed in the thermograms in Fig. 5.2 b for BSA don't seem to consist of multiple peaks, suggesting that the population of water that crystallizes upon cooling

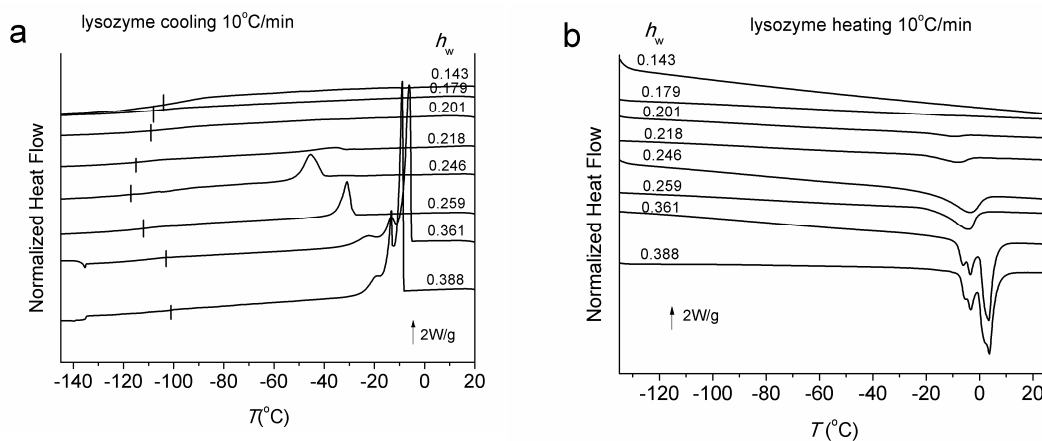


Fig. 7. 10 Normalized heat flow during **a)** cooling and **b)** heating against temperature, both at 10°C/min, for hydrated lysozyme at different water fraction values h_w indicated on the plots. The estimated glass transition temperature, T_g , during cooling, is highlighted on the plot by vertical solid lines

mainly of one kind of water, with respect to the connectivity of the latter or the size of the water crystals, at each hydration level. This observation supports the hypothesis that a great part of water in the secondary hydration shell of the protein behaves as unfrozen water. In case of lysozyme in Fig. 7.10b the shape of the melting peaks at higher water fractions is more complicated, consisting clearly of more than one contribution, showing that multiple populations of crystals are present even at water fractions where bulk dynamics is dominant. This can be explained in terms of the higher degree of swelling for BSA, as it was shown by ESI measurements (see above), which causes a more homogeneous distribution of water at high water contents.

The amount of uncrystallized water in the samples has been calculated for all the hydrated systems, from the melting enthalpies of water during heating, according to the methodology described for BSA in chapter 5. The fraction of uncrystallized water, X_{ucw} is plotted against total water fraction h_w , for all of the systems studied, in Fig. 7.11 a. The number of uncrystallized water molecules, n_{ucw} , per aminoacid residue, against h_w are plotted in Fig. 7.11 b for the hydrated proteins. These results will be taken into account in the upcoming evaluation of the experimental results.

The results so far regarding the glass transition of the hydrated systems suggest that the latter is highly associated to the amount of uncrystallized water in the samples. First of all, the glass transition is not present for the completely dry samples in the case of BSA, casein peptone and HA. In the case of elastin the dry sample exhibits a glass transition, but the evolution of its magnitude with hydration level was found to depend non linearly on hydration level, and was significantly enhanced for water fractions where water clustering is significant according to ESI (see chapter 6). On the other hand, no glass transition was recorded for hydrated collagen. In the case of globular proteins, the α relaxation associated to the glass transition is recorded by dielectric techniques [Panagopoulou 2011a,b, 2012]. The α relaxation peak is followed by TSDC for h_w higher than about h_m for lysozyme [Panagopoulou 2011a] and BSA [Panagopoulou 2011b] and the results for BSA have been described in detail in chapter 5. Although the DSC results regarding the glass transition are

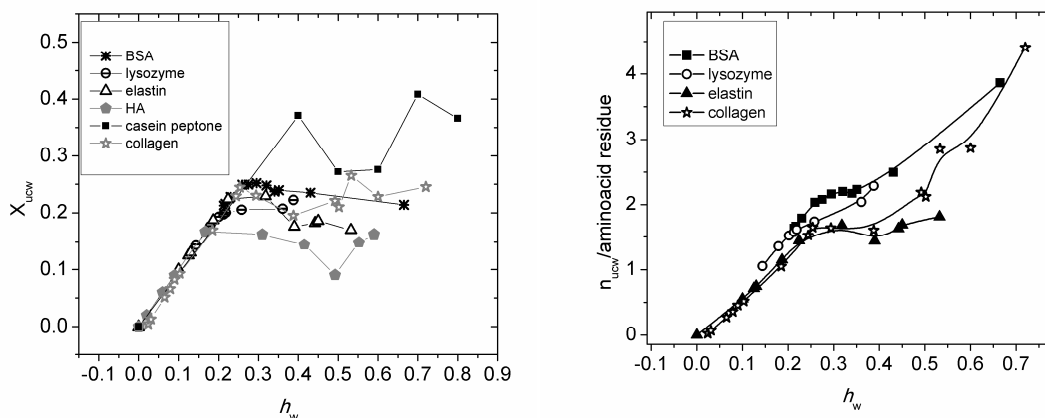


Fig. 7. 11 a) Fraction of uncrystallized water, X_{ucw} , against water fraction, h_w , for several hydrated systems indicated on the plot and b) number of uncrystallized water molecules, n_{ucw} , per aminoacid residue, against water fraction, h_w , for several hydrated proteins indicated on the plot

quite different for the different hydrated systems (glass transition only during cooling for lysozyme, glass transition in agreement to dielectric α relaxation for BSA, high glass transition temperature values for elastin, no glass transition for collagen), the dielectric response and the evolution of its relaxation time with hydration level is quite similar in the temperature region where the α relaxation was detected for BSA in chapter 5. In particular, we recall that a relaxation denoted as p was detected for hydrated elastin at h_w values higher than about 0.10, suggesting that this relaxation due to uncrystallized water is associated with the polarization process within clusters at the protein surface. It must be mentioned that in the case of collagen an analogous peak is recorded by the dielectric techniques, although no glass transition is detected by DSC. Those similarities of the α relaxation peak for BSA to the p peak for elastin, probe to the comparison of the two processes and the evaluation of their relation to the calorimetric glass transition. The raw data obtained by TSDC for the hydrated proteins at comparable h_w values are shown in Fig. 7.12 a. The characteristic temperatures for the α relaxation for BSA and lysozyme and the p relaxation for elastin and collagen, are plotted against water fraction h_w in Fig. 7.12 b, together with the T_g values recorded by DSC during cooling and/or heating for all of the systems studied. The main observation in Fig. 7.12 b regarding the evolution of the TSDC data, is that the T_α values (we use T_α for T_p in the case of collagen and elastin) move systematically to lower temperatures with the increase of h_w until a water fraction value of about 0.3 is reached, which corresponds to the onset of crystallization effects during cooling for the hydrated protein systems, as it was shown by DSC results. At higher h_w values the data obtain stabilized values in all cases. These are at about $T = -80^\circ\text{C}$ for BSA and lysozyme, and at about $T = -65^\circ\text{C}$ for the fibrous proteins elastin and collagen. The hydration dependence of the T_g values obtained by DSC is similar for all of the systems studied, regarding the stabilization above the water fraction where crystallization effects of water set in during cooling. The glass transition temperatures of elastin, which obtain significantly higher values than the ones for hydrated proteins and HA, decrease "in parallel" to the reduction of the T_α values with h_w increase. This fact induces a possible implication that the uncrystallized water

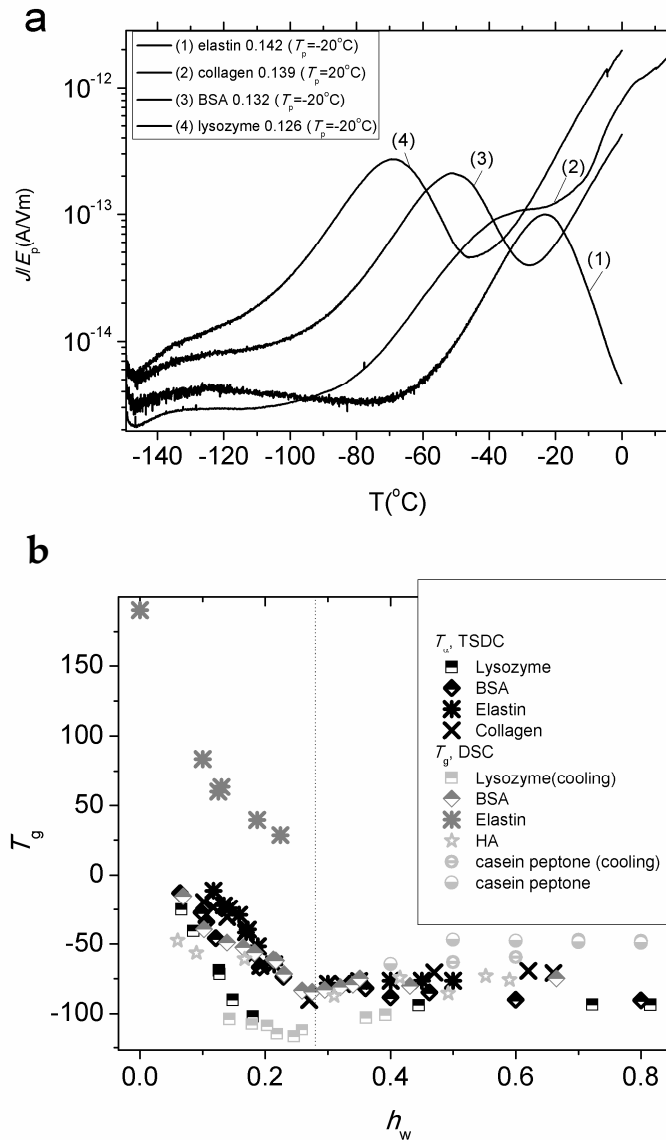


Fig. 7.12 a) Normalized TSDC thermograms (density of depolarization current divided by polarizing electric field, J/E_p) against temperature T for several hydrated protein pellets (samples 1-4) of water fractions h_w indicated on the plot. **b)** Characteristic temperatures calculated by TSDC and DSC, T_{α} and T_g , respectively, for the α relaxation associated with the glass transition (TSDC) and the calorimetric glass transition (DSC), against water fraction, h_w , for several hydrated systems indicated on the plot

molecules associated with the p relaxation might be connected to the protein glass transition. A possible decoupling of the calorimetric glass transition from the segmental dynamics observed dielectrically, in the sense that dielectric techniques probe mainly electrical polarization processes within the water clusters, could be suggested. In what follows this assumption will be further evaluated.

The heat capacity step, ΔC_p , of the glass transition detected by DSC, for all of the hydrated systems studied is plotted against h_w in Fig. 7.13. The normalized ΔC_p values with

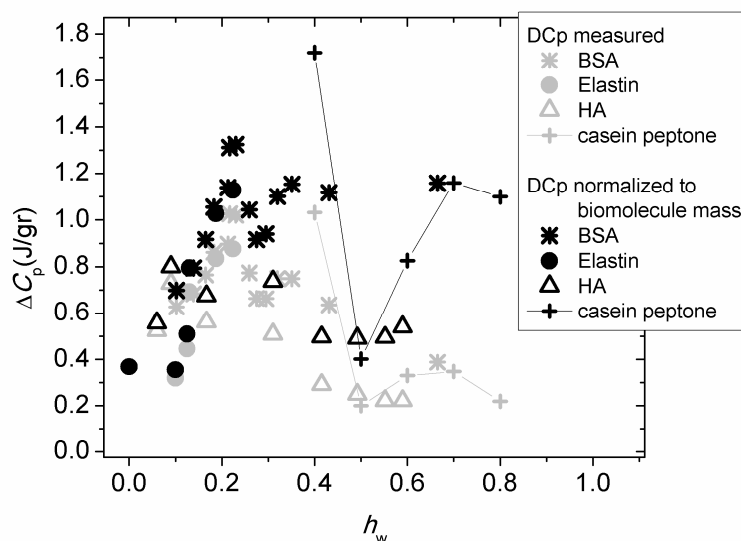


Fig. 7. 13 Heat capacity step, ΔC_p , of the glass transition of hydrated BSA, elastin, HA and casein peptone. The normalized ΔC_p values with respect to the biomolecule mass, are also added to the diagram.

respect to the biopolymer mass is also added to the diagram. The results on BSA have been already described in chapter 5 (Fig. 5.5). The ΔC_p values for elastin, are almost identical with the ones for BSA, an exception being the value for the dry sample. In particular, they increase with h_w increase until a value of about $h_w=0.2$ (we recall that the glass transition could not be detected for elastin at higher water fraction values, although a stabilization of its position is estimated, chapter 6, Fig. 6.2b). The results on HA show an initial increase of ΔC_p with h_w and a subsequent decrease, which is in agreement to the dielectrically recorded data by DRS for the α relaxation (not shown here, see [Panagopoulou 2013b]). It has been shown that the reduction is associated to the reorganization of water in the HA matrix, attributed to swelling. This fact, supports the assumption that the dielectrically observed segmental dynamics is connected to the dynamics of water in the hydration shell. The ΔC_p values for HA at higher water fraction values stabilize when normalized to the biopolymer mass, like in the case of BSA, but exhibit significantly lower values in Fig.7.13. Finally, the ΔC_p values for casein peptone may also be seen in Fig. 7.13. It is interesting to note that the value for $h_w=0.40$ is enhanced when compared to the respective ones for the other systems at similar h_w values. This is attributed to the fact that the casein peptone sample of $h_w=0.40$ contains only uncrystallized water as it was shown by DSC. The ΔC_p values decrease dramatically for $h_w=0.50$, where crystallization of water during cooling sets in. Finally, the normalized ΔC_p values for casein peptone at high hydration levels, obtain a stabilized value, comparable to the one for BSA. It is interesting to note at this point the analogy between the measured ΔC_p values in Fig. 7.13 to the fraction of uncrystallized water, X_{ucw} , in Fig. 7.11a.

This fact provides more evidence that the glass transition is related to the amount of uncrystallized water molecules in the systems.

Moving further, the dielectric map for the systems studied is presented, including the temperature dependence of the relaxation times for the α and p relaxations, the w relaxation (see chapters 5 and 6 and section 7.3.2) and the ν relaxation (i.e. excluding the relaxations attributed to ice-forms), according to the results by analysis. These are presented in Fig. 7.14 a and b for BSA and lysozyme, Fig. 7.15 a and b for elastin and collagen and in Fig. 7.16 a and b for HA and casein peptone, respectively. The results for BSA and elastin have been thoroughly presented in chapters 5 and 6, respectively. In this section, the discussion will focus on the comparative study between the different systems, regarding the connection of the α to the p relaxation.

Starting with the evolution of the trace of the α/p relaxation with hydration level, a global observation for all of the systems is that it is being plasticized by the addition of water, until a water fraction value, where crystallization events of water set in, is reached. Additional increase in hydration level, results in the stabilization of the trace, and the slight antistabilization at extremely high hydration levels. This may be seen in Fig. 7.14 a and b for BSA and lysozyme, in Fig. 7.15 a and b for elastin and collagen and in Fig. 7.16 a and b for HA and casein peptone, respectively. In all cases, except from elastin and collagen, the trace of the α relaxation shows good agreement with the results by DSC. In all cases, the final, antiplasticized trace at high h_w values is located at the boundary of the trace of hexagonal ice Ih [Johari 1981] in the Arrhenius diagram. The results suggest that the origin of the glass transition in hydrated biopolymers should be associated with the dynamics of the uncrystallized water population which relaxes via the α/p relaxations. In the case of the globular protein BSA the coupling of the segmental dynamics and the dynamics of water causes a huge dielectric strength as it was shown in chapter 5 (Fig. 5.16 b). Such huge dielectric loss values have been also observed in the case of hydrated gelatin in reference [Sasaki 2013] and interestingly enough, have been predicted by molecular dynamics simulations on hydrated heme proteins [Matyushov 2011], where it is suggested that the interfacial water is being polarized by protein charges. On the other hand, in the case of the fibrous proteins elastin and collagen, the dynamics of the p relaxation is decoupled from the segmental protein dynamics and the dielectric strength obtains lower values even at high hydration levels (see chapter 6, Fig. 6.19 a). This could be explained by the fact that the only charged polar group of elastin, i.e. lysine, is mostly associated into crosslinking. We recall at this point that the α relaxation for BSA and the p relaxation for elastin, both exhibit a dynamic behavior characterized by cooperativity, depending on the hydration level. By all the above statements we may conclude that, in general, the α/p relaxation as studied in the present thesis might reflect the dynamics of a glassy state of interfacial water at the vicinity of the protein surface, which is affected by protein fluctuations and is associated to the protein glass transition.

The results regarding the w relaxation will be discussed in the upcoming section 7.3.5 (ice-like structures and confinement effects).

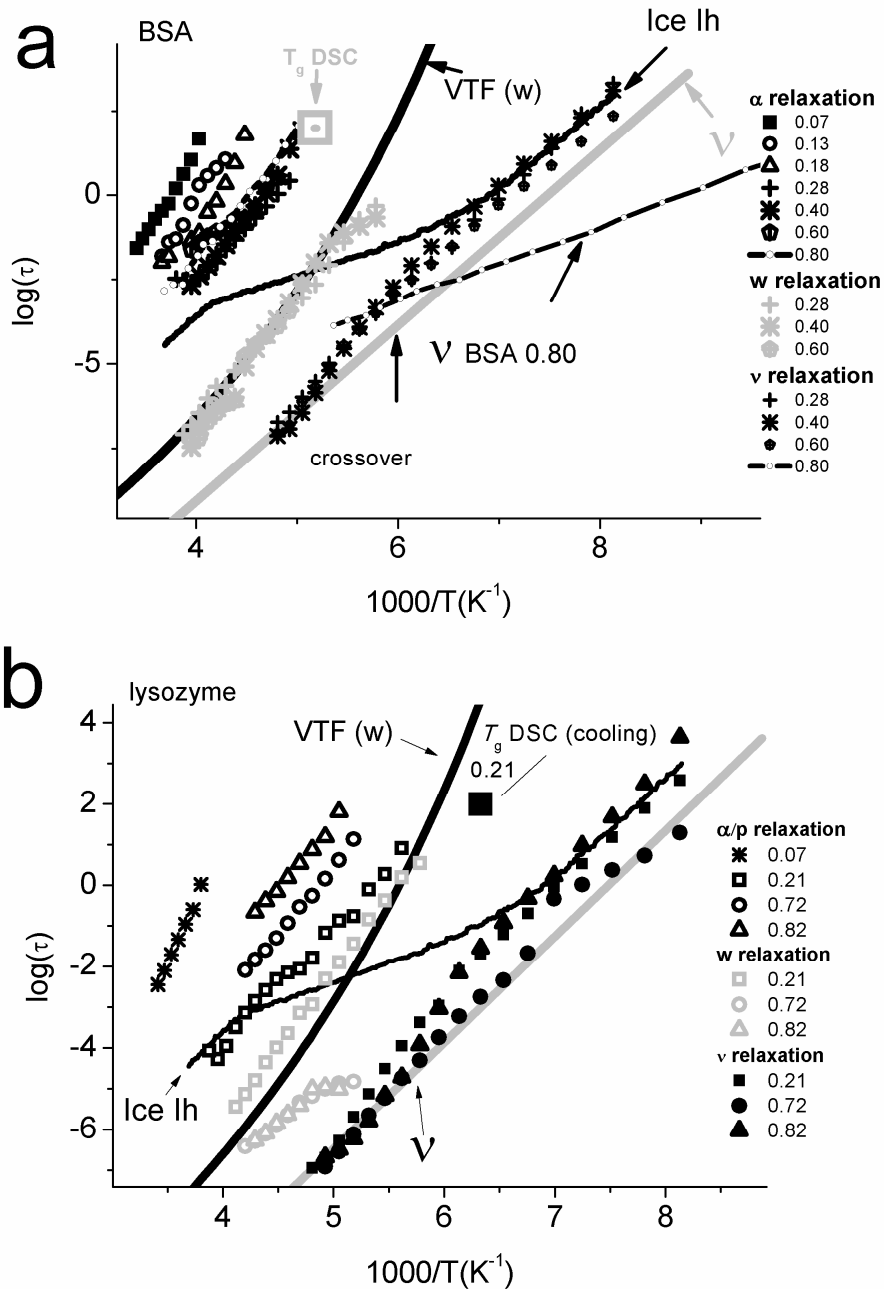


Fig. 7.14 a) Temperature dependence of the relaxation times for the α relaxation associated with the glass transition, the w relaxation and the ν relaxation for hydrated BSA at several water fraction values h_w indicated on the plot. The data for a BSA solution of $h_w=0.80$ from reference [Shinyashiki 2009] are also added to the diagram. **b)** Temperature dependence of the relaxation times for the α relaxation associated with the glass transition, the w relaxation and the ν relaxation for hydrated

lysozyme at several water fraction values h_w indicated on the plot. The glass transition temperatures T_g as measured by DSC are added to the diagrams (at $\tau=100s$), for selected h_w indicated on the plots.

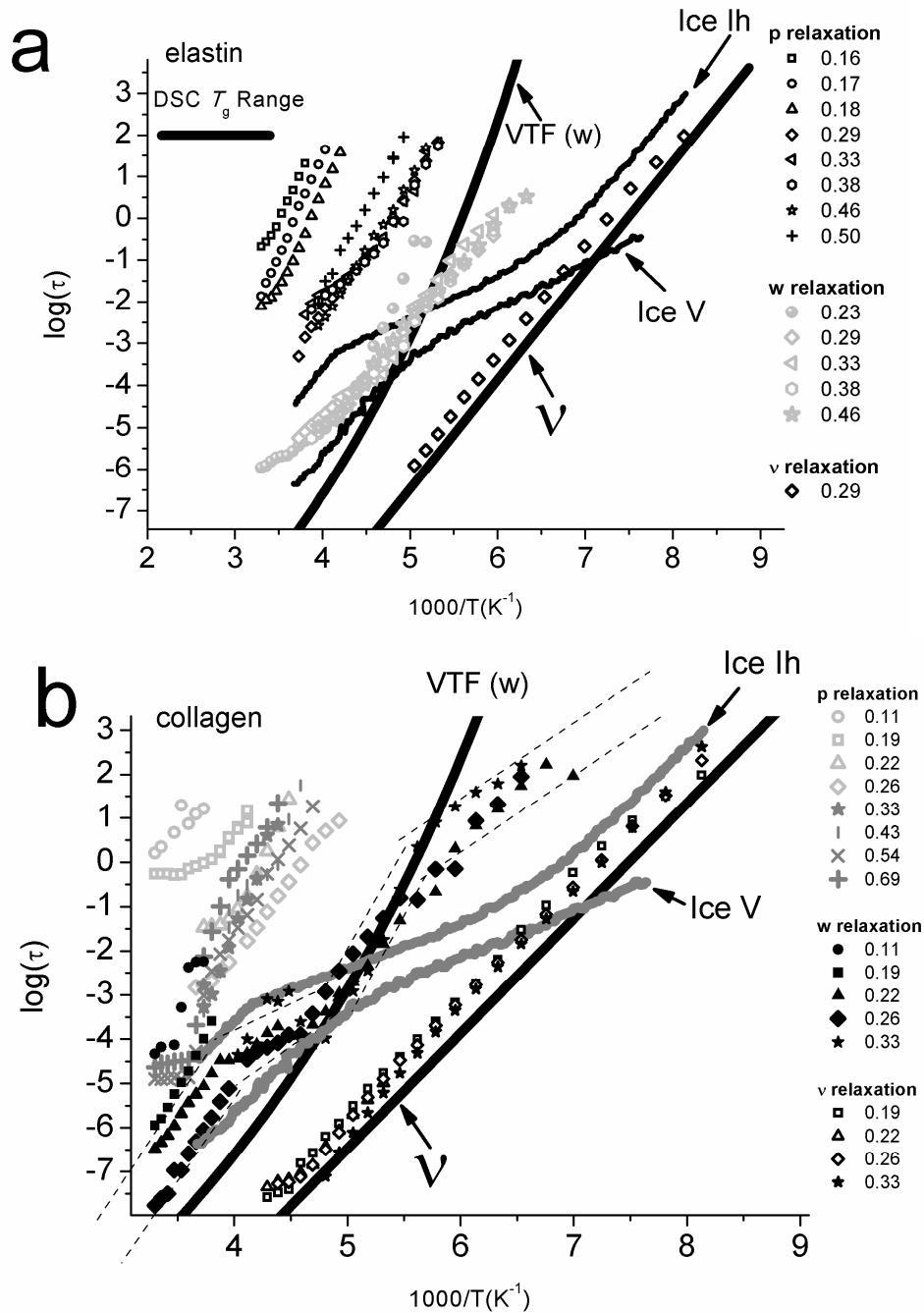


Fig. 7. 15 a) Temperature dependence of the relaxation times for the p relaxation, the w relaxation and the ν relaxation for hydrated elastin at several water fraction values h_w indicated on the plot. The range of the glass transition temperature T_g as measured by DSC is added to the diagram (at $\tau=100s$)
b) Temperature dependence of the relaxation times for the p relaxation, the w relaxation and the ν

relaxation for hydrated collagen at several water fraction values h_w indicated on the plot. The trace of ice V from [Johari 2001] is also added to the plots.

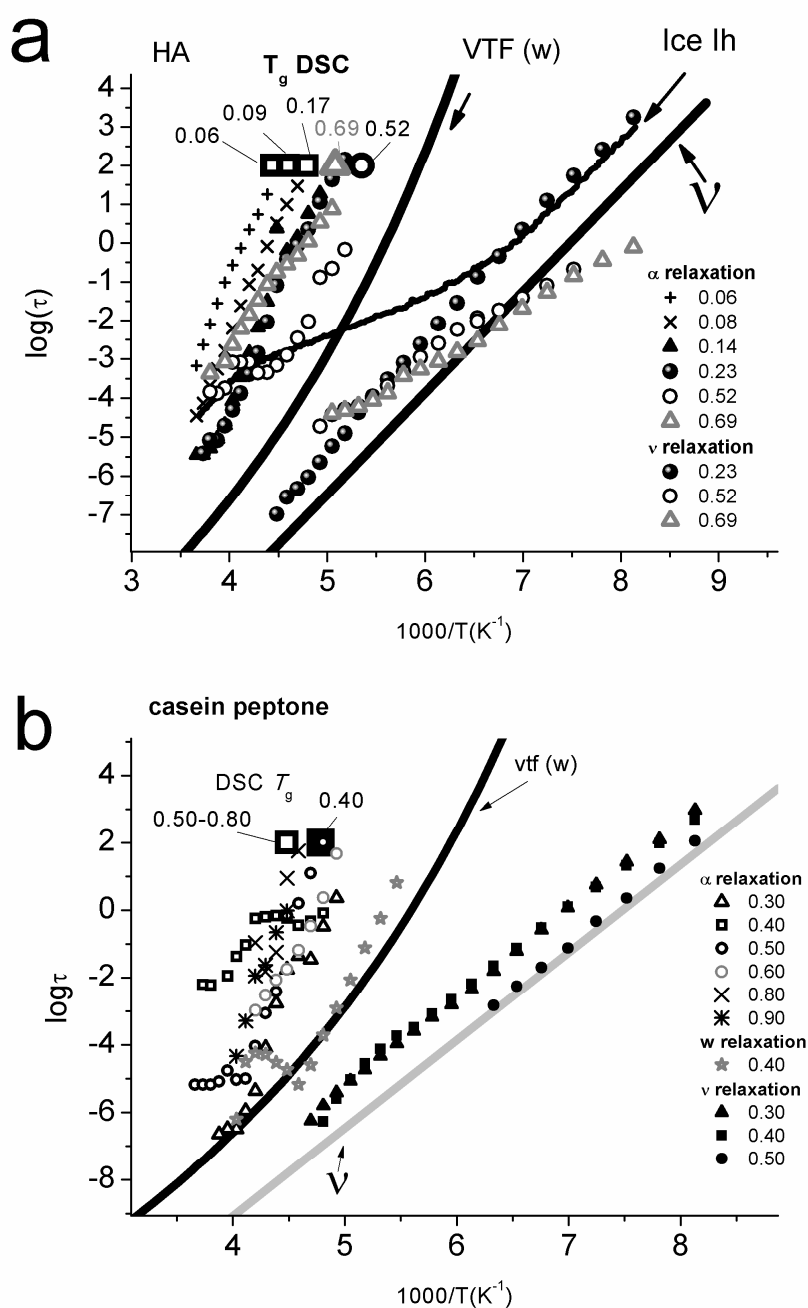


Fig. 7. 16 a) Temperature dependence of the relaxation times for the α relaxation associated with the glass transition and the ν relaxation for hydrated HA at several water fraction values h_w indicated on the plot. **b)** Temperature dependence of the relaxation times for the α relaxation associated with the glass transition, the w relaxation and the ν relaxation for hydrated casein peptone at several water fraction values h_w indicated on the plot. The glass transition temperatures T_g as measured by DSC are added to the diagrams (at $\tau=100s$), for selected h_w indicated on the plots.

7.3.5 Ice like structures - Confinement effects

The w relaxation

A dielectric relaxation denoted as w has been recorded for BSA and elastin and its characteristics have been well described in chapters 5 and 6. In all cases the relaxation is classified as a relaxation due to excess water, in the sense that it remains to some extent in the uncrystallized form, while at the same time its relaxation time is much higher than the one of the main relaxation of uncrystallized water, i.e. the ν relaxation. We recall that the w relaxation in the case of the globular protein BSA is detected for the first time upon increasing h_w for water fraction values in the cold crystallization range (as estimated by DSC) and its relaxation time and dielectric strength exhibit nonlinear temperature dependence, the changes occurring around the homogeneous nucleation temperature (see chapter 5, Fig. 5.21). On the contrary, in the case of the fibrous protein elastin, the w relaxation is followed already at lower water fractions, where no crystallization of water occurs in the hydrated samples. Its relaxation time shows a hydration dependence and it becomes faster with h_w increase until a critical water fraction value of $h_w=0.23$. At higher water fraction values, in the case of hydrated elastin, the trace of the w relaxation saturates in position in the Arrhenius diagram. At the same time, DSC measurements at comparable hydration levels, reveal the existence of a crystallization peak, the position and magnitude of which does not depend drastically on hydration level, suggesting that it comes from the crystallization of confined water molecules. Possibly the small voids available within the elastin structure become larger due to swelling of the protein matrix (we recall that crystallization of water is recorded only for the elastin samples which have been hydrated through immersion in water). The DRS and DSC measurements alone are not able to conclude a straightforward assignment of the w relaxation to a specific confined population of water molecules, as proposed. Nevertheless, the various results so far and the comparison of the trace of the w relaxation to the results by Murata et al. [Murata2012] and also the calorimetric results in the case of confined internal water by Oguni et al. [Oguni 2007] favor this possible explanation. In the case of hydrated collagen the temperature dependence of the relaxation times for the w relaxation may be seen in Fig. 7.15 b. Like in the case of elastin, the trace attributed to the w relaxation may be followed from low h_w values, exhibiting a plasticization by water. The trace seems to stabilize in position at $h_w=0.22$. Two crossover temperatures are clearly seen in the data. The first one, located at low temperatures in the range $5 < 1000/T < 5.5$, seems to be common for the w relaxation in BSA, elastin and collagen. A general picture is that the trace follows the VTF line (see chapter 5) of the w relaxation for the above mentioned hydrated proteins in the range $4.5 < 1000/T < 5.5$, while it appears to deviate at lower temperatures. Interestingly enough, the value of this low temperature crossover is comparable to the universally observed one, in the case of confined water or biological hydration water (see chapters 2 and 3). In addition, an explanation of the latter according to the LLPT observed in a water-glycerol mixture was hypothesized in section 7.3.2.

Moving the discussion on the dynamics of the w relaxation further, we should highlight the similarities and differences regarding the latter, for the systems studied in this thesis. The common characteristic of the w relaxation is that its trace in the Arrhenius

diagram, stabilizes in general at the boundary of the VTF curve (see chapter 5), in Fig. 7.14, 7.15 and 7.16. An exception holds for hydrated HA, where there is no apparent contribution of the w relaxation, at least for the hydration levels measured, lysozyme, where the w relaxation is recorded for $h_w=0.21$ but seems to be absent or different at higher hydration levels (see gray points in Fig. 7.14b) and casein peptone, where a relaxation of similar temperature dependence of the relaxation times of the w relaxation, apart from the α relaxation, is recorded only for the sample of $h_w=0.40$. The average 'mean' position of the trace on the VTF curve, despite the differences, suggests that the latter corresponds to some temperature/frequency domain, critical for the dynamics of water. The trace of the w relaxation is more simple in the case of globular proteins and casein peptone, i.e. more soft systems. In the case of the fibrous proteins elastin and collagen, as already mentioned, the trace of the w relaxation shows more crossover temperatures and deviates from the VTF curve more profoundly in the high temperature side. This may be observed in Fig. 7.15 a and 7.15 b. In particular, the trace of the w relaxation deviates from the VTF curve upon increasing temperature, approximately at temperatures higher than the homogeneous nucleation temperature ($1000/T \sim 4.4$). The traces of hexagonal ice Ih and ice V (see chapter 2, section 2.1), from references [Johari 1981] and [Johari 2001], respectively, are also added in Fig. 7.15 a and 7.15b. It is very interesting that the trace of the w relaxation lies in between the traces of the above mentioned ices, above the homogeneous nucleation temperature, for both hydrated elastin and collagen, more profoundly in the case of collagen. Although ice V is a crystalline form which occurs naturally under high values of pressure, it has been recently shown that high pressure ices may be stabilized due to confinement effects inside carbon nanotubes [Jadzevska 2011]. Such pressure effects have been also verified in the case of water-glycerol mixtures in [Murata 2012]. This kind of an approach to explain the current results would be very interesting and could suggest that a 'visualization' of a triple point may be possible in the protein hydration shell. Furthermore, it supports the existence of a LLPT in water.

Although the indications for such an explanation are strong, the exact location of the water molecules which relax via the w relaxation is not clear, nor its relation to the ν relaxation. Nevertheless, the findings are significant and promising for understanding protein hydration. The main conclusion regarding the w relaxation is that it probably originates from the dynamics of a metastable form of confined water.

Crystalline water structures

Next to dielectric relaxations associated to the dynamics of uncrystallized water, i.e. the α/p relaxations and the ν relaxation, several relaxations due to crystalline structures have been recorded by the dielectric techniques. The assignment of those to ice forms is made mainly according to the detection of crystallization by DSC. The relaxation modes which have been attributed to ice structures for BSA and elastin have been described in detail in chapters 5 and 6. It is found that the relaxations modes do not resemble the temperature dependence of the common hexagonal ice Ih, although they are comparable to some extent. In the case of BSA, a VTF behavior was found at high temperatures for the relaxation due to ice for an intermediate hydration level of $h_w=0.40$ (ice1 in chapter 5) and this behavior was

suggested to be associated to the α relaxation of the hydrated system. The temperature dependence of the relaxation times for the dielectric relaxations due to ice, at relatively high hydration levels, is shown in Fig. 7.17 a and b, for lysozyme and collagen, respectively. The points in the high temperature side, denoted as ice1, in the diagrams, follow an Arrhenius behavior and their trace is located at the projection of the high temperature part of the trace of hexagonal ice. This trace is comparable to the trace of deionized ice measured by Auty and Cole [Auty 1952]. It should be mentioned at this point, that this relaxation in both systems coexists with the α/p relaxation, the trace of which is located at higher temperatures. We also recall that the α/p relaxation antiplasticizes at high h_w values, when after its trace becomes comparable to this 'boundary' position. In the case of hydrated lysozyme in Fig. 7.17 a, the trace of the relaxations due to ice at low temperatures (ice2), are similar to the one observed for BSA of $h_w=0.60$ (chapter 5). It exhibits a crossover from an Arrhenius behavior at low temperatures to a VTF one at higher temperatures at about $1000/T=5$ and its trace is continuously followed in the entire temperature range. We will come back to this comparison later on. In the case of hydrated collagen, in Fig. 7.17 b, a relaxation similar to ice 2 for lysozyme, but even faster, is detected for $h_w=0.43$. The crossover in this case cannot be associated to the p relaxation in collagen, as this is located at even higher temperatures. When increasing the water fraction, the relaxations due to ice become even faster and the temperature dependence of their relaxation times changes. The assignment of the ice2 relaxation to a different class of crystallized or uncrystallized water cannot be excluded. After all, the coexistence of all, ice 1, w and ice 2, at the same time makes the evaluation more complicated. Furthermore, it has been already shown in Fig. 7.11a and b that both the fraction of uncrystallized water and the number of uncrystallized water molecules per aminoacid residues increase significantly at high h_w for hydrated collagen, suggesting a deep reorganization of water in the material. The trace of ice 2 for collagen of $h_w=0.54$ and 0.69 , is comparable to the one of Ih at low temperatures, exhibits a crossover from Arrhenius to Arrhenius of lower activation energy at higher temperatures, like in Ih, but shows lower relaxation times when compared to the latter, and finally meets the trace of Ih at very high temperatures. Furthermore, its relaxation times in the intermediate temperature region are comparable to the ones of ice V, as it may be seen in Fig. 7.17 b. By these observations a possible explanation would be that the rigid collagen matrix induces pressure effects, so that some form of high pressure ice is stabilized by confinement, as it has been recently observed in water confined within carbon nanotubes [Jadzewska 2011].

The temperature dependence of the relaxation times of the relaxations due to ice for BSA of $h_w=0.40$ and for hydrated HA of $h_w=0.52$ and 0.69 are shown in Fig. 7.18. The characteristics of the two ices (at low and high T) have been described for BSA in chapter 5 [Panagopoulou 2012]. The situation is similar for the hydrated HA hydrogels. The important information which is derived from this comparison is that the trace of ice1 at high temperatures seems to be connected to the trace of the VTF curve, which is derived from the w relaxation. The dielectric data on a relaxation recorded in hydrated lysozyme of water fraction $h_w=0.23$ [Mazza 2011], are also added to Fig. 7.18. It may be seen that the trace of the "proton peak" coincides with the trace of ice 1. The trace of ice1 is also similar to the trace of the w relaxation in the case of elastin and collagen (compare Fig. 5.15).

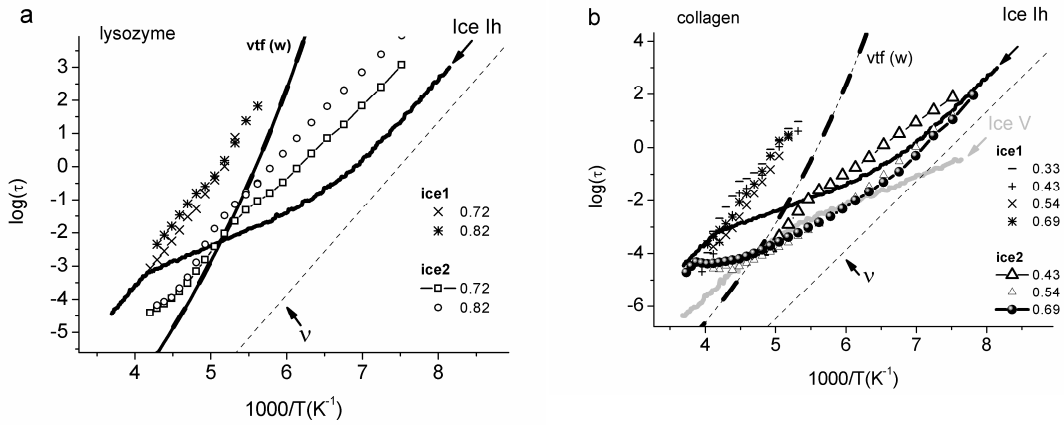


Fig. 7. 17 Temperature dependence of the relaxation times for ice1 at high temperatures and ice2 at lower temperatures, a) for hydrated lysozyme and b) hydrated collagen, of h_w values indicated on the plot

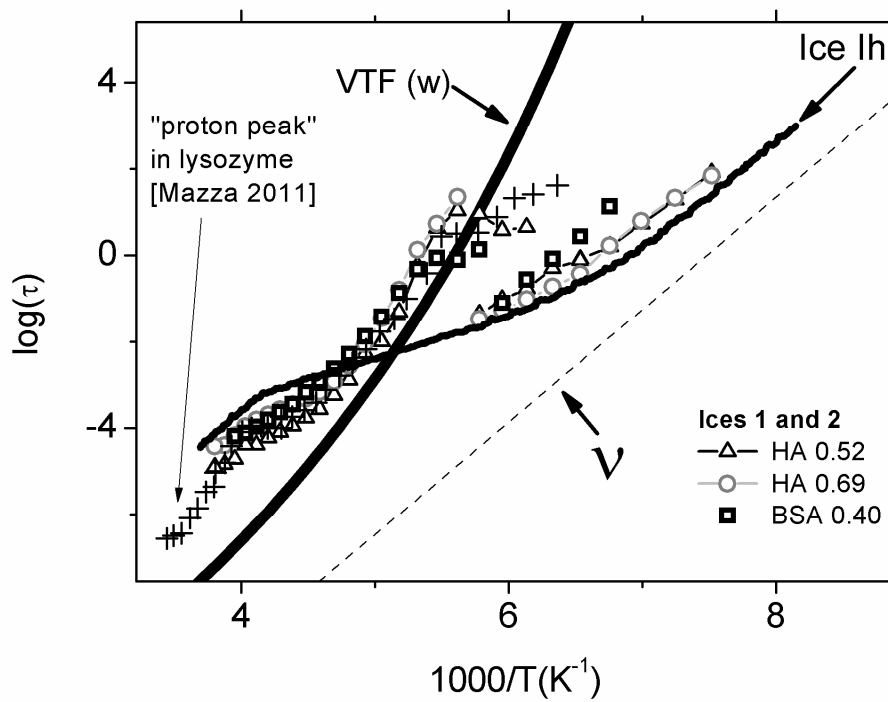


Fig. 7. 18 Temperature dependence of the relaxation times for ice1 at high temperatures and ice2 at lower temperatures for hydrated systems of h_w values indicated on the plot. The dielectric data on a so called "proton relaxation" from reference [Mazza 2011 and references therein] are added in the plot.

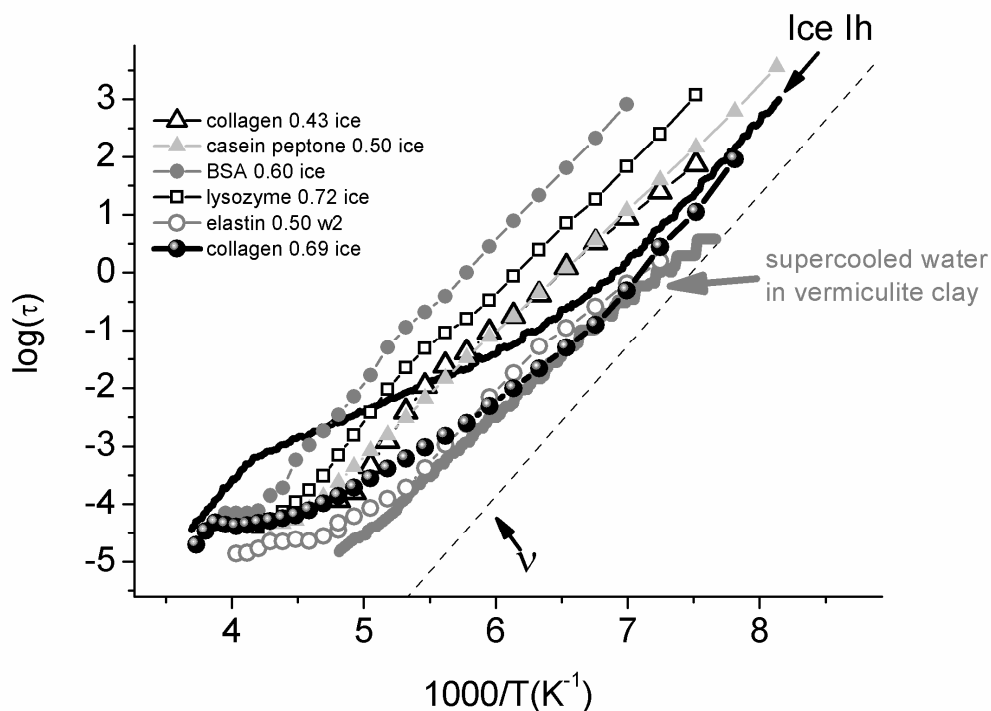


Fig. 7. 19 Temperature dependence of the relaxation times for relaxations attributed to ice forms, for several hydrated systems at selected h_w indicated on the plot.

Finally, the temperature dependence of the relaxation times for relaxations due to ice, for several hydrated systems at relatively high hydration levels, is shown in the comparative diagram of Fig. 7.19. The behavior observed has been already described in the previous paragraphs and the previous chapters. Summarizing the behavior of ice, we may suggest:

- a) the ice formed in hydrated biomolecules exhibits differentiated dynamics than the normal hexagonal ice Ih
- b) a crossover from Arrhenius at low T to VTF behavior at high T is observed in some cases in the range of about $5 < 1000/T < 5.5$. This crossover seems to be associated to some structural transition in the HB network of water, rather than to be associated to segmental dynamics in the system
- c) different relaxation modes due to ice, resembling more the dynamics observed in the case of confined water dynamics, are recorded in the case of rigid fibrous proteins, i.e. collagen and elastin

7.3.4 Percolation

Finally, having in mind the overall picture regarding the phase transitions and dynamics studied so far for the hydrated systems, we will try to evaluate the effects of water organization in the systems to the electrical conductivity in the materials. The picture derived from the so far investigation is that the main population of uncrystallized water in the materials, is manifested through the ν relaxation of water. The trace of the latter was found to saturate in position in the Arrhenius diagram and its magnitude was found to saturate also, in parallel with the formation of a percolating water cluster on the biopolymer surface. The abrupt increase of the conductivity above some critical hydration level is highly associated to a percolation type proton displacement and to the onset of enzymatic activity in globular proteins [Rupley 1991].

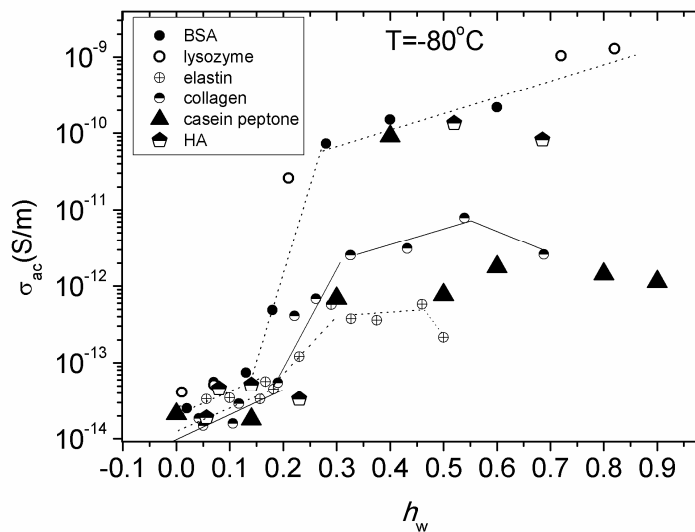


Fig. 7. 20 σ_{ac} values measured at $f = 1$ Hz at the temperature of -80°C on several hydrated samples as a function of water fraction h_w . The lines are guides for the eye.

The interrelation between conduction and polarization effects has been shown by our measurements in the case of the globular proteins BSA and lysozyme [Kyrtsis 2012]. In order to observe the enhancement of conductivity for h_w higher than a critical value for all of the systems studied, we plot in Fig. 7. 20 the values of σ_{ac} measured at the frequency of 1Hz, at -80°C for the hydrated samples as a function of the water fraction. The overall behavior in Fig. 7.20 suggests that in all cases, the abrupt increase in the conductivity values occurs for h_w higher than about 0.15, depending slightly on the system. This is a value for which in all cases the trace of the ν relaxation of water stabilizes in position in the Arrhenius diagram. In general, the conductivity values are lower for the fibrous proteins collagen and elastin. The data for casein peptone of $h_w=0.40$ shows an enhanced conductivity value (comparable to the ones for the globular proteins) which is then reduced and stabilized at high h_w . This is an additional indication that the percolation effects are enhanced when the magnitude of the ν relaxation is also enhanced, like in the case of casein peptone of $h_w = 0.40$.

Chapter 7. Comparative studies of glass transition and dynamics

The overall conclusions arising from the comparative study of the systems in this chapter will be presented in the next chapter (chapter 8, Conclusions) together with the ones derived individually throughout this thesis.

8. Conclusions

The present PhD Thesis deals with the systematic investigation of the phase transitions and dynamics in the case of hydrated proteins. The main techniques employed are water equilibrium sorption isotherms (ESI) measurements at room temperature, in order to study the hydration properties, differential scanning calorimetry (DSC), in order to study the thermal glass transition and crystallization and melting events of water, and two dielectric techniques, dielectric relaxation spectroscopy (DRS) and thermally stimulated depolarization currents (TSDC), in order to study the molecular mobility in the hydrated systems.

The systems under study include globular and fibrous proteins as well as other simple biomolecules, in terms of comparison. In particular, these are:

1. The globular protein bovine albumin serum (BSA)
2. The globular protein lysozyme
3. The fibrous protein elastin
4. The fibrous protein collagen
5. The digest derivative of the globular protein casein, casein peptone
6. A hyaluronic acid (HA) hydrogel, crosslinked by divinyl sulfone

A main aspect of the present study is the variation of hydration level in small steps and over wide ranges of water composition in the hydrated systems. This is achieved by varying the hydration of the samples starting from dry samples, including solid samples hydrated through vapor adsorption or by immersion in deionized water, concentrated solutions and dilute solutions. By this way, the parameter of hydration level is incorporated and the detection of critical hydration levels is possible. In addition, the parallel investigation of structurally different systems, involves more parameters, such as molecular weight, stiffness, chemical structure etc.

The main results that come out of this PhD Thesis, may be described as follows, according to several categories:

1) Critical water contents and crystallization effects

The hydration properties of the systems were studied by ESI measurements. The technique provides the possibility to estimate two important critical hydration levels, relevant to the water organization in the materials. The first one is the critical water content for the coverage of the primary hydration sites on the molecule surface, h_m (g of water per g of dry sample), above which clustering of water molecules sets in. In particular, $h_m = 0.073, 0.088, 0.067, 0.096$ and 0.114 for BSA, lysozyme, elastin, collagen and HA, respectively. Thus, the value of h_m was calculated in the range of $0.067 \leq h_m \leq 0.114$ for the hydrated systems

depending on the structure. For hydration levels lower than h_m the hydration water interacts with primary hydration sites, i.e. surface groups on the protein/biopolymer surface, and does not form extended clusters. Additionally, an estimation was made for the number of aminoacid residues which interact with water molecules at a hydration level respective to h_m , for hydrated globular proteins. It was found that 71 out of 129 aminoacid residues are accessible to water for lysozyme, while 270 out of 607 are accessible in the case of BSA, the other being hidden within the protein structure. A reorganization of the structure at each new hydration level is proposed, due to swelling. The second critical water content estimated by ESI is the one above which clustering of water is significant. In the case of hydrated globular proteins BSA and lysozyme and the fibrous protein collagen, this is at around $h=0.25$ (g of water per g of protein), corresponding to a water fraction h_w (g of water per g of hydrated sample), of $h_w=0.2$. In the case of the fibrous protein elastin the respective water content value for significant clustering is at about $h=0.13$, corresponding to $h_w=0.12$. Finally, for HA the respective value is located at around $h=0.4$, corresponding to $h_w=0.29$. This information obtained by ESI regarding the organization of water molecules in the samples is taken into account in order to evaluate the results obtained by dielectric techniques at different hydration levels. A general conclusion which derives from the comparative study of the majority of the systems by ESI is that the water uptake is similar in all cases in the range of water activity values which correspond to water contents lower than the one for which significant clustering occurs in the systems. When increasing further the water activity large differences in the values of water uptake are seen and the maximum water uptake value is quite different for each system. It was concluded that the swelling degree of the system along with the hydrophilic or hydrophobic character of the latter is reflected by the difference in the water uptake out of the primary sorption layer, i.e. for the water populations which start to organize into clusters or to diffuse into less accessible domains of the host material. The systems studied are listed in the order of increasing maximum water uptake in the following order: elastin, lysozyme, collagen, BSA, HA. It was also concluded that the swelling degree increases with increasing molecular weight, for globular proteins.

The crystallization and melting events of water were investigated by DSC. Several critical hydration levels were estimated, regarding the onsets for crystallization of water (upon increasing hydration level), first during heating (cold crystallization, if present) and then during cooling. In addition, the amount of uncrystallized water in the samples could be estimated by the melting enthalpies of water and the melting enthalpy of bulk ice.

The characteristic temperatures of crystallization and melting peaks gives information on the state of water in the systems (crystal size) and its evolution with hydration level. It was found that the crystallization behavior depends on the structure and the stiffness of the material. In particular, for the globular protein BSA cold crystallization of water during heating occurs for the first time at about $h_w=0.26$ and during cooling at about $h_w=0.30$. The respective values for lysozyme are $h_w=0.18$ and 0.21 , during heating and cooling, respectively. The values are lower when compared to the respective ones for BSA. This is an indication that the crystallization behavior is not unique for globular proteins in general. Another difference between BSA and lysozyme, is the fact that the crystallization peaks are more simple (mostly a unique peak at each hydration level) for BSA, while

multiple peaks are observed for lysozyme. This difference has been attributed to a difference in the swelling degree between the two proteins (BSA exhibits higher swelling degree than lysozyme), which has been also observed by ESI measurements. For globular proteins the characteristic temperatures of crystallization and melting show a hydration dependence, increasing in general with hydration level. The crystallization behavior of water in case of hydrated HA is similar to the one observed for globular proteins. In particular, the crystallization during cooling and heating is observed simultaneously at about $h_w=0.31$ and the multiple crystallization peaks show a strong hydration dependence. The hydrated system casein peptone, exhibits no crystallization of water during cooling for water fraction values up to $h_w=0.4$. Cold crystallization during heating is observed for the same water fraction. At higher h_w both cold crystallization and crystallization during cooling occur in the samples.

The crystallization in the case of the fibrous proteins exhibits two distinct crystallization peaks during cooling. The position of the peaks is almost independent of water fraction, in contrast to globular proteins HA and casein peptone. In the case of hydrated elastin crystallization during cooling occurs at $h_w=0.32$, for the first time, upon increasing hydration level. One crystallization peak is centered at about -40°C and its magnitude is independent of hydration level increase. This behavior suggests the existence of primary crystal forms, which originate to the crystallization of confined water molecules. A second peak is recorded at higher temperatures and increases in magnitude with increasing water fraction. Cold crystallization during heating is also evident. These two distinct crystallization peaks are also present in the case of hydrated collagen. The peak at about -40°C is recorded for collagen in the entire hydration range studied and its magnitude is almost independent of hydration level. The fact that this crystallization peak is attributed to water crystallization is verified by specific DSC experiments. It is suggested that the water molecules involved are under severe confinement, which is supported by the complex structure of the collagen triple helix. The second crystallization peak at higher temperatures in the case of collagen is observed for $h_w=0.32$ upon increasing water fraction. Finally, no clear cold crystallization is recorded for hydrated collagen.

The fraction of uncrystallized water in the samples, which remains uncrystallized both during cooling and heating, has been calculated. For all systems the fraction obtains an almost stable value, in the hydration range where crystallization events of water are evident. This value is in the range of $h_w=0.20-0.25$ for hydrated proteins and it obtains the lowest value for elastin. The respective value was $h_w\sim 0.15$ and $h_w\sim 0.35$ for HA and casein peptone, respectively. In addition, the number of uncrystallized water molecules per aminoacid residue was calculated for the hydrated protein systems. This was in the range of 1.5 to 4.5 water molecules per aminoacid residue, being higher in general at high hydration levels for BSA, lysozyme and collagen while it is kept almost stable at 1.5 for elastin, in the whole hydration range where crystallization of water is evident.

2) Glass transition of hydrated proteins

The thermal glass transition was recorded by DSC for hydrated BSA, lysozyme, elastin, casein peptone and HA hydrogel, while it was absent for hydrated collagen. In the case of globular proteins and HA the glass transition was detected for hydration levels

higher than about h_m , while in the case of elastin the glass transition was already detected for the dry sample and, in addition, the glass transition temperature, T_g , was positioned at quite higher temperature ranges, than the one for globular proteins and HA. In particular, the T_g in the system BSA-water is located at about $T_g=-40^\circ\text{C}$ for $h_w=0.10$ and decreases significantly with increasing hydration level, until a value of about $T_g=-80^\circ\text{C}$ where it stabilizes, for water fractions at which crystallization of water occurs during cooling. The corresponding heat capacity step ΔC_p , which is analogous to the magnitude of the transition, increases initially with the increase of hydration level and then decreases simultaneously with the stabilization of the T_g . In addition, the ΔC_p values obtain a stable value if normalized to the mass of BSA, in the hydration range where crystallization of water occurs during cooling. These results suggest that the thermal glass transition originates from the combined motion of protein segments and water molecules in the uncrystallized phase. For the system lysozyme-water the T_g was recorded by DSC only during cooling with no apparent explanation for that. The results on hydrated HA are quite similar to the ones for BSA. On the other hand, the T_g of hydrated elastin was recorded already for the dry protein showing higher values than the rest of the systems. In particular, the glass transition value for dry elastin, $T_g=190^\circ\text{C}$, decreased to a value of about $T_g\sim 30^\circ\text{C}$ for $h_w=0.22$. Finally, despite the differences in T_g values, the values and hydration dependence of ΔC_p are similar for BSA, elastin and HA, suggesting a similar origin for the transitions.

A dielectric relaxation, which is associated with the thermal glass transition was recorded by TSDC and DRS. In the case of the globular protein BSA and the HA hydrogel, the dielectric manifestation of the α relaxation are quite in a good accordance to each other. The major result is that a relaxation similar to the particular dielectric relaxation is recorded in a similar frequency/temperature range, even for the systems which do not exhibit a thermal glass transition in the same temperature range, i.e. elastin and collagen and also for lysozyme, the thermal glass transition of which was tricky to detect. The comparative study of the hydrated protein systems showed that this dielectric relaxation is recorded in a temperature range, where the dynamical transition appears in fully hydrated proteins and confined supercooled water. The dynamical characteristics of the relaxation in question depend on hydration level. In some cases the dielectric strength of the relaxation increases with temperature decrease and, therefore, is characterized by cooperativity, although this is not a unique result in the entire hydration range. Furthermore, the results obtained by TSDC, a technique which is characterized by a peak resolving power, revealed that the relaxation in question involves two distinct contributions in some cases.

The origin and interrelation of the thermal glass transition and the dielectric relaxation has been discussed. Finally, it is suggested that the thermal glass transition and the respective dielectric relaxation, are decoupled. In particular, the two transitions show the following common characteristics:

- a) they are detected above a critical hydration level, of about $h_w=0.6-0.11$, which corresponds to the critical water content for the coverage of the primary sorption sites by uncrystallized water molecules
- b) their characteristic temperature decreases with increasing hydration level, implying plasticization effects (increased mobility) until a critical water fraction of about $h_w=0.3$, above which crystallization effects set in and the characteristic temperature values finally stabilize.

These characteristics imply that the recorded transitions are connected mainly to the dynamics of uncrystallized water molecules.

By analysis of the experimental results, it comes out that the origin of the thermal glass transition is the combined motion of protein segments, triggered by uncrystallized water molecules, which are probably parts of extended clusters within the hydration shell. The detection and temperature range of the thermal glass transition depends also on the stiffness of the protein. The respective dielectric relaxation, is present independently of the glass transition and reflects mainly the polarization processes within the uncrystallized water clusters in the hydration shell. In other words, the glass transition may be attributed to large scale protein motions which are triggered by glassy water in the secondary hydration shell of the protein.

3) Dynamics of uncrystallized water in the protein hydration shell

A main dielectric relaxation due to the uncrystallized water molecules in the protein hydration shell was recorded. The systematic recording of the temperature dependence of the relaxation time and the dielectric strength of the relaxation versus the hydration level, revealed a strong dependence on the hydration level and, consequently, on the protein dynamics. In particular, it was found that the dynamics is associated to the motion of small polar groups on the protein surface. At low hydration levels, where water molecules are attached mainly on to primary hydration sites (according to water ESI measurements) the motion of polar groups dominates, the latter being plasticized with hydration level increase. This critical hydration level is equal to about $h_w=0.10$. At higher hydration levels, water clusters are gradually formed and the subsequent formation of a percolating water cluster, covering the entire protein surface, is gradually achieved. The temperature dependence of the relaxation times and the dielectric strength of the relaxation are being stabilized with the coverage of the surface and, at the same time, the excess water molecules are being involved in different configurations, in crystallized or uncrystallized formations. The stabilization of the characteristic relaxation times of the relaxation (trace in the Arrhenius diagram) is achieved at hydration levels in the range of $0.14 < h_w < 0.2$. The stabilization of both the trace and dielectric strength of the main relaxation, is achieved at hydration levels equal to about $h_w=0.3$. At the same hydration level ice formation during cooling is recorded by DSC. The main relaxation due to uncrystallized water was also detected in the case of the other biopolymers (other than proteins) studied. The hydration dependence of its dynamical characteristics was different than the one for hydrated proteins and the differences were attributed to the structural differences between the different systems. In all cases, the main result is that the main relaxation is a secondary relaxation as its dielectric strength increases universally with temperature increase. It is suggested that it corresponds to the Johari Goldstein relaxation of water, although it is clearly interrelated with the material surface. Finally, the dynamics of the main relaxation is differentiated at extremely high hydration levels, in general at about $h_w > 0.5$, suggesting that the uncrystallized water molecules follow different organization motives. The modification of the main relaxation with hydration level is expressed via the gradual reduction of its activation energy. In general, the activation energy in the intermediate hydration levels, i.e. at around $h_w=0.30$, obtains values in the range of 0.55 eV which corresponds to the energy required to brake 2 hydrogen bonds. Upon

increasing hydration levels, the activation energy values decrease gradually down to a value of about 0.22 eV, which corresponds to the energy required to break 1 hydrogen bond. The modification of the observed dynamics depends also on the structure. In the case of lysozyme this modification is suppressed.

In addition, two slower dielectric relaxations were detected due to the contribution of uncrystallized water molecules. The slower one is the one which is associated with the thermal glass transition of the hydrated system and was described in the previous section. This relaxation corresponds to water molecules in the secondary hydration shell of the molecule surface. The second one is suggested to originate to the contribution of an additional class of uncrystallized water, probably metastable against crystallization. Its relaxation times show a complex behavior, exhibiting crossovers from Arrhenius to VTF and vice versa, depending on the particular system studied. In the case of hydrated BSA the relaxation is detected for the first time upon increasing water fraction for $h_w=0.23$, its relaxation times show similarities to the α relaxation of a water glycerol solution above the liquid-liquid phase transition, and the VTF behavior changes to an Arrhenius one when crossing the homogeneous nucleation temperature at about -40°C . In the case of the fibrous proteins elastin and collagen this relaxation is followed from lower hydration levels, approximately above h_m , and it shows a hydration dependence. Its relaxation times become faster with hydration level increase and finally its trace stabilizes at a position comparable to the one of BSA, although not identical. In the case of fibrous proteins there are indications that the water molecules which are involved into this relaxation form confined crystal structures, possibly similar to ice forms under high pressure.

4) Crystalline water populations in hydrated biological systems

The crystallization of water in the hydrated systems studied, was recorded through differential scanning calorimetry. A dependence of the characteristics of the crystallization on the morphology of the sample was found. In the case of less rigid systems, such as globular proteins or HA, the dielectric response due to crystalline water populations was comparable but different than the one of the normal hexagonal ice (Ih). The observed temperature dependence, at high temperatures, was more similar to a dielectric relaxation observed on hydrated lysozyme, which is attributed to protonic conductivity, according to several literature studies. In the case of the more rigid systems studied, i.e. the fibrous proteins, the observed dielectric relaxations due to crystalline structures, obtain shorter relaxation times with respect to temperature, when compared to the respective ones for the less rigid systems. The confinement effect could possibly be similar to the effects of pressure.

References

- [Anagnostopoulou-Konsta 1987] A. Anagnostopoulou-Konsta, P. Pissis, A study of casein hydration by the thermally stimulated depolarisation currents method, *J. Phys. D Appl. Phys.* 20 (1987) 1168–1174.
- [Andrade 2011] R. D. P. Andrade, R. M. Lemus, C.E.C. Pérez, Models of sorption isotherms for foods: uses and limitations, *VITAE, REVISTA DE LA FACULTAD DE QUÍMICA FARMACÉUTICA*, 8(3) (2011) 325-334.
- [Angell 2008] C.A. Angell, Supercooled water, in: F. Franks (Ed.), *Water: A Comprehensive Treatise*, vol. 7, Plenum, New York, 2008, pp. 1–81.
- [Alberts 2002] B. Alberts, A. Johnson, J. Lewis, M. Raff, K. Roberts, P. Walter, *Molecular Biology of the Cell*, 4th ed., Garland Science, New York, 2002. ISBN-10:0-8153-3218-1 ISBN-10: 0-8153-4072-9
- [Auty 1952] R. P. Auty, R. H. Cole, Dielectric properties of ice and solid D₂O, *J. Chem. Phys.* 20 (1952) 1309-1314.
- [Barut 1998] G. Barut, P. Pissis, R. Pelster, G. Nimtz, Glass transition in liquids: two versus three-dimensional confinement, *Phys. Rev. Lett.*, 80 (1998) 3543–3546.
- [Bergman 2000] R. Bergman, J. Swenson, Dynamics of supercooled water in confined geometry, *Nature communications*, 403 (2000) 283-286.
- [Bertolini 1982] D. Bertolini, M. Cassettari, G. Salvetti, The dielectric relaxation time of supercooled water, *J. Chem. Phys.* 76 (1982) 3285–3290.
- [Blahovec 2007] J. Blahovec, S. Yanniotis, GAB Generalized equation for sorption phenomena, *Food Bioprocess Tech.*, (2007)
- [Böttcher 1978] C.J.F. Böttcher, P. Bordewijk. *Theory of electric polarization*, vol. ii. dielectrics in its time dependent fields. Elsevier, 1978.
- [Brodsky 2005] B. Brodsky, A. V. Persikov, Molecular structure of the collagen triple helix, *Adv. Prot. Chem.* 70 (2005) 301-339.

- [Brunauer 1938] S. Brunauer, P. H. Emmet, E. Teller, Adsorption of gases in multimolecular layers, *J. Am. Chem. Soc.*, 60 (2) (1938) 309-319.
- [Brunauer 1940] S. Brunauer, L. S. Deming, W. E. Deming, E. Teller, On a theory of the van der Waals adsorption of gases, *J. of The American Chemical Society*, 62(7) (1940) 1723-1732.
- [Bruni 2011] F. Bruni, R. Mancinelli, M. A. Ricci, Multiple relaxation processes versus the fragile to strong transition in confined water, *Phys. Chem. Chem. Phys.*, 13 (2011) 19773–19779.
- [Capaccioli 2007] S. Cappaccioli, K. L. Ngai, N. Shinyashiki, The Johari-Goldstein β -Relaxation of Water, *J. Phys. Chem. B*, 111 (2007) 8197-8209.
- [Capaccioli 2010] S. Capaccioli, K. L. Ngai, S. Ancherbak, P.A. Rolla, N. Shinyashiki, The role of primitive relaxation in the dynamics of aqueous mixtures, nano-confined water and hydrated proteins, *J. Non-Cryst. Solids* 257 (2010) 641-654.
- [Capaccioli 2011] S. Capaccioli, K. L. Ngai, Resolving the controversy of the glass transition temperature of water?, *J. Chem. Phys.* 135 (2011) 104504–104512.
- [Careri 1998] G. Careri, Cooperative charge fluctuations by migrating protons in globular proteins, *Prog. Biophys. Mol. Biol.* 70 (1998) 223–249.
- [Cerveny 2004] S. Cerveny, G. A. Schwarz, R. Bergman, J. Swenson, Glass transition and relaxation processes in supercooled water, *Physical Review Letters* 93 (2004) 245702-245704.
- [Cerveny 2005] S. Cerveny, J. Colmenero, A. Alegria, Dielectric investigation of the low temperature water dynamics in the poly(vinyl methyl ether)/H₂O system, *Macromolecules* 38 (2005) 7056–7063.
- [Cerveny 2006] S. Cerveny, G.A. Schwartz, A. Alegria, R. Bergman, J. Swenson, Water dynamics in n-propylene glycol aqueous solutions, *J. Chem. Phys.* 124 (2006) 194501–194509.
- [Cerveny 2008] S. Cerveny, A. Alegria, and J. Colmenero, Universal features of water dynamics in solutions of hydrophilic polymers, biopolymers, and small glass-forming materials, *Physical. Review E* 77 (2008) 031803-031807.

- [Chen 2009] S. H. Chen, Y. Zhang, M. Lagi, S. C. Chong, P. Baglioni, F. Mallamace, Evidence of dynamic crossover phenomena in water and other glass-forming liquids: Experiments, MD Simulations and theory, *J. Phys.: Condens. Matter*, 21 (2009) 504102-504112.
- [Collins 2005] M. D. Collins, G. Hummer, M. L. Quillin, B. W. Matthews, S. M. Gruner, Cooperative water filling of a nonpolar protein cavity observed by high-pressure crystallography and simulation, *Proc. Natl. Acad. Sci. USA* 102 (2005) 16668–71.
- [Collins 2007] M. D. Collins, M. L. Quillin, G. Hummer, B.W. Matthews, S. M. Gruner, Structural rigidity of a large cavity-containing protein revealed by high-pressure crystallography, *J. Mol. Biol.* 367(2007)752–63.
- [Conn 2008] P. M. Conn, *Progress in Molecular Biology and Translational Science*, Volume 83, *Molecular Biology of Protein Folding Part A*, Elsevier, 2008.
- [Cooke 1974] R. Cooke, I.D. Kuntz, The properties of water in biological systems, *Annu. Rev. Biophys. Bioeng.* 3 (1974) 95–126.
- [Cole 1942] R. H. Cole, K. S. Cole, Dispersion and absorption in dielectrics II. Direct current characteristics, *J. Chem. Phys.* 10 (1942) 98-105.
- [Cowman 2005] M. K. Cowman, S. Matsuoka, Experimental approaches to hyaluronan structure, *Carbohydrate Res.*, 340 (2005) 791-809.
- [Daoukaki-Diamanti 1984] D. Daoukaki-Diamanti, P. Pissis, G. Boudouris, Depolarization thermocurrents in frozen aqueous solutions of mono- and di-saccharides, *Chem. Phys.* 91 (1984) 315–325.
- [Darwin 2001] B. L. Darwin, O.V. Alonso, B.J. Bennion, V. Daggett, Hydrophobic hydration is an important source of elasticity in elastin-based polymers, *J. Am. Chem. Soc.*, 123 (2001) 11991-11998.
- [Debelle 1999] L. Debelle, A. J. P. Alix, The structures of elastins and their function, *Biochimie*, 81 (1999) 981-994.
- [Debenedetti 1996] P. G. Debenedetti, *Metaestable Liquids*; Princeton University Press: Princeton, NJ, 1996.

- [Debenedetti 2003] P.G. Debenedetti, Supercooled and glassy water, J. Phys. Condens. Matter 15 (2003) R1669–R1726.
- [Dean 1999] J.A. Dean, Lange's Handbook of Chemistry, McGraw-Hill, New York, 1999, p. 6.115.
- [Doster 1986] W. Doster, A. Bachleitner, R. Dunau, M. Hiebl, E. Luscher, Thermal properties of water in myoglobin crystals and solutions at subzero temperatures, Biophysical J., 50 (1986) 213-219.
- [Doster 2010] W. Doster, S. Busch, A.M. Gaspar, M.S. Appavu, J. Wuttke, H. Scheer, Dynamical transition of protein–hydration water, Phys. Rev. Lett. 104 (2010) 098101–098104.
- [Fenimore 2004] P.W. Fenimore, H. Frauenfelder, B.H. McMahon, R.D. Young, Bulk-solvent and hydration-shell fluctuations, similar to α - and β -fluctuations in glasses, control protein motions and functions, Proc. Nat. Acad. Sci. 101 (2004) 14408–14413.
- [Finney 2002] J. L. Finney, D.T. Bowron, A. K. Soper, T. Loerting, E. Mayer E. and A. Hallbrucker, Structure of a new dense amorphous ice, Phys. Rev. Lett., 89 (2002) 503-506.
- [Fragiadakis 2006] D. Fragiadakis, "Πειραματική μελέτη της σχέσης δομής-ιδιοτήτων σε ναοσύνθετα πολυμερικά υλικά", Διδακτορική Διατριβή, ΕΜΠ, Αθήνα, 2006.
- [Franks 1972] F. Franks, A Comprehensive Treatise, Plenum Press, New York, 1972.
- [Franks 1977] F. Franks, Solvation interactions of proteins in solution, Philos. Trans. R. Soc. Lond. B Biol. Sci. 278 (1977) 89–96.
- [Franzese 2011] G. Franzese, V. Bianco, S. Iskov, Water at interface with proteins, Food Biophys. 6 (2011) 186–198.
- [Fox 1956] T.G. Fox, Bull. Am. Phys. Soc. 1 (1956) 123.
- [Gainaru 2009] C. Gainaru, A. Fillmer, R. Böhmer, Dielectric response of deeply supercooled hydration water in the connective tissue proteins collagen and elastin, J. Phys. Chem. B 113 (2009) 12628-12631.

- [Gallo 2000] P. Gallo, M. Rovere, E. Spohr, Glass transition and layering effects in confined water: a computer simulation study, *J. Phys. Chem.*, 113 (25) (2000) 11324–11335.
- [Giovambattista 2004] N. Giovambattista, C.A. Angell, F. Sciortino, H.E. Stanley, Glass-transition temperature of water: a simulation study, *Phys. Rev. Lett.* 93 (2004) 047801/1–047801/4.
- [Gionambattista 2012] N. Giovambattista, T. Loerting, B. R. Lukanov, F. Starr, Interplay of the glass transition and the liquid-liquid phase transition in water, *Scientific Reports*, 2(390) (2012) 1-8.
- [grafity] <http://grafitylabs.com>
- [Grant 1978] E. H. Grant, R. J. Sheppard, G.P. South, Dielectric behavior of biological molecules in solution, Oxford, Clarendon, 1978.
- [Greenspan 1977] L. Greenspan, Humidity Fixed Points of Binary Saturated Aqueous Solutions, *J. Res. Nat. Bur. Stand. A Phys. Chem.* 81A (1977) 89-96.
- [Gregory 2003] R.B. Gregory, Protein–solvent Interactions, New York, USA, Marcel Dekker, 1995.
- [Gutina 2003] A. Gutina, T. Antropova, E. Rysiakiewicz-Pazec, K. Virnik, Y. Feldman, Dielectric relaxation in porous glasses, *Microporous Mesoporous Mater.* 58 (2003) 237–254.
- [Harrington 1997] Harrington S., Zhang R., Poole P. H., Sciortino F. and Stanley H. E., Liquid-liquid phase transition: evidence from simulations, *Phys. Rev. Lett.*, 78 (1997) 2409-2412.
- [Harvey 1972] S.C. Harvey, P. Hoekstra, Dielectric relaxation spectra of water absorbed on lysozyme, *J. Phys. Chem.* 76 (1972) 2987–2994.
- [Hatakeyama 1994] T. Hatakeyama, F.X. Quinn. *Thermal Analysis: Fundamentals and applications to polymer Science*. John Wiley and Sons, 1994.
- [Havriliak 1966] S. Havriliak, S. Negami. A complex plane analysis of α dispersion in some polymer systems. *J. Polym. Sci. C.*, 16 (1966) 99-117.

- [Hayashi 2006] Y. Hayashi, A. Puzenko, Y. Feldman, Slow and fast dynamics in glycerol–water mixtures, *J. NonCryst. Solids* 352 (2006) 4696–4703.
- [He 1992] X.M. He, D.C. Carter, Atomic structure and chemistry of human serum albumin, *Nature*, 358 (1992) 209-215.
- [Heyd 2006] A. Heyd, D.O. Kildsig, G.S. Banker, Dissolution of macromolecules I: surface phenomena associated with polymer dissolution, *J. Pharm. Sci.* 58 (5) (2006) 586–588.
- [Hoeve 1974] C. Hoeve and P. Flory, The elastic properties of elastin, *Biopolymers*, 13 (1974) 677-686.
- [Hoeve 1980] C. Hoeve and M. Hoeve, The glass point of elastin as a function of diluent concentration, *Polym. Eng. Sci.*, 20 (1980) 290-293.
- [Hummer 2001] G. Hummer, J. C. Rasaiah, P. J. Noworyta, Water conduction through the hydrophobic channel of a carbon nanotube, *Nature* 414 (2001)188–90.
- [Israelachvili 1983] J.N. Israelachvili, R.M. Pashley Molecular layering of water at surfaces and origin of repulsive hydration forces *Nature*, 306 (1983) 249–250.
- [Jadzewska 2011] M. Jadzewska, M. M. Sliwinska-Bartkowiak, A. I. Beskrovnyy, S. G. Vasilovskiy, S. W. Ting, K. Y. Chan, L. Huang, K. E. Gubbins, Novel ice structures in carbon nanopores: pressure enhancement effect of confinement, *Phys. Chem. Chem. Phys.*, 13 (2011) 9008-9013.
- [Jansson 2010] H. Jansson, J. Swenson, The protein glass transition as measured by dielectric spectroscopy and differential scanning calorimetry, *Biochim. Biophys. Acta* 1804 (2010) 20-26.
- [Jansson 2011] H. Jansson, R. Bergman, J. Swenson, Role of solvent for the dynamics and the glass transition of proteins, *J. Phys. Chem. B* 115 (2011), 4099–4109.
- [Johari 1981] G. P. Johari, E. Whalley, The dielectric properties of ice Ih in the range 272-133 K, *J. Chem. Phys.*, 75(1981) 1333-1340.
- [Johari 1987] G. P. Johari, A. Hallbrucker, E. Mayer, The glass-liquid transition of hyperquenched water, *Nature*. 330 (1987) 552–553.

- [Johari 2001] G. P. Johari, E. Whalley, The dielectric relaxation time of ice V, its partial anti-ferroelectric ordering and the role of Bjerrum defects, *J. Chem. Phys.*, 115(7) (2001) 3274-3280.
- [Kakinaya 1975] S. Kakivaya and C. Hoeve, The glass point of elastin, *Proc. Nat. Acad. Sci.*, 72 (1975) 3505-3507.
- [Kamb 1967] B. Kamb, A. Prakash and C. Knobler, Structure of ice V, *Acta Crystallogr.* 22 (1967) 706-715.
- [Kawai 2006] K. Kawai, T. Suzuki, M. Oguni, Low-temperature glass transitions of quenched and annealed bovine serum albumin aqueous solutions, *Biophys. J.* 90 (2006) 3732–3738.
- [Khodadadi 2008] S. Khodadadi, S. Pawlus, J. H. Row, V. Garcia Sakai, E. Mamontov, A. P. Sokolov, The origin of the dynamic transition in proteins, *J. Chem. Phys.* 128 (2008) 195106–195111.
- [Khodadadi 2010] S. Khodadadi, A. Malkovskiy, A. Kisliuk, A.P. Sokolov, A broad glass transition in hydrated proteins, *Biochim. Biophys. Acta* 1804 (2010) 15–19.
- [Kimmich 1990] R. Kimmich, T. Gneiting, K. Kotitschke, G. Schnur, Fluctuations, exchange processes, and water diffusion in aqueous protein systems, a study of bovine serum albumin by diverse NMR techniques, *Biophys. J.* 58 (1990) 1183–1197.
- [Kotitschke 1990] K. Kotitschke, R. Kimmich, E. Rommel, F. Parak, NMR study of diffusion in protein hydration shells, *Prog. Colloid Polym. Sci.* 83 (1990) 211–215.
- [Kremer 2002] F. Kremer, A. Schönhals (Eds.), *Broadband Dielectric Spectroscopy* (Springer, Berlin, 2002).
- [Kuntz 1974] I. D. Kuntz, W. Kauzman, Hydration of proteins and polypeptides, *Advances in protein chemistry* 28, 239-345, 1974.
- [Kyritsis 1995] A. Kyritsis, P. Pissis, J.L. Gómez Ribelles, M. Monleón Pradas, Polymer–water interactions in poly(hydroxyethyl acrylate) hydrogels studied by dielectric, calorimetric and sorption isotherm measurements, *Polym. Gels Netw.* 3 (1995) 445–469.
- [Kyritsis 2012] A. Kyritsis, A. Panagopoulou, P. Pissis, R.S.i Serra, J.L. Gomez Ribelles and N. Shinyashiki, Water and protein dynamics in protein-water mixtures over wide range of

composition, *IEEE Trans. Dielect. Electr. Insul.*, 19 (2012) 1239-1246.

[Lee 2013] S. W. Lee, D. Lee, Integrated study of water sorption/desorption behavior of weak polyelectrolyte layer by layer films, *Macromolecules* 46(7) 2013, 2793-2799.

[Leveque 1981] J.L. Leveque, J.C. Carson, P. Pissis, G. Boudouris, Free water in hair keratin? A depolarization thermal current study, *Biopolymers* 20 (1981) 2649-2656.

[Li 2002] B. Li and V. Daggett, Molecular basis for the extensibility of elastin, *J. Muscle Res. Cell Motil.*, 23 (2002) 561-573.

[Loerting 2001] Loerting T., Salzmann C., Kohl I., Mayer E. and Hallbrucker A., A second distinct structural "state" of high-density amorphous ice at 77 K and 1 bar, *Phys. Chem. Chem. Phys.*, 3 (2001) 5355-5357.

[Magazu 2011] S. Magazù, F. Migliardo, A. Benedetto, Puzzle of protein dynamical transition, *J. Phys. Chem. B* 115 (24) (2011) 7736-7743.

[Mackay 2005] J. Mackay, L. Muiznieks, A. Toonkool, A. Weiss, The hydrophobic domain 26 in human tropoelastin is unstructured in solution, *J. Struct. Biol.*, 150 (2005) 154-162.

[Mallamace 2007] F. Mallamace, C. Branca, M. Broccio, C. Corsaro, C.-Y. Mou and S.-H. Chen, The anomalous behavior of the density of water in the range $30\text{K} < T < 373\text{K}$, *Proc. Natl. Acad. Sci. U.S.A.*, 104 (2007) 18387-18391.

[Mallamace 2011] F. Mallamace, P. Baglioni, C. Corsaro, J. Spooren, H.E. Stanley, S.-H. Chen, Transport properties of supercooled confined water, *RIVISTA DI NUOVO CIMENTO*, 34(5) (2011) 253-388.

[Masciovecchio 2004] C. Masciovecchio, S. C. Santucci, A. Gessini, S. Di Fonzo, G. Ruocco, F. Sette, Structural relaxation in liquid water by inelastic UV scattering, *Phys. Rev. Lett.* 92 (2004) 255507-255510.

[Mathlouthi 2003] M. Mathlouthi, B. Rogé, Water vapor sorption isotherms and the caking of food powders, *Food Chem.* 82(1) (2003) 61-71.

- [Mathot 1994] V. B. F. Mathot, *Calorimetry and Thermal Analysis of Polymers*, Hanser Publishers, Munich, 1994.
- [Matyushov 2011] D. V. Matyushov, Nanosecond stokes shift dynamics, dynamical transition and gigantic reorganization energy of hydrated heme proteins, *J. Phys. Chem. B* 115 (2011) 10715-10724.
- [Mayer 1991] E. Mayer, Calorimetric glass transition in the amorphous forms of water: a comparison. *J. Mol. Struct.* 250 (1991) 403–411.
- [Mazza 2011] M. G. Mazza, K. Stokely, S. E. Pagnotta, F. Bruni, H.E. Stanley, G. Franzese, More than one dynamic crossover in protein hydration water, *PNAS* 108 (2011) 19873-19878.
- [Mishima 1984] O. Mishima, L. D. Calvert, E. Whalley, 'Melting ice' I at 77 K and 10 kbar: a new method of making amorphous solids. *Nature*. 310 (1984) 393–395.
- [Mishima 1985] O. Mishima, L. D. Calvert, E. Whalley, An apparently first-order transition between two amorphous phases of ice induced by pressure, *Nature* 314 (1985) 76-78.
- [Mishima 1998] O. Mishima, H. E. Stanley, The relationship between liquid, supercooled and glassy water, *Nature*, 396 (1998) 329-335.
- [Miyazaki 2000] Y. Miyazaki, T. Matsuo, H. Suga, Low-temperature heat capacity and glassy behavior of lysozyme crystal, *J. Phys. Chem. B* 104 (2000) 8044-8052.
- [Murata 2012] K. Murata, H. Tanaka, Liquid-liquid transition without macroscopic phase separation in water-glycerol mixture, *Nature Materials* 11(2012) 436-443.
- [Nakasako 2002] M. Nakasako, Structural characteristics in protein hydration investigated by cryogenic X-ray crystal structure analyses, *J. Biol. Phys.* 28 (2002) 129–137.
- [Ngai 2008] K. L. Ngai, S. Capaccioli, N. Shinyashiki, The protein glass transition and the role of the solvent, *J. Phys. Chem. B* 112 (2008) 3286-3832.
- [Ngai 2011] K. L. Ngai, S. Capaccioli, S. Ancherbak, N. Shinyashiki, Resolving the ambiguity of the dynamics of water and

clarifying its role in hydrated proteins, *Philos. Mag.*, 91 (2011) 1809–1835.

- [Oguni 2007] M. Oguni, S. Maruyama, K. Wakabayashi, A. Nagoe, Glass transitions of ordinary and heavy water within silica-gel nanopores, *Chem. Asian J.* 2 (4) (2007) 514–520.
- [Oodo 2011] K. Oodo, T. Masuda, H. Fujimori, Estimation of the pore diameter of organosilane modified silica based on the fusion temperature of ice, *J. NonCryst. Solids* 357 (2011) 683–685.
- [Pagnotta 2009] S. E. Pagnotta, F. Bruni, R. Senesi, A. Pietropaolo, Quantum behavior of water protons in protein hydration shell, *Biophys. J.* 96 (2009) 1939–1943.
- [Pagnotta 2010] S. A. Pagnotta, S. Cervený, A. Alegria, J. Colmenero, The dynamical behavior of hydrated glutathione: a model for protein water interactions, *Phys. Chem. Chem. Phys.* 12 (2010) 10512–10517.
- [Panagopoulou 2011a] A. Panagopoulou, A. Kyritsis, A. M. Aravantinou, Dionysios Nanopoulos, R. Sabater i Serra, J. L. Gómez Ribellez, N. Shinyashiki, P. Pissis, Glass Transition and Dynamics in Lysozyme-Water Mixtures Over Wide Ranges of Composition, *Food Biophysics*, 6 (2011) 199-209.
- [Panagopoulou 2011b] A. Panagopoulou, A. Kyritsis, R. Sabater i Serra, J.L. Gómez Ribelles, N. Shinyashiki, P. Pissis, Glass transition and dynamics in BSA-water mixtures over wide ranges of composition studied by thermal and dielectric techniques, *Biochim. et Biophys. Acta*, 1814 (2011) 1984-1996.
- [Panagopoulou 2012] A. Panagopoulou, A. Kyritsis, N. Shinyashiki, P. Pissis, Water and protein dynamics in bovine serum albumin-water mixtures over wide ranges of composition, *J. Phys. Chem. B*, 116 (2012) 4593-4602.
- [Panagopoulou 2013a] A. Panagopoulou, A. Kyritsis, M. Vodina, P. Pissis, Dynamics of uncrystallized water and protein in hydrated elastin studied by thermal and dielectric techniques, *Biochim. et Biophys. Acta*, 1834 (2013) 977-988.
- [Panagopoulou 2013b] A. Panagopoulou, J.V. Molina, A. Kyritsis, M.M. Pradas, A.V. Lluch, G.G. Ferrer, P. Pissis, Glass Transition and water dynamics in hyaluronic acid hydrogels, *Food Biophysics*, 8 (2013) 192-202.

- [Pandis 2011] C. Pandis, A. Spanoudaki, A. Kyritsis, P. Pissis, J. C. Rodríguez Hernández, J. L. Gómez Ribellez, M. Monleón Pradas, Water Sorption Characteristics of Poly(2-hydroxyethyl acrylate)/Silica Nanocomposite Hydrogels, *Polymer Physics*, 49 (2011) 657-668.
- [Pauling 1951] L. Pauling, R.B. Corey, H.R. Branson, The structure of proteins: two hydrogenbonded helical configurations of the polypeptide chain, *Proc. Natl. Acad. Sci. Wash.* 37 (1951) 205.
- [Partridge 1955] S. M. Partridge, H.F. Davies, G.S. Adair, The chemistry of connective tissues 2. SOLUBLE PROTEINS DERIVED FROM PARTIAL HYDROLYSIS OF ELASTIN, *Biochemical J.*, 61 (1955) 11-21.
- [Partridge 1969] S. Partridge, in *Chemistry and molecular biology of the extracellular matrix*, vol.1, E. Bazas, Ed., London, Academic press (1969) 593-616.
- [Petsko 2004] G. A. Petsko, D. Ringe, *Protein Structure and Function (Primers in Biology)*, NSP, New Science Press, 2004.
- [Pissis 1981] P. Pissis, G. Boudouris, J.C. Garson, J.L. Leveque, Depolarization thermocurrents in ice Ih at low temperature, *Z. Naturforsch.* 36a (1981) 321–328.
- [Pissis 1982] P. Pissis, L. Apeki, C. Christodoulides, G. Boudouris, Dielectric behavior of ice microcrystals dispersed within suspensions, *Z. Naturforsch.* 37a (1982) 1000–1004.
- [Pissis 1985] P. Pissis, A study of sorbed water on cellulose by the thermally stimulated depolarisation technique, *J. Phys. D: Appl. Phys.* 18 (1985) 1897-1908.
- [Pissis 1989] P. Pissis, Dielectric studies of protein hydration, *J. Mol. Liq.* 41 (1989) 271–289.
- [Pissis 1990] P. Pissis, The Dielectric Relaxation of Water in Plant Tissue, *J. Exper. Botany* 41 (1990) 677-684.
- [Pissis 1991] P. Pissis, A. Anagnostopoulou-Konsta, L. Apeki, D. Daoukaki-Diamanti, C. Christodoulides, Dielectric effects of water in water-containing systems, *J. Non-Cryst. Solids* 131–133 (1991) 1174–1181.

- [Ping 2001] Z. H. Ping, Q. T. Nguyen, S.M. Chen, J.Q. Zhou, Y.D. Ding, States of water in different hydrophilic polymers – DSC and FTIR studies, *Polymer* 42 (2001) 8461–8467.
- [Poole 2002] P. H. Poole, F. Sciortino, U. Essmann and H. E. Stanley, Phase behavior of metastable water, *Nature*, 360 (1992) 324–328.
- [Porter 2012] D. Porter, F. Vollrath, Water mobility, denaturation and the glass transition in proteins, *Biochim. Biophys. Acta* 1824 (2012) 785–791.
- [Prouzet 2010] E. Prouzet, J.B. Brubach, P. Roy, Differential scanning calorimetry study of the structure of water confined within AOT lamellar mesophases, *J. Phys. Chem. B* 114 (2010) 8081–8088.
- [Rasaiah 2008] J. C. Rasaiah, S. Garde, G. Hummer, Water in non polar confinement: from nanotubes to proteins and beyond, *Annu. Rev. Phys. Chem.*, 59 (2008) 713-740.
- [Ratkovic 1997] S. Ratkovic, P. Pissis, Water binding to biopolymers in different cereals and legumes: proton NMR relaxation, dielectric and water imbibition studies, *J. Mater. Sci.* 32 (1997) 3061-3068.
- [Rault 1997] J. Rault, A. Lucas, R. Neffati, M. Monleon Pradas, Thermal transitions in hydrogels of poly(ethyl acrylate)/poly(hydroxyethyl acrylate) interpenetrating networks, *Macromolecules* 30 (1997) 7866–7873.
- [Ribeiro 2009] A. Ribeiro, F. Javier Arias, J. Reguera, M. Alonso, J. C. Rodríguez-Cabello, Influence of the aminoacid sequence on the inverse temperature transition of elastin-like polymers, *Biophysical J.*, 97 (2009) 312-320.
- [Richert 2011] R. Richert, A. Agapov, A. P. Sokolov, Appearance of a Debye process at the conductivity relaxation frequency of a viscous liquid, *J. Chem. Phys.*, 134, (2011) 104508-104514.
- [Ringe 2003] D. Ringe, G.A. Petsko, The ‘glass transition’ in protein dynamics: what it is, why it occurs, and how to exploit it, *Biophys. Chem.* 105 (2003) 667–680.
- [Rønne 1997] C. Rønne, P.O. Åstrand, S.R. Keidung, Investigation of the temperature dependence of dielectric relaxation in liquid

water by THz reflection spectroscopy and molecular dynamics simulation, *J. Chem. Phys.* 107 (1997) 5319–5331.

- [Rossmmeisl 2004] J. Rossmmeisl, J. K. Nørskov, K. W. Jakobsen, Elastic effects behind cooperative bonding in beta-sheets, *J. Am. Chem. Soc.*, 126 (2004) 13140-13143.
- [Rupley 1991] J. A. Rupley, G. Careri, Protein hydration and function, *Adv. Protein Chem.* 41(1991) 37–172.
- [Rusiniak 2004] L. Rusiniak, Electric properties of ice near solidification and melting temperature, *Acta Geophysica Polonica*, 52(3)(2004) 363-380.
- [Russo 2011] D. Russo, J. Teixeira, L. Kneller, L. Copley, J. R. D. Ollivier, S. Perticaroni, E. Pellegrini, M. A. Gonzalez, Vibrational density of states of hydration water at biomolecular sites: Hydrophobicity promotes low density amorphous ice behavior, *J. Am. Chem. Soc.* 133(13) (2011) 4882-4888.
- [Sasaki 2013] K. Sasaki, A. Panagopoulou, M. Miyara, K. Fujita, W. Yamamoto, P. Pissis, A. Kyritsis, R. Kita, N. Shinyashiki, S. Yagihara, Dynamics of water and hydrated gelatin in partially crystallized mixtures, *AIP Conf. Proc.*, 1518 (2013) 288-291.
- [Saenger 1987] W. Saenger, Structure and dynamics of water surrounding biomolecules, *Annu. Rev. Biophys. Chem.* 16 (1987) 93–114.
- [Salmeron Sanchez 2002] M. Salmeron Sanchez, M. Monleon Pradas, J.L. Gomez Ribelles, Thermal transitions of benzene in a poly (ethyl acrylate) network, *J. NonCryst. Solids* 307–310 (2002) 750–757.
- [Salveti 2002] G. Salvetti, E. Tombari, L. Mikheeva, G.P. Johari, The endothermic effects during denaturation of lysozyme by temperature modulated calorimetry and an intermediate reaction equilibrium, *J. Phys. Chem. B* 106 (23) (2002) 6081-6087.
- [Samouillan 2000] V. Samouillan, A. Lamure, C. Lacabanne, Dielectric relaxations of collagen and elastin in the dehydrated state, *Chemical Physics*, 255 (2000) 259-271.
- [Samouillan 2011] V. Samouillan, D. Tintar, C. Lacabanne, Hydrated elastin: Dynamics of water and protein followed by dielectric spectroscopies, *Chem. Phys.* 385 (2011) 19-26.

- [Sandberg 1984] L. B. Sandberg and J. M. Davidson, *Elastin and its Gene*, *Peptide Protein. Rev.*, 3 (1984) 169-226.
- [Sartor 1992] G. Sartor, A. Hallbrucker, K. Hofer, E. Mayer, Calorimetric glass-liquid transition and crystallization behaviour of a vitrous, but freezable, water fraction in hydrated matemoglobin, *J. Phys. Chem.* 96 (1992) 5133-5138.
- [Sartor 1994a] G. Sartor, E. Mayer, G.P. Johari, Calorimetric studies of the kinetic unfreezing of molecular motions in hydrated lysozyme, hemoglobin, and myoglobin, *Biophys. J.* 66 (1994) 249-258.
- [Sartor 1994b] G. Sartor, E. Mayer, Calorimetric study of crystal growth of ice in hydrated matemoglobin and of redistribution of the water clusters formed on melting the ice, *Biophys. J.* 67 (1994) 1724-1732.
- [Sartor 1995] G. Sartor, A. Hallbrucker, E. Mayer, Characterizing the secondary hydration shell on hydrated myoglobin, hemoglobin, and lysozyme powders by its vitrification behaviour on cooling and its calorimetric glass-liquid transition and crystallization behaviour on reheating, *Biophys. J.* 69 (1995) 2679-2694.
- [Serrano 2007] V. Serrano, W. Liu, S. Franzen, *Biophysical Journal*, An infrared spectroscopic study of the conformational transition of elastin-like polypeptides, 93 (2007) 2429-2435.
- [Seidl 2011] M. Seidl, M. S. Elsaesser, K. Winkel, G. Zifferer, E. Mayer, T. Loerting, Volumetric study consistent with a glass-to-liquid transition in amorphous ices under pressure, *Phys. Rev. B*, 83 (2011) 100201-100204(R).
- [Servaty 2001] R. Servaty, J. Schiller, H. Binder, K. Arnold, Hydration of polymeric components of cartilage – an infrared spectroscopic study on hyaluronic acid and chondroitin sulfate, *International Journal of Biological Macromolecules* 28 (2001) 121-127.
- [Shinyashiki 2007a] N. Shinyashiki, M. Shimomura, T. Ushiyama, T. Miyagawa, S. Yagihara, Dynamics of water in partially crystallized polymer/water mixtures studied by dielectric spectroscopy, *J. Phys. Chem. B* 111 (2007) 10079-10087.

- [Shinyashiki 2007b] N. Shinyashiki, S. Sudo, S. Yagihara, A. Spanoudaki, A. Kyritsis, P. Pissis, Relaxation processes of water in the liquid to glassy states of water mixtures studied by broadband dielectric spectroscopies, *J. Phys.: Condens. Matter* 2007, 19, 205113–205125.
- [Shinyashiki 2009] N. Shinyashiki, W. Yamamoto, A. Yokoyama, T. Yoshinari, S. Yagihara, K.L. Ngai, S. Capaccioli, Glass transitions in aqueous solutions of protein (Bovine Serum Albumin), *J. Phys. Chem. B* 113 (2009) 14448–14456.
- [Stanley 2000] H. E. Stanley, S. V. Buldyrev, M. Canpolat, O. Mishima, M. R. Sadr-Lahijany, A. Scala and F. W. Starr, The puzzling behavior of water at very low temperature, *Phys. Chem. Chem. Phys.*, 2 (2000) 1551-1558.
- [Starr 2003] F. W. Starr, C.A. Angell, H.E. Stanley, Prediction of entropy and dynamic properties of water below the homogeneous nucleation temperature, *Phys. A* 323 (2003)51–66.
- [Stathopoulos 2011] A. T. Stathopoulos, A. Kyritsis, F.J. Romero Colomer, J.L. Gomez Ribelles, N. Shinyashiki, C. Christodoulides, P. Pissis, Polymer segmental dynamics and solvent thermal transitions in Poly(ethyl acrylate)/p-xylene mixtures, *J. Polym. Sci. B Polym. Phys.* 49 (2011) 455–466.
- [Sugimoto 2008] H. Sugimoto, T. Miki, K. Kanayama, M. Norimoto, Dielectric relaxation of water adsorbed on cellulose, *J. Non-Cryst. Solids* 354 (2008) 3220-3224.
- [Suherman 2002] P. M. Suherman, P. Taylor, G. Smith, Low frequency dielectric study on hydrated ovalbumin, *J. Non-Cryst. Solids* 305 (2002) 317–321.
- [Sun 2010] C. Sun, G. S. Boutis, Investigation of the dynamical properties of water in elastin by deuterium Double Quantum Filtered NMR, *J. of Magnetic Resonance*, 205 (2010) 86-92.
- [Sun 2011] C. Sun, G. S. Boutis, Measurement of the exchange rate of waters of hydration in elastin by 2D $T_2 - T_2$ correlation nuclear magnetic resonance spectroscopy, *New Journal of Physics*, 13 (2011) 025026-025042.
- [Sjöström 2010] J. Sjöström, J. Mattsson, R. Bergman, E. Johansson, K. Josefsson, D. Svantesson, J. Swenson, *Phys. Chem. Chem. Phys.* 12 (2010) 10452–10456.

- [Swenson 2006] J. Swenson, H. Jansson, R. Bergman, Relaxation processes in supercooled confined water and implications to protein dynamics, *Phys. Rev. Lett.* 96 (2006) 247802–247805.
- [Swenson 2010] J. Swenson, J. Teixeira, The glass transition and relaxation behavior of bulk water and a possible relation to confined water, *J. Chem. Phys.* 132 (2010) 014508–014513.
- [Tamburro 2003] A. Tamburro, B. Bochicchio and A. Pepe, Dissection of human tropoelastin-by-exon chemical synthesis and related conformational studies, *Biochemistry*, 42 (2003) 13347-13362.
- [Tamburro 2006] A. Tamburro, A. Pepe and B. Bochicchio, Localizing alpha-helices in human tropoelastin: assembly of the elastin “puzzle”, *Biochemistry*, 45 (2006) 9518-9530.
- [Teixeira 1997] J. Teixeira, J. M. Zanotti, M. C. Bellissent-Funel, S. H. Chen, Water in confined geometries, *Physica B*, 234–236 (1997) 370–374.
- [Timmermann 1989] E. O. Timmermann, A BET-like three sorption stage isotherm, *J. Chem. Soc. Faraday Trans.*, 1 85 (1989) 1631-1645.
- [Tournier 2003] A. L. Tournier, J. Xu, J.C. Smith, Translational hydration water dynamics drives the protein glass transition, *Biophys. J.* 85 (2003) 1871–1875.
- [Turnhout 1980] J. van Turnhout, in: G.M. Sessler (Ed.), *Electrets*, Topics in Applied Physics, vol. 33, Springer, Berlin, 1980, pp. 81–215.
- [Urry 1984] D. Urry, Protein elasticity based on conformations of sequential polypeptides: The biological elastic fiber, *J. Prot. Chem.*, 3 (1984) 403-436.
- [Urry 1988] D. W. Urry, Entropic elastic processes in protein mechanisms.I. Elastic structure due to an inverse temperature transition and elasticity due to internal chain dynamics, *J. Protein Chem.*, 7 (1988) 1-34.
- [Urry 2002] D. W. Urry, T. Hugel, M. Seitz, H. E. Gaub, L. Sheiba, J. Dea, J. Xu, T. Parker, Elastin: A representative ideal protein elastomer, *Phil. Trans. R. Soc. Lond. B*, 357 (2002) 169-184.
- [Van der Sman 2012] R. G. M. Van der Sman, Thermodynamics of meat proteins, *Food Hydrocolloids*, 27 (2012) 529-535.

- [Vanderschueren 1979] J. Vanderschueren, J. Gasiot, Field-Induced Thermally Stimulated Currents. In P. Braunlich ed., *Thermally Stimulated Currents in Solids*, volume 37 of *Topics in Applied Physics*, 135-223. Springer-Verlag, 1979.
- [Vázquez 2010] M. Vázquez, E. Pallé, P. Montañés Rodríguez, *The earth as a distant planet: A Rosetta Stone for the search of Earth-Like Worlds*, Springer, 2010.
- [Velikov 2001] V. Velikov, S. Borick, C.A. Angell, The glass transition of water, based on hyperquenching experiments, *Science* 294 (2001) 2335–2338.
- [Vogel 1921] H. Vogel, The law of the relationship between viscosity of liquids and the temperature, *Physik. Z.*, 22 (1921) 645–646.
- [Wübbenhorst 2002] M. Wübbenhorst, J. van Turnhout, Analysis of complex dielectric spectra. I. One-dimensional derivative techniques and three-dimensional modelling, *J. Non-Cryst. Solids* 305 (2002) 40–49.
- [Yu 2004] Y. Yu, C.A. Angell, Clarifying the glass-transition behaviour of water by comparison with hyperquenched inorganic glasses, *Nature* 427 (2004) 717–720.
- [Zhang 2000] J. Zhang, G. Zografi, The relationship between 'BET'- and 'Free Volume' derived parameters for water vapor adsorption into amorphous solids, *J. Pharm. Scienc.* 89(8) (2000) 1063-1072.
- [Zhang 2007] F. Zhang, M. W. A. Skoda, R. M. J. Jacobs, R. A. Martin, C. M. Martin, F. Schreiber, Protein Interactions Studied by SAXS: Effect of Ionic Strength and Protein Concentration for BSA in Aqueous Solutions, *J. Phys. Chem. B*, 111 (2007) 251-259.

Summary

This PhD Thesis deals with the systematic investigation of molecular dynamics and phase transitions in the case of hydrated proteins and other biomolecules, in a wide range of hydration levels. The main goal is the study of the dynamical characteristics of the observed transitions in relation to the coupling of hydration water to the biomolecules. In long terms, the main goal is to explain biological function in physical terms.

The hydrated systems studied in this thesis are: two globular proteins, bovine serum albumin (BSA) and lysozyme and two fibrous proteins, elastin and collagen. In addition to hydrated proteins, two structurally simpler biopolymers were chosen, in order to compare the results to the ones obtained for hydrated proteins as well as to literature results obtained on more simple synthetic polymers. In particular, these are, hydrated solid samples and aqueous solutions of casein peptone (a digest derivative of the protein casein), as well as hydrated solid hydrogels of hyaluronic acid (HA).

The crystallization and melting events of water and the glass transition were studied through differential scanning calorimetry (DSC). Molecular mobility (α relaxation of the hydrated systems and secondary relaxations of water in the uncrystallized and/or crystallized phase) was investigated in detail using two dielectric techniques, thermally stimulated depolarization currents (TSDC) and dielectric relaxation spectroscopy (DRS), in a wide frequency and temperature range. Additional information on the hydration properties of the samples was obtained by water equilibrium sorption measurements (ESI) at room temperature.

The thermal glass transition in the hydrated systems was recorded by DSC. Depending on the system the glass transition was recorded in different temperature regions, while it could not be detected for hydrated collagen. In general, the glass transition shows a strong hydration dependence. The variation of the glass transition temperature and the heat capacity step with hydration level leads to the conclusion that the motion associated with the transition includes contributions from the uncrystallized water molecules in the mixtures as well as segments of the biopolymer.

The dielectric response which is associated with the thermal glass transition was studied by DRS and TSDC. A relaxation which exhibits cooperative character, according to the temperature dependence of its dielectric strength, was recorded in quite good accordance with the results from calorimetry, in the case of less rigid systems. On the other hand, in the case of the fibrous protein elastin which exhibits a glass transition at higher temperatures than the rest of the systems, but also for the fibrous protein collagen, which does not exhibit a glass transition, a dielectric relaxation, similar to the dielectric manifestation of the glass transition previously mentioned for the rest of the systems, is still recorded. The striking result is that the relaxation in question is recorded in a specific temperature interval, independently of the calorimetric glass transition. It is suggested that the dielectric relaxation probes mainly the polarization of uncrystallized water molecules within clusters on the surface of the hydrated molecules.

The main dielectric relaxation due to uncrystallized water molecules in the hydration shell of the hydrated systems was systematically studied. An interrelation of the latter to a

Summary

secondary relaxation of polar groups on the surface of the hydrated systems was observed. In particular, the uncrystallized water molecules at low hydration levels trigger the motion of small polar groups on the surface of the biomolecules. The characteristic relaxation times are being reduced as the hydration level increases. The dynamical characteristics of the relaxation depend on the polar groups sequence and proportionality. In a critical region of hydration levels of about 20-30 wt% the surface of the biopolymer is gradually covered by water molecules and a percolative uncrystallized water cluster is formed, in parallel to the stabilization of both the relaxation time and the dielectric strength of the relaxation. In general, the relaxation is of secondary character and is well described by an Arrhenius law at low temperatures. In the region where the characteristics of the relaxation stabilize, the dielectric response corresponds to a mode within the uncrystallized water layer which covers the underlying surface. The excess water molecules beyond the main uncrystallized water layer, are being organized into various uncrystallized or crystalline forms depending on the structure. Finally, there are implications for a transition of the uncrystallized water molecules from a high density amorphous form (HDA) to a low density amorphous form (LDA) at high temperatures, at least in the case of the globular protein BSA.

Περίληψη

Αντικείμενο της διδακτορικής διατριβής είναι η παράλληλη μελέτη της μοριακής δυναμικής και των μεταπτώσεων φάσης πρωτεϊνών και βιοπολυμερών, σε ευρεία περιοχή επιπέδων υδάτωσης. Προσδοκώμενο τελικό αποτέλεσμα είναι, βραχυπρόθεσμα, η παραγωγή νέας γνώσης σε θέματα που αναφέρονται στην διαμόρφωση της δομής, της μοριακής δυναμικής και των μεταπτώσεων φάσης της πρωτεΐνης (ή του βιοπολυμερούς) και του διαλύτη ως αποτέλεσμα της αλληλεπίδρασής τους, και, μακροπρόθεσμα, η συμβολή στη ποσοτική περιγραφή και κατανόηση βιολογικών λειτουργιών με όρους Φυσικής.

Τα υδατωμένα συστήματα που μελετήθηκαν σε αυτή την διδακτορική διατριβή είναι: δύο σφαιρικές πρωτεΐνες, αλβουμίνη βοείου ορού (bovine serum albumin, BSA) και λυσοζύμη (lysozyme) και δύο ινώδεις πρωτεΐνες, ελαστίνη και κολλαγόνο. Εκτός από πρωτεΐνες, επιλέχθηκαν δύο δομικά απλούστερα βιοπολυμερή, προκειμένου να γίνει σύγκριση των αποτελεσμάτων με τα αντίστοιχα που προκύπτουν για τις πρωτεΐνες, καθώς και με αντίστοιχα αποτελέσματα από τη μελέτη υδροπηκτωμάτων συνθετικών πολυμερών. Συγκεκριμένα, μελετήθηκαν ενυδατωμένα στερεά δοκίμια και υδατικά διαλύματα πεπτόνης της καζεΐνης (παράγωγο πέψης της πρωτεΐνης καζεΐνης) και ενυδατωμένα στερεά υδροπηκτώματα (hydrogels) υαλουρικού οξέος (hyaluronic acid, HA).

Τα φαινόμενα κρυστάλλωσης και τήξης του νερού καθώς και το φαινόμενο της υαλώδους μετάβασης των μακρομορίων, μελετήθηκαν μέσω της διαφορικής θερμιδομετρίας σάρωσης (differential scanning calorimetry, DSC). Η μοριακή δυναμική (ο α μηχανισμός διηλεκτρικής αποκατάστασης των ενυδατωμένων συστημάτων και οι δευτερεύοντες μηχανισμοί των μορίων νερού στην μη κρυσταλλική και/ή κρυσταλλική φάση) μελετήθηκαν διεξοδικά μέσω δύο διηλεκτρικών τεχνικών, θερμικώς διηγερόμενα θερμορεύματα αποπόλωσης (thermally stimulated depolarization currents (TSDC)) και διηλεκτρική φασματοσκοπία εναλλασσομένου πεδίου (dielectric relaxation spectroscopy (DRS)), σε ευρεία περιοχή συχνοτήτων και θερμοκρασιών. Επιπλέον πληροφορίες για την οργάνωση των μορίων νερού κατά την υδάτωση προήλθαν από μετρήσεις ισόθερμης υδάτωσης σε ισορροπία (water equilibrium sorption measurements, ESI) σε θερμοκρασία περιβάλλοντος.

Η θερμική υαλώδης μετάβαση στα ενυδατωμένα συστήματα καταγράφηκε με την τεχνική DSC. Ανάλογα με το προς μελέτη σύστημα, η υαλώδης μετάβαση εκδηλώνεται σε διαφορετική θερμοκρασιακή περιοχή ενώ στην περίπτωση του κολλαγόνου δεν είναι ανιχνεύσιμη. Ένα γενικό συμπέρασμα είναι ότι η υαλώδης μετάβαση εξαρτάται άμεσα από το επίπεδο υδάτωσης. Η μελέτη της μεταβολής της θερμοκρασίας υαλώδους μετάβασης και του βήματος θερμοχωρητικότητας με το επίπεδο υδάτωσης οδηγεί στο συμπέρασμα ότι η μοριακή κίνηση που συσχετίζεται με το φαινόμενο περιέχει συνεισφορές από τα μη κρυσταλλωμένα μόρια νερού καθώς και από τμήματα των βιοπολυμερών.

Η διηλεκτρική απόκριση που σχετίζεται με τη θερμική υαλώδη μετάβαση μελετήθηκε με τις τεχνικές DRS και TSDC. Ένας μηχανισμός διηλεκτρικής

αποκατάστασης που εμφανίζει χαρακτηριστικά συνεργασιμότητας, όπως προκύπτει από τη θερμοκρασιακή εξάρτηση της διηλεκτρικής ισχύος, καταγράφηκε σε αρκετά καλή συμφωνία με τα αποτελέσματα της θερμοδομετρίας, προκειμένου για τα πιο εύκαμπτα συστήματα. Αντιθέτως, στην περίπτωση της ινώδους πρωτεΐνης ελαστίνης η οποία παρουσιάζει την υαλώδη μετάβαση σε περιοχή υψηλότερων θερμοκρασιών σε σχέση με τα υπόλοιπα συστήματα, αλλά επίσης στην περίπτωση της ινώδους πρωτεΐνης κολλαγόνο, η οποία δεν εμφανίζει υαλώδη μετάβαση, καταγράφεται ένας μηχανισμός διηλεκτρικής αποκατάστασης ο οποίος είναι παρόμοιος με τον αντίστοιχο μηχανισμό που σχετίζεται με την υαλώδη μετάβαση, και καταγράφηκε για τα υπόλοιπα συστήματα. Το κύριο αποτέλεσμα είναι ότι ο εν λόγω μηχανισμός εκδηλώνεται σε συγκεκριμένη θερμοκρασιακή περιοχή, ανεξάρτητα από την θερμική υαλώδη μετάβαση. Προτείνεται σχετικά, ότι ο μηχανισμός διηλεκτρικής αποκατάστασης εκφράζει κυρίως την πόλωση μη κρυσταλλωμένων μορίων νερού εντός συσσωματωμάτων στην επιφάνεια των ενυδατωμένων μορίων.

Ο κύριος μηχανισμός διηλεκτρικής αποκατάστασης των μη κρυσταλλωμένων μορίων νερού στα διεπιφανειακά στρώματα των ενυδατωμένων συστημάτων μελετήθηκε διεξοδικά. Παρατηρήθηκε μια αλληλοσυσχέτιση αυτού με ένα δευτερεύοντα μηχανισμό πολικών ομάδων στην επιφάνεια των ενυδατωμένων συστημάτων. Συγκεκριμένα, τα μη κρυσταλλωμένα μόρια νερού σε χαμηλά ποσοστά υδάτωσης διεγείρουν την κίνηση μικρών πολικών ομάδων στην επιφάνεια των βιοπολυμερών. Οι χαρακτηριστικοί χρόνοι αποκατάστασης μειώνονται με την αύξηση του επιπέδου υδάτωσης. Τα δυναμικά χαρακτηριστικά του μηχανισμού εξαρτώνται από την διαδοχή και αναλογία των πολικών ομάδων στην επιφάνεια. Σε μία κρίσιμη περιοχή επιπέδων υδάτωσης περίπου ίση με 20 - 30% κ. β. η επιφάνεια του βιοπολυμερούς καλύπτεται σταδιακά από μη κρυσταλλωμένα μόρια νερού και δημιουργείται ένα συνεχές επιφανειακό στρώμα νερού, ενώ παράλληλα σταθεροποιούνται οι τιμές των χαρακτηριστικών χρόνων χαλάρωσης και της διηλεκτρικής ισχύος του μηχανισμού. Σε γενικές γραμμές ο μηχανισμός είναι δευτερεύων, τοπικού χαρακτήρα και περιγράφεται ικανοποιητικά από την εξίσωση Arrhenius σε χαμηλές θερμοκρασίες. Στην περιοχή όπου σταθεροποιούνται τα χαρακτηριστικά του μηχανισμού η διηλεκτρική απόκριση αντιστοιχεί στην χαλάρωση μέρους του επιφανειακού στρώματος μη κρυσταλλωμένων μορίων νερού που καλύπτουν την επιφάνεια του μορίου. Τα επιπλέον μόρια νερού που βρίσκονται εκτός του κύριου επιφανειακού στρώματος μη κρυσταλλωμένων μορίων νερού, οργανώνονται σε άλλες δομές στην κρυσταλλική ή μη φάση, ανάλογα με την μορφολογία. Τέλος, υπάρχουν ενδείξεις για μετάβαση των μορίων νερού από μία άμορφη κατάσταση υψηλής πίεσης (high density amorphous, HDA) προς μία άμορφη κατάσταση χαμηλής πίεσης σε υψηλές θερμοκρασίες (low density amorphous, LDA), τουλάχιστον στην περίπτωση της σφαιρικής πρωτεΐνης BSA.

1^η ΕΝΟΤΗΤΑ

ΠΡΟΛΟΓΟΣ

Η παρούσα διδακτορική διατριβή με τίτλο "Μεταπτώσεις φάσης και μοριακή δυναμική σε συστήματα πρωτεΐνης-νερού" πραγματοποιήθηκε στον Τομέα Φυσικής του ΕΜΠ, στη Σχολή Εφαρμοσμένων Μαθηματικών και Φυσικών Επιστημών, στα πλαίσια του προγράμματος ΗΡΑΚΛΕΙΤΟΣ ΙΙ.

Τα μέλη της τριμελούς συμβουλευτικής επιτροπής συμπεριλαμβάνουν τον Καθηγητή Naoki Shinyashiki του πανεπιστημίου του Τόκυο στην Ιαπωνία. Ως εκ τούτου, η συγγραφή της διατριβής πραγματοποιήθηκε στην αγγλική γλώσσα.

Η παρούσα περίληψη στην ελληνική παρουσιάζει συνοπτικά τα κύρια πειραματικά αποτελέσματα που προέκυψαν από την διδακτορική διατριβή, συγκεκριμένα για το σύστημα της σφαιρικής πρωτεΐνης: αλβουμίνη βοείου ορού (bovine serum albumin, BSA). Αναφέρονται επίσης και χαρακτηριστικά παραδείγματα από αντίστοιχα αποτελέσματα που προέκυψαν για επιπρόσθετα υδατωμένα συστήματα, καθώς και τα γενικά συμπεράσματα που προκύπτουν από την συγκριτική μελέτη των διαφόρων συστημάτων.

Στην 2η Ενότητα περιγράφεται συνοπτικά η σχετική βιβλιογραφία αναφορικά με τη μελέτη των υδατωμένων πρωτεϊνών και παρουσιάζονται τα ανοιχτά προς συζήτηση ζητήματα, τα οποία οριοθετούν και το στόχο της παρούσας μελέτης.

Στη 3η Ενότητα περιγράφονται συνοπτικά οι κύριες πειραματικές τεχνικές που χρησιμοποιήθηκαν και δίνονται πληροφορίες για τις πειραματικές διατάξεις των μετρήσεων και την προετοιμασία των δοκιμών.

Στην 4η Ενότητα της περιλήψης παρουσιάζονται τα πειραματικά αποτελέσματα για το σύστημα BSA-νερό και ακολουθεί συζήτηση των αποτελεσμάτων σε αντιπαραβολή με την αντίστοιχη βιβλιογραφία.

Στην 5η Ενότητα παρουσιάζονται χαρακτηριστικά παραδείγματα από αντίστοιχα αποτελέσματα που προέκυψαν για επιπρόσθετα υδατωμένα συστήματα, όπως η ινώδης πρωτεΐνη ελαστίνη (elastin) ή το υδροπήκτωμα υαλουρικού οξέος (HA hydrogel), και ακολουθεί συζήτηση των αποτελεσμάτων σε αντιπαραβολή με την αντίστοιχη βιβλιογραφία.

Στην 6η Ενότητα παραθέτονται τα γενικά συμπεράσματα.

Η Εκτενής Περίληψη ολοκληρώνεται με τη Βιβλιογραφία.

Αναλυτική περιγραφή των αποτελεσμάτων για το σύστημα BSA-νερό δίδεται στις αναφορές:

1. A. Panagopoulou, A. Kyritsis, R. Sabater i Serra, J.L. Gómez Ribelles, N. Shinyashiki, P. Pissis, Glass transition and dynamics in BSA-water mixtures over wide ranges of

ΕΚΤΕΝΗΣ ΠΕΡΙΛΗΨΗ

composition studied by thermal and dielectric techniques, *Biochim. et Biophys. Acta*, 1814 (2011) 1984-1996.

2. A. Panagopoulou, A. Kyritsis, N. Shinyashiki, P. Pissis, Water and protein dynamics in bovine serum albumin-water mixtures over wide ranges of composition, *J. Phys. Chem. B*, 116 (2012) 4593-4602.

ενώ για τα συστήματα ελαστίνη-νερό και HA-νερό στις αναφορές 3, 4, αντίστοιχα:

3. A. Panagopoulou, A. Kyritsis, M. Vodina, P. Pissis, Dynamics of uncrystallized water and protein in hydrated elastin studied by thermal and dielectric techniques, *Biochim. et Biophys. Acta*, 1834 (2013) 977-988.

4. A. Panagopoulou, J.V. Molina, A. Kyritsis, M.M. Pradas, A.V. Lluch, G.G. Ferrer, P. Pissis, Glass Transition and water dynamics in hyaluronic acid hydrogels, *Food Biophysics*, 8 (2013) 192-202.

2 η ΕΝΟΤΗΤΑ

ΒΙΒΛΙΟΓΡΑΦΙΚΗ ΕΠΙΣΚΟΠΗΣΗ

Οι πρωτεΐνες αποτελούν κύριο συστατικό των βιολογικών κυττάρων και επιτελούν εξαιρετικά εξειδικευμένες λειτουργίες, όμως μόνο παρουσία ενός διαλύτη (νερού) και σε μια ορισμένη περιοχή θερμοκρασιών, δηλαδή στις συνθήκες που συναντούμε σε ένα ζωντανό κύτταρο [1]. Για τον Φυσικό όμως οι πρωτεΐνες είναι μακρομόρια και οι κινήσεις τους, τόσο οι μικρής κλίμακας (θερμικά διεγερόμενες [2]) όσο και οι συνεργασιακές μεγάλης εμβέλειας [3], αμφότερες απαραίτητες για τη σταθερότητα, την αναδίπλωση και τη λειτουργία των πρωτεϊνών, περιγράφονται και ερμηνεύονται με τους ίδιους όρους όπως οι χαλαρώσεις των (απλούστερων στη δομή) συνθετικών πολυμερών. Οι μοριακοί μηχανισμοί κίνησης του διαλύτη, που χρειάζεται να ενεργοποιηθούν για να επαχθεί η δομική χαλάρωση της πρωτεΐνης δεν είναι επακριβώς γνωστοί, εν τούτοις το κατώφλι στη θερμοκρασία και στην ενυδάτωση για τη βιολογική λειτουργία της πρωτεΐνης μπορεί να κατανοηθεί με όρους υαλώδους μετάβασης [4]. Η σχέση μεταξύ δυναμικής της πρωτεΐνης και δυναμικής του διαλύτη αποτελεί κομβικό σημείο στη μελέτη των πρωτεϊνών [4]. Πειράματα και προσομοιώσεις σε υπολογιστή [5-7]) υποδεικνύουν ότι τα μόρια του διαλύτη κοντά στην επιφάνεια της πρωτεΐνης είναι σε άμορφη κατάσταση, ενώ η δυναμική τους είναι μερικές τάξεις μεγέθους πιο αργή και εκτεταμένη στο χρόνο (stretched exponential) σε σύγκριση με τον μακροσκοπικό (bulk) διαλύτη. Ειδικότερα στη περίπτωση του νερού η διεργασία αυτή μοιάζει με τη χαλάρωση υπέρψυκτου νερού [8], καθώς και οργανικών υαλοποιητών και συνθετότερων πολυμερικών συστημάτων [9]. Η τεράστια σημασία που έχουν τα πρώτα επιφανειακά στρώματα νερού για τη βιολογική λειτουργία των πρωτεϊνών γίνεται προφανής, αν αναλογισθεί κανείς ότι στα βιολογικά κύτταρα οι πρωτεΐνες διαχωρίζονται μεταξύ τους με 2-3 στρώματα νερού [10]. Παράλληλα με την επίδραση της πρωτεΐνης στη δομή και στη δυναμική συμπεριφορά του διαλύτη, η δυναμική

συμπεριφορά της πρωτεΐνης επηρεάζεται σημαντικά από τη παρουσία του διαλύτη μέσω αλληλεπιδράσεων πρωτεΐνης-διαλύτη, συχνά μέσω δεσμών υδρογόνου [6]. Σε υδατικό διάλυμα το ποσοστό ενυδάτωσης απαιτείται να υπερβεί μία κρίσιμη τιμή (κατώφλι), προκειμένου να έχουμε μεταβολές στη διαμόρφωση της πρωτεΐνης [6, 11, 12]. Οι Frauenfelder και συνεργάτες πρότειναν μια διάκριση των μεταβάσεων (χαλαρώσεων) στις πρωτεΐνες σε μη-συζευγμένες (non-slaved), που καθορίζονται από τη διαμόρφωση και τη δυναμική της πρωτεΐνης, και σε συζευγμένες (slaved) με το διαλύτη [14]. Τα αποτελέσματα πρόσφατων πειραμάτων ενισχύουν όμως την άποψη ότι δεν είναι η μακροσκοπική φάση νερού που είναι συζευγμένη με τις κινήσεις της πρωτεΐνης αλλά τα πρώτα στρώματα ενυδάτωσης και ότι μάλλον έχουμε αμοιβαία τροποποίηση της δυναμικής παρά σύζευξη και επιβολή της δυναμικής του διαλύτη στη πρωτεΐνη [15, 16].

3 η ΕΝΟΤΗΤΑ

ΠΕΙΡΑΜΑΤΙΚΕΣ ΤΕΧΝΙΚΕΣ & ΔΙΑΤΑΞΕΙΣ

3.1 Μετρήσεις ισόθερμης ρόφησης/εκρόφησης νερού σε ισοροπία (ESI)

Οι μετρήσεις ισόθερμης ρόφησης/εκρόφησης σε ισοροπία παρέχουν πολύτιμες πληροφορίες για την αλληλεπίδραση του μορίου του νερού με το προς μελέτη δοκίμιο. Οι μετρήσεις ρόφησης/εκρόφησης πραγματοποιούνται με τον πειραματικό προσδιορισμό της μάζας του νερού που απορροφάται ή αποβάλλεται από το υλικό όταν, ευρισκόμενο σε ισοροπία σε μία αρχική σχετική υγρασία (ενεργότητα $a_w=rh$, relative humidity) μεταβαίνει σε νέα κατάσταση ισοροπίας, σε διαφορετική σχετική υγρασία, υπό σταθερή θερμοκρασία.

Ένα τυπικό πείραμα ισόθερμης ρόφησης νερού παρίσταται γραφικά μέσω της λεγόμενης 'ισόθερμης' καμπύλης, η οποία αποτελεί την γραφική αναπαράσταση του ποσοστού υδάτωσης, h (g νερού/ g ξηρού δοκιμίου) συναρτήσει της αντίστοιχης τιμής σχετικής υγρασίας/ενεργότητας, a_w .

Η ποσοτική επεξεργασία των δεδομένων πραγματοποιείται, στην περίπτωση υδάτωσης πολλαπλών επιπέδων, υδρόφιλων πολυμερών και λοιπών βιοπολυμερών, μέσω της εξίσωσης Guggenheim-Anderson-de Boer (GAB) [17] η οποία προσαρμόζεται στα πειραματικά σημεία:

$$\frac{h}{h_m} = \frac{cfa_w}{(1-fa_w)[1+(c-1)fa_w]} \quad (3.1)$$

όπου, h_m , το ποσοστό μορίων νερού που είναι συνδεδεμένα σε πρωταρχικές θέσεις υδάτωσης (πρώτο επίπεδο υδάτωσης), ενώ c, f , σταθερές που αφορούν στο δεύτερο και διαδοχικά επίπεδα υδάτωσης.

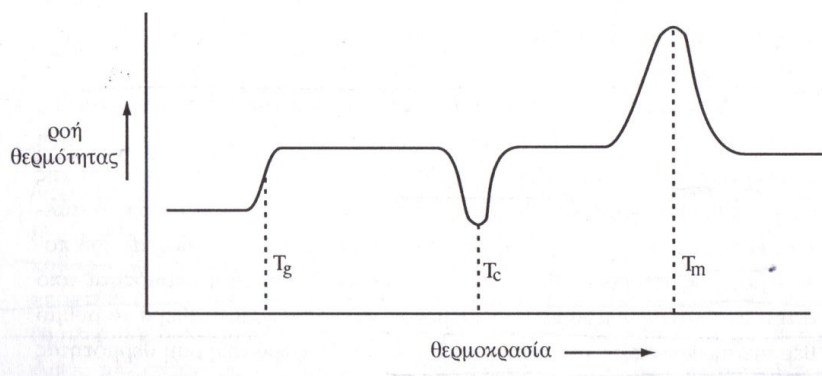
3.2 Διαφορική θερμοδομετρία σάρωσης (DSC)

Η διαφορική θερμοδομετρία σάρωσης (Differential Scanning Calorimetry) αποτελεί παραδοσιακή τεχνική θερμικής ανάλυσης. Το φυσικό μέγεθος που εξάγεται με αυτή την τεχνική είναι η ειδική θερμότητα του υπό μελέτη δοκιμίου. Η τιμή της υπολογίζεται έμμεσα από τη μετρούμενη θερμότητα που εκλύεται ή απορροφάται από το δοκίμιο, προκειμένου αυτό να ακολουθεί τη θερμοκρασία αδρανούς δοκιμίου αναφοράς, καθώς τα δύο δοκίμια υπόκεινται σε ίδιες θερμικές διαδικασίες (π.χ. θέρμανση ή ψύξη με σταθερό ρυθμό).

Υπάρχουν δύο τύποι διατάξεων DSC, οι οποίοι διαφοροποιούνται ως προς τη λειτουργία τους. Το DSC ροής θερμότητας (heat flux) και το DSC αντιστάθμισης ισχύος (power compensation). Στο heat flux DSC τα δύο δοκίμια βρίσκονται σε καλή θερμική επαφή μέσω μεταλλικού δίσκου, ενώ περιβάλλονται από κοινό φούρνο. Οι μεταβολές στην ενθαλπία και τη θερμοχωρητικότητα που λαμβάνουν χώρα στο υπό μελέτη δοκίμιο έχουν ως αποτέλεσμα τη μεταβολή της θερμοκρασίας του σε σχέση με αυτή του δοκιμίου αναφοράς. Αυτή η διαφορά θερμοκρασίας μετράται, και γνωρίζοντας τη θερμική αντίσταση συνδέεται με τη ροή θερμότητας στο σύστημα. Στο DSC αντιστάθμισης ισχύος οι θερμοκρασίες του υπό μελέτη δοκιμίου και του δοκιμίου αναφοράς ελέγχονται ανεξάρτητα μέσω ανεξάρτητων φούρνων. Η εξίσωση των θερμοκρασιών των δύο δοκιμίων επιτυγχάνεται μεταβάλλοντας την ισχύ εισόδου των δύο φούρνων που συμπίπτει με τη ροή θερμότητας στο σύστημα.

Ένα τυπικό πείραμα θερμοδομετρίας διεξάγεται θερμαίνοντας ή ψύχοντας με σταθερό ρυθμό, αλλά είναι επίσης δυνατό να παρατηρηθεί υπό σταθερή θερμοκρασία η εξέλιξη μίας διεργασίας (κρυστάλλωση, χημική αντίδραση) συναρτήσει του χρόνου.

Στο Σχήμα 3.1 φαίνεται η συνολική καμπύλη DSC ενός ημικρυσταλλικού πολυμερούς. Οι μεταπτώσεις που παρατηρούνται αυξανόμενης της θερμοκρασίας είναι η υαλώδης μετάβαση με τη μορφή ενός σκαλοπατιού, η κρυστάλλωση, και τέλος η τήξη των κρυσταλλιτών. Από το σκαλοπάτι λαμβάνεται η τιμή της θερμοκρασίας υαλώδους μετάβασης T_g . Από τις κορυφές τήξης και κρυστάλλωσης λαμβάνεται, εκτός από τις αντίστοιχες θερμοκρασίες T_m , T_c , η ενθαλπία τήξης (ΔH_m), ή κρυστάλλωσης (ΔH_c), από το εμβαδό της αντίστοιχης κορυφής.



Σχήμα 3.1: Η συνολική καμπύλη DSC ενός ημικρυσταλλικού πολυμερούς. Στο διάγραμμα η σύμβαση είναι η ενδόθερμη κορυφή να δείχνει προς τα πάνω.

Εκτίμηση του βαθμού κρυσταλλικότητας

Είναι δυνατόν να γίνει μία εκτίμηση του βαθμού κρυσταλλικότητας ενός υλικού μέσω της ενθαλπίας τήξης (ή κρυστάλλωσης). Η εκτιμώμενη τιμή για τον χ_c δίνεται από τη σχέση

$$\chi_c = \frac{\Delta H}{\Delta H_{100\%}} \quad (3.2)$$

όπου ΔH είναι η τιμή της ενθαλπίας τήξης ή κρυστάλλωσης, και $\Delta H_{100\%}$ η ενθαλπία τήξης του 100% κρυσταλλικού πολυμερούς.

3.2.1 Διάταξη DSC

Οι μετρήσεις διαφορικής θερμιδομετρίας σάρωσης στα πλαίσια της παρούσας διδακτορικής διατριβής για το σύστημα αλβουμίνης - νερού πραγματοποιήθηκαν στο Κέντρο Βιοπολυμερών στο Πολυτεχνείο της Βαλένθια στην Ισπανία (Center of Biomaterials, UPV, Valencia, Spain). Η διάταξη που χρησιμοποιήθηκε είναι ένα θερμιδόμετρο Mettler Toledo 823e. Οι μετρήσεις πραγματοποιήθηκαν σε ατμόσφαιρα αζώτου στη θερμοκρασιακή περιοχή $-150 \leq T \leq 40^\circ\text{C}$. Τα δείγματα, μάζας μεταξύ 5 και 15 mg, τοποθετήθηκαν σε καψίδια αλουμινίου. Οι τιμές των ρυθμών ψύξης-θέρμανσης ήταν $10^\circ\text{C}/\text{min}$.

3.3 Διηλεκτρική φασματοσκοπία εναλλασσομένου πεδίου (DRS)

Η διηλεκτρική φασματοσκοπία εναλλασσομένου πεδίου (Dielectric Relaxation Spectroscopy) αποτελεί μία μέθοδο διηλεκτρικής φασματοσκοπίας, δηλαδή αποσκοπεί στη μελέτη των διηλεκτρικών ιδιοτήτων ενός υλικού, οι οποίες εκφράζονται με τη μιγαδική διηλεκτρική σταθερά $\varepsilon^* = \varepsilon'(\omega) - i\varepsilon''(\omega)$. Η μιγαδική διηλεκτρική σταθερά συνδέει το ηλεκτρικό πεδίο κυκλικής συχνότητας ω που εφαρμόζεται στο δοκίμιο με την απόκριση του υλικού, την πόλωση. Το ε' είναι ένα μέτρο της ηλεκτρικής ενέργειας που αποθηκεύτηκε στο υλικό, ενώ οι διηλεκτρικές απώλειες ε'' είναι ένα μέτρο της ενέργειας που μετατρέπεται σε θερμότητα.

Η συνεισφορά στην πόλωση για ένα υλικό σε εναλλασσόμενο πεδίο προέρχεται από τους εξής μηχανισμούς: πόλωση προσανατολισμού (μόνιμα δίπολα), ηλεκτρονική πόλωση, ατομική ή ιοντική πόλωση και παγίδευση φορέων φορτίου σε διεπιφάνειες μεταξύ περιοχών με διαφορετική αγωγιμότητα (διεπιφανειακή πόλωση). Η μεταβολή της πόλωσης συναρτήσει του χρόνου εισάγει την έννοια του χρόνου αποκατάστασης τ , δηλαδή του χρόνου στον οποίο, μετά την απομάκρυνση του πεδίου, η πόλωση έχει μειωθεί στο $1/e$ της τιμής ισορροπίας της (με εφαρμοσμένο πεδίο). Η διηλεκτρική φασματοσκοπία εναλλασσομένου πεδίου εφαρμόζεται σε μία ευρεία περιοχή συχνοτήτων ($10^4 - 10^{12}$ Hz). Σε αυτή την περιοχή συχνοτήτων η ηλεκτρονική και ιοντική πόλωση ακολουθούν χωρίς καθυστέρηση το πεδίο, ενώ μόνο η διπολική και η επιφανειακή καθυστερούν. Από τη θεωρία προκύπτει ότι

$$\varepsilon^*(\omega) = \varepsilon_\infty + \frac{\varepsilon_s - \varepsilon_\infty}{1 + i\omega\tau} = \frac{\Delta\varepsilon}{1 + i\omega\tau} \quad (3.3)$$

ΕΚΤΕΝΗΣ ΠΕΡΙΛΗΨΗ

όπου ε_∞ η διηλεκτρική σταθερά σε πολύ μεγάλες συχνότητες, δηλαδή αυτή που οφείλεται στην ατομική και ηλεκτρονική πόλωση. Το $\Delta\varepsilon$ είναι η σεινισφορά του συγκεκριμένου μηχανισμού στη στατική διηλεκτρική σταθερά ε_s . Για το πραγματικό και φανταστικό μέρος προκύπτουν οι εξισώσεις Debye

$$\begin{aligned}\varepsilon'(\omega) &= \varepsilon_\infty + \frac{\varepsilon_s - \varepsilon_\infty}{1 + \omega^2 \tau^2} \\ \varepsilon''(\omega) &= \frac{\varepsilon_s - \varepsilon_\infty}{1 + \omega^2 \tau^2} \omega \tau\end{aligned}\quad (3.4)$$

για ένα μηχανισμό Debye ενός μόνο χρόνου αποκατάστασης τ . Στην πράξη λίγα υλικά συμπεριφέρονται σύμφωνα με τις εξισώσεις Debye, διότι συνήθως οι μηχανισμοί δεν έχουν ένα μόνο χρόνο αποκατάστασης, αλλά περιγράφονται από μία κατανομή χρόνων αποκατάστασης. Μία εμπειρική εξίσωση για την περιγραφή του φαινομένου αποτελεί η εξίσωση Havriliak-Negami

$$\begin{aligned}\varepsilon^*(\omega) &= \varepsilon_\infty + \frac{\Delta\varepsilon}{[1 + (i\omega\tau_{HN})^a]^b} \\ ab &\leq 1\end{aligned}\quad (3.5)$$

Στο Σχήμα 3.2 φαίνεται η μορφή του πραγματικού και του φανταστικού μέρους της διηλεκτρικής συνάρτησης σύμφωνα με το μοντέλο Debye (διακεκομμένη γραμμή) και με την εξίσωση HN (συνεχής γραμμή). Όπως φαίνεται για το μοντέλο Debye, σε μία περιοχή συχνοτήτων γύρω από την τιμή $f = 1 / (2\pi\tau)$ παρατηρείται α) μία κορυφή στο ε'' με μέγιστο στη συχνότητα $\omega_{\max} = 1 / \tau$, η οποία αντιστοιχεί στη μεγιστοποίηση των απωλειών ενέργειας, και β) ένα σκαλοπάτι στο ε' , με ύψος $\Delta\varepsilon$. Η αντίστοιχη εικόνα για την εξίσωση HN δίνει μια πιο πλατειά και ασύμμετρη κορυφή διηλεκτρικών απωλειών. Οι παράμετροι a, b της εξίσωσης 3.5 περιγράφουν αντίστοιχα τη συμμετρική και μη συμμετρική διεύρυνση της κορυφής διηλεκτρικών απωλειών.

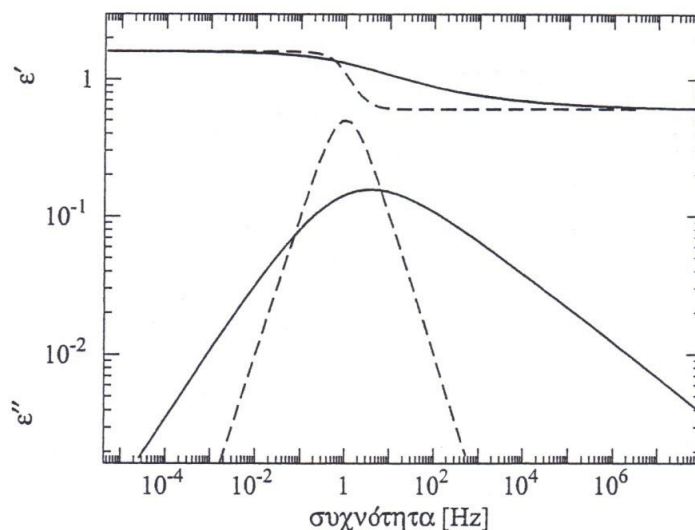
Θερμοκρασιακή εξάρτηση του χρόνου αποκατάστασης

Ο χρόνος αποκατάστασης ενός μηχανισμού δεν είναι ο ίδιος σε όλες τις θερμοκρασίες, αλλά γενικά μειώνεται με τη θερμοκρασία, το οποίο οφείλεται στο πλεόνασμα κινητικής ενέργειας που έχουν τα μόρια ενός υλικού σε υψηλότερες θερμοκρασίες. Οι πιο συχνά παρατηρούμενες σχέσεις $\tau(T)$ είναι οι Arrhenius και Vogel-Tammann-Fulcher (VTF) [3].

Η σχέση Arrhenius είναι:

$$\tau = \tau_0 \exp\left(\frac{W}{kT}\right) \quad (3.6)$$

όπου W είναι η ενέργεια ενεργοποίησης του μηχανισμού, το τ_0 είναι ο προεκθετικός παράγοντας και k η σταθερά του Boltzmann. Η εξίσωση αυτή υποδηλώνει ότι τα δίπολα δεν αλληλεπιδρούν μεταξύ τους, αλλά μόνο με το πεδίο.



Σχήμα 3.2: Πραγματικό μέρος ϵ' και φανταστικό μέρος ϵ'' της διηλεκτρικής συνάρτησης συναρτήσει της συχνότητας για ένα μηχανισμό τύπου Debye (διακεκομμένη γραμμή) και τύπου Havriliak-Negami (συνεχής γραμμή).

Η σχέση VFT είναι:

$$\tau = \tau_0 \exp\left(\frac{B}{T - T_0}\right) \quad (3.7)$$

όπου B , τ_0 , και T_0 (θερμοκρασία Vogel) είναι παράμετροι ανεξάρτητες της θερμοκρασίας. Τέτοιου είδους εξάρτηση είναι χαρακτηριστική για μηχανισμούς που οφείλονται σε συνεργασιακές κινήσεις των διπόλων.

Αγωγιμότητα

Στη διηλεκτρική συνάρτηση $\epsilon^*(\omega)$ εκτός από τους διπολικούς μηχανισμούς πόλωσης συνεισφέρουν και οι μηχανισμοί αγωγιμότητας που εμφανίζονται στο υλικό λόγω μετατόπισης φορτίων. Η αγωγιμότητα (όταν πρόκειται για dc αγωγιμότητα) συνεισφέρει στο φανταστικό μέρος της διηλεκτρικής συνάρτησης τον όρο $(\sigma_0/\epsilon_0\omega)$. Η αγωγιμότητα σ_0 ονομάζεται και dc αγωγιμότητα και σε μεγάλες συχνότητες η συνεισφορά της μηδενίζεται. Η διηλεκτρική σταθερά τελικά γράφεται $\epsilon''(\omega) = \sigma'(\omega)/\epsilon_0\omega$.

3.3.1 Διάταξη DRS

Για τις μετρήσεις διαφορικής διηλεκτρικής φασματοσκοπίας εναλλασσομένου πεδίου στα πλαίσια της παρούσας διδακτορικής διατριβής, χρησιμοποιήθηκε η διάταξη DRS του Εργαστηρίου Διηλεκτρικής Φασματοσκοπίας του Τομέα Φυσικής του ΕΜΠ.

Η διάταξη διαθέτει αναλυτή απόκρισης συχνότητας Alpha Analyzer, καθώς και κυψελίδα μέτρησης τύπου BDS 1200 της Novocontrol. Το εύρος μετρήσεων σύνθετης αντίστασης κυμαίνεται από $10\text{m}\Omega$ έως $100\text{M}\Omega$. Η διάταξη δίνει τη δυνατότητα μετρήσεων των διηλεκτρικών ιδιοτήτων με μεγάλη ακρίβεια στην περιοχή

συχνοτήτων 10^{-1} έως 10^6 Hz. Το επιτρεπόμενο εύρος θερμοκρασιών είναι από -150 έως 400°C .

3.3 Θερμορεύματα αποπόλωσης (TSDC)

Η τεχνική των θερμορευμάτων αποπόλωσης (Thermally Stimulated Depolarization Currents) αποτελεί μία μέθοδο διηλεκτρικής φασματοσκοπίας στην περιοχή της θερμοκρασίας (δηλαδή με ανεξάρτητη μεταβλητή τη θερμοκρασία). Στην τεχνική TSDC το υλικό τοποθετείται ανάμεσα στους οπλισμούς ενός επίπεδου πυκνωτή και πολώνεται ηλεκτρικά σε σταθερή θερμοκρασία T_p , με την εφαρμογή συνεχούς ηλεκτρικού πεδίου E_p για χρονικό διάστημα $t_p \gg \tau(T_p)$, (όπου τ ο χρόνος αποκατάστασης των μοριακών διπόλων), ώστε να επιτευχθεί πόλωση κορεσμού. Στους οπλισμούς του πυκνωτή δεσμεύονται τότε φορτία λόγω επαγωγής. Στη συνέχεια, με εφαρμοσμένο ακόμα το πεδίο το υλικό ψύχεται σε μία θερμοκρασία T_0 αρκετά χαμηλή, ώστε ο χρόνος αποκατάστασης $\tau(T_0)$ να γίνει πολύ μεγάλος, της τάξης μερικών ωρών. Έτσι, όταν αποσυνδεθεί το πεδίο, παραμένουν τόσο η πόλωση όσο και τα φορτία στους οπλισμούς του πυκνωτή. Στη συνέχεια οι οπλισμοί του πυκνωτή βραχυκυκλώνονται μέσω ενός ηλεκτρομέτρου, και το υλικό θερμαίνεται με σταθερό ρυθμό θέρμανσης $b = dT/dt$. Με την αύξηση της θερμοκρασίας δίνεται θερμική ενέργεια στα μόρια και ο χρόνος αποκατάστασης μειώνεται. Όταν η θερμοκρασία αυξηθεί αρκετά, τα δίπολα ανακατανέμονται στατιστικά και τα αντίστοιχα φορτία στους οπλισμούς απελευθερώνονται με αποτέλεσμα την εμφάνιση ηλεκτρικού ρεύματος στο εξωτερικό κύκλωμα. Αυτό το ρεύμα καταγράφεται τελικά από το ηλεκτρόμετρο και αποτελεί την απόκριση της μεθόδου. Ένα από τα κύρια πλεονεκτήματα της τεχνικής αυτής είναι ότι πολύ γρήγορα και μη καταστροφικά για το δοκίμιο, δίνεται μια συνολική εικόνα των μηχανισμών σε μία ευρεία περιοχή θερμοκρασιών.

Η πυκνότητα ρεύματος που λαμβάνεται κατά την αποπόλωση ενός μηχανισμού διηλεκτρικής αποκατάστασης, όταν ισχύει κινητική πρώτης τάξης, εκφράζεται ως:

$$J(T) = \frac{P_0}{\tau(T)} \exp\left(-\frac{1}{b} \int_{T_0}^T \frac{dT'}{\tau T'}\right) \quad (3.8)$$

ενώ όταν η θερμοκρασιακή εξάρτηση του χρόνου αποκατάστασης είναι τύπου Arrhenius, ως:

$$J(T) = \frac{P_0}{\tau_0} \exp\left(-\frac{E_a}{kT} - \frac{1}{b\tau_0} \int_{T_0}^T \exp\left(\frac{E_{act}}{kT'}\right) dT'\right) \quad (3.9)$$

Λόγω του γεγονότος ότι η τεχνική TSDC εφαρμόζεται σε πολύ στενή περιοχή συχνοτήτων, δεν είναι εύκολο πειραματικά να προσδιορισθούν οι εξαρτήσεις $\tau(T)$. Έτσι πολλές φορές εφαρμόζεται η εξίσωση 2.8 ακόμα και αν ο μηχανισμός που εξετάζεται δεν είναι τύπου Arrhenius. Σε αυτές τις περιπτώσεις οι τιμές που λαμβάνονται για τις παραμέτρους της ενέργειας ενεργοποίησης θα θεωρούνται ενεργές (effective) τιμές.

ΕΚΤΕΝΗΣ ΠΕΡΙΛΗΨΗ

Στο Σχήμα 2.3 (αριστερό σκέλος) φαίνεται σχηματικά η διαδικασία ενός τυπικού πειράματος TSDC, καθώς και το διάγραμμα του ρεύματος αποπόλωσης συναρτήσει της θερμοκρασίας (θερμόγραμμα αποπόλωσης). Η κορυφή που λαμβάνεται από το θερμόγραμμα αντιστοιχεί σε κάποιο μηχανισμό αποπόλωσης. Ένα θερμόγραμμα αποπόλωσης είναι δυνατόν να περιέχει μία ή περισσότερες τέτοιες κορυφές. Εκτός από τη θερμοκρασία μέγιστου του ρεύματος αποπόλωσης, μία σημαντική πληροφορία που λαμβάνεται από το θερμόγραμμα αποπόλωσης είναι η συνεισφορά ενός μηχανισμού διηλεκτρικής αποκατάστασης στη στατική διηλεκτρική σταθερά στη θερμοκρασία πόλωσης T_p , που προκύπτει από τη σχέση:

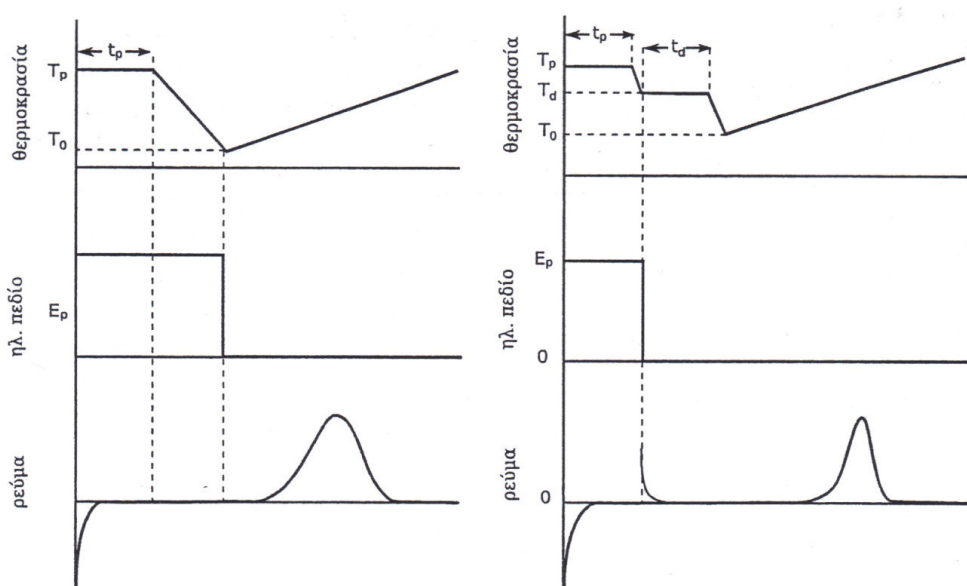
$$\Delta\varepsilon = \frac{J}{\varepsilon_0 E_p} = \frac{Q}{\varepsilon_0 A E_p} = \int I(T') dT' \quad (3.10)$$

όπου A το εμβαδόν διατομής του δοκιμίου και Q το φορτίο αποπόλωσης που υπολογίζεται με γραφική ολοκλήρωση της καμπύλης του ρεύματος αποπόλωσης.

2.3.1 Διάταξη TSDC

Για τις μετρήσεις θερμορευμάτων αποπόλωσης στα πλαίσια της παρούσας διδακτορικής διατριβής, χρησιμοποιήθηκε η διάταξη TSDC του Εργαστηρίου Διηλεκτρικής Φασματοσκοπίας του Τομέα Φυσικής του ΕΜΠ.

Η διάταξη διαθέτει ηλεκτόμετρο Keithley 617 μεγάλης ευαισθησίας ($10^{-14}A$), καθώς και σύστημα ελέγχου θερμοκρασίας Quatro Novocontrol. Η επιτρεπόμενη περιοχή σάρωσης θερμοκρασιών είναι από -160 έως $400^\circ C$.



Σχήμα 3.3: Μεταβολή της θερμοκρασίας, του επιβαλλόμενου ηλεκτρικού πεδίου και του παρατηρούμενου ρεύματος αποπόλωσης κατά τη διάρκεια ενός τυπικού πειράματος θερμορευμάτων αποπόλωσης (αριστερά) και ενός πειράματος επιλεκτικής πόλωσης (δεξιά).

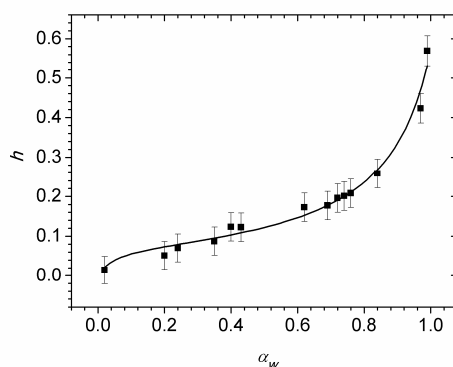
4 η ΕΝΟΤΗΤΑ

ΠΕΙΡΑΜΑΤΙΚΑ ΑΠΟΤΕΛΕΣΜΑΤΑ-ΔΙΕΡΕΥΝΗΣΗ-BSA

4.1 Ισόθερμες ρόφησης νερού σε ισορροπία (ESI)

Πραγματοποιήθηκαν μετρήσεις ισόθερμης υδάτωσης σε θερμοκρασία δωματίου, $T=25\text{ }^{\circ}\text{C}$, για ένα δοκίμιο αλβουμίνης βοείου ορού (bovine serum albumin, BSA). Η ξηρή μάζα της πρωτεΐνης μετρήθηκε μετά από ξήρανση παρουσία κενού σε φούρνο στους 70°C , για διάστημα 48 h.

Τα πειραματικά σημεία, ποσοστό νερού h (ως προς την ξηρή μάζα, g νερού/ g πρωτεΐνης) συναρτήσει της ενεργότητας a_w ($a_w=rh$, σχετική υγρασία), φαίνονται στο Σχήμα 4.1.



Σχήμα 4.1: Ισόθερμες καμπύλες υδάτωσης για το BSA. Η συμπαγής γραμμή που διαπερνά τα πειραματικά σημεία αποτελεί προσαρμογή της εξίσωσης GAB στα πειραματικά σημεία.

Η εξίσωση Guggenheim-Anderson-de Boer (GAB) [17]

$$\frac{h}{h_m} = \frac{cfa_w}{(1-fa_w)[1+(c-1)fa_w]} \quad (4.1)$$

προσαρμόστηκε στα πειραματικά σημεία.

Όπως φαίνεται στο Σχήμα 4.1, μια γραμμική περιοχή επικρατεί αρχικά για $a_w < 0.8$, η οποία ακολουθείται από απόκλιση σε μεγαλύτερες τιμές σχετικής υγρασίας. Η απόκλιση αυτή εξηγείται με βάση φαινόμενα οργάνωσης των μορίων νερού σε συσσωματώματα [18]. Αντιστοιχεί σε ποσοστό υδάτωσης $h=0.25$, δηλαδή σε κλάσμα $h_w=0.2$ (ορίζουμε ως h_w το κλάσμα νερού, δηλαδή $h_w = \text{g νερού/g υδατωμένου δοκιμίου}$). Επιπλέον, η παράμετρος h_m της εξίσωσης GAB, η οποία αντιστοιχεί στο ποσοστό μορίων νερού που απορροφώνται από το δοκίμιο και προσδένονται σε

ΕΚΤΕΝΗΣ ΠΕΡΙΛΗΨΗ

πρωταρχικές θέσεις υδάτωσης, υπολογίστηκε για το BSA, $h_m=0.073$, που αντιστοιχεί σε κλάσμα νερού $h_w=0.068$.

Έτσι προκύπτουν δύο κρίσιμα επίπεδα υδάτωσης για το BSA:

1. $h_w=0.2$, για την έντονη δημιουργία συσσωματωμάτων νερού
2. $h_w=0.068$, για την κάλυψη των πρωταρχικών θέσεων υδάτωσης

4.2 Διαφορική θερμοδομετρία σάρωσης (DSC)

Στο Σχήμα 4.2 a και 4.2 b φαίνονται θερμογράμματα DSC που καταγράφηκαν κατά την ψύξη και θέρμανση, αντίστοιχα, για υδατωμένα δοκίμια BSA. Κατά την ψύξη καταγράφεται εμφανώς η κρυστάλλωση του νερού στα δοκίμια, για κλάσμα υδάτωσης $h_w \geq 0.30$. Κατά την θέρμανση η τήξη καταγράφεται εμφανώς για $h_w \geq 0.26$. Μία ενδιάμεση περιοχή όπου εκδηλώνεται ψυχρή κρυστάλλωση κατά τη θέρμανση, εκτιμάται ως $0.23 \leq h_w \leq 0.30$.

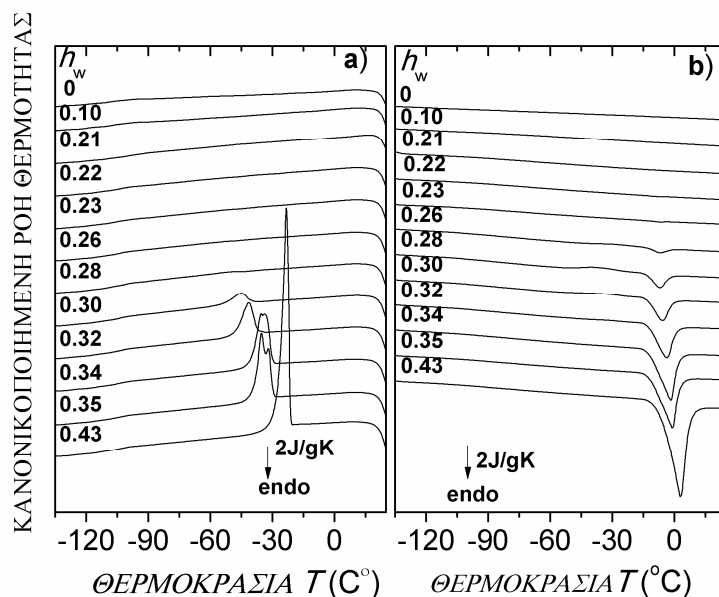
Κατά τη θέρμανση καταγράφεται ένα ευρύ σκαλοπάτι, το οποίο αποδίδεται σε φαινόμενα θερμοκίνησης υαλώδους μετάβασης. Η κλίμακα του Σχήματος 4.2b δεν επιτρέπει την άμεση παρατήρησή του φαινομένου. Για το λόγω αυτό μία μεγέθυνση στην θερμοκρασιακή περιοχή της υαλώδους μετάβασης αποτυπώνεται στο Σχήμα 4.3. Η εκτιμώμενη θερμοκρασία υαλώδους μετάβασης, T_g , αναδεικνύεται στο διάγραμμα με κάθετα ευθύγραμμα τμήματα. Σημαντική παρατήρηση είναι ότι η υαλώδης μετάβαση ανιχνεύεται μόνο για επίπεδα υδάτωσης $h_w > 0.07$. Η T_g φαίνεται να μειώνεται με την προσθήκη νερού στα δοκίμια, γεγονός που σηματοδοτεί την διευκόλυνση της μοριακής κίνησης στην οποία οφείλεται η μετάβαση, μέσω πλαστικοποίησης από τα μόρια νερού. Επιπλέον, στο Σχήμα 4.3 φαίνονται καθαρά οι εξώθερμες κορυφές ψυχρής κρυστάλλωσης οι οποίες καταγράφονται κατά τη θέρμανση, πιο έντονα για $h_w = 0.26$.

Το βήμα της υαλώδους μετάβασης καταγράφηκε για όλα τα δοκίμια που μετρήθηκαν, όπου αυτό εμφανίστηκε, και υπολογίστηκαν τα χαρακτηριστικά μεγέθη της μετάβασης. Η θερμοκρασία υαλώδους μετάβασης, T_g , καθώς και οι θερμοκρασίες κρυστάλλωσης, T_c , και τήξης, T_m , συναρτήσει του κλάσματος υδάτωσης h_w , καταγράφονται στο Σχήμα 4.4. Η θερμοκρασία υαλώδους μετάβασης μειώνεται σταθερά με την αύξηση του επιπέδου υδάτωσης, έως ένα κρίσιμο κλάσμα υδάτωσης $h_w = 0.30$. Όπως είδαμε νωρίτερα, το κλάσμα αυτό αποτελεί κατώφλι για την κρυστάλλωση νερού κατά την ψύξη. Περαιτέρω αύξηση του επιπέδου υδάτωσης προκαλεί σταθεροποίηση της T_g , περίπου στους -80 °C. Η σταθεροποίηση αυτή μπορεί να αποδοθεί στο γεγονός ότι τα επιπλέον μόρια νερού που προστίθενται στο δοκίμιο δεν συνεισφέρουν πλέον στην υαλώδη μετάβαση, πιθανότατα γιατί αποτελούν πλέον πληθυσμούς κρυσταλλωμένου νερού.

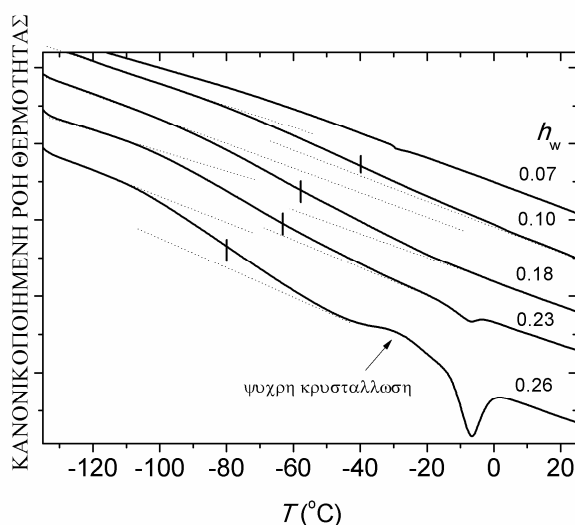
Η μεταβολή του βήματος θερμοχωρητικότητας της υαλώδους μετάβασης, ΔC_p , συναρτήσει του κλάσματος νερού στα δοκίμια, h_w , φαίνεται στο Σχήμα 4.5. Επιπλέον, το ίδιο μέγεθος, κανονικοποιημένο ως προς τη μάζα της ξηρής πρωτεΐνης, έχει προστεθεί στο διάγραμμα. Το ΔC_p αυξάνεται με την προσθήκη νερού έως ένα κρίσιμο κλάσμα υδάτωσης, περίπου ίσο με $h_w = 0.20$. Για ανώτερα επίπεδα υδάτωσης, όπου φαινόμενα ψυχρής κρυστάλλωσης και κρυστάλλωσης κατά την ψύξη λαμβάνουν χώρα στα

ΕΚΤΕΝΗΣ ΠΕΡΙΛΗΨΗ

δοκίμια, το ΔC_p μειώνεται ή μένει σταθερό. Η σταθεροποίηση παρατηρείται στην περίπτωση της κανονικοποιημένης τιμής ως προς την μάζα της πρωτεΐνης.



Σχήμα 4.2: Θερμογράμματα DSC κατά την a) ψύξη και b) θέρμανση με ρυθμό 10 °C/min για υδατωμένα δοκίμια BSA σε διάφορα κλάσματα υδάτωσης, h_w (g νερού/g υδατωμένης πρωτεΐνης). Η ροή θερμότητας είναι κανονικοποιημένη ως προς τη μάζα των δοκιμίων.



Σχήμα 4.3: Θερμογράμματα DSC κατά την θέρμανση με ρυθμό 10 °C/min, για υδατωμένα δοκίμια BSA, σε διάφορα κλάσματα υδάτωσης, h_w . Η θερμοκρασία ναλώδους μετάβασης, T_g , αναδεικνύεται στο διάγραμμα με κάθετα ευθύγραμμα τμήματα.

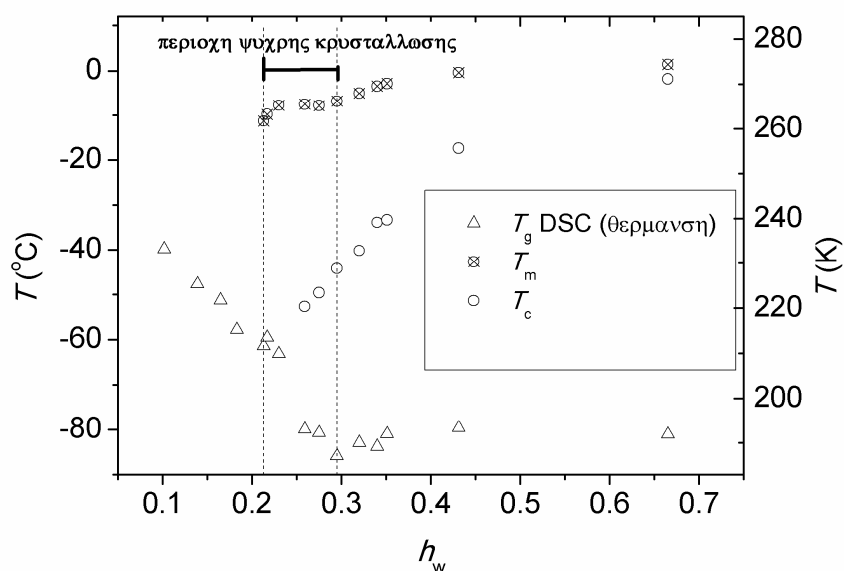
Περαιτέρω συσχέτιση των αποτελεσμάτων με τους διάφορους πληθυσμούς νερού στα δοκίμια μπορεί να επιτευχθεί, αφού ποσοτικοποιηθούν τα αποτελέσματα του

ΕΚΤΕΝΗΣ ΠΕΡΙΛΗΨΗ

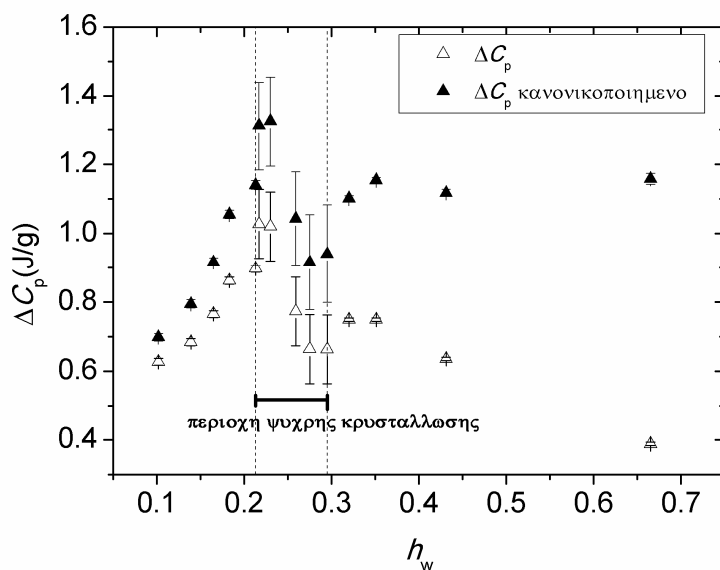
DSC. Συγκεκριμένα, από τις τιμές ενθαλπίας κρυστάλλωσης και τήξης, πολύ συχνά πραγματοποιείται ο υπολογισμός του κρυσταλλικού κλάσματος στα δοκίμια. Στην περίπτωση της κρυστάλλωσης νερού, το κλάσμα του κρυσταλλικού νερού στα δοκίμια υπολογίζεται με βάση την ενθαλπία τήξης και την αντίστοιχη ενθαλπία τήξης του εξαγωνικού πάγου (333.55J/g). Τα διάφορα ποσοτικά αποτελέσματα που προέκυψαν από τέτοιου τύπου υπολογισμούς καταγράφονται στον Πίνακα 4.1. Με βάση τα στοιχεία του Πίνακα 4.1 τα ποσοστά κρυσταλλωμένου, $h_{d,cw}$, και μη κρυσταλλωμένου, $h_{d,ucw}$, νερού στα δοκίμια, υπολογισμένα ως προς την ξηρή μάζα των δοκιμίων, παριστάνονται συναρτήσει του συνολικού, ως προς την ξηρή μάζα, ποσοστού νερού, h_d , στο Σχήμα 4.6. Το ποσοστό του μη κρυσταλλωμένου νερού αυξάνεται αρχικά, στη συνέχεια σταθεροποιείται στην περιοχή της ψυχρής κρυστάλλωσης και στην συνέχεια αυξάνεται πάλι για επιπλέον προσθήκη νερού. Συγκρίνοντας με τα αποτελέσματα για τον αριθμό μορίων νερού ανά μόριο πρωτεΐνης (βλ. Πίνακα 4.1) και έχοντας υπόψη τον αριθμό των υπολοίπων αμινοξέων του μορίου BSA, που είναι 607, μπορούμε να έχουμε μία εικόνα για την κάλυψη των θέσεων υδάτωσης από μόρια νερού, αν θεωρήσουμε όσο το δυνατόν ομοιόμορφη κατανομή των μορίων νερού. Δεδομένων των παραπάνω, η αύξηση του ποσοστού μη κρυσταλλωμένου νερού, για $h_d > 0.4$, όπου το πρώτο στρώμα υδάτωσης έχει ολοκληρωθεί και η κρυστάλλωση είναι πλέον παγιωμένη στα δοκίμια, υπονοεί ότι αναδιοργάνωση των μορίων νερού οδηγεί στο σχηματισμό νέου τύπου μη κρυσταλλωμένων δομών.

Πίνακας 4.1 Αποτελέσματα από τις μετρήσεις DSC, κλάσμα νερού h_w (ως προς τη συνολική μάζα) και ποσοστό νερού h_d , ενθαλπία τήξης ΔH_m , ποσοστά κρυσταλλωμένου ($h_{d,cw}$) και μη κρυσταλλωμένου νερού ($h_{d,ucw}$), κλάσματα κρυσταλλωμένου (X_{cw}) και μη κρυσταλλωμένου νερού (X_{ucw}), και αριθμός μορίων νερού ανά μόριο BSA συνολικών (n), κρυσταλλωμένων (n_{cw}) και μη κρυσταλλωμένων (n_{ucw})

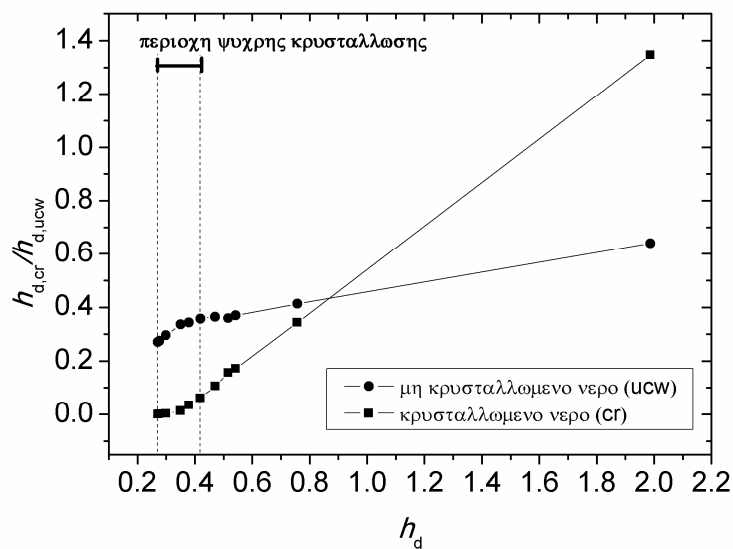
h_w	h_d	ΔH_m (J/gr)	$h_{d,cw}$	$h_{d,ucw}$	X_{cw}	X_{ucw}	n	n_{cw}	n_{ucw}
0.18	0.23	0	0	0.225	0	1	825	0	825
0.21	0.27	-0.17	0.001	0.270	0.002	0.998	993	2	991
0.22	0.28	-0.34	0.001	0.276	0.005	0.995	1015	5	1010
0.23	0.30	-0.66	0.002	0.297	0.009	0.991	1096	10	1086
0.26	0.35	-3.27	0.013	0.337	0.038	0.962	1283	49	1234
0.28	0.38	-8.49	0.045	0.334	0.092	0.908	1390	129	1261
0.30	0.42	-14.36	0.061	0.358	0.146	0.854	1536	224	1312
0.32	0.47	-24.23	0.106	0.365	0.226	0.774	1726	390	1336
0.34	0.52	-34.4	0.156	0.360	0.303	0.697	1891	573	1318
0.35	0.54	-37.34	0.173	0.369	0.318	0.682	1987	632	1355
0.43	0.76	-65.33	0.344	0.413	0.454	0.546	2775	1260	1515
0.67	1.99	-150.7	1.348	0.639	0.678	0.322	7283	4938	2345



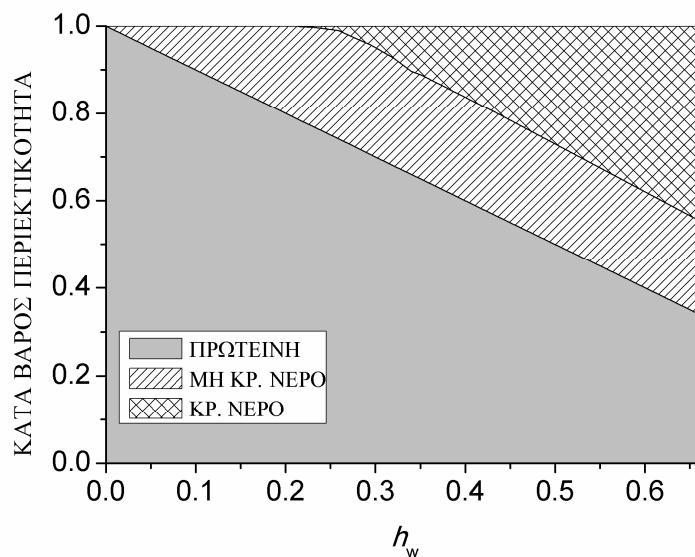
Σχήμα 4.4: Χαρακτηριστικές θερμοκρασίες υαλώδους μετάβασης, T_g , τήξης, T_m , και κρυστάλλωσης T_c , συναρτήσει του κλάσματος υδάτωσης, h_w , για υδατωμένα δοκίμια BSA.



Σχήμα 4.5: Μεταβολή της θερμοχωρητικότητας, ΔC_p , συναρτήσει του κλάσματος υδάτωσης, h_w , για υδατωμένα δοκίμια BSA. Οι κανονικοποιημένες τιμές ως προς τη μάζα της πρωτεΐνης έχουν προστεθεί στο διάγραμμα.



Σχήμα 4.6: Ποσοστό κρυσταλλωμένου, $h_{d,cr}$, και μη κρυσταλλωμένου, $h_{d,ucw}$, νερού, συναρτήσει του συνολικού ποσοστού υδάτωσης, h_d , υπολογισμένα ως προς την ξηρή μάζα του δοκιμίου (g νερού/g ξηρής πρωτεΐνης) για υδατωμένα δοκίμια BSA.



Σχήμα 4.7: Διάγραμμα περιεκτικότητας, όπου φαίνονται το κλάσμα της πρωτεΐνης, του κρυσταλλωμένου και μη κρυσταλλωμένου νερού συναρτήσει του συνολικού κλάσματος υδάτωσης για υδατωμένα δοκίμια BSA.

Από μια άλλη οπτική γωνία, αν εξετάσουμε το κλάσμα του νερού που δεν κρυσταλλώνεται ως προς τη συνολική μάζα του δοκιμίου, φαίνεται στο διάγραμμα σύστασης του Σχήματος 4.7, ότι αυτό μένει σταθερό και περίπου ίσο με το 20% της συνολικής μάζας του δοκιμίου, για κλάσματα υδάτωσης μεγαλύτερα από αυτά για τα οποία πραγματοποιείται κρυστάλλωση του νερού κατά την ψύξη.

Επομένως, η υαλώδης μετάβαση που ανιχνεύθηκε με τις μετρήσεις DSC, μπορεί πλέον να αποδοθεί στη συνεργασιακή κίνηση των μορίων νερού που δεν κρυσταλλώνονται με τμήματα της πρωτεΐνης.

4.3 Θερμορεύματα αποπόλωσης (TSDC)

Το κανονικοποιημένο ρεύμα αποπόλωσης συναρτήσει της θερμοκρασίας φαίνεται στο Σχήμα 4.8 για υδατωμένα δοκίμια BSA και υδατικά διαλύματα του τελευταίου, σε διάφορα κλάσματα νερού h_w .

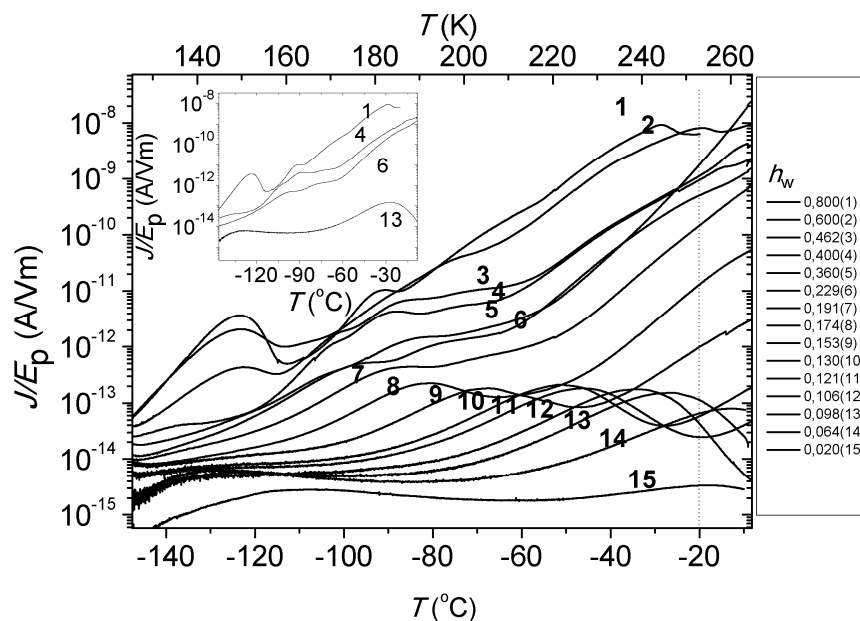
Ξεκινώντας από χαμηλά επίπεδα υδάτωσης και χαμηλές θερμοκρασίες, μία πλατιά κορυφή διηλεκτρικής αποκατάστασης ανιχνεύεται ήδη για το ξηρό δοκίμιο ($h_w=0.02$, εναπομένον νερό). Το μέγιστο της κορυφής τοποθετείται περίπου στους -110°C . Με την αύξηση του επιπέδου υδάτωσης η κορυφή μετακινείται σε χαμηλότερες θερμοκρασίες (πλαστικοποίηση). Με βάση προηγούμενες μελέτες σε υδατωμένες πρωτεΐνες και άλλα βιομόρια [19,20], ο μηχανισμός αποδίδεται στην αποκατάσταση μικρών πλευρικών πολικών ομάδων στην επιφάνεια της πρωτεΐνης, η κίνηση των οποίων ενεργοποιείται και ενισχύεται από τα αλληλεπιδρώντα μόρια νερού. Σε αρκετά υψηλότερα επίπεδα υδάτωσης, η συνεισφορά του μηχανισμού δεν είναι ανιχνεύσιμη, καθώς επικαλύπτεται από συνεισφορές μορίων νερού που είναι πλέον οργανωμένες σε άλλου τύπου δομές, όπως π.χ. σε κρυσταλλικές δομές. Με βάση αποτελέσματα TSDC από προηγούμενες μελέτες [21,22], η έντονη κορυφή που καταγράφεται για τα δοκίμια 1,2,3 στο Σχήμα 4.8, και είναι κεντραρισμένη περίπου στους -125°C , αποδίδεται σε συνεισφορές πάγου.

Στην περιοχή υψηλών θερμοκρασιών, για τα δοκίμια χαμηλού επιπέδου υδάτωσης, ένας μηχανισμός διηλεκτρικής αποκατάστασης εκδηλώνεται με μία κορυφή αποπόλωσης η οποία είναι κεντραρισμένη περίπου στους -30°C , για το δοκίμιο με $h_w=0.098$. Πρέπει να αναφερθεί σε αυτό το σημείο, ότι η κορυφή για τα δοκίμια 14 και 15 στους -20°C , δεν μπορεί να αξιολογηθεί ως μηχανισμός διηλεκτρικής αποκατάστασης, καθώς βρίσκεται στην θερμοκρασιακή περιοχή επιβολής της πόλωσης. Παρόλα αυτά, βάση μετρήσεων σε μεγαλύτερες θερμοκρασίες (που δεν παρουσιάζονται εδώ), εκτιμάται ότι ο εν λόγω μηχανισμός εμφανίζεται πάνω από ένα κρίσιμο επίπεδο υδάτωσης. Στο Σχήμα 4.8 φαίνεται ότι η εν λόγω κορυφή μετακινείται σε χαμηλότερες θερμοκρασίες με αύξηση του ποσοστού υδάτωσης και ενισχύεται σε ένταση. Για κλάσματα υδάτωσης μεγαλύτερα του $h_w=0.191$ (δοκίμιο 7 στο Σχήμα 4.8.), παρατηρείται μία διάσπαση της κορυφής σε δύο συνεισφορές ή μία επιπλέον συνεισφορά σε μεγαλύτερες θερμοκρασίες, με παράλληλη σταθεροποίηση των θερμοκρασιών μέγιστου. Όπως προκύπτει από τη σύγκριση με τις μετρήσεις DSC, οι μηχανισμοί διηλεκτρικής αποκατάστασης πιθανότατα σχετίζονται με την θερμική υαλώδη μετάβαση, καθώς έχουν παρόμοια χαρακτηριστικά. Προκειμένου να αξιολογηθεί

ΕΚΤΕΝΗΣ ΠΕΡΙΛΗΨΗ

καλύτερα η θερμοκρασιακή εξάρτηση των κορυφών, οι θερμοκρασίες μεγίστου για τους μηχανισμούς που συνδέονται με την υαλώδη μετάβαση και αυτές που αντιστοιχούν στη συνεισφορά του πάγου, καταγράφονται στο Σχήμα 4.9 σε συνάρτηση του κλάσματος υδάτωσης h_w .

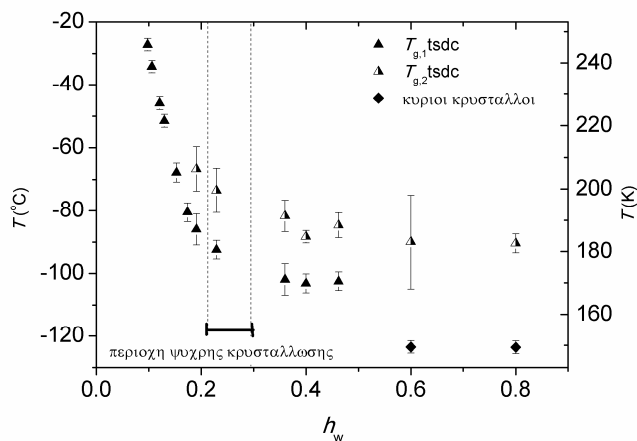
Η σύγκριση των αποτελεσμάτων DSC και TSDC, σύμφωνα με τα δεδομένα από τα Σχήματα 4.4 και 4.9, καταλήγει στο συμπέρασμα ότι η θερμοκρασία υαλώδους μετάβασης, T_g , έτσι όπως καταγράφεται από τη θερμομετρία, συμφωνεί περισσότερο με την T_{g2} , δηλαδή με την θερμοκρασία μεγίστου που εκδηλώνεται σε μεγαλύτερες θερμοκρασίες στο Σχήμα 4.8. Η διακριτική ικανότητα της τεχνικής TSDC καθιστά εφικτή την καταγραφή και ενός δεύτερου μηχανισμού χαμηλότερης έντασης.



Σχήμα 4.8: Κανονικοποιημένα θερμογράμματα TSDC (πυκνότητα ρεύματος αποπόλωσης προς ηλεκτρικό πεδίο πόλωσης, J/E_p), συναρτήσει της θερμοκρασίας για τα υδατικά διαλύματα BSA (δοκίμια 1-4) και τα υδατωμένα στερεά δοκίμια (δοκίμια 5-15) σε διάφορα κλάσματα υδάτωσης, h_w . Η κάθετη διακεκομμένη ευθεία δηλώνει την θερμοκρασία επιβολής της πόλωσης. Το ένθετο δείχνει τα θερμογράμματα 1,4,6,13, για λόγους ευκρίνειας.

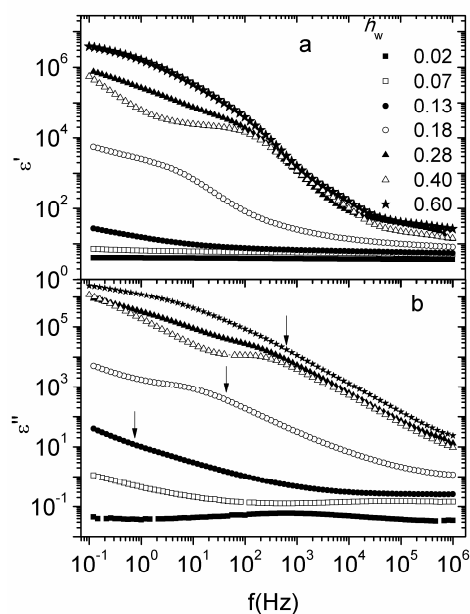
4.4 Διηλεκτρική φασματοσκοπία εναλλασσομένου πεδίου (DRS)

Αντίστοιχοι μηχανισμοί διηλεκτρικής αποκατάστασης με αυτούς που ανιχνεύθηκαν με την τεχνική TSDC μελετήθηκαν για το υδατωμένο σύστημα BSA/νερού και με την τεχνική DRS.

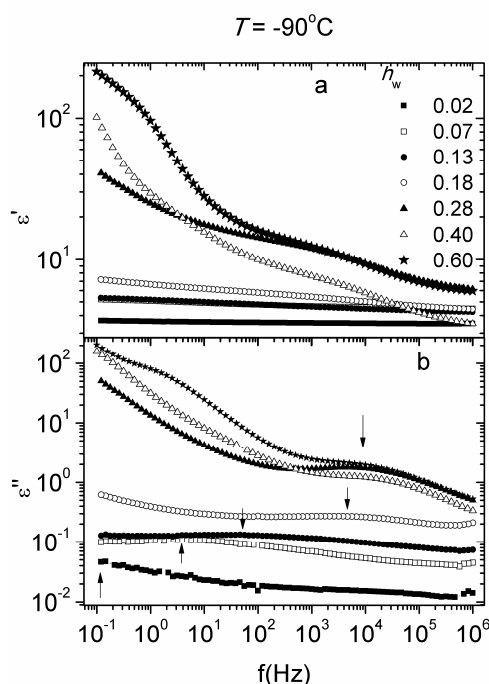


Σχήμα 4.9: Χαρακτηριστικές θερμοκρασίες που υπολογίστηκαν με τις τεχνική TSDC για τις θερμοκρασίες υαλώδους μετάβασης, $T_{g,1}$, $T_{g,2}$ και τη θερμοκρασία μεγίστου της κορυφής αποπόλωσης που αντιστοιχεί στον μηχανισμό αποκατάστασης των κυρίων κρυστάλλων νερού στα δοκίμια (πάγος). Οι κάθετες ευθείες οριοθετούν την περιοχή ψυχρής κρυστάλλωσης.

$T = -15^{\circ}\text{C}$



Σχήμα 4.10: **a)** Πραγματικό, ϵ' , και **b)** φανταστικό, ϵ'' , μέρος της διηλεκτρικής συνάρτησης συναρτήσει της συχνότητας, f , σε θερμοκρασία $T = -15^{\circ}\text{C}$ για υδατωμένα δοκίμια BSA σε διάφορα κλάσματα υδάτωσης h_w . Τα βέλη στο (b) καταδεικνύουν την εκτιμώμενη κορυφή μεγίστου για τον μηχανισμό διηλεκτρικής αποκατάστασης α .



Σχήμα 4.11: **a)** Πραγματικό, ϵ' , και **b)** φανταστικό, ϵ'' (απώλειες), μέρος της διηλεκτρικής συνάρτησης συναρτήσει της συχνότητας, f , σε θερμοκρασία $T=-90^{\circ}\text{C}$, για υδατωμένα δοκίμια BSA σε διάφορα κλάσματα υδάτωσης h_w . Τα βέλη στο (b) καταδεικνύουν την εκτιμώμενη κορυφή μεγίστου.

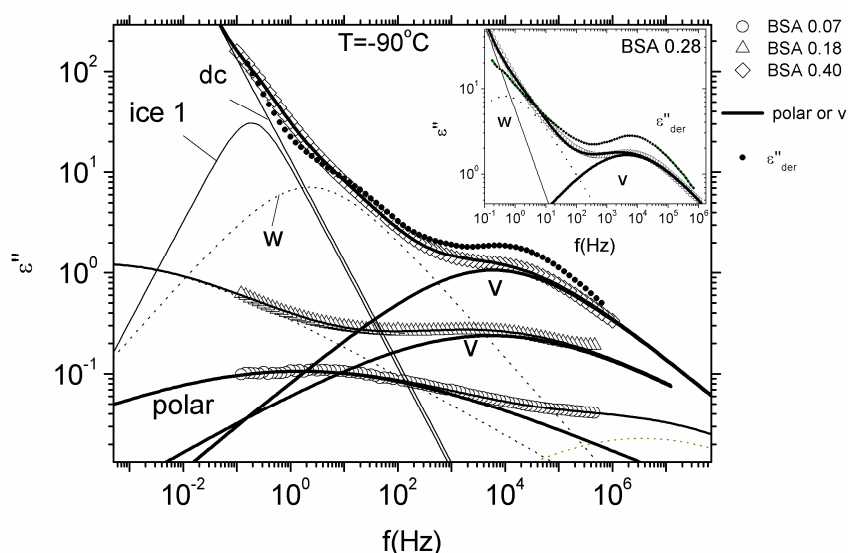
Στο Σχήμα 4.10a και 4.10b φαίνονται τα πειραματικά δεδομένα του πραγματικού και φανταστικού μέρους της διηλεκτρικής συνάρτησης, αντίστοιχα, σε συνάρτηση της συχνότητας, για υδατωμένα δοκίμια BSA σε διάφορα επίπεδα υδάτωσης h_w , σε θερμοκρασία $T=-15^{\circ}\text{C}$. Στην συγκεκριμένη θερμοκρασία βρίσκεται εντός του πειραματικού παραθύρου ο κύριος μηχανισμός διηλεκτρικής αποκατάστασης, ο οποίος αποδίδεται στον α μηχανισμό που συσχετίζεται με τη θερμική υαλώδη μετάβαση. Λόγω της περιοχής συχνοτήτων που εξετάζει η τεχνική DRS, η οποία περιλαμβάνει συχνότητες υψηλότερες από την αντίστοιχη της τεχνικής TSDC, ενδείκνυται ανάλυση των φασμάτων με βάση πρότυπες συναρτήσεις, προκειμένου για καλύτερο διαχωρισμό των διαφόρων συνεισφορών. Παραδείγματα της ανάλυσης στην περιοχή του α μηχανισμού ακολουθούν στη συνέχεια.

Στο Σχήμα 4.11a και 4.11b φαίνονται τα πειραματικά δεδομένα του πραγματικού και φανταστικού μέρους της διηλεκτρικής συνάρτησης, αντίστοιχα, σε συνάρτηση της συχνότητας, για υδατωμένα δοκίμια BSA σε διάφορα επίπεδα υδάτωσης h_w , σε θερμοκρασία $T=-90^{\circ}\text{C}$. Στην συγκεκριμένη θερμοκρασία βρίσκεται εντός του πειραματικού παραθύρου ο κύριος μηχανισμός διηλεκτρικής αποκατάστασης, ο οποίος αποδίδεται στην κίνηση πλευρικών πολικών ομάδων στην επιφάνεια της πρωτεΐνης, ο οποίος περιέχει συνεισφορές από μη κρυσταλλωμένα μόρια νερού στο πρώτο

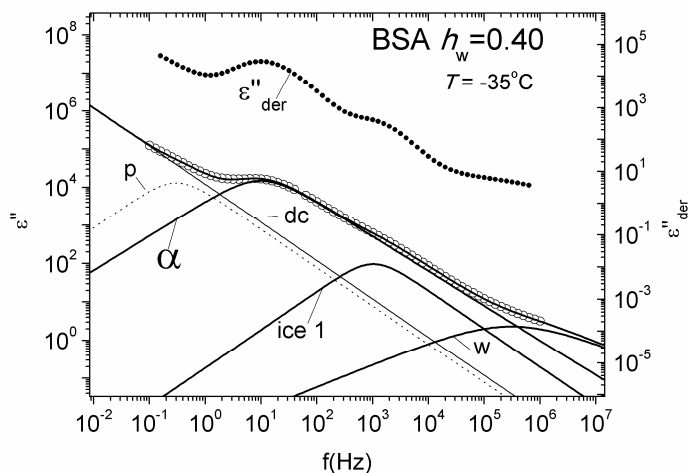
ΕΚΤΕΝΗΣ ΠΕΡΙΛΗΨΗ

επιφανειακό στρώμα υδάτωσης. Σε υψηλά επίπεδα υδάτωσης η θέση και η ένταση της κορυφής απωλειών σταθεροποιείται στο Σχήμα 4.11b.

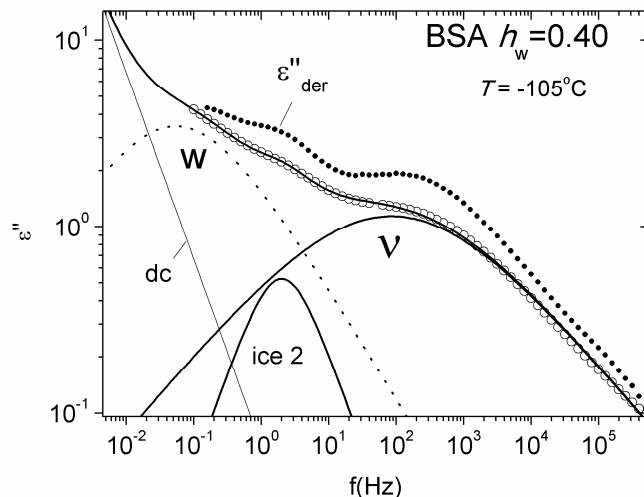
Περεταίρω διερεύνηση των πειραματικών αποτελεσμάτων ακολουθεί μετά την ανάλυση των κορυφών με βάση πρότυπες συναρτήσεις. Συγκεκριμένα, στα πειραματικά σημεία των διηλεκτρικών απωλειών προσαρμόστηκε άθροισμα συναρτήσεων Cole-Cole και ενός όρου αγωγιμότητας (βλ. Ενότητα 3, παράγραφος 3.2). Παραδείγματα των προσαρμογών φαίνονται σε διάφορες θερμοκρασίες στα Σχήματα 4.12, 4.13, 4.14. Στο Σχήμα 4.12 φαίνεται για διάφορα δοκίμια η εξέλιξη της κορυφής του διηλεκτρικού μηχανισμού που αντιστοιχεί στην κίνηση πλευρικών πολικών ομάδων (polar), με το επίπεδο υδάτωσης. Σε υψηλά επίπεδα υδάτωσης η σταθεροποιημένη κορυφή ως προς τη θέση ονομάζεται πλέον 'ν' μηχανισμός, ο οποίος σύμφωνα με τη βιβλιογραφία είναι ο κύριος δευτερεύων μηχανισμός διηλεκτρικής αποκατάστασης που εντοπίζεται σε υδατωμένα συστήματα και αποδίδεται σε δυναμική μη κρυσταλλωμένων μορίων νερού. Στο Σχήμα 4.13 φαίνεται η συνεισφορά του α μηχανισμού, καθώς και διαφόρων άλλων συνεισφορών. Σε γενικές γραμμές ανιχνεύτηκαν, εκτός από τους μηχανισμούς α και πολικών ομάδων- ν , ο μηχανισμός w , ο οποίος αντιστοιχεί στη δεύτερη συνιστώσα σε χαμηλότερες θερμοκρασίες του α μηχανισμού (βλ. TSDC), ένας μηχανισμός p σε υψηλές θερμοκρασίες που οφείλεται πιθανότατα σε πόλωση φορτίων χώρου και δύο μηχανισμοί που αντιστοιχούν σε κρυσταλλικές δομές, ice1 και ice2, στην περιοχή υψηλών και χαμηλών θερμοκρασιών, αντίστοιχα. Σε αυτή την ενότητα θα επικεντρωθούμε περισσότερο στον σχολιασμό του α μηχανισμού και του μηχανισμού πλευρικών ομάδων που ενισχύεται από μη κρυσταλλωμένα μόρια νερού.



Σχήμα 4.12: Διηλεκτρικές απώλειες, ϵ'' , συναρτήσει της συχνότητας, f , σε θερμοκρασία $T=-90^\circ\text{C}$ για υδατωμένα δοκίμια BSA σε κλάσματα υδάτωσης 0.07, 0.18, 0.28(ένθετο) και 0.40. Οι συμπαγείς κύκλοι αντιστοιχούν στις διηλεκτρικές απώλειες όπως υπολογίστηκαν με την μέθοδο της πρώτης παραγώγου, ϵ''_{der} [23]. Οι συνεχείς γραμμές αποτελούν τις συνεισφορές απωλειών στο συνολικό φάσμα όπως προέκυψαν από ανάλυση με πρότυπες συναρτήσεις. Η συμπαγής συνεχής γραμμή που διαπερνά τα πειραματικά σημεία είναι το άθροισμα των συνεισφορών.



Σχήμα 4.13: Διηλεκτρικές απώλειες, ϵ'' , συναρτήσει της συχνότητας, f , σε θερμοκρασία $T=-35^{\circ}\text{C}$ για ένα υδατωμένο δοκίμιο BSA με $h_w=0.40$. Οι συμπαγείς κύκλοι αντιστοιχούν στις διηλεκτρικές απώλειες όπως υπολογίστηκαν με την μέθοδο της πρώτης παραγώγου, ϵ''_{der} . Οι συνεχείς γραμμές αποτελούν τις συνεισφορές απωλειών στο συνολικό φάσμα όπως προέκυψαν από ανάλυση με πρότυπες συναρτήσεις. Η συμπαγής συνεχής γραμμή που διαπερνά τα πειραματικά σημεία είναι το άθροισμα των συνεισφορών.



Σχήμα 4.14: Διηλεκτρικές απώλειες, ϵ'' , συναρτήσει της συχνότητας, f , σε θερμοκρασία $T=-105^{\circ}\text{C}$ για ένα υδατωμένο δοκίμιο BSA με $h_w=0.40$. Οι συμπαγείς κύκλοι αντιστοιχούν στις διηλεκτρικές απώλειες όπως υπολογίστηκαν με την μέθοδο της πρώτης παραγώγου, ϵ''_{der} . Οι συνεχείς γραμμές αποτελούν τις συνεισφορές απωλειών στο συνολικό φάσμα όπως προέκυψαν από ανάλυση με πρότυπες συναρτήσεις. Η συμπαγής συνεχής γραμμή που διαπερνά τα πειραματικά σημεία είναι το άθροισμα των συνεισφορών.

Ο α μηχανισμός

Στο Σχήμα 4.15a φαίνεται η θερμοκρασιακή εξάρτηση του χρόνου αποκατάστασης για τον α μηχανισμό. Αυτός ανιχνεύεται για επίπεδα υδάτωσης μεγαλύτερα ή ίσα του $h_w=0.07$, όπως στην περίπτωση των μετρήσεων TSDC. Η πλαστικοποίηση του ίχνους είναι εμφανής, καθώς και η σταθεροποίηση του τελευταίου για υψηλά επίπεδα υδάτωσης. Η προέκταση του σταθεροποιημένου ίχνους είναι σε καλή συμφωνία με την θερμοκρασία υαλώδους μετάβασης από το DSC. Επίσης, το ίχνος είναι συγκρίσιμο με το ίχνος του α μηχανισμού για ένα υδατικό διάλυμα BSA με $h_w=0.80$, από τη βιβλιογραφία [24].

Στο Σχήμα 4.15b φαίνεται η θερμοκρασιακή εξάρτηση της διηλεκτρικής ισχύος του α μηχανισμού. Η ένταση σε γενικές γραμμές ενισχύεται με την προσθήκη νερού. Η δυναμική του μηχανισμού φαίνεται να αυξομειώνεται επιδεικνύοντας ή όχι χαρακτηριστικά συνεργασιμότητας. Τέλος, η ένταση είναι υπερβολικά υψηλή σε υψηλά επίπεδα υδάτωσης, πιθανότατα ως αποτέλεσμα της συνεισφοράς ιόντων στις διηλεκτρικές απώλειες.

Η περίεργη δυναμική συμπεριφορά του μηχανισμού και το γεγονός ότι αυτός απαιτεί ένα κατώφλι επιπέδου υδάτωσης, προκειμένου να εμφανιστεί, μας οδηγεί στο συμπέρασμα ότι το φαινόμενο περιέχει συνεισφορές τόσο από την πρωτεΐνη, όσο και από το ποσοστό του μη κρυσταλλωμένου νερού στην επιφάνεια της πρωτεΐνης.

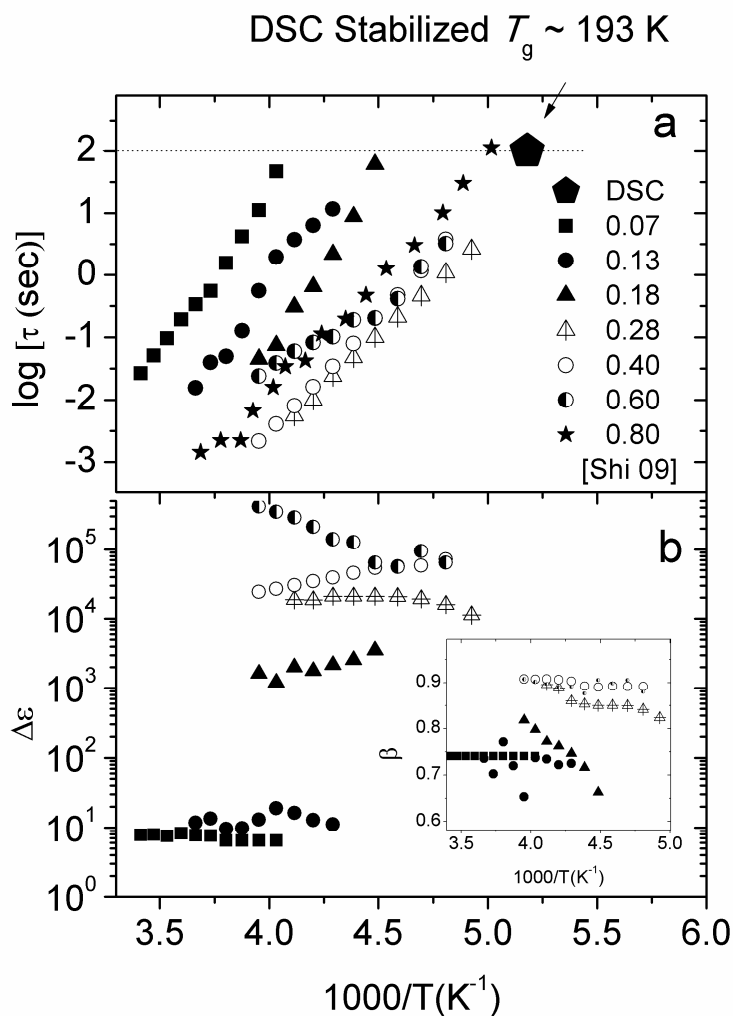
Ο δευτερεύων μηχανισμός πολικών ομάδων και η σχέση του με το ν μηχανισμό

Ο δευτερεύων μηχανισμός που ήδη αποδόθηκε στην κίνηση πλευρικών ομάδων στην επιφάνεια της πρωτεΐνης, η οποία ενισχύεται από την αλληλεπίδραση με μόρια νερού, θα διερευνηθεί ως προς τα δυναμικά του χαρακτηριστικά. Η θερμοκρασιακή εξάρτηση του χρόνου αποκατάστασης καταγράφεται στο Σχήμα 4.16. Η αντίστοιχη θερμοκρασιακή εξάρτηση της διηλεκτρικής ισχύος φαίνεται στο Σχήμα 4.17.

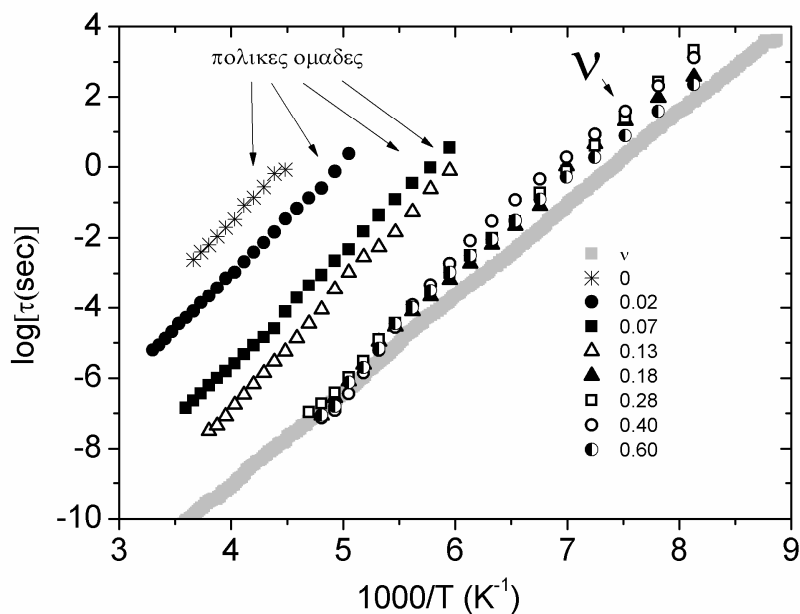
Η αρχική εικόνα είναι ότι το ίχνος του μηχανισμού των πολικών ομάδων μετακινείται σε χαμηλότερες θερμοκρασίες με την προσθήκη μορίων νερού (πλαστικοποίηση) και εν συνεχεία σταθεροποιείται για επίπεδα υδάτωσης $h_w \geq 0.18$. Η θέση του σταθεροποιημένου ίχνους είναι συγκρίσιμη με το κατώτατο όριο συχνοτήτων για τη δυναμική του νερού, που συμβολίζεται με την συμπαγή γκρι γραμμή στο Σχήμα 4.16 [25]. Πλέον ο μηχανισμός ονομάζεται ν . Μια προσεκτικότερη παρατήρηση των σημείων οδηγεί στο συμπέρασμα ότι το ίχνος του ν μηχανισμού παρουσιάζει μία μετάβαση (μεταβολή, σπάσιμο), όπου μεταβάλλεται η ενέργεια ενεργοποίησης (κλίση), περίπου σε θερμοκρασία $1000/T=6$. Η παράμετρος σχήματος $\beta(T)$ της έκφρασης Cole-Cole, για τους εν λόγω μηχανισμούς καταγράφεται στον Πίνακα 5.2. Το ίχνος του μηχανισμού πολικών ομάδων και του ν μηχανισμού για θερμοκρασίες μικρότερες της μεταβολής, προσαρμόστηκε σε εξίσωση Arrhenius (Εξ. 3.6). Οι τιμές της ενέργειας ενεργοποίησης και του προεκθετικού παράγοντα παρουσιάζονται στον Πίνακα 5.3. Όπως φαίνεται στον Πίνακα 5.3, η ενέργεια ενεργοποίησης του μηχανισμού σε υψηλά επίπεδα υδάτωσης είναι περίπου ίση με $E_{act}=0.55$ eV, δηλαδή ίση με την ενέργεια που απαιτείται για το σπάσιμο 2 δεσμών υδρογόνου, σύμφωνα με τιμές της βιβλιογραφίας

ΕΚΤΕΝΗΣ ΠΕΡΙΛΗΨΗ

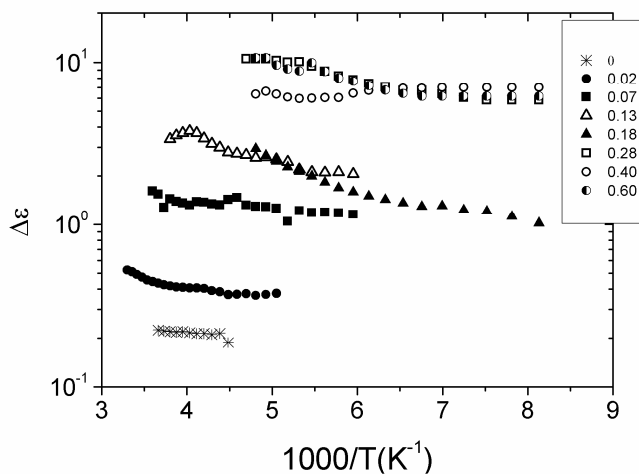
για την αντίστοιχη ενέργεια ενεργοποίησης του κύριου μηχανισμού διηλεκτρικής αποκατάστασης σε νερό υδάτωσης πρωτεϊνών και άλλων υδατωμένων συστημάτων.



Σχήμα 4.15: a) Θερμοκρασιακή εξάρτηση του λογαρίθμου του χρόνου αποκατάστασης $\log(\tau)$ για τον α μηχανισμό διηλεκτρικής αποκατάστασης για υδατωμένα δοκίμια BSA σε διάφορα κλάσματα υδάτωσης h_w . Τα αστέρια αντιστοιχούν στον α μηχανισμό για ένα υδατικό διάλυμα BSA με $h_w=0.80$ [24]. **b)** Θερμοκρασιακή εξάρτηση της διηλεκτρικής ισχύος, $\Delta \epsilon$, για τον α μηχανισμό διηλεκτρικής αποκατάστασης για υδατωμένα δοκίμια BSA σε διάφορα κλάσματα υδάτωσης h_w . Το ένθετο περιέχει τον συντελεστή σχήματος, $\beta(T)$, της συνάρτησης Cole-Cole του α μηχανισμού.



Σχήμα 4.16: Θερμοκρασιακή εξάρτηση του λογαρίθμου του χρόνου αποκατάστασης $\log(\tau)$ για τον μηχανισμό διηλεκτρικής αποκατάστασης πολικών ομάδων (polar groups) και για τον ν μηχανισμό για υδατωμένα δοκίμια BSA σε διάφορα κλάσματα υδάτωσης h_w .



Σχήμα 4.17: Θερμοκρασιακή εξάρτηση της διηλεκτρικής ισχύος, $\Delta\epsilon$, για τον μηχανισμό διηλεκτρικής αποκατάστασης πολικών ομάδων (polar groups) και για τον ν μηχανισμό για υδατωμένα δοκίμια BSA σε διάφορα κλάσματα υδάτωσης h_w .

ΕΚΤΕΝΗΣ ΠΕΡΙΛΗΨΗ

Πίνακας 4.2 Συντελεστής σχήματος, $\beta(T)$, της συνάρτησης Cole-Cole για τον μηχανισμό πολικών ομάδων ($h_w=0, 0.02, 0.07, 0.13$) και για το ν μηχανισμό ($h_w=0.18, 0.28, 0.40, 0.60$) για υδατωμένα δοκίμια BSA.

h_w	0	0.02	0.07	0.13	0.18	0.28	0.40	0.60
$\beta(T)$	0.38	0.32	0.23	0.15	0.30	0.43	0.43	0.48

Πίνακας 4.3 Ενέργεια ενεργοποίησης, E_{act} , και προεκθετικός παράγοντας $\log f_0$ για τον μηχανισμό πολικών ομάδων ($h_w=0, 0.02, 0.07, 0.13$) και για το ν μηχανισμό ($h_w=0.18, 0.28, 0.40, 0.60$), για υδατωμένα δοκίμια BSA.

h_w	E_{act} (eV)	$\log f_0$
0	0.67±0.01	14.14±0.20
0.02	0.62±0.01	14.67±0.12
0.07	0.63±0.01	17.60±0.09
0.13	0.70±0.01	20.08±0.15
0.18	0.55±0.02	18.83±0.75
0.28	0.59±0.01	19.92±0.32
0.40	0.50±0.01	16.95±0.19
0.60	0.49±0.01	16.70±0.16

Συμπεράσματα-BSA

Η δυναμική και οι μεταπτώσεις φάσης στο σύστημα BSA-νερό, διερευνήθηκε με τις τεχνικές ESI, DSC, TSDC και DRS, σε ευρεία περιοχή επιπέδων υδάτωσης.

Η θερμική υαλώδης μετάβαση ανιχνεύτηκε με την τεχνική DSC για επίπεδα υδάτωσης μεγαλύτερα ενός κατωφλίου. Αντίστοιχη εκδήλωση ενός α μηχανισμού διηλεκτρικής αποκατάστασης παρατηρήθηκε μέσω των διηλεκτρικών τεχνικών. Γενικό συμπέρασμα είναι ότι το φαινόμενο περιέχει συνεισφορές τόσο από την πρωτεΐνη, όσο και από το ποσοστό του μη κρυσταλλωμένου νερού στην επιφάνεια της πρωτεΐνης. Επίσης φαίνεται ότι οι διαφορετικές τεχνικές ανιχνεύουν διαφορετικές συνιστώσες του φαινομένου.

Επιπλέον, ο κύριος δευτερεύων μηχανισμός διηλεκτρικής αποκατάστασης στη σφαίρα υδάτωσης της πρωτεΐνης μελετήθηκε διεξοδικά ως προς την δυναμική του. Τα πειραματικά αποτελέσματα κατέδειξαν ότι το μη κρυσταλλωμένο νερό στην πρώτη σφαίρα υδάτωσης αλληλεπιδρά με μικρές πλευρικές πολικές ομάδες στην επιφάνεια της πρωτεΐνης και ενισχύει την κίνησή τους. Για επίπεδα υδάτωσης μεγαλύτερα του ποσοστού μορίων νερού σε πρωταρχικές θέσεις υδάτωσης, η βαθμιαία οργάνωση των μορίων νερού σε συσσωματώματα οδηγεί στη βαθμιαία κάλυψη της επιφάνειας και πλέον κυριαρχεί η δυναμική του δευτερεύοντα μηχανισμού του υπέρψυκτου νερού σε ένα επιφανειακό στρώμα στην επιφάνεια της πρωτεΐνης.

5 η ΕΝΟΤΗΤΑ

ΧΑΡΑΚΤΗΡΙΣΤΙΚΑ ΑΠΟΤΕΛΕΣΜΑΤΑ ΣΕ ΔΙΑΦΟΡΑ ΥΔΑΤΩΜΕΝΑ ΣΥΣΤΗΜΑΤΑ

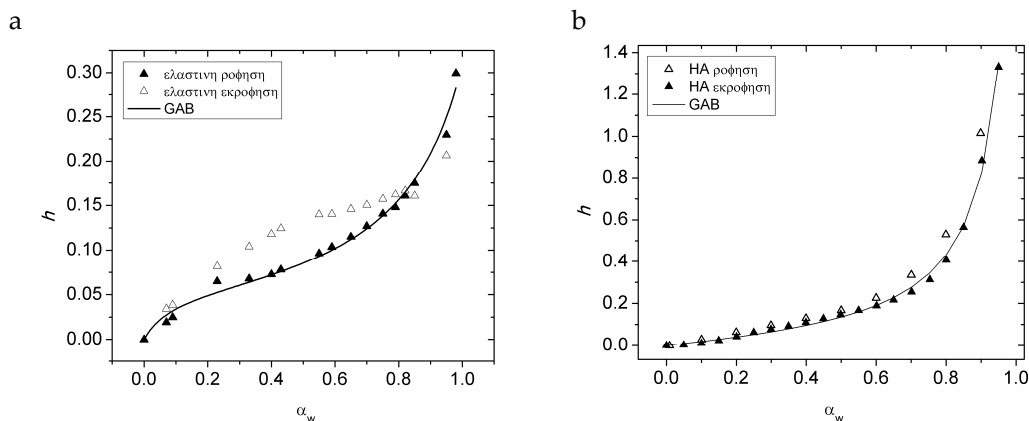
Στα πλαίσια της παρούσας διδακτορικής διατριβής πραγματοποιήθηκε σειρά πειραματικών μετρήσεων σε διάφορα υδατωμένα συστήματα, προκειμένου να πραγματοποιηθεί η συγκριτική μελέτη αυτών. Εκτός από το σύστημα BSA-νερό (τα κύρια αποτελέσματα από το οποίο παρουσιάστηκαν και σχολιάστηκαν στην 4η Ενότητα της παρούσας περίληψης) μελετήθηκαν επίσης υδατωμένες ινώδεις πρωτεΐνες, π.χ. η ινώδης ελαστίνη, και πολυσακχαρίτες όπως π.χ. το υδροπήκτωμα υαλουρικού οξέος (HA). Κατά αυτόν τον τρόπο, εισάγεται και η παράμετρος των δομικών διαφοροποιήσεων, εκτός από το ποσοστό υδάτωσης, στην αξιολόγηση των πειραματικών αποτελεσμάτων. Στην παρούσα ενότητα θα παρουσιαστούν κάποια χαρακτηριστικά αποτελέσματα και ο σχολιασμός θα εστιαστεί στη δυναμική του μη κρυσταλλωμένου νερού στο πρώτο επίπεδο υδάτωσης.

5.1 Ισόθερμες ρόφησης νερού σε ισορροπία (ESI)

Πραγματοποιήθηκαν μετρήσεις ισόθερμης ρόφησης/εκρόφησης σε θερμοκρασία δωματίου, $T=25$ °C, για ένα δοκίμιο ελαστίνης και ένα δοκίμιο υδροπηκτώματος υαλουρικού οξέος (HA). Οι διαδικασίες ρόφησης και εκρόφησης έλαβαν χώρα διαδοχικά.

Τα πειραματικά σημεία, ποσοστό νερού h (ως προς την ξηρή μάζα, g νερού/ g ξηρού δοκιμίου) συναρτήσει της ενεργότητας a_w ($a_w=rh$, σχετική υγρασία), για τις διαδικασίες ρόφησης (sorption) και εκρόφησης (desorption) φαίνονται στο Σχήμα 5.1a και 5.1b, για την ελαστίνη και το HA, αντίστοιχα.

Όπως φαίνεται στο Σχήμα 5.1 a και 5.1 b, η μορφή των ισόθερμων καμπυλών διαφέρει για τα δύο δοκίμια. Ξεκινώντας από τα πειραματικά σημεία που αντιστοιχούν στη διαδικασία ρόφησης, παρατηρούμε σημαντική διαφοροποίηση στο μέγιστο ποσοστό υδάτωσης σε υψηλές τιμές σχετικής υγρασίας, και, συγκεκριμένα, $h\sim 0.30$, $h\sim 1.4$ για την ελαστίνη και το HA, αντίστοιχα. Το γεγονός αυτό αντανακλά τον υδρόφοβο και υδρόφιλο χαρακτήρα της ελαστίνης και του HA, αντίστοιχα. Επιπλέον, όσον αφορά τα σημεία που αντιστοιχούν στη διαδικασία εκρόφησης, παρατηρούνται έντονα φαινόμενα υστέρησης (μεγαλύτερες τιμές h κατά την εκρόφηση για αντίστοιχες τιμές a_w με αυτές της ρόφησης) στην περίπτωση της ελαστίνης, τα οποία απουσιάζουν στην περίπτωση του HA. Τα φαινόμενα υστέρησης είναι δυνατό να αποδοθούν σε δομικές διαφοροποιήσεις του δοκιμίου κατά την ρόφηση.



Σχήμα 5.1 Ισόθερμες καμπύλες ρόφησης/εκρόφησης για **a)** την ελαστίνη **β)** το HA. Η συμπαγής γραμμή που διαπερνά τα πειραματικά σημεία αποτελεί προσαρμογή της εξίσωσης GAB στα πειραματικά σημεία.

Η εξίσωση GAB (Εξ. (3.1)) προσαρμόστηκε στα πειραματικά σημεία ρόφησης. Η προσαρμογή των σημείων είναι ικανοποιητική. Επιπλέον, η παράμετρος h_m της εξίσωσης GAB, η οποία αντιστοιχεί στο ποσοστό μορίων νερού που απορροφώνται από το δοκίμιο και προσροφώνται σε πρωταρχικές θέσεις υδάτωσης, υπολογίστηκε για την ελαστίνη ως $h_m=0.067$, που αντιστοιχεί σε κλάσμα νερού $h_w=0.063$ και για το HA ως $h_m=0.114$, που αντιστοιχεί σε κλάσμα νερού $h_w=0.102$.

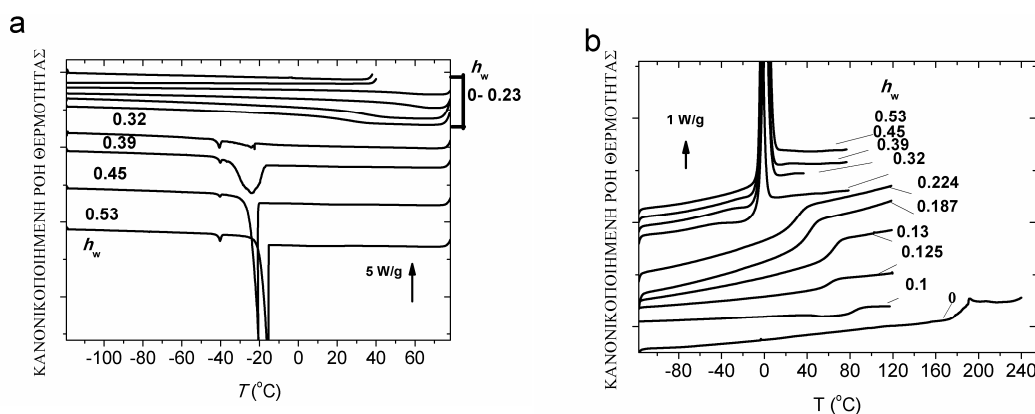
5.2 Διαφορική θερμιδομετρία σάρωσης (DSC)

Στο Σχήμα 5.2 a και 5.2 b φαίνονται θερμογράμματα DSC που καταγράφηκαν κατά την ψύξη και θέρμανση, αντίστοιχα, για υδατωμένα δοκίμια ελαστίνης με ρυθμό ψύξης/θέρμανσης $10^\circ\text{C}/\text{min}$. Όπως διαπιστώθηκε από τις μετρήσεις ισόθερμης υδάτωσης, το μέγιστο κλάσμα νερού που δύνανται να απορροφήσουν τα δοκίμια ελαστίνης μέσω ρόφησης από ατμούς, είναι $h_w \sim 0.23$ (που αντιστοιχεί σε $h \sim 0.30$, βλέπε Σχήμα 5.1 a). Η υδάτωση των δοκιμίων που παρουσιάζουν μεγαλύτερα κλάσματα υδάτωσης ($h_w > 0.23$ στο Σχήμα 5.2) έχει επιτευχθεί μέσω εμβάπτισης σε απιονισμένο νερό και ακόλουθη αποκατάσταση της ομοιογενούς υδάτωσης εντός ερμητικά σφραγισμένων δοχείων για δεδομένα χρονικά διαστήματα. Κατά την ψύξη καταγράφεται εμφανώς η κρυστάλλωση του νερού στα δοκίμια, για κλάσμα υδάτωσης $h_w \geq 0.32$. Καταγράφηκαν δύο διακριτές κορυφές κρυστάλλωσης, με θερμοκρασίες κρυστάλλωσης, $T_c \sim -40$ και -20°C . Η θέση και η ένταση της κορυφής χαμηλότερων θερμοκρασιών δεν μεταβάλλονται ιδιαίτερα με την αύξηση του κλάσματος υδάτωσης. Το γεγονός αυτό αποτελεί ένδειξη ότι αυτή οφείλεται στην κρυστάλλωση μορίων νερού που βρίσκονται υπό περιορισμό σε περιοχές στο εσωτερικό του πολύπλοκου δικτύου της πρωτεΐνης. Η ένταση της δεύτερης κορυφής σε υψηλότερες θερμοκρασίες ενισχύεται με την αύξηση του κλάσματος υδάτωσης, ενώ η θερμοκρασία μέγιστου αυτής αυξάνεται αμυδρά. Η εν λόγω κορυφή αποδίδεται πιθανότατα στην κρυστάλλωση μορίων νερού

ΕΚΤΕΝΗΣ ΠΕΡΙΛΗΨΗ

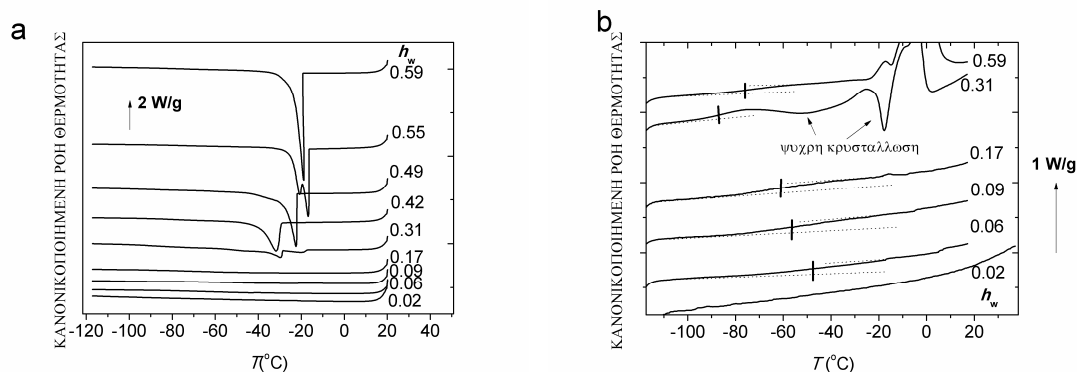
που παρουσιάζουν χαμηλότερο βαθμό συνδεσιμότητας με την πρωτεΐνη, σε σχέση με αυτά που δεν κρυσταλλώνονται σε χαμηλότερα επίπεδα υδάτωσης. Κατά την θέρμανση η τήξη καταγράφεται εμφανώς για $h_w \geq 0.32$, μέσω μίας κορυφής η οποία παρουσιάζει θερμοκρασία τήξης, $T_c \sim 0^\circ\text{C}$.

Κατά τη θέρμανση των δοκιμίων, είναι δυνατή η καταγραφή της υαλώδους μετάβασης του συστήματος ελαστίνη-νερό, ως βήμα θερμοχωρητικότητας, στο Σχήμα 5.2 b. Η θερμοκρασία υαλώδους μετάβασης, T_g , μειώνεται (η υαλώδης μετάβαση πλαστικοποιείται) με την αύξηση του επιπέδου υδάτωσης, από $T_g \sim 190^\circ\text{C}$ για την ξηρή ελαστίνη, έως $T_g \sim 30^\circ\text{C}$ για $h_w \sim 0.23$. Σε μεγαλύτερα ποσοστά υδάτωσης δεν είναι δυνατός ο υπολογισμός της T_g , καθώς το βήμα θερμοχωρητικότητας επικαλύπτεται από την κορυφή τήξης. Η ισχυρή πλαστικοποίηση της υαλώδους μετάβασης πιθανότατα οφείλεται στην διευκόλυνση της κίνησης λόγω αλληλεπίδρασης με τα μόρια νερού.



Σχήμα 5.2. Θερμογράμματα DSC κατά την a) ψύξη και b) θέρμανση με ρυθμό $10^\circ\text{C}/\text{min}$ για υδατωμένα δοκίμια ελαστίνης σε διάφορα κλάσματα υδάτωσης, h_w (g νερού/g υδατωμένης πρωτεΐνης). Η ροή θερμότητας είναι κανονικοποιημένη ως προς τη μάζα των δοκιμίων.

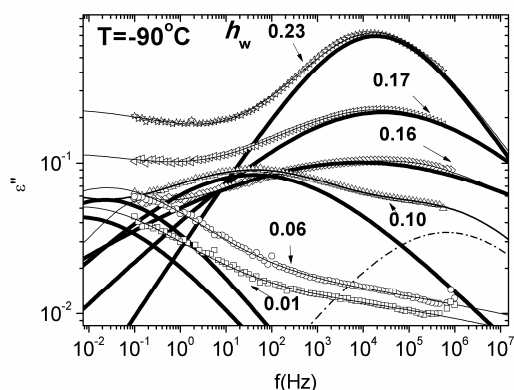
Στο Σχήμα 5.3 a και 5.3 b φαίνονται θερμογράμματα DSC που καταγράφηκαν κατά την ψύξη και θέρμανση, αντίστοιχα, για υδατωμένα δοκίμια HA με ρυθμό ψύξης/θέρμανσης $10^\circ\text{C}/\text{min}$. Η εικόνα που λαμβάνεται από τα θερμογράμματα DSC για το σύστημα HA-νερό είναι παρόμοια με αυτή στην περίπτωση του συστήματος BSA-νερό. Συγκεκριμένα, η κρυστάλλωση κατά την ψύξη ανιχνεύεται για κλάσματα υδάτωσης $h_w \geq 0.31$ (Σχήμα 5.3 a), ενώ παρατηρείται ψυχρή κρυστάλλωση κατά την θέρμανση (Σχήμα 5.3 b). Επιπλέον, η υαλώδης μετάβαση ανιχνεύεται για κλάσματα υδάτωσης $h_w \geq 0.06$, ενώ δεν είναι ανιχνεύσιμη για το δοκίμιο με $h_w \geq 0.02$. Η εκτιμώμενη T_g ελαττώνεται από $T_g \sim -45^\circ\text{C}$ για $h_w = 0.06$, αυξανόμενου του κλάσματος υδάτωσης, έως $T_g \sim -80^\circ\text{C}$ για $h_w = 0.59$, όπου και σταθεροποιείται (η σταθεροποίηση επιβεβαιώνεται από φάσματα που δεν παρουσιάζονται στο Σχήμα 5.3 b, για λόγους ευκρίνειας).



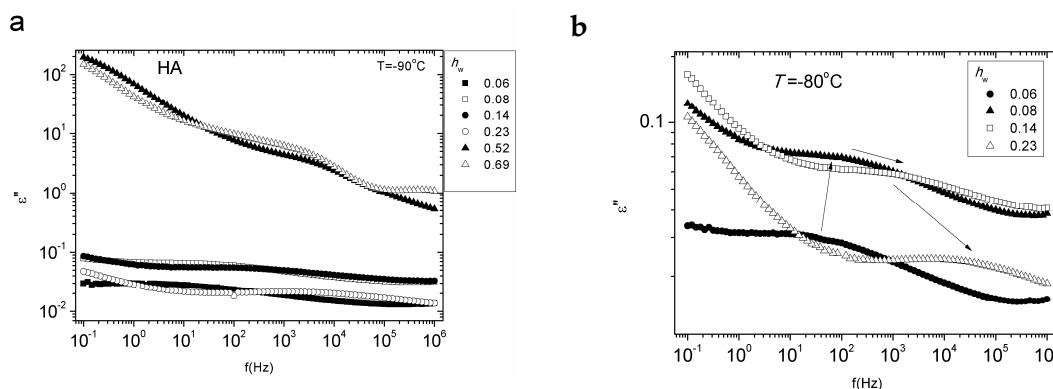
Σχήμα 5.3. Θερμογράμματα DSC κατά την α) ψύξη και β) θέρμανση με ρυθμό 10 °C/min για υδατωμένα δοκίμια ΗΑ σε διάφορα κλάσματα υδάτωσης, h_w (g νερού/g υδατωμένου ΗΑ). Η θερμοκρασία υαλώδους μετάβασης, T_g , αναδεικνύεται στο διάγραμμα με κάθετα ευθύγραμμα τμήματα. Η ροή θερμότητας είναι κανονικοποιημένη ως προς τη μάζα των δοκιμών.

5.3 Διηλεκτρική φασματοσκοπία εναλλασσομένου πεδίου (DRS)

Στο Σχήμα 5.4 φαίνεται για διάφορα δοκίμια η εξέλιξη της κορυφής του διηλεκτρικού μηχανισμού που αντιστοιχεί στην κίνηση πλευρικών πολικών ομάδων (polar), με το επίπεδο υδάτωσης, για το σύστημα ελαστίνη-νερό στο εύρος υδάτωσης $h_w \leq 0.23$. Σε υψηλά επίπεδα υδάτωσης η σταθεροποιημένη κορυφή ως προς τη θέση ονομάζεται πλέον 'ν' μηχανισμός, ο οποίος σύμφωνα με τη βιβλιογραφία είναι ο κύριος δευτερεύων μηχανισμός διηλεκτρικής αποκατάστασης που εντοπίζεται σε υδατωμένα συστήματα και αποδίδεται σε δυναμική μη κρυσταλλωμένων μορίων νερού. Στα πειραματικά σημεία των διηλεκτρικών απωλειών προσαρμόστηκε άθροισμα συναρτήσεων Cole-Cole και ενός όρου αγωγιμότητας (βλ. Ενότητα 3, παράγραφος 3.2). Παραδείγματα των προσαρμογών φαίνονται επίσης στο Σχήμα 5.4. Με διακεκομμένη



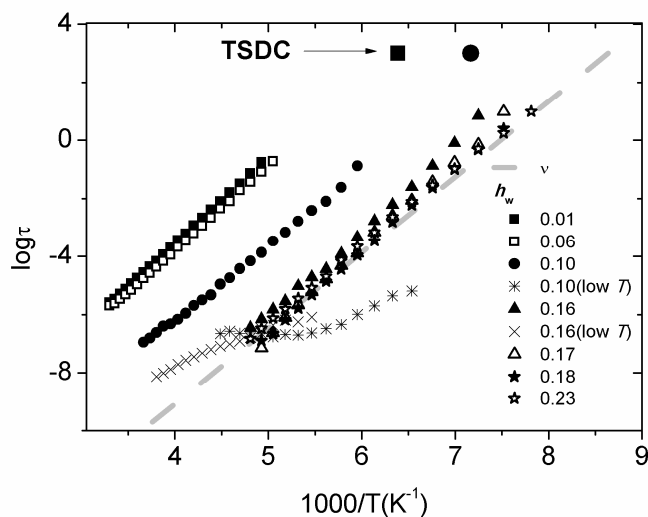
Σχήμα 5.4. Διηλεκτρικές απώλειες, ϵ'' , συναρτήσει της συχνότητας, f , σε θερμοκρασία $T=-90^\circ\text{C}$ για υδατωμένα δοκίμια ελαστίνης σε κλάσματα υδάτωσης h_w . Οι συμπαγείς (ή διακεκομμένες) γραμμές αποτελούν τις συνεισφορές απωλειών στο συνολικό φάσμα όπως προέκυψαν από ανάλυση με πρότυπες συναρτήσεις. Οι συνεχείς γραμμές που διαπερνούν τα πειραματικά σημεία είναι το άθροισμα των συνεισφορών.



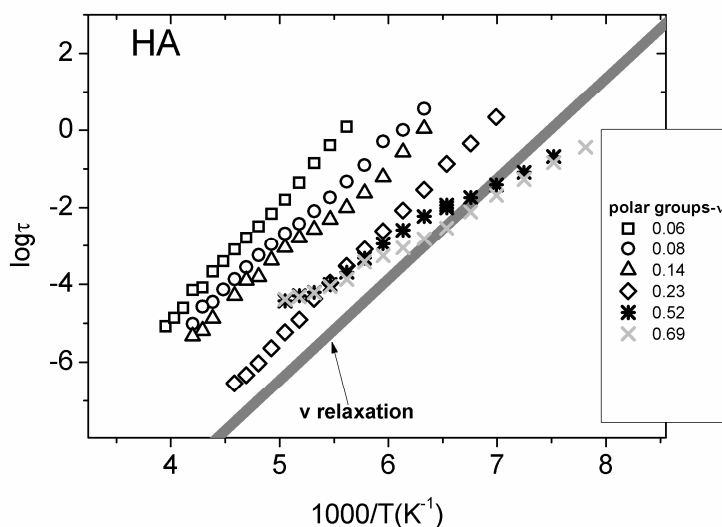
Σχήμα 5.5. Διηλεκτρικές απώλειες, ϵ'' , συναρτήσει της συχνότητας, f , σε θερμοκρασία **a)** $T=-90^{\circ}\text{C}$ και **b)** $T=-80^{\circ}\text{C}$ για υδατωμένα δοκίμια HA σε κλάσματα υδάτωσης h_w .

γραμμή φαίνεται και η συνεισφορά ενός επιπλέον μηχανισμού διηλεκτρικής αποκατάστασης που ανιχνεύτηκε για κάποια δοκίμια σε χαμηλές θερμοκρασίες. Ο εν λόγω μηχανισμός δεν θα σχολιαστεί περαιτέρω στην παρούσα Ενότητα. Αντίστοιχα αποτελέσματα σχετικά με την εξέλιξη του μηχανισμού πολικών ομάδων με το επίπεδο υδάτωσης προέκυψαν και για το σύστημα HA-νερό. Στο Σχήμα 5.5 a και b φαίνεται η εξέλιξη της κορυφής του διηλεκτρικού μηχανισμού που αντιστοιχεί στην κίνηση πλευρικών πολικών ομάδων (polar), με το επίπεδο υδάτωσης, για το σύστημα HA-νερό στο εύρος υδάτωσης στους -90°C και στους -80°C , αντίστοιχα. Στο Σχήμα 5.5 a φαίνεται ότι οι διηλεκτρικές απώλειες αυξάνονται έντονα σε μεγάλα ποσοστά υδάτωσης, όπου και το φάσμα γίνεται πολύπλοκο καθώς περιέχει συνεισφορές από επιπρόσθετους μηχανισμούς αποκατάστασης, με του οποίους δεν θα ασχοληθούμε στο παρούσα ενότητα. Στο Σχήμα 5.5 b φαίνεται καλύτερα η εξέλιξη του μηχανισμού πολικών ομάδων για τα χαμηλά ποσοστά υδάτωσης στην περιοχή $h_w < 0.23$. Αυτό που πρέπει να τονιστεί είναι, εκτός από την πλαστικοποίηση του μηχανισμού η οποία παρατηρείται και στα υπόλοιπα συστήματα που παρουσιάστηκαν έως τώρα, η εξάρτηση της έντασης του μηχανισμού από το ποσοστό υδάτωσης. Παρατηρούμε ότι η ένταση ενισχύεται αρχικά αλλά στη συνέχεια ελαττώνεται με την αύξηση του κλάσματος υδάτωσης από $h_w=0.14$ σε $h_w=0.23$. Το γεγονός αυτό οφείλεται στην αναδιοργάνωση του νερού στη σφαίρα υδάτωσης του μορίου, λόγω διόγκωσης. Το αποτέλεσμα αυτό ενισχύεται από την ολοκληρωμένη ανάλυση των αποτελεσμάτων σε περισσότερες θερμοκρασιακές περιοχές (αποτελέσματα που δεν παρουσιάζονται εδώ). Αντιθέτως, η ένταση του μηχανισμού αυξάνεται μονότονα με την αύξηση του ποσοστού υδάτωσης για τα συστήματα BSA και ελαστίνη (Ενότητα 4, Σχήμα 5.4).

Η θερμοκρασιακή εξάρτηση του χρόνου αποκατάστασης του μηχανισμού πολικών ομάδων και του ν μηχανισμού (βλ. Ενότητα 4) καταγράφεται στα Σχήματα 5.5 και 5.6. για τα συστήματα ελαστίνη-νερό και HA-νερό, αντίστοιχα, σε συγκεκριμένα επίπεδα υδάτωσης h_w .



Σχήμα 5.5. Θερμοκρασιακή εξάρτηση του λογαρίθμου του χρόνου αποκατάστασης $\log(\tau)$ για τον μηχανισμό διηλεκτρικής αποκατάστασης πολικών ομάδων (polar groups) και για τον ν μηχανισμό για υδατωμένα δοκίμια ελαστίνης σε διάφορα κλάσματα υδάτωσης h_w . Τα αντίστοιχα σημεία από μετρήσεις TSDC καταγράφονται στην ισοδύναμη συχνότητα της τεχνικής. Τα σημεία που αντιστοιχούν σε έναν επιπλέον μηχανισμό που ανιχνεύτηκε σε χαμηλές θερμοκρασίες (low T) παρουσιάζονται επίσης στο διάγραμμα για κάποια δοκίμια.



Σχήμα 5.6. Θερμοκρασιακή εξάρτηση του λογαρίθμου του χρόνου αποκατάστασης $\log(\tau)$ για τον μηχανισμό διηλεκτρικής αποκατάστασης πολικών ομάδων (polar groups) και για τον ν μηχανισμό για υδατωμένα δοκίμια HA σε διάφορα κλάσματα υδάτωσης h_w .

Στο Σχήμα 5.5 φαίνεται ότι το ίχνος του μηχανισμού πολικών ομάδων για την υδατωμένη ελαστίνη μετακινείται σε χαμηλότερες θερμοκρασίες (πλαστικοποίηση) με

την αύξηση του ποσοστού υδάτωσης και σταθεροποιείται για $h_w \geq 0.16$ σε θέση συγκρίσιμη με αυτή του ν μηχανισμού (διακεκομμένη γκρι ευθεία στο Σχήμα 5.4, βλέπε ενότητα 5). Στο Σχήμα 5.6 φαίνεται η πλαστικοποίηση του μηχανισμού πολικών ομάδων για το σύστημα HA-νερό, έως ένα κλάσμα υδάτωσης $h_w = 0.23$. Σε μεγαλύτερα ποσοστά υδάτωσης ο αντίστοιχος μηχανισμός διαφοροποιείται ως προς την ενέργεια ενεργοποίησης (κλίση), γεγονός που αντανακλά την αναδιοργάνωση του νερού η οποία αναφέρθηκε προηγουμένως στο σχολιασμό του Σχήματος 5.5. Αναφέρεται εδώ ότι για τα συστήματα BSA-νερό και ελαστίνη-νερό η ενέργεια ενεργοποίησης είναι περίπου ίση με $E_{act} = 0.55$ eV, η οποία αντιστοιχεί στην ενέργεια που απαιτείται για το σπάσιμο 2 δεσμών υδρογόνου.

Τα αποτελέσματα από τις τεχνικές ESI, DSC, DRS, για τα συστήματα ελαστίνη-νερό και HA-νερό θα σχολιαστούν στην 6η Ενότητα, η οποία αφορά στα γενικά συμπεράσματα, σε αντιπαράβολη με τα αντίστοιχα αποτελέσματα για το σύστημα BSA-νερό.

6 η ΕΝΟΤΗΤΑ

ΓΕΝΙΚΑ ΣΥΜΠΕΡΑΣΜΑΤΑ

Η δυναμική και οι μεταπτώσεις φάσης στα συστήματα BSA-νερό, ελαστίνη-νερό και HA-νερό διερευνήθηκε με τις τεχνικές ESI, DSC, TSDC και DRS, σε ευρεία περιοχή επιπέδων υδάτωσης.

Η θερμική υαλώδης μετάβαση για το σύστημα BSA-νερό ανιχνεύτηκε με την τεχνική DSC για επίπεδα υδάτωσης μεγαλύτερα ενός κατωφλίου. Παρόμοια συμπεριφορά ανιχνεύτηκε στην περίπτωση του συστήματος HA-νερό, με τη μέθοδο DSC. Η απουσία ανίχνευσης της υαλώδους μετάβασης για τα ξηρά συστήματα, ενισχύει την άποψη ότι στην θερμική υαλώδη μετάβαση συνεισφέρει συγκεκριμένος πληθυσμός μη κρυσταλλωμένων μορίων νερού. Αντιθέτως, οι μετρήσεις DSC κατέδειξαν την υαλώδη μετάβαση για την ελαστίνη ήδη από το ξηρό δοκίμιο. Οι τιμές της υαλώδους μετάβασης στην περίπτωση της ελαστίνης λαμβάνουν υψηλότερες τιμές από τις αντίστοιχες για το BSA και το HA. Σε όλες τις περιπτώσεις η κίνηση των τμημάτων που συμμετέχουν στην υαλώδη μετάβαση διευκολύνεται από τα μόρια νερού που συμμετέχουν σε αυτήν. Γενικό συμπέρασμα είναι ότι το φαινόμενο περιέχει συνεισφορές τόσο από την πρωτεΐνη, όσο και από το ποσοστό του μη κρυσταλλωμένου νερού στην επιφάνεια της πρωτεΐνης.

Ο κύριος δευτερεύων μηχανισμός διηλεκτρικής αποκατάστασης στη σφαίρα υδάτωσης της πρωτεΐνης μελετήθηκε διεξοδικά ως προς την δυναμική του. Τα πειραματικά αποτελέσματα κατέδειξαν ότι το μη κρυσταλλωμένο νερό στην πρώτη σφαίρα υδάτωσης αλληλεπιδρά με μικρές πλευρικές πολικές ομάδες στην επιφάνεια της πρωτεΐνης και ενισχύει την κίνησή τους. Για επίπεδα υδάτωσης μεγαλύτερα του ποσοστού μορίων νερού σε πρωταρχικές θέσεις υδάτωσης, η βαθμιαία οργάνωση των

ΕΚΤΕΝΗΣ ΠΕΡΙΛΗΨΗ

μορίων νερού σε συσσωματώματα οδηγεί στη βαθμιαία κάλυψη της επιφάνειας και πλέον κυριαρχεί η δυναμική του δευτερεύοντα μηχανισμού του υπέρψυκτου νερού σε ένα επιφανειακό στρώμα στην επιφάνεια της πρωτεΐνης. Στην περίπτωση της σφαιρικής πρωτεΐνης BSA και της ινώδους πρωτεΐνης ελαστίνης οι χαρακτηριστικοί χρόνοι αποκατάστασης μειώνονται με την αύξηση του ποσοστού υδάτωσης και η ένταση του μηχανισμού αυξάνεται. Η εν λόγω εξέλιξη με το ποσοστό υδάτωσης παγιώνεται με τη βαθμιαία κάλυψη της επιφάνειας και τη δημιουργία ενός ενιαίου επιφανειακού στρώματος νερού. Στην περίπτωση του HA και στα χαμηλά επίπεδα υδάτωσης, η οργάνωση των μη κρυσταλλωμένων μορίων νερού είναι παρόμοια με αυτή στην περίπτωση των BSA και ελαστίνης, ενώ για κλάσματα υδάτωσης μεγαλύτερα του 14% κ.β. παρατηρείται μία αναδιοργάνωση των μορίων νερού, η οποία συνδέεται με τον ιδιαίτερα υδροφιλικό χαρακτήρα του HA και τη διόγκωση του πλέγματος. Η ενέργεια ενεργοποίησης του μηχανισμού μειώνεται σε αυτήν την περίπτωση.

Βιβλιογραφία

- [1] H. Lodish et al. *Molecular Cell Biology* 5th ed. WH Freeman and Company: New York, NY. (2004).
- [2] C. Branden and J. Tooze, *Introduction to Protein Structure* 2nd ed. Garland Publishing: New York, NY (1999).
- [3] E. Donth, *The Glass Transition: Relaxation Dynamics in Liquids and Disordered Materials*. Springer: Berlin (2001).
- [4] R. B. Gregory in: R.B. Gregory (ed.) *Protein-Solvent Interactions*, Marcel Dekker: New York, (1995), p. 191.
- [5] B.J. Halle, *Chem. Phys.* 119, 12372 (2003).
- [6] M.C. Belissent-Funel, *J. Mol. Liq.* 84, 39 (2000).
- [7] Bhattacharayya, B. Bagchi, *J. Phys. Chem. A* 104, 10603 (2000).
- [8] J. Swenson, H. Jansson, R. Bergman, *Phys. Rev. Lett.* 96, 247802 (2006).
- [9] G. Careri, G. Consolini, F. Bruni, *Solid State Ionics* 125, 257 (1999).
- [10] P. Mentre *Cell. Mol. Biol.* 47, 709 (2001).
- [11] A.R. Bizzarini, S. Cannistrato, *J. Phys. Chem. B* 106, 6617 (2002).
- [12] P. Chen, L. Zhang, *Macromol. BioSci.* 5, 237 (2005).
- [13] K. Kawai, T. Suzuki, M. Oguni, *Biophys. J.* 90, 3732 (2006).
- [14] H. Frauenfelder, P.W. Fenimore, G. Chen, B.H. McMahon, *Proc. Natl. Acad. Sci. USA* 103, 15469 (2006).
- [15] W. Doster, M. Settles, *BBA-Proteins Proteom.* 1749, 173 (2005).
- [16] K. L. Ngai, S. Capaccioli, N. Shinyashiki, *J. Phys. Chem. B* 112, 3826 (2008).
- [17] E. O. Timmermann, A BET-like three sorption stage isotherm, *J. Chem. Soc. Faraday Trans.*, 1 85 (1989) 1631-1645.
- [18] C. Pandis, A. Spanoudaki, A. Kyritsis, P. Pissis, J. C. Rodríguez Hernández, J. L. Gómez Ribellez, M. Monleón Pradas, *Water Sorption Characteristics of Poly(2-hydroxyethyl acrylate)/Silica Nanocomposite Hydrogels*, *Polymer Physics*, 49 (2011) 657-668.

ΕΚΤΕΝΗΣ ΠΕΡΙΛΗΨΗ

- [19] P. Pissis, A study of sorbed water on cellulose by the thermally stimulated depolarisation technique, *J. Phys. D: Appl. Phys.* 18 (1985) 1897-1908.
- [20] A. Anagnostopoulou-Konsta, P. Pissis, A study of casein hydration by the thermally stimulated depolarisation currents method, *J. Phys. D Appl. Phys.* 20 (1987) 1168–1174.
- [21] P. Pissis, G. Boudouris, J.C. Garson, J.L. Leveque, Depolarization thermocurrents in ice Ih at low temperature, *Z. Naturforsch.* 36a (1981) 321–328.
- [22] P. Pissis, L. Apekis, C. Christodoulides, G. Boudouris, Dielectric behavior of ice microcrystals dispersed within suspensions, *Z. Naturforsch.* 37a (1982) 1000–1004.
- [23] M. Wübbenhorst, J. van Turnhout, Analysis of complex dielectric spectra. I. One-dimensional derivative techniques and three-dimensional modelling, *J. Non-Cryst. Solids* 305 (2002) 40–49.
- [24] N. Shinyashiki, W. Yamamoto, A. Yokoyama, T. Yoshinari, S. Yagihara, K.L. Ngai, S. Capaccioli, Glass transitions in aqueous solutions of protein (Bovine Serum Albumin), *J. Phys. Chem. B* 113 (2009) 14448–14456.
- [25] K. L. Ngai, S. Capaccioli, S. Ancherbak, N. Shinyashiki, Resolving the ambiguity of the dynamics of water and clarifying its role in hydrated proteins, *Philos. Mag.*, 91 (2011) 1809–1835.